SYNTHESIS, STRUCTURE AND PROPERTIES OF $Cu^{II}/Ln^{III}(NO_3)_x$ COMPLEXES

A Thesis

Submitted for the Degree of

Doctor of Philosophy

By

KRISHNA CHARY THATIPAMULA

SCHOOL OF CHEMISTRY

UNIVERSITY OF HYDERABAD

HYDERABAD – 500 046

INDIA

SEPTEMBER 2015

With the Blessings of

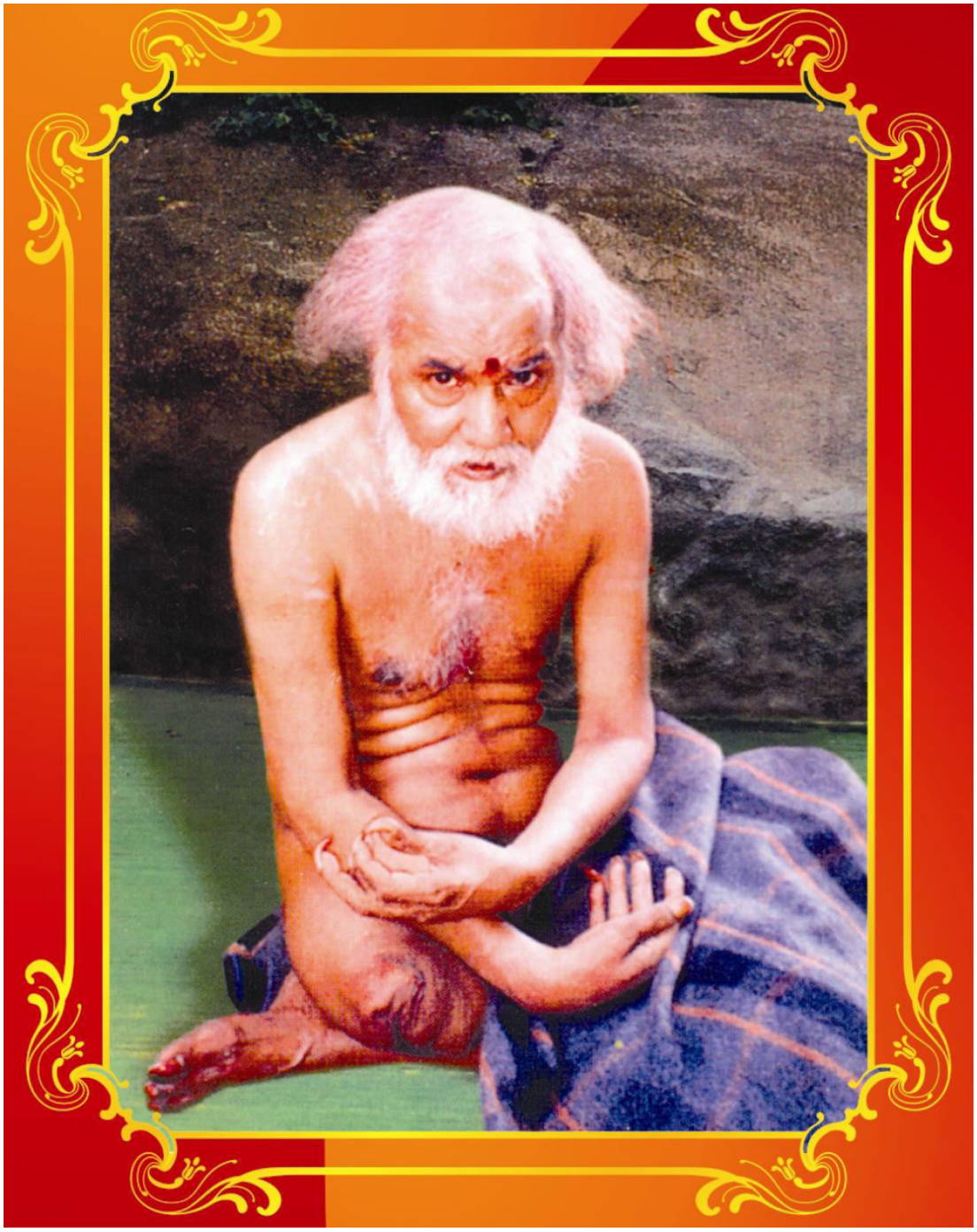

The 6th incarnation of Lord Datta Prabhu

Sadguru Sri Nampally Baba

Dedicated to the Holy and Lotus Feet of my Revered Spiritual Master

Pujya Sri ***Kolipaka Appa Rao***

CONTENTS

CHAPTER II

Synthesis, structural and spectral characterization of the lanthanide nitrato complex anions crystallised using Cu(II) nitrate and 2,2'-bipyridine

STATEMENT

I hereby declare that the matter embodied in this thesis is the result of investigations carried out by me in the School of Chemistry, University of Hyderabad, Hyderabad, Telangana, India under the supervision of **Prof. M. V. Rajasekharan.** In keeping with the general practice of reporting scientific observations, due acknowledgement has been made wherever the work described is based on the finding of other investigators.

Krishna Chary Thatipamula

CERTIFICATE

Certified that the work embodied in this thesis entitled **"SYNTHESIS, STRUCTURE AND PROPERTIES OF $Cu^{II}/Ln^{III}(NO_3)_x$ COMPLEXES"** has been carried out by **Mr. Krishna Chary Thatipamula** under my supervision and the same has not been submitted elsewhere for any degree.

Hyderabad
September 2015

M. V. RAJASEKHARAN
(Thesis Supervisor)

DEAN
School of Chemistry

Acknowledgements

*Thanks and again thanks to "**Sadguru Sri Nampally Baba**" for his kind blessing and divine support that this report is finally completed.*

*I gratefully acknowledge my thesis supervisor, **Prof. M. V. Rajasekharan** for his guidance, encouragement and support. My association with him throughout my research tenure in this lab was a rewarding experience, which I never wish to forget.*

I thank the present and past Dean(s) of the School of Chemistry, Doctoral committee members and all the faculty members of the school for their cooperation.

I thank Centre for Nanotechnology (CNF), University of Hyderabad, for the variable temperature magnetic susceptibility measurements. My sincere thanks are also due to Mr. Ravi, Mr. Uma Shanker, Mr. Pavan and Mr. Binay for the immense help I received from them.

I thank the librarian and other staff of Indira Gandhi Memorial Library (IGML) of the university for the books and journals.

I thank all the technical and non-teaching staff of the School of Chemistry and Central Instrumentation Lab (CIL) for their help and guidance on various occasions.

Let me also thank the present and past Warden(s) of NRS (E) hostel and all the staff members of the mess for providing quality food and accommodation.

I thank my seniors Dr. A. R. Biju, Dr. G. Bhargavi, labmates Dr. S. M. Elahi, Mr. R. Babu, Dr. N. Srinivasan, Dr. B. Kishore Babu, Dr. P. M. Vimal, Dr. Laxmi Prabha, Mrs. Sneha and project students Mr. Shiva and Satya Krishna for their timely help and cooperation.

I thank all my teachers especially Dr. J. P., Dr. P. V. Rao, Mr. Ravi Kumar, Mr. Janga Reddy, whose lectures, made chemistry more convincing and interesting to me.

I would like to thank all my friends, colleagues and well wishers especially to Kishore, Srinivas, Rama Raju, Swamy, Shiva, Naveen, Obaiah, Sudhansu, Singh, Abao, Satish Bhat, Venkatesh, Malli, Rajini akka, Shashi-Visu garu, Ajay babu garu, Kumar anna, Sarkar, Srinivas, Rani-Yadaiah garu, Smt. Ravitha, Krishna Swamy, Linga Reddy uncle, Kusuma-Prabhakar garu, Madhu-Anil garu, Gangapur, Chandu, Mr. Rama Krishna, Radha-Narasimha garu, Thatha Rao garu, Uma Pathi garu, Smt. Jyothi, Prasad garu, Dr. Suresh, Manjunatha garu, Varun garu, Latha akka, Smt. Laxmi and Smt. Sandhya for their support, whole-hearted cooperation. I wish to express my profound gratitude to my father, mother, sister, brother-in-law, aunty and two brothers for their encouragement and support throughout my life.

I owe my deepest gratitude to Sri Dattatreya Swamy, Sri Sripada Sri Vallabha Swamy, Sri Nrisimha Saraswathi Swamy, Sri Manik Prabhu Maharaj, Sri Akkalkot Maharaj, Sri Shiridi Sai Baba, Pujya Acharya Sri Ekkirala Bharadwaja, Sri Chaitanya Swamy, Sri Gopal Baba, Sri Polaiah thatha, Sri Patny Baba, The Lord Michael oliver Raju who molded me to be a modest worker in my life. I would like to thank all my gurus, who teach me right way.

Financial Assistance from UGC and CSIR is gratefully acknowledged.

Finally, I thank all those who gave suggestions and guidance before and during the research. I sincerely regret the omission of references to any special help of suggestions.

Krishna Chary Thatipamula

PREFACE

The thesis work deals with the structural and magnetic properties of Cu(II) complexes. The main objective of this thesis is to synthesize Cu(II)/*Ln*(III) heteropolynuclear complexes with 2,2'-bipyridine (bpy) as a co-ligand and to observe the influence of lanthanide complex anions on the composition of the Cu(II) complex cations. In addition, with a view to the investigation of magnetic exchange interactions between adjacent magnetic nuclei, Cu(II) complexes bridged by water molecules as well as halogenated acetates have been investigated. The thesis work is divided into six chapters. Chapter I gives a brief introduction to the lanthanides and their chemistry. Besides these, a brief introduction to the mixed heterometallic Cu(II)/*Ln*(III) coordination complexes. Chapter II deals with the synthesis, structural and spectral properties of a series of novel heterometallic Cu(II)/*Ln*(III) complexes containing 2,2'-bipyridine (bpy) as a co-ligand are discussed. Chapter III describes the synthesis, structural and spectral properties of a series of novel heterometallic tris-chelated Cu(II) complexes containing 2,2'-bipyridine (bpy) accompanied by lanthanide anions. Synthesis structural and spectral properties of heterometallic Cu(II)/*Ln*(III) compounds with 5,5'-dimethyl-2,2'-bipyridine (dmbpy) are discussed in chapter IV. The synthesis and structural characterization of four mixed-ligand Cu(II) complexes containing 2,2'-bipyridine (bpy) or 1,10-phenanthroline (phen) in presence of isonicotinate (IN) are discussed in chapter V. The chapter VI deals with the synthesis, structural and spectral properties of four Cu(II) complexes with 2,2'-bipyridine and different halogenated carboxylate ligands.

In the thesis only essential crystallographic data and selected geometrical parameters of the compounds are given. For isomorphous compounds, only for the first compound geometrical parameters and thermal ellipsoid plot are given and for other compounds the range in the bond

lengths are presented in text. Throughout the thesis, in thermal ellipsoid plots atoms are represented as 30% probability ellipsoids and all hydrogen atoms and solvent molecules are omitted for clarity. Part of the work reported in this thesis has been published or communicated in a preliminary form and are given at the end of the thesis.

Abbreviations and definitions

$R1$ $= \Sigma||F_o| - |F_c|| \,/\, \Sigma|F_o|$

$wR2$ $= \{\Sigma\,[w(F_o^2 - F_c^2)^2]/\,[\Sigma(w(F_o^2)^2)]\}^{1/2}$

w $= 1/[\sigma^2(F_o)^2 + (AP)^2 + BP];\ P = [2F_c^2 + \text{Max}\,(F_o^2, 0)]/3$

GooF $= \{\Sigma[w(F_o^2 - F_c^2)^2]/(n\text{-}p)\}^{1/2}$

CHAPTER I

Lanthanides and their chemistry: A brief introduction

According to IUPAC,[1] the 'Rare Earths' is a group of 17 elements including 15 elements from lanthanum to lutetium (Z = 57 to 71), scandium (Z = 21) and yttrium (Z = 39) (Figure 1.1). However, promethium (Z = 61), a fission reaction product, is excluded from this group since it has not been found in nature. Scandium is not readily available, owing partly to the lack of rich sources and partly due to the difficulty of separation. And also, the chemistry of scandium is intermediate between that of aluminium (Z = 13) and lanthanides (*Ln*). The remaining 15 elements of this group generally occur together in nature and it is difficult to separate them from each other.

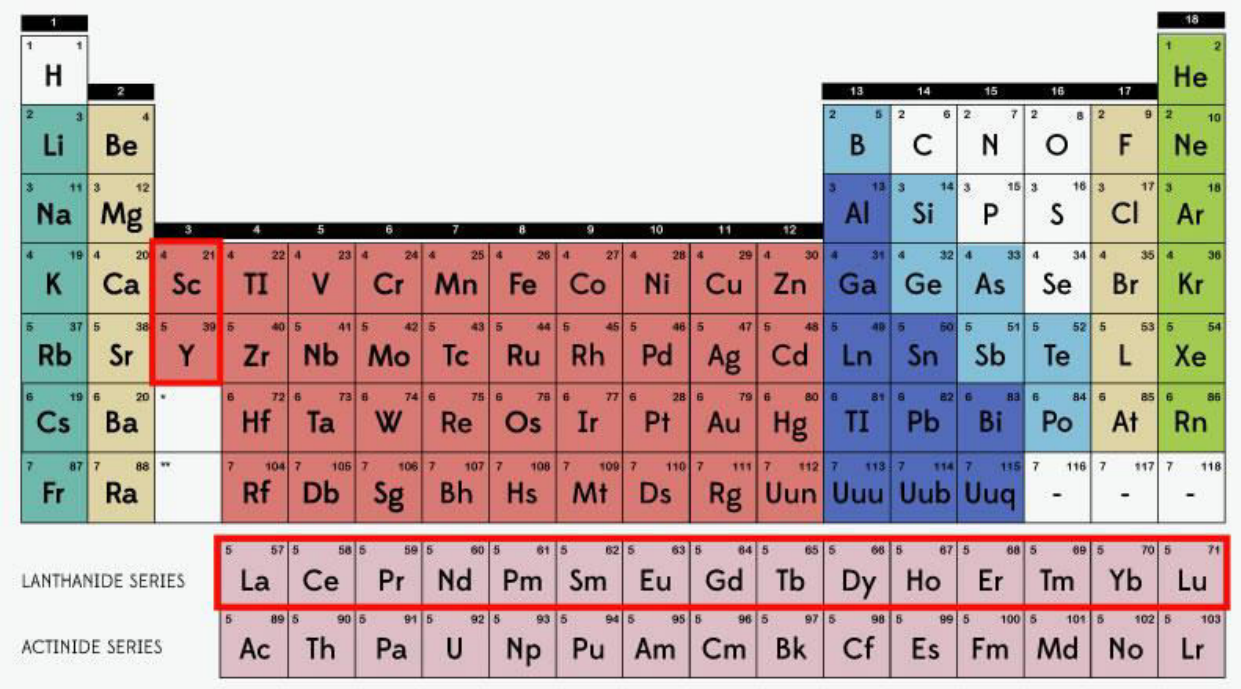

Figure 1.1. The periodic table of the elements (Reproduced from Google images via http://trer.com/ree/)

Based on their separability, the rare earths are usually divided into two sub groups: light rare earths or ceric group representing the first seven lanthanides La, Ce, Pr, Nd, Sm, Eu and Gd. Heavy rare earths or yttric group representing the rest of the eight lanthanides Y, Tb, Dy, Ho, Er, Tm, Yb and Lu. As the atomic and ionic radii of yttrium are in between that of Ho and Er, it shows greater similarity to the heavier lanthanides rather than to the lighter ones.

1.1. Coordination chemistry of lanthanides

The coordination chemistry of lanthanides has gained significant attention due to their unique physical and chemical properties and magnetic characteristics.[2] It is clear that over the past three decades, more importance has been given to find applications in the isolation and separation of the members of series by fractional crystallization and precipitation. Nowadays, more efforts have been made to study the intricate problems of structure and bonding in these complexes as well as to find new emerging area of applications in detail.

1.1.1. General properties

The complex formation of lanthanides is rather difficult because of the placement of the well shielded 4f electrons inside the completely filled outer electronic configuration of $[Xe]5s^2 5p^6$. Hence, practically the 4f orbitals are not involved in bond formation. Thus the metal-ligand bonds are substantially electrostatic in nature and the geometry of their complexes is usually determined by steric factor rather than by electronic factors. The important consequence of this shielding is the large similarity in the chemical behavior of the 15 lanthanide ions. Differences in chemical behavior may be ascribed to the decrease in ionic radius from La^{3+} to Lu^{3+}, a particular feature of these elements, the decrease in atomic size and radius with

increasing atomic number, a property known as the lanthanide contraction.[3] The ionic radii of *Ln*(III) ions in aqueous solution and crystal ionic radii for CN 8 and CN 9 are given in Table 1.1 and Figure 1.2.

The outer electronic configuration of lanthanides is generally $[Xe]4f^n5d^06s^2$ with the exceptions being cerium, $[Xe]4f^15d^16s^2$; gadolinium, $[Xe]4f^75d^16s^2$ and lutetium, $[Xe]4f^{14}5d^16s^2$. The lanthanide complexes are formed mainly from +3 oxidation state ($[Xe]4f^n$), but Ce^{4+}, Eu^{2+} and Yb^{2+} complexes are also known. The size of these ions is larger than that of other ions with similar charge and consequently the aftinity towards ligand is much less. As a result, appreciably stable complexes are obtained only when strongly chelating ligands, particularly ligands having highly electronegative donor atoms like oxygen, nitrogen etc., are used.

Table 1.1: Ionic radii (Å) of lanthanoid(III) cations in aqueous solution and crystal ionic radii listed by Shannon for 8-Fold and 9-Fold coordination[4]

Ln(III)	Ionic radii	Crystal radii for CN 8	Crystal radii for CN 9
La(III)	1.250	1.16	1.216
Ce(III)	1.220	1.143	1.196
Pr(III)	1.200	1.126	1.179
Nd(III)	1.175	1.109	1.163
Sm(III)	1.140	1.079	1.132
Eu(III)	1.120	1.066	1.120
Gd(III)	1.105	1.053	1.107
Tb(III)	1.090	1.040	1.095
Dy(III)	1.075	1.027	1.083
Ho(III)	1.055	1.015	1.072
Er(III)	1.040	1.004	1.062
Tm(III)	1.025	0.994	1.052
Yb(III)	1.010	0.985	1.042
Lu(III)	0.995	0.977	1.032

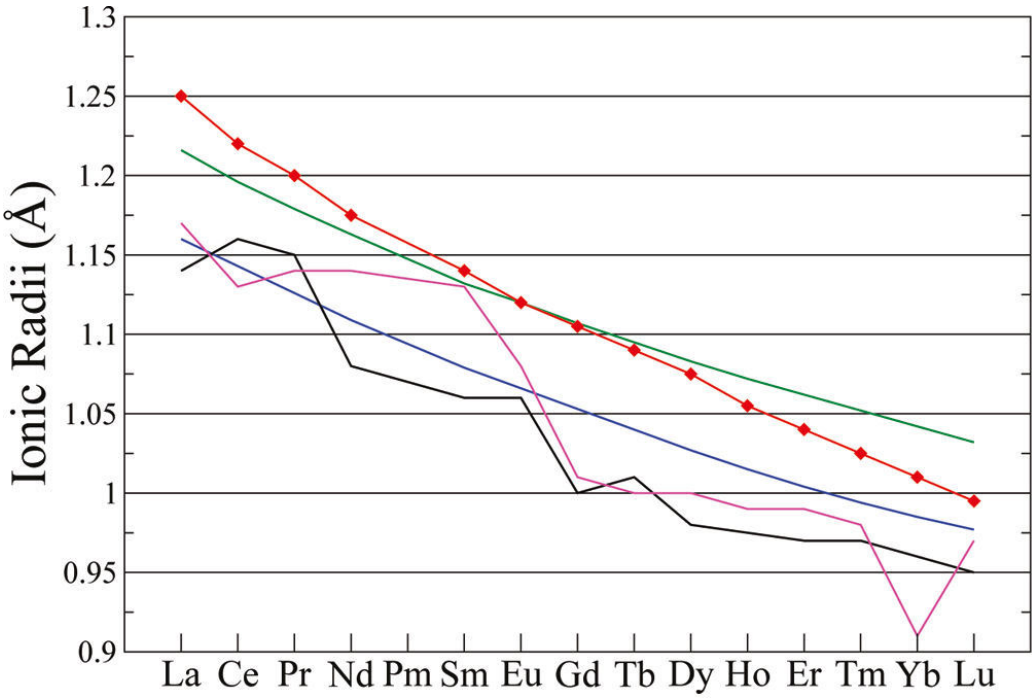

Figure 1.2. Ionic radii of *Ln*(III) in aqueous solution as determined by Marcus[5] (black line), by Heyrovska[6] (magenta line), by D'Angelo[4] (red line) together with the Shannon[7] 8-fold (blue line) and 9-fold (green line) crystal ionic radii.

Water molecule is a strong coordinating ligand towards lanthanide ions.[8] In the alkaline medium, OH^- ions are much stronger than water molecule towards coordination. Besides, the lanthanide hydroxides or hydrous oxides may get precipitated due to their extremely low solubility, this may prevent the formation of complexes with other ligands present in the medium. In addition to this, water is a solvent of high dielectric constant. Because of the above said reasons, it is often difficult to precipitate lanthanide complexes of neutral ligands from aqueous solutions. Therefore, the synthesis of lanthanide complexes are usually carried out in non-aqueous solvents like acetone, acetonitrile, methanol, ethanol, ethyl acetate, etc. under anhydrous condition.

In terms of hard-soft acid-base theory (HSAB),[9] lanthanide ions are typical hard acids (small ionic radius, low polarisability and high oxidation state) that prefer to bind hard bases

such as oxygen and nitrogen donors over softer donors such as sulfur and phosphorus.[10] As coordination is ionic in nature, charged groups such as carboxylates, phosphonates and phosphinates are favoured. According to Forsberg,[11] *Ln*-O interaction is stronger than *Ln*-**N** interaction that is why majority of the lanthanide complexes so far prepared contain oxygen donor ligands. Among the common ligands, the order of preference of donor sites for the interaction of the lanthandes is O > N > S.

1.1.2. Coordination number and molecular geometry

Unlike transition metals, the lanthanide complexes are characterised by high coordination numbers. The coordination number of lanthanides ranges from 3-12 with 8 and 9 being the most common. The coordination numbers of 3-5 are observed only in the case of bulky ligands.[12] Coordination numbers of 10 and over require chelating ligands with small "bites", such as NO_3^- or SO_4^{2-}. The high coordination numbers encountered is a consequence of the predominant electrostatic nature of the bonding between the metal ion and the ligand and the large size of the lanthanide ions. As the 4f orbitals are sufficiently shielded by the $[Xe]5s^25p^6$ octet as to be largely unavailable for bonding with the ligand orbitals, they do not have significant bond orienting character. As a result, the structure of a lanthanide complex is dictated by the following considerations:[13] (a) preserving (near) spherical symmetry for the central metal ion, (b) minimizing metal-metal and ligand-ligand repulsions, and (c) steric requirements of the ligands. And also it is generally observed that due to the decrease in the ionic size along the series the coordination number also decreases for the complexes with the same ligand. Ideal polyhedra which describe high coordination number are given in Table 1.2 and Figure 1.3.

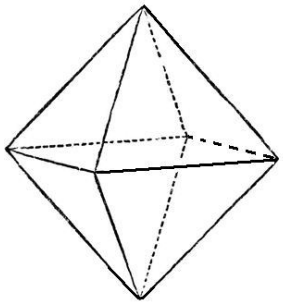

Octahedron (CN 6)

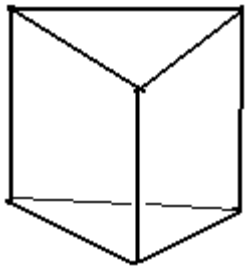

Trigonal prism (CN 6)

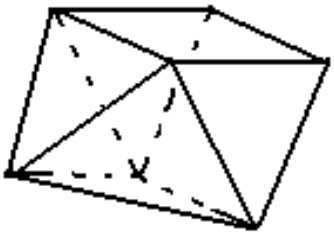

Monocapped trigonal prism(CN 7)

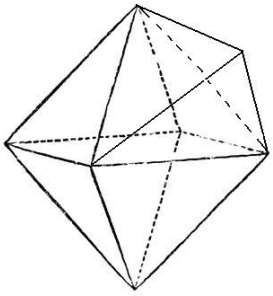

Monocapped octahedron (CN 7)

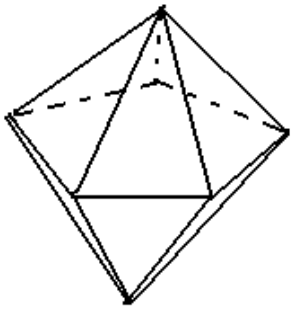

Pentagonal bipyramid (CN 7)

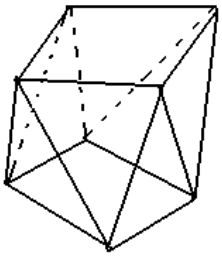

Square antiprism (CN 8)

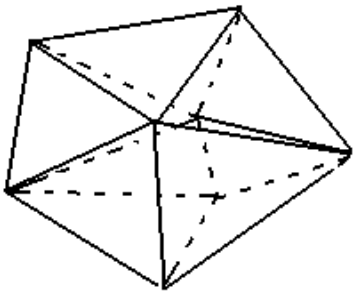

Trigonal dodecahedron (CN 8)

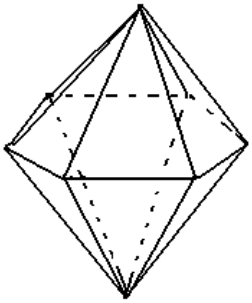

Hexagonal bipyramid (CN 8)

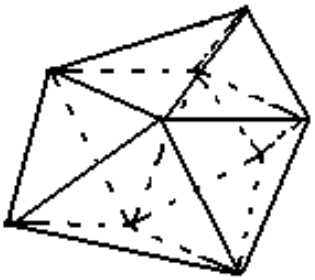

Tricapped trigonal prism (CN 9)

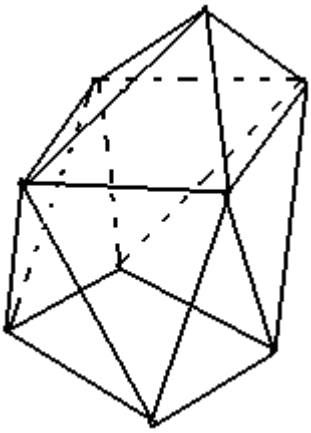

Monocapped squareantiprism (CN 9)

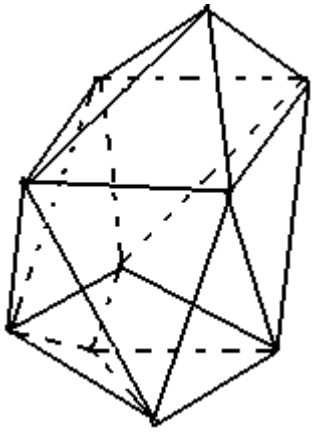

Bicapped square antiprism (CN 10)

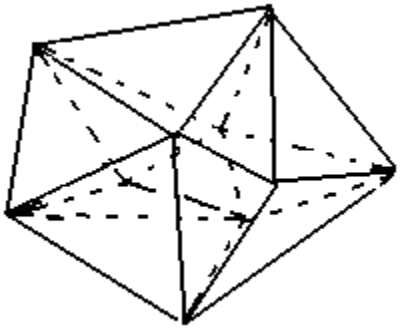

Bicapped dodecahedron (CN 10)

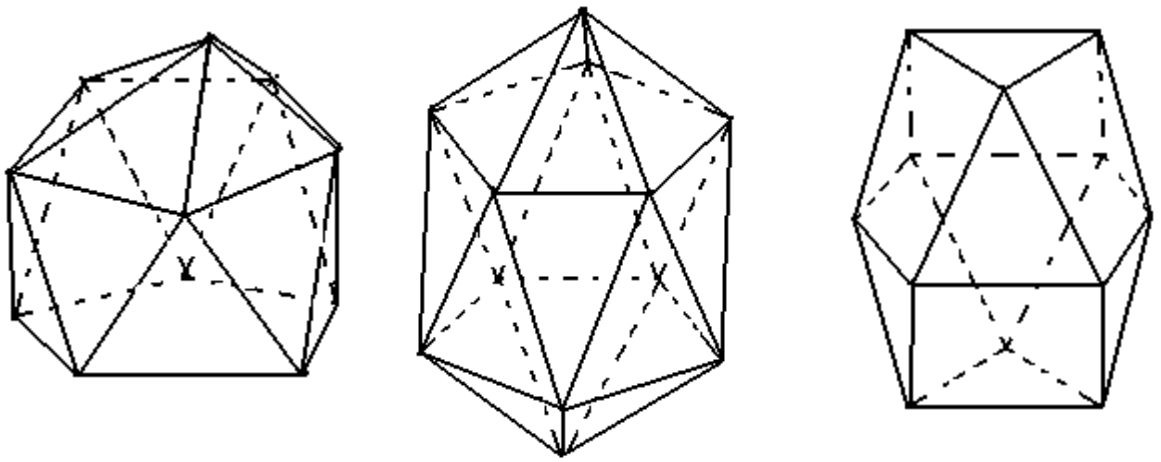

Monocapped pentagonal antiprism (CN11) | Icosahedron (CN 12) | Cuboctahedron (CN 12)

Figure 1.3. Ideal polyhedra for various high coordination numbers

Table 1.2: various coordination numbers and corresponding molecular geometry

Coordination number	Polyhedron
6	Octahedron (O_h), Trigonal prism (D_{3h})
7	Pentagonal bipyramid (D_{5h}), Monocapped trigonal prism (C_{2v}), Monocapped octahedron (C_{3v})
8	Trigonal dodecahedron (D_{2d}), Cube (O_h), Square antiprism (D_{4d}), Hexagonal bipyramid (D_{6h})
9	Tricapped trigonal prism (D_{3h}), Monocapped square antiprism
10	Bicapped square antiprism (D_{4d}), Bicapped dodecahedron
11	Monocapped pentagonal antiprism (C_{5v})
12	Icosahedron (I_h), Cuboctahedron (O_h)

1.1.3. Spectral properties

The electronic configurations of the lanthanides are described by using the Russell-Saunders (or L - S) coupling scheme. Because of 4f electrons are largely burried in the inner core, they are effectively shielded from their chemical environment. As a result, the spin-orbit coupling is much larger than the crystal field (2000 cm^{-1} compared to 100 cm^{-1}). Electronic absorption spectra of the lanthanides from J to J' state are extremely sharp, originating from *f-f* transitions (orbitally forbidden), where as transition elements give broad spectra. Most of the lanthanide elements have weak absorption in the visible range. The colours of *Ln*(III) ions are given in Table 1.3.

A further consequence of the relatively small effect of the crystal field is that the energies of the electronic states are slightly affected by the nature of the ligands or by thermal vibrations, so the absorption bands are very much sharper than those for d-d transitions. Because of this, they provide a useful means of characterizing, and quantitatively estimating, Ln^{3+} ions.[14]

1.1.4. Luminescent properties

The emission colors of the lanthanide ions cover the entire spectrum from UV to visible and near-infrared (NIR) ranges. Although most lanthanide ions are luminescent (except La^{3+} and Lu^{3+}), they are not luminescent to an equal degree, and thus not equally useful or commonly applied. The luminescence intensity of the lanthanide ion is dependent on the quantum yield, which is related to the extent of the energy gap between the lowest excited energy level of the ion and the highest sub-level of its ground state multiplet.[15] The partial energy level diagram for aqueous lanthanide ions, illustrating also the energy gaps, is shown in Figure 1.4.[16]

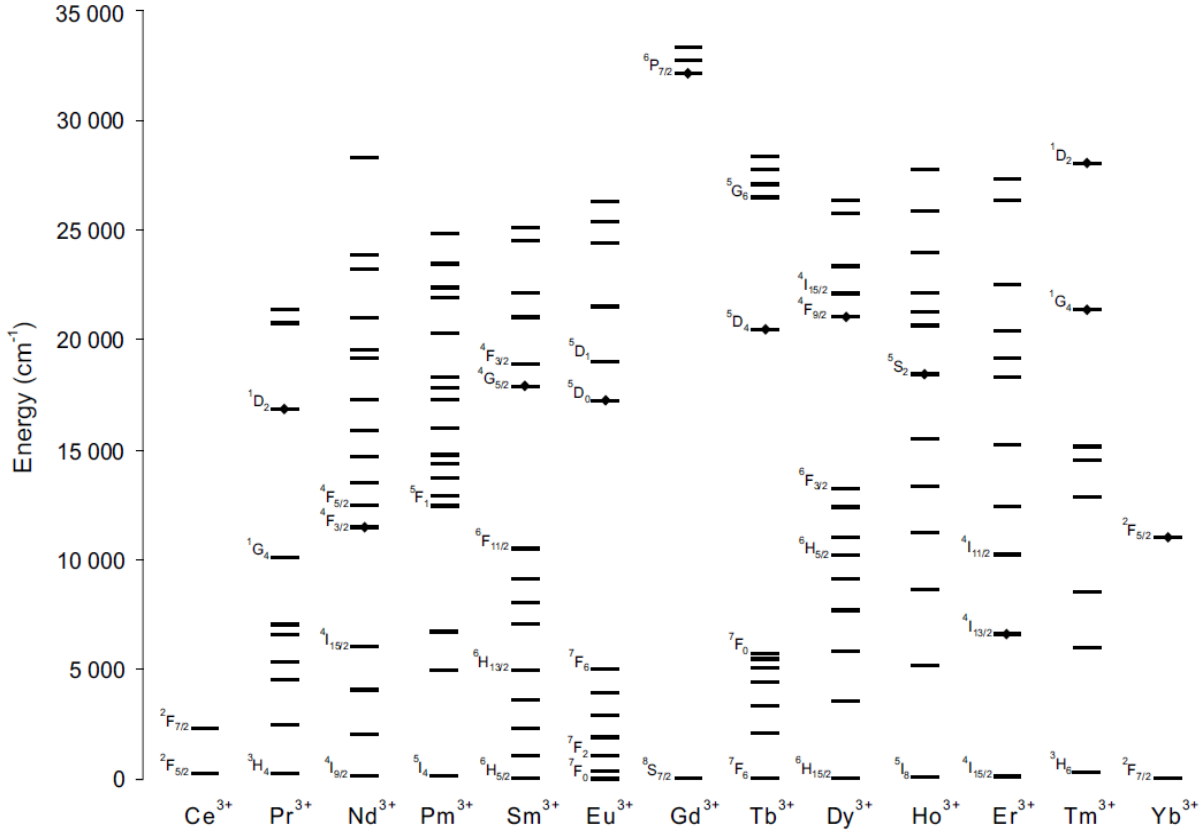

Figure 1.4. A diagram depicting the approximate energy levels for aqueous lanthanide ions. The commonly observed emittive levels are marked with closed tilted squares (Reproduced from Ref. 16a).

From the energy gap criterion, Eu^{3+}, Tb^{3+}, and Gd^{3+} ions have the strongest luminescence. The most commonly used lanthanide ions in bio analytical applications are Eu^{3+} and Tb^{3+}. In addition to their intense emission in the visible wavelength, this is due to their particularly long lifetime.[17] The usefulness of Gd^{3+} as a luminescent reporter is, however, limited, as it emits in the UV instead of the visible wavelength region.[18] Dy^{3+} and Sm^{3+} have also found many applications, but their use has been limited because of their inferior luminescence quantum yields and shorter lifetimes.[19] The applicability of the NIR emitting lanthanides (Nd^{3+}, Er^{3+}, and Yb^{3+}) has long been restricted, but recently their utility has increased because of the technical advances in the detection of the weak NIR emission, and because of the development

of novel sensitizing structures.[20] The photon upconversion phenomenon (a process where the energy of two or more sequentially absorbed photons combine to produce a higher energy photon) is demonstrated by several lanthanide ions, such as Tm^{3+}, Dy^{3+}, Er^{3+}, and Ho^{3+}.[21]

1.1.5. Electronic transitions

The electronic configuration of lanthanide ions is first divided into terms because of the Coulombic repulsion between the electrons within the orbitals. These terms are again split into J-levels because of spin-orbit coupling. These represent the free ion levels and are described by the term symbols S, L, and J with the formula $^{2S+1}L_J$, where 2S+1 is the spin multiplicity, L is the total orbital angular momentum, and J the total angular momentum of the f electrons. Because of the shielding of the 4f orbitals by the filled 5s and 5p sub-shells, the energies of the J-levels are well-defined, and the transitions between these levels are sharp, resulting in narrow, lanthanide-specific emission bands.[22] If the lanthanide ion is in a coordinating environment, the J levels can be further split into sub-levels because of the electric field of the matrix. These splittings may be seen as the fine structure of the main emission bands of the lanthanide ion.[23] Splitting of the electronic energy levels of a Eu^{3+} ion is shown in Figure 1.5.

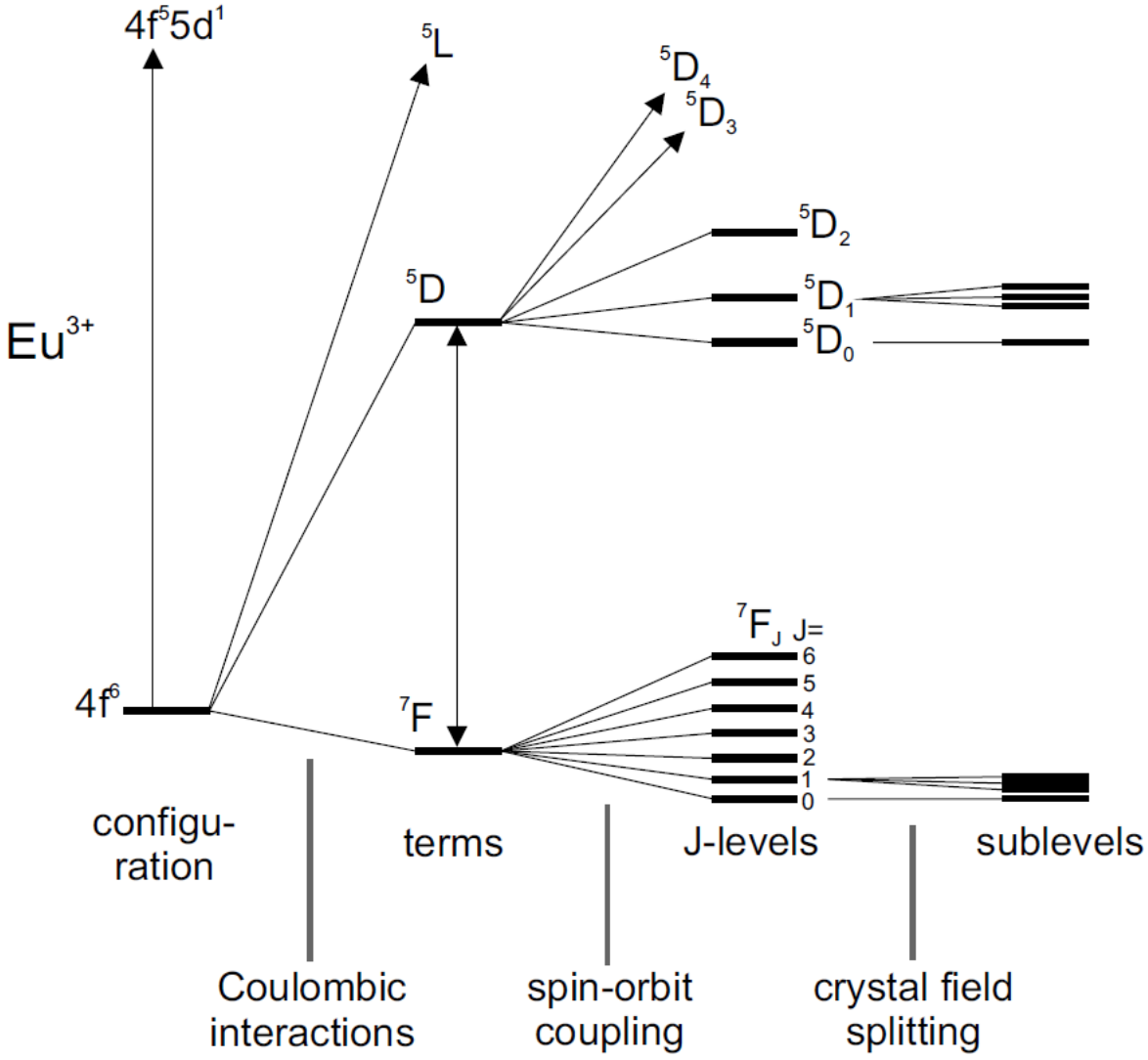

Figure 1.5. The interactions leading to the splitting of the electronic energy levels of a Eu^{3+} ion. In the diagram, energy increases when going up (Reproduced from Ref. 18).

1.1.6. Magnetic properties

All lanthanide(III) ions are paramagnetic in nature with the exception of La(III) and Lu(III) ions. The magnetic moments can be determined with equations using the *J* state.[24] Depending upon the number of unpaired electrons, the lanthanide ions produce varying paramagnetic effects. Some of them are strongly paramagnetic (Dy(III), Tb(III), Tm(III)) and others only moderate (Er(III), Ho(III), Yb(III)). The experimental magnetic moment values

closely match the expected values with two exceptions, Sm(III) and Eu(III) (Table 1.3). These two ions have excited *J* states close to the ground state at room temperature, resulting in an underestimation of their magnetic moments.[25]

Table 1.3: Magnetic properties and colours of Ln^{III} ions[25]

At. No.	*Ln*	unpaired electrons($4f^n$)	Ground state term	Colour	μ_{eff} (BM) $g\sqrt{J(J+1)}$	μ_{eff} (BM)[(a)] Observed
57	La[(b)]	$0(4f^0)$	$^1S_0$	Colourless	0	
58	Ce	$1(4f^1)$	$^2F_{5/2}$	Colourless	2.535	2.3-2.5
59	Pr	$2(4f^2)$	$^3H_4$	Green	3.578	3.4-3.6
60	Nd	$3(4f^3)$	$^4I_{9/2}$	Lilac	3.618	3.5-3.6
61	Pm	$4(4f^4)$	$^5I_4$	Pink	2.683	-
62	Sm	$5(4f^5)$	$^6H_{5/2}$	Yellow	0.845	1.4-1.7[(c)]
63	Eu	$6(4f^6)$	$^7F_0$	Pale pink	0	3.3-3.5[(c)]
64	Gd	$7(4f^7)$	$^8S_{7/2}$	Colourless	7.937	7.9-8.0
65	Tb	$6(4f^8)$	$^7F_6$	Pale pink	9.721	9.5-9.8
66	Dy	$5(4f^9)$	$^6H_{15/2}$	Yellow	10.646	10.4-10.6
67	Ho	$4(4f^{10})$	$^5I_8$	Yellow	10.607	10.4-10.7
68	Er	$3(4f^{11})$	$^4I_{15/2}$	Lilac	9.581	9.4-9.6
69	Tm	$2(4f^{12})$	$^3H_6$	Pale green	7.561	7.1-7.5
70	Yb	$1(4f^{13})$	$^2F_{7/2}$	Colourless	4.536	4.3-4.9
71	Lu	$0(4f^{14})$	$^1S_0$	Colourless	0	

[(a)] Definition: $\chi_m = \mu_0 N_A \mu_B^2 \mu_{eff}^2/(3k_B T)$

[(b)] diamagnetic

[(c)] These are the values of μ_e at room temperature. The values fall when the temperature is lowered.

1.1.7. Applications

Lanthanide ions have been used in a various types of applications in biological sciences. They have been used as luminescent chemosensors for biological imaging and drug delivery,[26]

anion sensors in aqueous solution,[27] catalysts for organic synthesis,[28] contrast agents for magnetic resonance imaging (MRI),[29] biomedical applications for the determination of cellular activity, and as paramagnetic centers for high resolution nuclear magnetic resonance spectroscopy (NMR).[30]

The lanthanide complexes with optically active β-diketones have been used to determine the purity of optical isomers.[31] Some of lanthanide β-diketonates have been shown to act as antiknock additive for gasoline and are good replacements for tetraethyl lead (TEL).[31] Lanthanides were used as catalyst for 'fluid catalytic cracking process' in the petroleum-refining industry.[32] With the help of these lanthanide catalysts, the heavy crude oil is converted into gasoline and other valuable products. Some metallopolymers containing lanthanide ions were used in photovoltaics, electro, and photoluminescent materials.[33] The lanthanide compounds combined with triethyl aluminium are used as Ziegler-Natta catalyst, which shows very high activity for the polymerisation of ethylene.[34] Some of lanthanide carboxylates are used as antioxidants.[35] The lanthanides with Schiff bases possess antifungal activity, and it has been found that toxicity decreases with chelation.[36]

Since lanthanide ions and alkaline earths have comparable ionic sizes, their complexes find similarities in properties. As far as it is known, the lanthanide ions have not any essential role in biology. However due to similar ionic radius, *Ln*(III) can substitute Ca(II) in calcium binding proteins. This characteristic is really useful in structural biology once it permits the direct introduction of the probe in the protein without any structural changes.[37] It is also important to refer that due to the similar size of different *Ln*(III) ions, a binding site in a protein can bind different lanthanides with similar affinities, with only a minimum distortion in the protein.

1.2. Coordination compounds of rare earth complex ions with organic ligands

Investigation of coordination compounds of lanthanide ions has attracted significant attention, for example the search for new highly efficient luminophores,[38] with focus on several potential applications in the lighting industry for the engineering of lamps, electroluminescent material for organic light emitting diodes (OLEDs) and optical fibers for telecommunications, as well as to make functional complexes for biological assays and medical imaging purposes.[39]

Unlike organic fluorescent and phosphorescent materials, lanthanide coordination compounds emit within a rather narrow spectral range due to the specifics of their electronic structures. Among lanthanides coordination compounds, the Eu(III) and Tb(III) complexes are most studied, which exhibit strong luminescence in visible range. Characteristic red and green intensive luminescence, respectively, due to structure of their electronic energy levels are typical for them. However, there are also lanthanide compounds that emit light in other spectral regions such as NIR (Nd(III), Yb(III) and Er(III)), visible (orange for Sm(III), yellow for Dy(III), blue for Tm(III)) and near-UV (Ce(III) and Gd(III)) range. The efficiency of excitation energy transfer to a luminescence center in lanthanide complexes depends on the ratio of energies of the triplet level of the organic ligand and the meta-stable excited electronic level of the lanthanide ion. Therefore, searching for new chelating ligands that would satisfy the efficient energy transfer requirements is topical. Some types of organic ligands are convenient for the molecular design of luminescent lanthanides complexes, among them are β−diketones, carboxylic acids, acylpyrazolones and their derivatives.[40]

1.3. Mixed heterometallic 3d-4f coordination complexes: an overview

1.3.1. Survey of 3d-4f coordination complexes

So far, plenty of mixed heterometallic 3d–4f complexes have been synthesized and investigated,[41] such as binuclear,[42] trinuclear[43] and tetranuclear[44] complexes with a variety of ligands including schiff bases, pyridonates, amino alcohols, oxalate, oximates etc.., the high dimensional magnets constructed by cyano bridges,[45] the polynuclear M_2Ln_2,[46] M_3Ln,[47] M_4Ln_2,[48] M_6Ln,[49] M_4Ln_4[50] with designed organic ligands, the heterometallic analogue of the Mn_{12} family,[51] the unusual discrete molecules with novel topologies like Mn_9Dy_8,[52] $Fe_{12}Sm_4$,[53] Co_2Dy_{10},[54] Ni_8Dy_8[55] and so on. However, the construction of polynuclear 3d-4f complexes is still a formidable challenge, because of some intricate factors, such as the choice of organic ligands, the variable and high coordination numbers with low stereochemical preference of *Ln*(III) ions, and the competitive reaction between transition and lanthanide ions with organic ligands.[56]

1.3.2. Synthetic strategies

It is well known that lanthanide ions behave as hard acids and that they prefer O-donors to N-donors, whereas d-block metal ions are borderline acids, having a strong tendency to coordinate to both O-donors and N-donors.[57] In contrast, 4f metal ions have variable and flexible coordination behavior, and have different coordination characteristics to those of transition metals. Therefore, choosing appropriate organic ligands as structure-directing agents is a successful synthetic strategy for the construction 3d-4f MOFs.

Desired architectures of heterometallic complexes might be achieved by the application of building blocks possessing bridging possibilities due to the presence of sterically accessible donor atoms, H-bonding centers and/or fragments capable of π–π stacking. These building blocks

could be formed by self-assembly of components in the one pot reaction. For the construction of the mixed heterometallic 3d-4f complexes there emerged two general synthetic approaches. The first is based on "one pot" procedures and requires a mixture of the appropriate M(II) and *Ln*(III) salts (M = 3d metals, *Ln* = lanthanines), and a ligand featuring distinct coordination compartments for preferential binding of the M(II) and the *Ln*(III) ion. The second strategy is the ''metal complexes as ligands'' approach. These ligands can be involved in rich non-covalent interactions, π-stacking and hydrogen-bonding, and therefore could extend molecular units into supramolecular networks.

1.3.3. Heterometallic 3d-4f clusters

The construction of mixed metal materials are an important research area for many groups in the fields of solid state chemistry and condensed matter physics.[58] Molecular chemists have also developed a great interest in mixed metal complexes during the last 2 decades. One reason for this is the search for compounds with interesting magnetic properties, such as single molecule magnets (SMMs),[59] single chain magnets[60] and 3D molecule based magnets.[61] Another reason is that the continuing effort for the preparation of molecular compounds that simultaneously show two different properties, e.g. ferromagnetism and ferroelectricity,[62a] or SMM behaviour and electronic conductivity.[62b]

Polynuclear 3d-4f metal complexes such as coordination clusters[63] or simply clusters[64] occupy a special place among mixed metal molecular materials because they offer alternatives[65] to homometallic 3d-metal SMMs and magnetic refrigerants. Compared with the studies dealing with heteronuclear system comprising 3d-metal ions, relatively few concern heterometallic complexes containing 3d-metal and *Ln*(III) ions (so-called d–f heteronuclear complexes), due to

a lanthanide's often high spin and/or its often significant anisotropy, as reflected in a large zero field splitting parameter D, will lead to 3d-4f metal SMMs with properties significantly different from those of homometallic 3d-metal ones. Indeed, this approach has been successfully led to Cr/*Ln*,[66] Mn/*Ln*,[67] Fe/*Ln*,[68] Co/*Ln*,[69] Ni/*Ln*[70] and Cu/*Ln*[71] SMMs, with the majority of them being Mn/*Ln* species containing some Mn(III) centres.

1.3.4. 3d-4f coordination complexes bridged by nitrate ion

The design and synthesis of heteronuclear complexes containing both 3d/4f ions have attracted special attention in view of their magnetic and electronic properties.[72] Indeed, the synthesis of discrete heteronuclear complexes affords simple models to understand the respective influences of two different metal centres in modulating the electronic, magnetic and electrochemical properties of such compounds. A CCDC search reveals that a plethora of transition metals[73] and heterometallic transition metal–lanthanide complexes with polydentate ligands coordinating the metal ions. On the other hand, structural studies showing these metals bridged by nitrate are scarce, although nitrate ion represents a common bridging ligand acting through different coordination modes (Scheme 1.1).[74-84]

In the past few years, several heteronuclear complexes of salen derivatives containing Cu_4Ln_2, Cu_2Ln, Cu_4Ln_4 and recently Cu_2/Gd_2 systems have been studied.[85] All the cited examples contain a bridging nitrate between Cu(II) and the *Ln*(III) ions. Jianmin et al.[86] described a unique compound $[La(NO_3)_6\{Cu(bpy)_2)\}_2][La(NO_3)_6Cu(bpy)_2]\cdot CH_3CN$, where $[La(NO_3)_6]^{3-}$ connecting either a single or two $[Cu(bpy)_2]^{2+}$ units in the same compound.

The ligands which coordinate through oxygen atoms to a rare-earth metal ion may form stable lanthanide complexes.

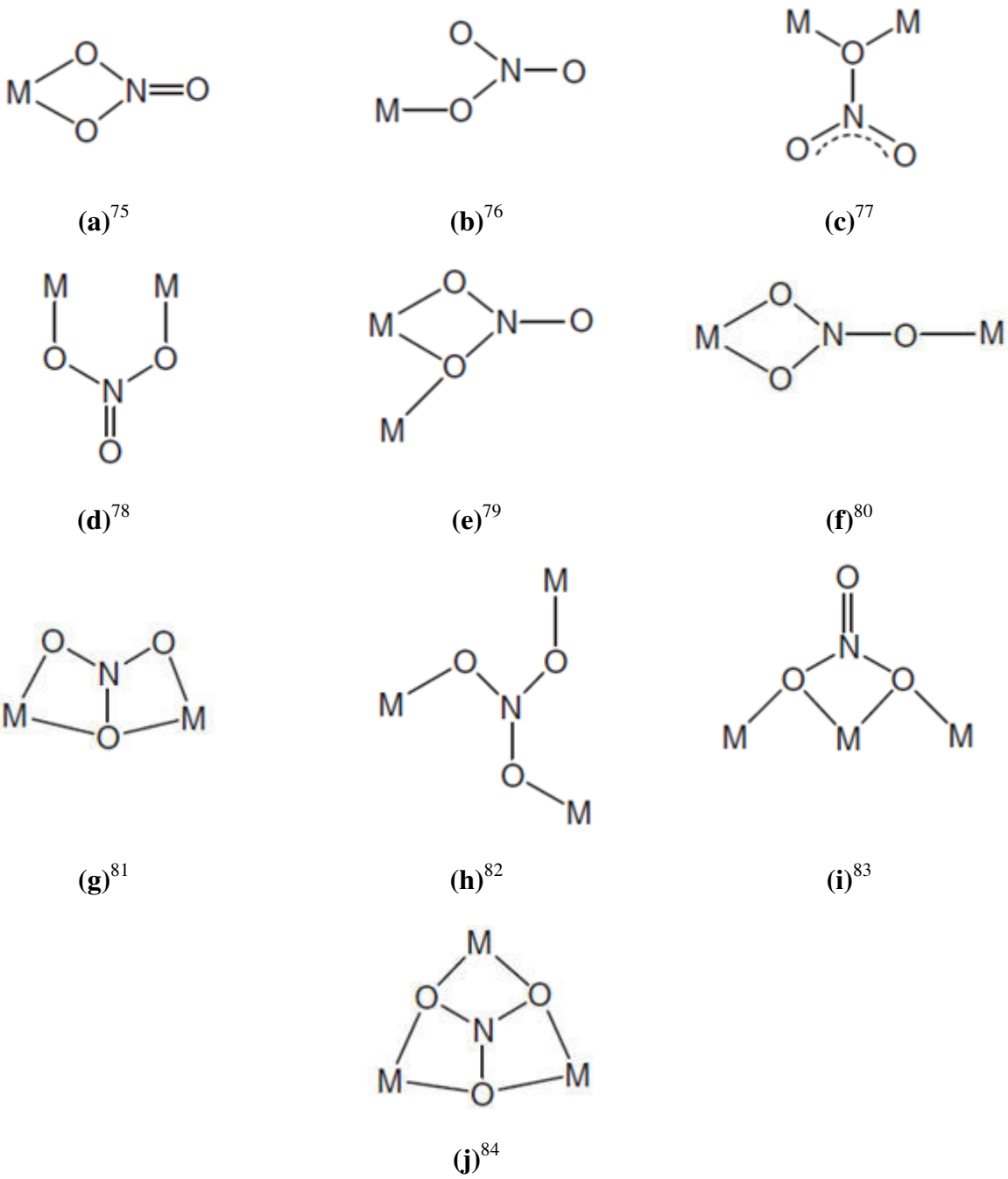

Scheme 1.1. Different possible coordination modes of nitrate ion.

The nitrate ion (relatively small, bidentately coordinates with a short bite) is regarded as a suitable ligand of lanthanide for lanthanide complexes stable to water or air. Lanthanide (III) nitrates have been used to form polynitrato organic[87] and inorganic salts.[88] These salts contain

either a pentanitrato or a hexaanitrato ion. In the solid state, hexanitratolanthanates are isolated only with the early and middle lanthanide ions *Ln* = La–Dy, whereas pentanitratolanthanates are isolated for the entire rare-earth series, provided by the suitable counter ions. Previously studied lanthanide nitrato complex anions are given in Table 1.4.

A considerable amount of structural work has been done on pentanitratolanthanates, and crystallographic data are available. In all of these species, the lanthanide ion is surrounded by five chelating bidentate nitrates. For La-Eu, one or two water molecules are also coordinated to the metal ion, which is therefore eleven- or twelve-coordinate. The site symmetry of the lanthanide ion is low, C_2 or even C_1, which may be the reason why detailed spectroscopic study has not been published so far. However, the crystal structure reveals that this low symmetry sometimes arises from distortions of a more symmetrical arrangement. A significant series of hexanitratolanthanates ($[Cat+]_3[Ln(NO_3)_6]$; Cat+ = cation)[89] have been synthesized and structurally characterized.

Table 1.4. Previously studied lanthanide nitrato complex anions.

Coord. No.	complex ion	*Ln*	Reference
12	$[Ln(NO_3)_6]^{3-}$	La − Dy	89
12	$[Ln(NO_3)_5(H_2O)_2]^{2-}$	La – Pr	90
11	$[Ln(NO_3)_5(H_2O)]^{2-}$	La − Eu	91
11	$[Ln(NO_3)_4(H_2O)_3]^{-}$	Ce and Nd	92
10	$[Ln(NO_3)_5]^{2-}$	La − Lu	93
10	$[Ln(NO_3)_4(H_2O)_2]^{-}$	Sm, Eu, Gd and Er	94, 97d
10	$[Ln(NO_3)_3(H_2O)_4]$	La, Pr, Nd, Sm, Eu, Tb, Er and Yb	95
10	$[Ln(NO_3)_2(H_2O)_6]^{+}$	La – Nd	96
9	$[Ln(NO_3)_3(H_2O)_3]$	La – Lu (except Ce)	97,89b
9	$[Ln(NO_3)_2(H_2O)_5]$	Dy	98
8	$[Ln(NO_3)(H_2O)_7]$	Sm, Eu and Gd	96b

1.3.5. Co-crystallization of inorganic *Ln*(III) coordination complex

Co-crystals or multi-component crystals constitute an interesting class of compounds in crystal engineering in which two or more chemical species, which can form stable solids by themselves under ambient conditions, co-exist in the same crystal lattice.[99] Co-crystallization of two or more different chemical species is a possible way to study the hierarchy of intermolecular interactions within a crystalline solid with newly generated macroscopic properties. So far, many organic systems have been reported to comprise co-crystal structures, especially those with acid–base pairs.[99] The reports on co-crystallization in lanthanide complexes still remain rare. The design and synthesis of lanthanide compounds that can exhibit inherent co-crystallization behavior remains a challenging task. Recently, only a few examples of the crystallization of organic ligand-coordinated or inorganic anion-bonded lanthanide units with uncoordinated ligands have been reported.[100]

1.4. Objectives of the work

The main objective of this thesis is to synthesise Cu(II)/*Ln*(III) heteropolynuclear complexes with 2,2'-bipyridine (bpy) as a co-ligand and to observe the influence of lanthanide complex anions on the composition of the Cu(II) complex cations. The lanthanide nitrato complex anions, $[Ln(NO_3)_x(OH_2)_{6-x}]^{(x-3)-}$ (x = 5 or 6), which have relatively smaller volume in anionic lanthanide complexes and show favorable crystallinity with a number of Cu(II) complex cations. In addition, co-crystallisation of lanthanide coordination complexes with Cu(II) complex salt was also investigated.

As a part of a research on Cu(II) complexes bridged by water molecules as well as halogenated acetates with a view to the investigation of magnetic exchange interactions between

adjacent magnetic nuclei, complexes with the core $[Cu(OH_2)_2Cu]^{4+}$ and $[Cu(RCOO)_2Cu]^{2+}$ containing bpy have been synthesized.

1.5. References

1. N. G. Connelly, *Nomenclature of inorganic chemistry*: IUPAC recommendations 2005 The red book. Royal Society of Chemistry, Cambridge, **2005**, P. 51.
2. S. P. Fricker, *Chem. Soc. Rev.*, **2006**, *35*, 524.
3. J. D. Lee, *Concise of Inorgnic Chemistry.* 4th edn., ELBS, London, **1995**.
4. P. D'Angelo, A. Zitolo, V. Migliorati, G. Chillemi, M. Duvail, P. Vitorge, S. Abadie, R. Spezia, *Inorg. Chem.*, **2011**, *50*, 4572.
5. Y. Marcus, *Chem. Rev.*, **1988**, *88*, 1475.
6. R. Heyrovska, *Chem. Phys. Lett.*, **2006**, *429*, 600.
7. R. D. Shannon, *Acta Crystallogr., Sect. A*, **1976**, *32*, 751.
8. T. Moeller, *MTP International Review of Science, inorganic Chemistry,* Butterworths, London, **1972**, Series 1, *Vol. VII,* 275.
9. R. G. Pearson, *J. Am. Chem. Soc.*, **1963**. *85,* 3533.
10. S. Cotton, *Lanthanide and Actinide Chemistry*, John Wiley & Sons. West Sussex, **2006**, P. 35.
11. J. H. Forsberg, *Coord. Chem. Rev.*, **1973**, *10*, 195.
12. S. A. Cotton, "Scandium, Yttrium & the Lanthanides: Inorganic & Coordination Chemistry", *Encyclopaedia of Inorganic Chemistry,* John Wiley & Sons. Inc., New York, **1994**.
13. R. K. Agarwal, H. Agarwal, N. Goel, S. K. Sindu, *Bull. Chem. Soc. Ethiop.*, **2001**, *15*, 79.

14. (a) F. A. Hart, *Comprehensive Coordination Chemistry*, vol. 3, Pergamon, Oxford, **1987**; (b) N. Sabbatini, M. Guardigli, J. M. Lehn, *Coord. Chem. Rev.*, **1993**, *123*, 201.

15. J. C. Bunzli, C. Piguet, *Chem. Soc. Rev.*, **2005**, *34*, 1048.

16. (a) E. G. Moore, A. P. Samuel, K. N. Raymond, *Acc. Chem. Res.*, **2009**, *42*, 542; (b) W. T. Carnall, P. R. Fields, K. Rajnak, *J. Chem. Phys.*, **1968**, *49*, 4424; (c) W. T. Carnall, P. R. Fields, K. Rajnak, *J. Chem. Phys.*, **1968**, *49*, 4443; (d) W. T. Carnall, P. R. Fields, K. Rajnak, *J. Chem. Phys.*, **1968**, *49*, 4447; (e) W. T. Carnall, P. R. Fields, K. Rajnak, *J. Chem. Phys.*, **1968**, *49*, 4450.

17. K. N. Allen, B. Imperiali, *Curr. Opin. Chem. Biol.*, **2010**, *14*, 247.

18. M. H. Werts, *Sci. Prog.*, **2005**, *88*, 101.

19. Y. Y. Xu, K. Pettersson, K. Blomberg, I. Hemmila, H. Mikola, T. Lovgren, *Clin. Chem.*, **1992**, *38*, 2038.

20. E. R. Trivedi, S. V. Eliseeva, J. Jankolovits, M. M. Olmstead, S. Petoud, V. L. Pecoraro, *J. Am. Chem. Soc.*, **2014**, *136*, 1526.

21. H. U. Gudel, M. Pollnau, *J. Alloys Compd.,* **2000**, *303-304*, 307.

22. S. T. Frey, W. D. J. Horrocks, *Small*, **1995***, 229*, 383.

23. J. C. Bunzli, *Chem. Rev.*, **2010**, *110*, 2729.

24. D. F. Evans, *J. Chem. Soc.* **1959**, 2003.

25. F. A. Cotton, G. Wilkinson, C. A. Murillo, M. Bochmann, *Advanced Inorganic Chemistry*, 6th Ed., John Wiley & Sons, Inc., New York, **1999**, P. 1109.

26. (a) F. Conti, M. Delfini, F. Scopinaro, U. Croatto, *Inorg. Chim. Acta.*, **1987**, *140,* 355; (b) C. Huang, Z. Bian, *Rare Earth Coordination Chemistry: Fundamentals and Applications*, John Wiley & Sons, Singapore, **2011**.

27. J. Massue, S. J. Quinn, T. Gunnlaugsson, *J. Am. Chem. Soc.*, **2008**, *130*, 6900.

28. (a) V. I. Parvulescu, C. Hardacre, *Chem. Rev.*, **2007**, *107*, 2615; (b) G. A. Molander, *Chem. Rev.*, **1992**, *92*, 29.

29. (a) D. A. Atwood, *The Rare Earth Elements: Fundamentals and Applications*, John Wiley & Sons, UK, **2012**; (b) J. Y. Park, M. J. Baek, E. S. Choi, S. Woo, J. H. Kim, T. J. Kim, J. C. Jung, K. S. Chae, Y. Chang, G. H. Lee, *ACS Nano*, **2009**, *3*, 3663; (c) H. Ur. Rashid, K. Yu, J. Zhou, *J. Struc. Chem.*, **2013**, *54*, 223.

30. (a) A. F. Cockrill, G. L. O. Davies, R. C. Harden, D. M. Rackham, *Chem. Rev.*, **1973**, *73*, 553; (b) S. Aime, M. Botta, M. Fasano, E. Terreno, *Chem. Soc. Rev.*, **1998**, *27*, 19; (c) K. Ifhkar, M. Sayed, N. Ahemad, *Bull. Chern. Snc. (Jpn.)*, **1982**, *55*, 2258.

31. (a) T. Verbiest, S. Houbrechts, M. Kauranen, K. Clays, A. Persoons, *J. Mater. Chem.*, **1997**, *7*, 2175; (b) K. Binnemans, *Handbook on the physics and chemistry of rare earths*, Elsevier, **2005**.

32. H. Xie, Q. Chang, *New Frontiers in Ram Earth Science and Applications.* Science Press, 1985, *Vol.2.;* (b) Y. Shu, A. Travert, R. Schiller, M. Ziebarth, R. Wormsbecher, W. –C. Cheng, *Top. Catal.*, **2015**, *58*, 334.

33. G. R. Whittell, M. D. Hager, U. S. Schubert, I. Manners, *Nat. Mater.*, **2011**, *10*, 176.

34. (a) Z. M. Hou, Y. Wakatsuki, *Coord. Chem. Rev.*, **2002**, *231*, 1; (b) M. J. Vitorino, T. Devic, M. Tromp, G. Ferey, M. Visseaux, *Macromol. Chem. Phys.*, **2009**, *210*, 1923.

35. I. Kostova, M. Traykova, V. K. Rastogi, *Medicinal Chemistry*, **2008**, *4*, 371.

36. W. M. Al Momani, Z. A. Taha, A. M. Ajlouni, Q. M. Abu Shaqra, M. Al Zouby, *Asian Pac. J. Trop. Biomed.*, **2013**, *3*, 367.

37. (a) C. W. Schwietert, J. P. McCue, *Coord. Chem. Rev.*, **1999**, *184,* 67; (b) R. K. W. Li, Y. Cheng, B. Zhu, *Coord. Chem. Rev.*, **1999***, 190-192,* 297; (c) V. Wing, W. Yarnand, K. Kam, L. Wing, *Coord. Chem. Rev.*, **1999**, *184,* 157.

38. (a) N. P. Kuzmina, S. V. Eliseeva, *Russ. J. Inorg. Chem.*, **2006**, *51*, 73; (b) V. F. Shulgin, S. V. Abkhairova, O. V. Konnik, S. B. Meshkova, Z. M. Topilova, E. B. Rusanov, G. G. Aleksandrov, I. L. Eremenko, *Russ. J. Inorg. Chem.,* **2013**, *58,* 678.

39. (a) V. F. Shulgin a, O. V. Konnik, S. V. Abkhairova, A. N. Gusev, S. B. Meshkova, A. V. Kiriyak, E. B. Rusanov, M. Hasegawa, W. Linert, *Inorg. Chim. Acta*, **2013**, *402*, 33; (b) J. P. Leonard, C. B. Nolan, F. Stomeo, Th Gunnlaugsson, *Top. Curr. Chem.*, **2007**, *281*, 1; (c) S.V. Eliseeva, J. -C. G. Bunzli, *Chem. Soc. Rev.*, **2010**, *39*, 189.

40. N. P. Kuzmina, S. V. Eliseeva, *Russ. J. Inorg. Chem.*, **2006**, *51*, 73.

41. Y. -G. Huang, F. -L. Jiang, M. -C. Hong, *Coord. Chem. Rev.*, **2009**, *253*, 2814.

42. (a) J. -P. Costes, B. Donnadieu, R. Gheorghe, G. Novitchi, J. -P. Tuchagues, L. Vendier, *Eur. J. Inorg. Chem.*, **2008**, *17*, 5235; (b) T. Kajiwara, M. Nakano, K. Takahashi, S. Takaishi, M. Yamashita, *Chem. Eur. J.*, **2011**, *17*, 196.

43. (a) T. Yamaguchi, J. -P. Costes, Y. Kisima, M. Kojima, Y. Sunatsuki, N. Brefuel, J. -P. Tuchagues, L. Vendier, W. Wernsdorfer, *Inorg. Chem.*, **2010**, *49*, 9125; (b) V. Chandrasekhar, B. M. Pandian, J. J. Vittal, R. Clerac, *Inorg. Chem.*, **2009**, *48*, 1148.

44. (a) J. -P. Costes, S. Shova, W. Wernsdorfer, *Dalton Trans.*, **2008**, *37*, 1843; (b) T. Hamamatsu, K. Yabe, M. Towatari, S. Osa, N. Matsumoto, N. Re, A. Pochaba,J. Mrozinski, J. -L. Gallani, A. Barla, P. Imperia, C. Paulsen, J. -P. Kappler, *Inorg.Chem.*, **2007**, *46*, 4458.

45. (a) D. -Y. Yu, L. Li, H. Zhou, A. -H. Yuan, Y. -Z. Li, *Eur. J. Inorg. Chem.*, **2012**, *21*, 3394; (b) S. A. Stoian, C. Paraschiv, N. Kiritsakas, F. Lloret, E. Munck, E. L. Bominaar, M. Andruh, *Inorg. Chem.*, **2010**, *49*, 3387.

46. (a) Z. -S. Meng, F. -S. Guo, J. -L. Liu, J. -D. Leng, M. -L. Tong, *Dalton Trans.*, **2012**, *41*, 2320; (b) A. S. R. Chesman, D. R. Turner, K. J. Berry, N. F. Chilton, B. Moubaraki, K. S. Murray, G. B. Deacon, S. R. Batten, *Dalton Trans.*, **2012**, *41*, 11402.

47. H. L. C. Feltham, R. Clerac, L. Ungur, L. F. Chibotaru, A. K. Powell, S. Brooker, *Inorg.Chem.*, **2013**, *52*, 3236.

48. (a) H. Ke, L. Zhao, Y. Guo, J. Tang, *Dalton Trans.*, **2012**, *41*, 2314; (b) A. Saha, M. Thompson, K. A. Abboud, W. Wernsdorfer, G. Christou, *Inorg. Chem.*, **2011**, *50*, 10476.

49. (a) G. J. Sopasis, M. Orfanoudaki, P. Zarmpas, A. Philippidis, M. Siczek, T. Lis, J. R. O'Brien, C. J. Milios, *Inorg. Chem.*, **2012**, *51*, 1170; (b) T. Peristeraki, M. Samios, M. Siczek, T. Lis, C. J. Milios, *Inorg. Chem.*, **2011**, *50*, 5175.

50. (a) M. Li, A. M. Ako, Y. Lan, W. Wernsdorfer, G. Buth, C. E. Anson, A. K. Powell, Z. Wang, S. Gao, *Dalton Trans.*, **2010**, *39*, 3375; (b) M. Li, Y. Lan, A. M. Ako, W. Wernsdorfer, C. E. Anson, G. Buth, A. K. Powell, Z. Wang, S. Gao, *Inorg. Chem.*, **2010**, *49*, 11587.

51. V. Mereacre, Y. Lan, R. Clerac, A. M. Ako, W. Wernsdorfer, G. Buth, C. E. Anson, A. K. Powell, *Inorg. Chem.*, **2011**, *50*, 12001.

52. S. K. Langley, B. Moubaraki, K. S. Murray, *Dalton Trans.*, **2010**, *39*, 5066.

53. Y. -F. Zeng, G. -C. Xu, X. Hu, Z. Chen, X. -H. Bu, S. Gao, E. C. Sanudo, *Inorg. Chem.*, **2010**, *49*, 9734.

54. L. -F. Zou, L. Zhao, Y. -N. Guo, G. -M. Yu, Y. Guo, J. -K. Tang, Y. -H. Li, *Chem. Comm.*, **2011**, *47*, 8659.

55. C. Papatriantafyllopoulou, T. C. Stamatatos, C. G. Efthymiou, L. Cunha-Silva, F. A. Almeida Paz, S. P. Perlepes, G. Christou, *Inorg. Chem.*, **2010**, *49*, 9743.

56. (a) L. Huang, H. Mei, L. Chen, Y. Xu, *Z. Anorg. Allg. Chem.*, **2012**, *638*, 996; (b) L. -Q. Fan, Y. Chen, J. -H. Wu, Y. -F. Huang, *J. Solid State Chem.*, **2011**, *184*, 899; (c) J. -W. Cheng, S. -T. Zheng, G. -Y. Yang, *Inorg. Chem.*, **2008**, *47*, 4930; (d) X. Gu, D. Xue, *Inorg. Chem.*, **2007**, *46*, 5349.

57. Q. Yue, J. Yang, G. -H. Li, G. -D. Li, W. Xu, J. -S. Chen, S. -N. Wang, *Inorg. Chem.*, **2005**, *44*, 5241.

58. (a) P. Baettig, R. Seshadri, N. A. Spaldin, *J. Am. Chem. Soc.*, **2007**, *129*, 9854; (b) S. -W. Cheong, M. Mostovoy, *Nat. Mater.*, **2007**, *6*, 13; (c) D. I. Khomskii, *J. Magn. Magn. Mater.*, **2006**, *306*, 1; (d) M. G. Kanatzidis, R. Pottgen, W. Jeitsckho, *Angew. Chem., Int. Ed.*, **2005**, *44*, 2; (e) N. A. Hill, R. Seshadri, *Chem. Mater.*, **2001**, *13*, 2892.

59. E. J. Schelter, F. Karadas, C. Avendano, A. V. Prosvirin, W. Wernsdorfer, K. R. Dunbar, *J. Am. Chem. Soc.*, **2007**, *129*, 8139.

60. H. Miyasaka, M. Julve, M. Yamashita, R. Clérac, *Inorg. Chem.*, **2009**, *48*, 3420.

61. O. Kahn, *Acc. Chem. Res.*, **2000**, *33*, 647.

62. (a) Th. C. Stamatatos, K. Oliver, K. A. Abboud, G. Christou, *Inorg. Chem.*, **2011**, *50*, 5272; (b) H. Hiraga, H. Miyasaka, T. Kajiwara, S. Takaishi, Y. Oshima, H. Nojiri, M. Yamashita, *Inorg. Chem.*, **2007**, *46*, 9661.

63. G. E. Kostakis, A. M. Ako, A. K. Powell, *Chem. Soc. Rev.*, **2010**, *39*, 2238.

64. M. H. Chisholm, *Polyhedron*, **1998**, *17*, 2773.

65. (a) R. Sessoli, A. K. Powell, *Coord. Chem. Rev.*, **2009**, *253*, 2328; (b) M. Andruh, J. -P. Costes, C. Diaz, S. Gao, *Inorg. Chem.*, **2009**, *48*, 3342; (c) Th. N. Hooper, J. Schnack, S. Piligkos, M. Evangelisti, E. K. Brechin, *Angew. Chem., Int. Ed.*, **2012**, *51*, 4633.

66. J. Rinck, G. Novitchi, W. Van den Heuvel, L. Ungur, Y. Lan, W. Wernsdorfer, C. E. Anson, L. F. Chibotaru, A. K. Powell, *Angew. Chem., Int. Ed.*, **2010**, *49*, 7583.

67. (a) A. Saha, M. Thompson, K. A. Abboud, W. Wernsdorfer, G. Christou, *Inorg. Chem.*, **2011**, *50*, 10476; (b) G. Rigaux, R. Inglis, S. Morrison, A. Prescimone, C. Cadiou, M. Evangelisti, E. K. Brechin, *Dalton Trans.*, **2011**, *40*, 4797; (c) C. Papatriantafyllopoulou, W. Wernsdorfer, K. A. Abboud, G. Christou, *Inorg. Chem.*, **2011**, *50*, 421; (d) V. Mereacre, M. N. Akhtar, Y. Lan, A. M. Ako, R. Clérac, C. E. Anson, A. K. Powell, *Dalton Trans.*, **2010**, *39*, 4918; (e) G. Karotsis, S. Kennedy, S. J. Teat, C. M. Beavers, D. A. Fowler, J. J. Morales, M. Evangelisti, S. J. Dalgarno, E. K. Brechin, *J. Am. Chem. Soc.*, **2010**, *132*, 12983; (f) A. M. Ako, V. Mereacre, R. Clérac, W. Wernsdorfer, I. J. Hewitt, C. E. Anson, A. K. Powell, *Chem. Commun.*, **2009**, 544; (g) Th. C. Stamatatos, S. J. Teat, W. Wernsdorfer, G. Christou, *Angew. Chem., Int. Ed.*, **2009**, *48*, 521; (h) A. Mishra, W. Wernsdorfer, S. Parsons, G. Christou, E. K. Brechin, *Chem. Commun.*, **2005**, 2086; (i) C. M. Zaleski, E. C. Depperman, J. W. Kampf, M. L. Kirk, V. L. Pecoraro, *Angew. Chem., Int. Ed.*, **2004**, *43*, 3912; (j) A. Mishra, W. Wernsdorfer, K. A. Abboud, G. Christou, *J. Am. Chem. Soc.*, **2004**, *126*, 15648.

68. (a) D. Schray, G. Abbas, Y. Lan, V. Mereacre, A. Sundt, J. Dreiser, O. Waldmann, G. E. Kostakis, C. E. Anson, A. K. Powell, *Angew. Chem., Int. Ed.*, **2010**, *49*, 5185; (b) Y. -F. Zeng, G. -C. Xu, X. Hu, Z. Chen, X. -H. Bu, S. Gao, E. C. Sanudo, *Inorg. Chem.*, **2010**, *49*, 9374; (c) G. Abbas, Y. Lan, V. Mereacre, W. Wernsdorfer, R. Clérac, G. Buth, M. T.

Sougrati, F. Grandjean, G. J. Long, C. E. Anson, A. K. Powell, *Inorg. Chem.*, **2009**, *48*, 9345.

69. (a) M. Orfanoudaki, I. Tamiolakis, M. Siczek, T. Lis, G. S. Armatas, S. A. Pergantis, C. J. Milios, *Dalton Trans.*, **2011**, *40*, 4793; (b) X. -Q. Zhao, Y. Lan, B. Zhao, P. Cheng, C. E. Anson, A. K. Powell, *Dalton Trans.*, **2010**, *39*, 4911.

70. (a) C. D. Polyzou, H. Nikolaou, C. Papatriantafyllopoulou, V. Psycharis, A. Terzis, C. P. Raptopoulou, A. Escuer, S. P. Perlepes, *Dalton Trans.,* **2012**, *41*, 13755; (b) E. Colacio, J. Ruiz-Sanchez, F. J. White, E. K. Brechin, *Inorg. Chem.*, **2011**, *50*, 7268; (c) T. D. Pasatoiu, M. Etienne, A. M. Madalan, M. Andruh, R. Sessoli, *Dalton Trans.*, **2010**, *39*, 4802.

71. (a) G. J. Sopasis, A. B. Canaj, A. Philippidis, M. Siczek, T. Lis, J. R. O'Brien, M. M. Antonakis, S. A. Pergantis, C. J. Milios, *Inorg. Chem.*, **2012**, *51*, 5911; (b) T. Shiga, H. Miyasaka, M. Yamashita, M. Morimoto, M. Irie, *Dalton Trans.*, **2011**, *40*, 2275; (c) H. L. C. Feltham, R. Clérac, A. K. Powell, S. Brooker, *Inorg. Chem.*, **2011**, *50*, 4232; (d) V. Baskar, K. Gopal, M. Helliwell, F. Tuna, W. Wernsdorfer, R. E. P. Winpenny, *Dalton Trans.,* **2010**, *39*, 4747.

72. (*a*) M. Sakamoto, K. Manseki, H. Okawa, *Coord. Chem. Rev.*, **2001**, *219–221*, 379; (*b*) C. Piguet, J. C. G. Bunzli, *Chem. Soc. Rev.*, **1999**, *28*, 347; (*c*) R. E. P. Winpenny, *Chem. Soc. Rev.*, **1998**, *27*, 447.

73. (a) Z. -L. You, L. -L. Ni, P. Hou, J. -C. Zhang, C. Wang, *J. Coord. Chem.*, **2010**, *63*, 515; (b) P. -P. Hao, S. -H. Li, X. -Z. Li, L. -N. Zhu, *J. Coord. Chem.*, **2010**, *63*, 464; (c) C. Demetg, M. Karakaplan, S. Serin, M. Digrak, *J. Coord. Chem.*, **2009**, *62*, 3544.

74. (a) L. W. Yang, S. Liu, S. J. Rettig, C. Orvig, *Inorg. Chem.*, **1995**, *34*, 4921; (b) P. N. V. Pavan Kumar, D. S. Marynick, *Inorg. Chem.*, **1995**, *32*, 1857; (c) R. Han, G. Parkin, *J. Am. Chem. Soc.*, **1991**, *113*, 9707; (d) F. Jhang, A. Odani, H. Masuda, O. Yamauchi, *Inorg. Chem.*, **1996**, *35*, 7148.

75. (a) J. Sniekers, N. R. Brooks, S. Schaltin, L. V. Meervelt, J. Fransaerb, K. Binnemans, *Dalton Trans.*, **2014**, *43*, 1589; (b) Q. –Y. Yang, K. Wu, J. –J. Jiang, C. –W. Hsu, M. Pan, J. –M. Lehnab, C. –Y. Su, *Chem. Commun.,* **2014**, *50*, 7702.

76. (a) M. A. Rhine, A. V. Rodrigues, R. J. Bieber Urbauer, J. L. Urbauer, T. L. Stemmler, T. C. Harrop, *J. Am. Chem. Soc.*, **2014**, *136*, 12560; (b) D. Vasilchenko, S. Tkachev, I. Baidina, S. Korenev, *Inorg. Chem.*, **2013**, *52*, 10532.

77. (a) R. Pedrero-Marin, A.V. Sanchez-Huertas, F. Luna-Giles, F. De la Cruz-Martinez, E. Vinuelas-Zahinos, *Polyhedron*, **2014**, *80*, 265; (b) G. Xiong, X. –Y. Qin, P. –F. Shi, Y. –L. Hou, J. –Z. Cuib, B. Zhao, *Chem. Commun.,* **2014**, *50*, 4255.

78. (a) S. Anbu, R. Ravishankaran, M. Fatima C. G. da Silva, A. A. Karande, A. J. L. Pombeiro, *Inorg. Chem.*, **2014**, *53*, 6655; (b) J. A. Sheikh, H. S. Jena, A. Adhikary, S. Khatua, S. Konar, *Inorg. Chem.*, **2013**, *52*, 9717.

79. (a) Z. Shi, X. Tang, X. Zhou, J. Cheng, Q. Han, J. Zhou, B. Wang, Y. Yang, W. Liu, D. Bai, *Inorg. Chem.*, **2013**, *52*, 12668; (b) E. Wong, J. Li, C. Seward, S. Wang, *Dalton Trans.*, **2009**, 1776.

80. (a) E. Brana, C. Mendoza, P. Vitoria, J. Gonzalez-Platas, S. Dominguez, C. Kremer, *Inorg. Chim. Acta*, **2014**, *417*, 192; (b) Y. Liu, D. –Z. Kuang, Y. –L. Feng, W. –W. Fu, *Trans. Met. Chem.*, **2013**, *38*, 849.

81. (a) P. I. Richards, A. Steiner, *Inorg. Chem.*, **2004**, *43*, 2810; (b) G. A. Bowmaker, Effendy, K. C. Lim, B. W. Skelton, D. Sukarianingsih, A. H. White, *Inorg. Chim. Acta*, **2005**, *358*, 4342.

82. (a) A. K. Chaudhari, B. Joarder, E. Riviere, G. Rogez, S. K. Ghosh, *Inorg. Chem.*, **2012**, 51, 9159; (b) A. Escuer, G. Vlahopoulou, S. P. Perlepes, F. A. Mautner, *Inorg. Chem.*, **2011**, *50*, 2468.

83. (a) A. Pramanik, G. Das, *Cryst. Eng. Comm.*, **2010**, *12*, 401; (b) V. K. Yadav, N. Kumari, L. Mishra, *Indian J. Chem., Sec. A*, **2011**, *50*, 1035.

84. J. –L. Liu, Y. –C. Chen, Q. –W. Li, S. Gomez-Coca, D. Aravena, E. Ruiz, W. –Q. Lin, J. –D. Lenga, M. –L. Tong, *Chem. Commun.,* **2013**, *49*, 6549.

85. (a) K. S. Banu, T. Ghosh, A. Guha, T. Chattopadhyay, D. Das, E. Zangrando, *J. Coord. Chem.*, **2010**, *63*, 3714; (b) G. Novitchi, J. -P. Costes, J. -P. Tuchagues, L. Vendier, W. Wernsdorfer, *New J. Chem.*, **2008**, *32*, 197; (c) A. M. Madalan, N. Avarvari, M. Fourmigue, R. Clerac, L. F. Chibotaru, S. Clima, M. Andruh, *Inorg. Chem.*, **2008**, *47*, 940; (d) K. G. Alley, A. Mukherjee, R. Cle´rac, C. Boskovic, *Dalton Trans.*, **2008**, 59; (e) T. Gao, W. B. Sun, P. F. Yan, G. M. Li, G. F. Hou, *Acta Crystallogr., Sect. E: Struct. Rep. Online*, **2007**, *63*, m2201; (f) J. -P. Costes, F. Dahan, A. Dupuis, *Inorg. Chem.*, **2000**, *39*, 5994; (g) M. Andruh, I. Ramade, E. Codjovi, O. Guillou, O. Kahn, J. C. Trombe, *J. Am. Chem. Soc.*, **1993**, *115*, 1822;; (h) W. Harrison, J. -C. G. Bunzli, *Inorg. Chim. Acta*, **1985**, *109*, 185.

86. L. Jianmin, Z. Huaqianga, Z. Yugen, C. Jinhua, K. Yanxiong, W. Quanming, W. Xintao, *Cryst. Res. Technol.*, **1999**, *34*, 925.

87. (a) L. He, S. –P. Ji, N. Tang, Y. Zhao, G. –H. Tao, *Dalton Trans.*, **2015**, *44*, 2325; (b) S. Lipstman, I. Goldberg, *Cryst. Growth Des.*, **2010**, *10*, 1823; (c) G. -H. Tao, Y. Huang, J. A. Boatz, J. M. Shreeve, *Chem. Eur. J.*, **2008**, *14*, 11167; (d) A. S. R. Chesman, D. R. Turner, G. B. Deacon, S. R. Batten, *J. Coord. Chem.*, **2007**, *60*, 2191; (e) T. Otsuka, H. Cui, A. Kobayashi, Y. Misaki, H. Kobayashiz, *J. Solid State Chem.*, **2002**, *168*, 444; (f) L. Zhang, Y. Zhou, L. Xu, Z. Yu, I. A. Razak, S. Chantrapromma, H. K. Fun, X. You, *Inorg. Chem. Commu*, **2001**, *4*, 368; (g) G. Y. S. Chan, M. G. B. Drew, M. J. Hudson, N. S. Issacs, P. Byers, *Polyhedron*, **1996**, *15*, 3385.

88. (a) S. Nayak, G. Novitchi, M. Hołynska, S. Dehnen, *Eur. J. Inorg. Chem.,* **2014**, 3065; (b) C. -B. Ma, M. –Q. Hu, H. Chen, C. –N. Chen, Q. –T. Liu, *Eur. J. Inorg. Chem.,* **2011**, 5043; (c) M. W. Chorab, A. Gorczyski, D. Marcinkowski, M. Kubicki, V. Patroniak, *J. Rare Earths*, **2010**, 61; (d) F. Benetollo, P. Di Bernardo, S. Tamburini , P. A. Vigato, P. Zanonato, *Inorg. Chem. Commun.*, **2008**, *11*, 246.

89. (a) T. Kawasaki, S. Okumura, Y. Sasaki, Y. Ikeda, *Bull. Chem. Soc. Jpn*, **2014**, *87*, 294; (b) M. del C. F. Fernandez, R. Bastida, A. Macias, P. Perez-Lourido, C. Platas-Iglesias, L. Valencia, *Inorg. Chem.*, **2006**, *45*, 4484; (c) A. N. Chekholv, *Zh. Neog. Khim. (Russ. J. Inorg. Chem.)*, **2007**, *52*, 1851.

90. (a) A. Fowkes, W. T. A. Harrison, *Acta Cryst.*, **2006**, *E62*, m1301; (b) A. Rohde, W. Urland, *Acta Cryst.*, **2006**, *E62*, m3026.

91. (a) D. J. Evans, P. C. Junk, M. K. Smith, *New J. Chem.*, **2002**, *26*, 1043; (b) C. –B. Ma, M. –Q. Hu, H. Chen, C. –N. Chen, Q. -T. Liu, *Eur. J. Inorg. Chem.,* **2011**, 5043; (c) H. Zhang, Y. Wu, L. Fang, *Acta Cryst.*, **2006**, *E62*, m854; (d) J. H. Burns, *Inorg. Chem.*,

1979, *18*, 3044; (e) J. M Martinez-Sanchez, R. Bastida, A. Macias, P. Perez-Lourido, L. Valencia, *Inorg. Chim. Acta*, **2011**, *378*, 127.

92. (a) A. Lennartson, C. J. McKenzie, *Acta Cryst.*, **2012**, *C68*, m347; (b) C. Nunez, R. Bastida, A. Macias, A. Aldrey, L. Valencia, *Polyhedron*, **2010**, *29*, 126.

93. (a) W. Urland, E. Warkentin, *Z. Naturforsch*. **1983**, *88b*, 299; (b) H. Cui, T. Otsuka, A. Kobayashi, N. Takeda, M. Ishikawa, Y. Misaki, H. Kobayashi, *Inorg. Chem.*, **2003**, *42*, 6114; (c) E. B. Dhoot, J. Fawcett, R. A. Kresinski, A. W. G. Platt, *Polyhedron*, **2009**, *28*, 1497; (d)A. N. Georgopoulou, R. Adam, C. P. Raptopoulou, V. Psycharis, R. Ballesteros, B. Abarca, A. K. Boudalis, *Dalton Trans*., **2011**, *40*, 8199; (e) T. Otsuka, H. Cui, A. Kobayashi, Y. Misaki, H. Kobayashiz, *J. Solid State Chem.*, **2002**, *168*, 444; (f) G. J. Sopasis, M. Orfanoudaki, P. Zarmpas, A. Philippidis, M. Siczek, T. Lis, J. R. O'Brien, C. J. Milios, *Inorg. Chem.*, **2012**, *51*, 1170.

94. (a) Z. Xu, L. K. Thompson, D. O. Miller, *Chem. Commun.*, **2001**, 1170; (b) J. Mao, Z. Jin, J. Ni, L. Yu, *Polyhedron,* **1994**, *13*, 313.

95. (a) C. V. K. Sharma, R. D. Rogers, *Chem. Commun.*, **1999**, 83; (b) T. J. R. Weakley, *Acta Cryst.*, **1989**, *C45*, 525; (c) K. T. Al Rasoul, M. G. B. Drew, *Acta Cryst.*, **1987**, *C43*, 2081; (d) J. C. Barnes, Private Communication, CCDC No. 611245, **2006**; (e) K. Li, Y. Liu, C. Yan, L. Fu, S. –C. Wei, H. –P. Wang, M. Pan, C. –Y. Su, *Cryst. Eng. Comm.*, **2012**, *14*, 3868; (f) K. Al-Rasoul, T. J. R. Weakley, *Inorg. Chim. Acta*, **1982**, *60*, 191.

96. (a) Nibha, B. P. Baranwal, Gurdip Singh, C. P. Singh, C. G. Daniliuc, P. K. Soni, Yogeshwar Nath, *J. Mol. Struc.*, **2014**, *1076*, 539; (b) A. T. Kruszynska, R. Kruszynski, M. Zalewicz, T. J. Bartczak, *J. Coord. Chem.*, **2010**, *63*, 1013.

97. (a) N. –G. Li, R. –M. Tao, B. –F. Fu, *Acta Cryst.*, **2007**, *E63*, m2715; (b) T. J. R. Weakley, *Inorg. Chim. Acta*, **1982**, *63*, 161; (c) T. J. R. Weakley, *Inorg. Chim. Acta*, **1984**, *95*, 317; (d) S. Lipstman, I. Goldberg, *Cryst. Growth & Des.*, **2010**, *10*, 1823 (f) A. G. Matveeva, Z. A. Starikova, R. R. Aysin, R. S. Skazov, S. V. Matveev, G. I. Timofeeva, M. P. Passechnik, E. E. Nifantev, *Polyhedron*, **2013**, *61*, 172.

98. P. Thuery, *Cryst. Eng. Comm.*, **2012**, *14*, 8128.

99. (a) H. Koshima, M. Nagano, T. Asahi, *J. Am. Chem. Soc.*, **2005**, *127*, 2455; (b) H. Koshima, H. Miyamoto, I. Yagi, K. Uosaki, *Cryst. Growth Des.*, **2004**, *4*, 807; (c) S. L. Childs, L. J. Chyall, J. T. Dunlap, V. N. Smolenskaya, B. C. Stahly, G. P. Stahly, *J. Am. Chem. Soc.*, **2004**, *126*, 13335; (d) J. F. Remenar, S. L. Morissette, M. L. Peterson, B. Moulton, J. M. MacPhee, H. R. Guzman, O. Almarsson, *J. Am. Chem. Soc.*, **2003**,*125*, 8456; (e) T. E. Keyes, R. J. Forster, A. M. Bond and W. Miao, *J. Am. Chem. Soc.*, **2001**, *123*, 2877; (f) X. -L. Zhang, X. -M. Chen, *Cryst. Growth Des.*, **2005**, *5*, 617; (g) S. Ohba, H. Hosomi, Y. Ito, *J. Am. Chem. Soc.*, **2001**, *123*, 634 (h) K. Li, Y. Liu, C. Yan, L. Fu, S. –C. Wei H.-P. Wang, M. Pan, C. –Y. Su, *Cryst Eng Comm.*, **2012**, *14*, 3868.

100. (a) S. Lipstman, I. Goldberg, *Cryst. Growth Des.*, **2010**, *10*, 1823; (b) K. L. Wong, P. A. Tanner, *J. Phys. Chem. B*, **2007**, *111*, 10858; (c) H. M. Titi, I. Goldberg, *Cryst Eng Comm.*, **2010**, *12*, 3914; (d) R. C. Holz, L. C. Thompson, *Inorg. Chem.*, **1993**, *32*, 5251; (e) W. J. Lu, L. P. Zhang, H. S. Chan, T. L. Chan, T. C. W. Mak, *Polyhedron*, **2004**, *23*, 1089.

CHAPTER II

Synthesis, structural and spectral characterization of the lanthanide nitrato complex anions crystallised using Cu(II) nitrate and 2,2'-bipyridine

2.1. Introduction

There is much current interest in the synthesis of Cu(II)/*Ln*(III) heteronuclear complexes due to their interesting structural and magnetic properties, especially in the field of molecular magnetism and single-molecule magnets.[1] Weak non-covalent interactions in lanthanide complexes are also the subject of intensive study as a new approach of developing materials science.[2] Several series of anionic lanthanide complexes have been synthesized with large organo-cations[3] and a few reported with complex-cations,[4] in which lanthanide ions were not coordinated directly to the cations. Only a few examples of $[Ln(NO_3)_x(OH_2)_{6-x}]^{(x-3)-}$ interacting with a cationic core via nitrate bridge have been reported.[5] A unique compound $[La(NO_3)_6\{Cu(bpy)_2)\}_2][La(NO_3)_6\ Cu(bpy)_2]\cdot CH_3CN$, where $[La(NO_3)_6]^{3-}$ connecting either a single or two $Cu(bpy)_2$ units in the same compound was reported.[5a]

In an attempt to generate nitrate ion linked Cu(II)/*Ln*(III) heteropolynuclear complexes with bpy as a co-ligand, with a view to investigate of magnetic properties, $Cu(NO_3)_2$ and $Ln(NO_3)_3$ were reacted with the bpy ligand sequentially. The resulting blue compounds, $\{[Cu_2(bpy)_4(\mu\text{-}NO_3)][Ln(NO_3)_6]\}$ [*Ln* = La (**1**), Ce (**2**), Pr (**3**) and Nd (**4**)], $\{[Cu(bpy)_2(NO_3)]_2[Ln(NO_3)_4(OH_2)_2](NO_3)\}$ [*Ln* = Sm (**5**), Eu (**6**), Gd (**7**), Tb (**8**) and Dy (**9**)] and $\{[Cu(bpy)_2(NO_3)]_2[Ln(NO_3)_5]\}$ [*Ln* = Ho (**10**), Er (**11**) and Tm (**12**)] have been shown to contain both Cu(II) and *Ln*(III), but the main fragments consist of the core $[Cu_2(\mu{-}NO_3)bpy_4]^{3+}$ (**1-4**) and $[Cu(bpy)_2(NO_3)]^+$ (**5-13**) cation distortion isomers accompanied by counter anions

$[Ln(NO_3)_x(OH_2)_{6-x}]^{(x-3)-}$ (**1-9**) and $[Ln(NO_3)_x]^{(x-3)-}$ (**10-12**). The reaction with Yb(III) nitrate salt leads to co-crystallization of a neutral *Ln*(III) coordination complex and a Cu(II) complex salt in one crystal, namely $\{[Cu(bpy)_2(NO_3)]_2[Yb(NO_3)_3(OH_2)_3](NO_3)_2{\cdot}2H_2O\}$ (**13**). There were two previous reports of $Yb(NO_3)_3(OH_2)_3$ cocrystallising with neutral organic molecules: $\{[Yb(NO_3)_3(H_2O)_3]{\cdot}$18-crown-6$\}$[6a] and $\{[Yb(NO_3)_3(H_2O)_3]{\cdot}$TPyP$\cdot$2(benzene)$\}$ (TPyP = *meso*-tetra(4-pyridyl)porphyrin).[6b]

Although the nitrate ion usually exhibits the terminal coordination mode in Cu(II) complexes, complexes with nitrato bridges (single, double or triple) are also reported in the literature.[7] Several Cu(II) complexes containing mono atomic nitrate bridge core $[Cu_2(\mu{-}NO_3)]^+$ along with other coordination bridges were reported.[8] No complex was isolated only with the mono atomic nitrate bridged core $[Cu_2(\mu{-}NO_3)]^+$. Only a few examples of Cu(II) complexes with $[Cu(bpy)_2(NO_3)]^+$ cation distortion isomers involving the counter anions, ONO_2^-, ClO_4^- and PF_6^- have been reported in the literature.[9] The Cu(II) geometries ranging from distorted trigonal bipyramidal to unsymmetrical bicapped square-pyramidal and unsymmetrical *cis*-distorted octahedral (4+1+1*) have been classified, based on the types of distortion from the regular *cis*-distorted octahedral geometry.[10] The present study deals with the formation of a new Cu(II)/*Ln*(III) heteropolynuclear complexes and the influence of lanthanide complex anions on the composition of the complex cations containing bpy as a co-ligand. Variable temperature magnetic susceptibility measurements in the range 3–300 K show weak antiferromagnetic behaviour for the complexes **1**–**4**. In addition, polycrystalline EPR spectra of all samples were measured at different temperature and the results are discussed.

2.2. Experimental

2.2.1. Reagents

All the chemicals were of reagent grade obtained from commercial sources and were used without further purification.

2.2.2. Synthesis

Preparation of {[Cu_2(bpy)$_4$(μ-NO_3)][*Ln*(NO_3)$_6$]} (1-4)

To 2,2'–bipyridine (0.187 g, 1.200 mmol) dissolved in acetonitrile (10 mL), $Cu(NO_3)_2 \cdot 3H_2O$ (0.145 g, 0.600 mmol) and $Ln(NO_3) \cdot 6H_2O$ (0.300 mmol) where *Ln* = La (0.130 g) (**1**), Ce (0.130 g) (**2**), Pr (0.131 g) (**3**) and Nd (0.133 g) (**4**) dissolved in acetonitrile solution (10 mL) was added slowly while stirring. The resulting dark blue solution was kept at room temperature for crystallization. Block shape blue crystals were obtained after 3 days.

For **1**: Yield 0.304 g, (0.230 mmol, 77%). *Anal.* Calc. for $C_{40}H_{32}N_{15}O_{21}Cu_2La$ (M.W. 1324.76 g): C, 36.27; H, 2.43; N, 15.86. Found: C, 36.38; H, 2.51; N, 15.71. Important IR absorptions (KBr disk, cm^{-1}): 3065, 2459, 2336, 1770, 1741, 1604, 1568, 1498, 1448, 1307, 1107, 1033, 819, 771, 731, 663 and 416.

For **2**: Yield 0.260 g, (0.196 mmol, 65%). *Anal.* Calc. for $C_{40}H_{32}N_{15}O_{21}Cu_2Ce$ (M.W. 1325.89 g): C, 36.23; H, 2.43; N, 15.84. Found: C, 36.41; H, 2.38; N, 15.96. Important IR absorptions (KBr disk, cm^{-1}): 3065, 2457, 2339, 1768, 1743, 1604, 1568, 1494, 1454, 1307, 1168, 1107, 1033, 817, 771, 731, 665 and 416.

For **3**: Yield 0.310 g, (0.234 mmol, 78%). *Anal.* Calc. for $C_{40}H_{32}N_{15}O_{21}Cu_2Pr$ (M.W. 1326.68 g): C, 36.21; H, 2.43; N, 15.83. Found: C, 36.05; H, 2.56; N, 15.71. Important IR absorptions (KBr

disk, cm^{-1}): 3070, 2461, 2341, 1780, 1743, 1604, 1570, 1498, 1448, 1309, 1170, 1107, 1032, 817, 771, 731, 663 and 414.

For **4**: Yield 0.380 g, (0.285 mmol, 95%). *Anal.* Calc. for $C_{40}H_{32}N_{15}O_{21}Cu_2Nd$ (M.W. 1330.09 g): C, 36.12; H, 2.43; N, 15.80. Found: C, 36.21; H, 2.51; N, 15.68. Important IR absorptions (KBr disk, cm^{-1}): 3065, 2453, 2341, 1768, 1745, 1604, 1568, 1498, 1448, 1317, 1172, 1107, 1032, 817, 771, 731, 663 and 416.

Preparation of {[Cu(bpy)$_2$(NO$_3$)]$_2$[*Ln*(NO$_3$)$_4$(OH$_2$)$_2$](NO$_3$)} (5-9)

To 2,2'–bipyridine (0.187 g, 1.200 mmol) dissolved in acetonitrile (10 mL), $Cu(NO_3)_2 \cdot 3H_2O$ (0.145 g, 0.600 mmol) and $Ln(NO_3) \cdot 6H_2O$ (0.300 mmol) where *Ln* = Sm (0.133 g) (**5**), Eu (0.129 g) (**6**), Gd (0.135 g) (**7**), Tb (0.131 g) (**8**) and Dy (0.132 g) (**9**) dissolved in acetonitrile (10 mL) was added slowly while stirring. The resulting clear blue solution was kept at room temperature for crystallization. Plate shaped blue crystals were obtained after 3 days.

For **5**: Yield 0.288 g, (0.210 mmol, 70%). *Anal.* Calc. for $C_{40}H_{36}N_{15}O_{23}Cu_2Sm$ (M.W. 1372.28 g): C, 35.01; H, 2.64; N, 15.31. Found: C, 35.16; H, 2.56; N, 15.18. Important IR absorptions (KBr disk, cm^{-1}): 3424, 3117, 3079, 2328, 2016, 1742, 1665, 1605, 1567, 1441, 1298, 1030, 898, 810 and 767.

For **6**: Yield 0.245 g, (0.178 mmol, 60%). *Anal.* Calc. for $C_{40}H_{36}N_{15}O_{23}Cu_2Eu$ (M.W. 1373.84 g): C, 34.97; H, 2.64; N, 15.29. Found: C, 34.79; H, 2.71; N, 15.16. Important IR absorptions (KBr disk, cm^{-1}): 3420, 3113, 3082, 2328, 2020, 1738, 1666, 1604, 1572, 1454, 1302, 1176, 1033, 902, 815, 767, 731, 661, 638 and 414.

For **7**: Yield 0.244 g, (0.180 mmol, 60%). *Anal.* Calc. for $C_{40}H_{36}N_{15}O_{23}Cu_2Gd$ (M.W. 1379.13 g): C, 34.84; H, 2.63; N, 15.23. Found: C, 34.75; H, 2.53; N, 15.36. Important IR absorptions

(KBr disk, cm^{-1}): 3443, 3119, 3084, 2329, 2020, 1741, 1659, 1602, 1570, 1446, 1315, 1032, 910, 827, 767, 731, 661 and 411.

For **8**: Yield 0.244 g, (0.180 mmol, 60%). *Anal.* Calc. for $C_{40}H_{36}N_{15}O_{23}Cu_2Tb$ (M.W. 1380.81 g): C, 34.79; H, 2.63; N, 15.21. Found: C, 34.65; H, 2.56; N, 15.36. Important IR absorptions (KBr disk, cm^{-1}): 3420, 3117, 3079, 2326, 2021, 1868, 1736, 1671, 1605, 1572, 1446, 1298, 1035, 898, 816 and 767.

For **9**: Yield 0.236 g, (0.170 mmol, 57%). *Anal.* Calc. for $C_{40}H_{36}N_{15}O_{23}Cu_2Dy$ (M.W. 1384.38 g): C, 34.70; H, 2.62; N, 15.18. Found: C, 34.48; H, 2.71; N, 15.07. Important IR absorptions (KBr disk, cm^{-1}): 3422, 3119, 3084, 2471, 2334, 2021, 1741, 1668, 1604, 1572, 1456, 1302, 1033, 902, 815, 767, 731, 638 and 412.

Preparation of {[Cu(bpy)$_2$(NO$_3$)]$_2$[*Ln*(NO$_3$)$_5$]} (10-12)

To 2,2'–bipyridine (0.125 g, 0.800 mmol) dissolved in acetonitrile (10 mL), $Cu(NO_3)_2 \cdot 3H_2O$ (0.145 g, 0.600 mmol) and $Ln(NO_3)_3 \cdot 5H_2O$ (0.200 mmol) where *Ln* = Ho (0.088 g) (**10**), Er (0.089 g) (**11**) and Tm (0.089 g) (**12**) dissolved in acetonitrile (10 mL) was added slowly while stirring. The resulting clear blue solution was kept at room temperature for crystallization. Plate shape blue crystals were obtained after 3 days.

For **10**: Yield 0.250 g, (0.185 mmol, 93%). *Anal.* Calc. for $C_{40}H_{32}N_{15}O_{21}Cu_2Ho$ (M.W. 1350.82 g): C, 35.57; H, 2.39; N, 15.55. Found: C, 35.68; H, 2.31; N, 15.43. Important IR absorptions (KBr disk, cm^{-1}): 3112, 3079, 1600, 1567, 1473, 1441, 1315, 1276, 1156, 1024, 810, 767, 728, 657 and 449.

For **11**: Yield 0.246 g, (0.182 mmol, 91%). *Anal.* Calc. for $C_{40}H_{32}N_{15}O_{21}Cu_2Er$ (M.W. 1353.15 g): C, 35.51; H, 2.38; N, 15.53. Found: C, 35.68; H, 2.46; N, 15.42. Important IR absorptions

(KBr disk, cm^{-1}): 3117, 3070, 1600, 1572, 1473, 1441, 1320, 1276, 1150, 1030, 816, 772, 723, 652 and 520.

For **12**: Yield 0.260 g, (0.192 mmol, 96%). *Anal.* Calc. for $C_{40}H_{32}N_{15}O_{21}Cu_2Tm$ (M.W. 1352.84 g): C, 35.46; H, 2.38; N, 15.51. Found: C, 35.50; H, 2.40; N, 15.60. Important IR absorptions (KBr disk, cm^{-1}): 3079, 1610, 1572, 1473, 1441, 1315, 1270, 1167, 1030, 810, 772, 728 and 646.

Preparation of $\{[Cu(bpy)_2(NO_3)]_2[Yb(NO_3)_3(OH_2)_3](NO_3)_2 \cdot 2H_2O\}$ (13)

To 2,2'–bipyridine (0.125 g, 0.800 mmol) dissolved in acetonitrile (10 mL), $Cu(NO_3)_2 \cdot 3H_2O$ (0.096 g, 0.400 mmol) and $Yb(NO_3) \cdot 5H_2O$ (0.090 g, 0.200 mmol) dissolved in acetonitrile (10 mL) was added slowly while stirring. The resulting clear blue solution was kept at room temperature for crystallization. Plate shape blue crystals were obtained after 3 days. Yield 0.279 g, (0.193 mmol, 96%). *Anal.* Calc. for $C_{40}H_{40}N_{15}O_{26}Cu_2Yb$ (M.W. 1446.99 g): C, 33.16; H, 2.92; N, 14.50. Found: C, 33.48; H, 2.45; N, 14.25. Important IR absorptions (KBr disk, cm^{-1}): 3380, 3084, 3065, 2021, 1665, 1610, 1570, 1441, 1380, 1298, 1035, 820 and 767.

2.3. Physical measurements

IR spectra were obtained for KBr pellets on a Jasco FT-IR 5300 spectrometer in the range 4000-400 cm^{-1}. Elemental analysis for C, H and N was performed on a Perkin-Elmer 240C elemental analyzer. Diffuse reflectance spectra were measured by using a Shimadzu UV-3100 spectrometer. EPR spectra were recorded on Bruker Xenon EMX-ER-073 spectrometer. Powder X-ray diffraction patterns were recorded on a Bruker D8-Advance diffractometer using graphite monochromated $CuK_{\alpha 1}$ (1.5406 Å) and $K_{\alpha 2}$ (1.54439 Å) radiations. Simulation of the P-XRD patterns was carried out using the Mercury program. Magnetic susceptibilities were measured in the temperature range of 3−300 K on a Quantum Design PPMS-VSM. The samples were pressed

into pellets to avoid orientation effects of the microcrystals during magnetic measurements. Diamagnetic corrections were made with Pascal's constants.[11] Fitting of the susceptibility data was done by using the program SUSCEP[12] based on the Bleaney-Bower equation[13] including temperature independent paramagnetism (TIP) for **1**. Data for compounds **2**–**4** were analyzed based on a modified SUSCEP program.[12]

2.4. X-ray crystallography

The unit cell parameters and the intensity data at 298 K for **1-3** were obtained on an Oxford Diffraction Xcalibur Gemini single crystal X-ray diffractometer using graphite-monochromated Mo-Kα radiation (λ = 0.71073 Å). The CrysAlisPro software[14] was used for data collection, reduction and absorption correction. The unit cell parameters and intensity data at 100 K for **4** and 298 K for **5-13** were obtained on a Bruker-Nonius SMART APEX CCD 1000 area detector, using graphite-monochromated Mo-Kα radiation (λ = 0.71073 Å). Data were reduced using SAINTPLUS[15] and a multi-scan absorption correction using SADABS[16] was performed. The structure of complexes were solved by direct methods and refined on F^2 by full-matrix least-squares procedures. The non-hydrogen atoms were refined using anisotropic thermal parameters. The hydrogen atoms were included in the structure factor calculations at idealized positions using a riding model, and the hydrogen atoms attached to oxygen atoms were located from the difference maps. The structures were solved using SHELXS-97 and refined using SHELXL-97.[17] Drawings were made using Mercury.[18] Crystallographic data and structure refinement details are given in Table 2.1, Table 2.4 and Table 2.7. Selected bond lengths and bond angles are listed in Table 2.2, Table 2.5, Table 2.8 and Table 2.10. Details of the hydrogen bonding and π–stacking interactions are given in Table 2.3, Table 2.6, Table 2.9 and Table 2.11.

Table 2.1: Crystallographic data and structure refinement for compounds **1−4**

Param	**1**	**2**	**3**	**4**
Formula	$C_{40}H_{32}N_{15}O_{21}Cu_2La$	$C_{40}H_{32}N_{15}O_{21}Cu_2Ce$	$C_{40}H_{32}N_{15}O_{21}Cu_2Pr$	$C_{40}H_{32}N_{15}O_{21}Cu_2Nd$
Formula weight	1324.80	1326.01	1326.80	1330.13
Crystal system	Monoclinic	Monoclinic	Monoclinic	Monoclinic
Space group	*C*2/*c*	*C*2/*c*	*C*2/*c*	*C*2/*c*
a (Å)	24.241(7)	24.191(2)	24.252(9)	24.140(11)
b (Å)	15.984(3)	15.964(13)	15.916(4)	15.959(11)
c (Å)	14.227(4)	14.185(12)	14.277(5)	14.195(7)
β (°)	118.155(4)	118.135(10)	118.218(5)	118.173(11)
V (Å^3)	4859.9(2)	4830.6(7)	4855.8(3)	4821(5)
Z	4	4	4	4
T(K)	298(2)	298(2)	298(2)	100(2)
λ (Å)	0.71073	0.71073	0.71073	0.71073
D_{calc} (g cm^{-3})	1.811	1.823	1.815	1.833
μ (mm^{-1})	1.829	1.898	1.954	2.034
F(000)	2640	2644	2648	2652
Crystal size (mm)	0.32 x 0.20 x 0.10	0.32 x 0.20 x 0.12	0.32 x 0.20 x 0.16	0.36 x 0.20 x 0.12
θ Range(°)	2.84 – 24.99	1.59 – 24.99	2.84 – 23.26	1.59 – 25.69
h/*k*/*l* indices	–28, 28/ –10, 18/ –13,16	–28, 28/ –15,18/ –16,16	–26,17/ –17,15/ –13,15	–29, 29/ –19,19/ –17,17
Refl^n collected	10345	14263	7554	18551
Unique refl^n [R_{int}]	4272 [0.0206]	4259 [0.0318]	3490 [0.0186]	4202 [0.0707]
GooF	1.055	1.032	1.071	1.007
R_1 [I>2σ(I)]	0.0484	0.0504	0.0533	0.0527
wR_2 (all data)	0.1448	0.1441	0.1590	0.1318

$w = 1/[\sigma^2(F_0^2) + (AP)^2 + BP]$; where $P = [2F_C^2 + Max(F_0^2, 0)]/3$

2.5. PXRD measurements

Powder X-ray diffraction experiments have been done to check the homogeneity of the bulk crystalline powders of **1–13** by comparison of the simulated and experimental X-ray powder diffraction patterns. The peak positions of the experimental patterns agree with the corresponding simulated patterns from the single-crystal X-ray diffraction data for **1–13** (Figure 2.4, Figure 2.14, Figure 2.24 and Figure 2.32).

2.6. $[Cu_2(bpy)_4(NO_3)][Ln(NO_3)_6]$ (*Ln* = La (1), Ce (2), Pr (3) and Nd (4))

2.6.1. Crystal structure of $\{[Cu_2(bpy)_4(NO_3)][Ln(NO_3)_6]\}$ (1-4)

Compounds **1-4** form isomorphous crystals. Crystallographic data and structure refinement details are listed in Table 2.1.

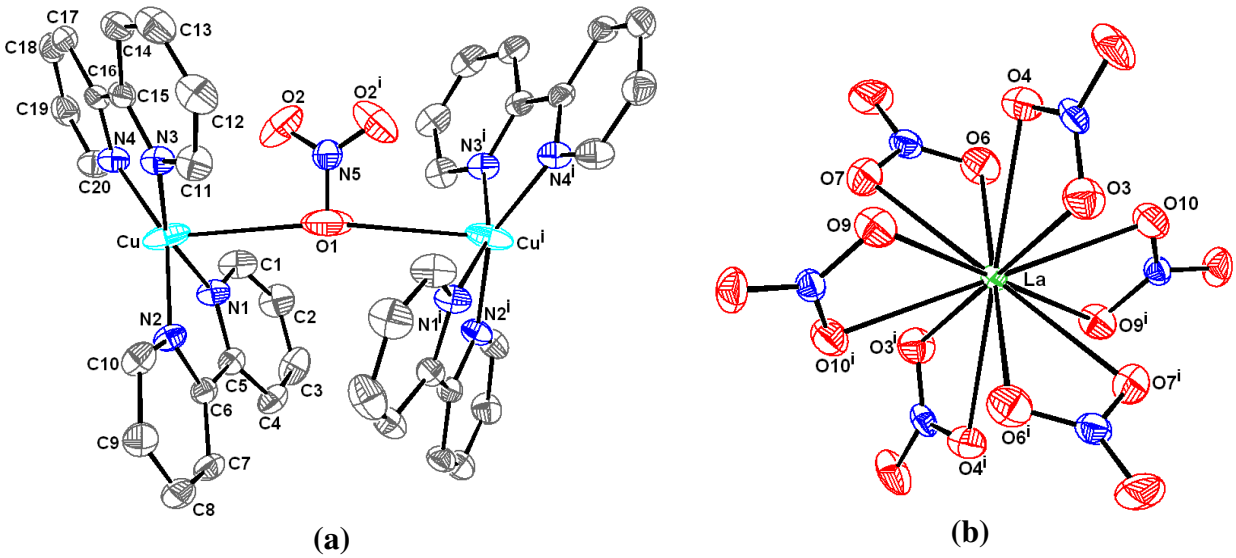

Figure 2.1. Thermal ellipsoid plot of the coordination environment of the (a) complex cation and (b) complex anion of **1**: Atoms are represented as 30% probability ellipsoids. Ring hydrogen atoms have been omitted for clarity. Symmetry code (i): $-x + {}^{3}/_{2}, -y + {}^{1}/_{2}, -z + 1$.

Since geometrical parameters of all compounds are similar the selected bond lengths and angles of compound **1** are given in Table 2.2. The asymmetric unit consists of a dinuclear cation, $[Cu_2(\mu{-}NO_3)bpy_4]^{3+}$, with monoatomic nitrate ion bridge accompanied by an isolated $[Ln(NO_3)_6]^{3-}$ anion is shown in Figure 2.1(a) and 2.1(b).

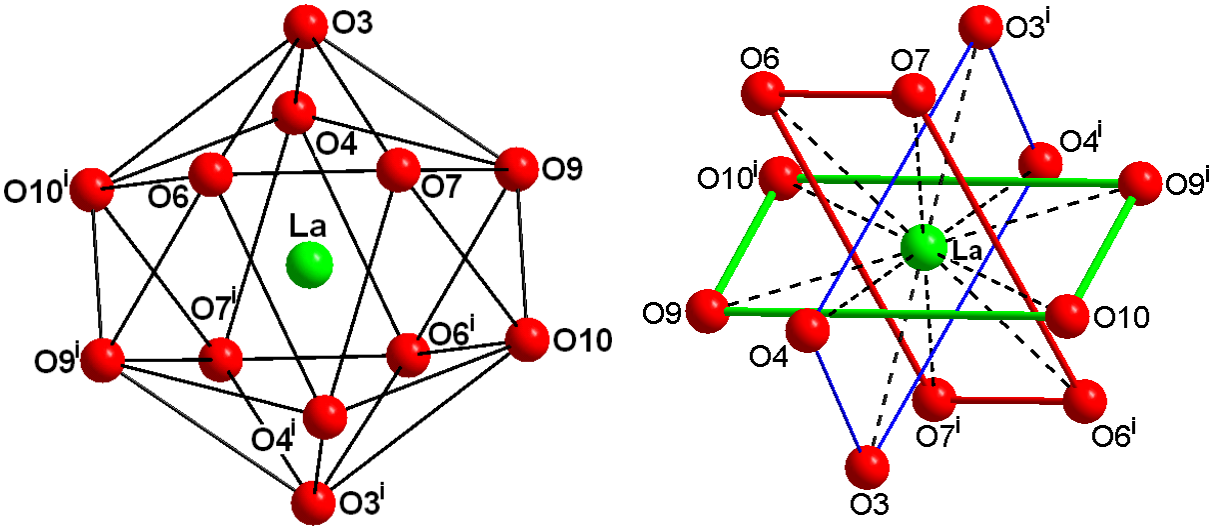

(a) **(b)**

Figure 2.2. (a) Icosahedral coordination polyhedron of La(III)ion. (b) Ligand atoms arranged in three mutually perpendicular planes (dihedral angles in the range, 87.1 - 89.8º) in $[La(NO_3)_6]^{3-}$.

The coordination geometry around Cu(II) in the complex cation is highly distorted square-pyramidal with an equatorial plane formed by four nitrogen atoms from two bpy ligands and an axial oxygen atom from bridged nitrate group. The Cu–N bond distances (Å) lie in the range 1.965(4)–1.989(4) in good agreement with the previously reported complexes.[19] The axial Cu–O(1) distance (Å) is quite large 2.879(1) and this value remains within the range reported for axial elongated Cu–O bonds (2.22-2.89 Å).[19] The Cu–O(2) distance (Å) is too far 2.911(8) to be considered even semi-coordination. The equatorial plane geometry is somewhat distorted toward the tetrahedron, the dihedral angle (º) between the N(1), Cu, N(2) and N(3), Cu, N(4) planes is

39.09, whereas the values of the angles (º) N(2)–Cu–N(4) and N(1)–Cu–N(3) are 151.9(2) and 157.4(2). The Cu–Cu distance (Å) is 5.737(2). The bpy ligands are not planar, but the individual pyridine rings are planar within 0.03 Å, the dihedral angles (º) between the two pyridine rings being 8.43-9.65.

The $Ln(NO_3)_6^{3-}$ anion has a distorted icosahedral structure with twelve oxygen atoms from six chelating nitrate ions and is similar to the previously reported centrosymmetric structures.[20] *Ln*(III) atom is located on a crystallographic inversion centre shown in Figure 2.2(a). The *Ln*–O bond lengths (Å): 2.635(5)-2.696(5) for **1**; 2.614(5)-2.674(5) for **2**; 2.599(6)-2.664(6) for **3**; 2.587(5)-2.642(5) for **4**, implying that nitrate ions are symmetrically bound to *Ln*(III). The O–*Ln*–O bond angles (º): 47.03(18)–132.97(18) for **1**; 47.19(17)–132.55(16) for **2**; 47.3(2)–132.7(2) for **3**; 47.98(18)–132.02(18) for **4**. In crystals of **1** (Figure 2.3), the $[La(NO_3)_6]^{3-}$ anion forms 1D zig-zag chain with cation by C-H···O interactions (C4-H4···O5, 2.407(5); C7-H7···O5, 2.480(5) Å) along *c*-axis. These are further interconnected with various π-stacking interactions (3.100-3.460 Å) forming a 2D network. However, the voids are blocked by a 3-fold parallel interpenetration of identical H-bonded networks shown in Figure 2.3(e). Details of the H-bonding and π- stacking interactions are given in Table 2.3.

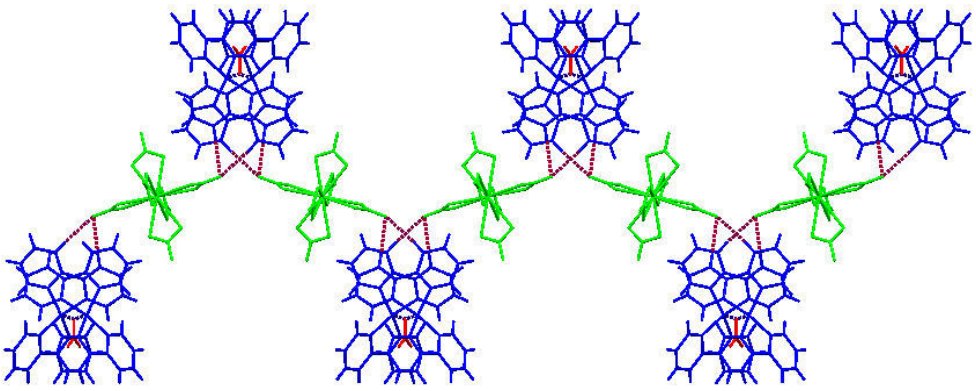

(a)

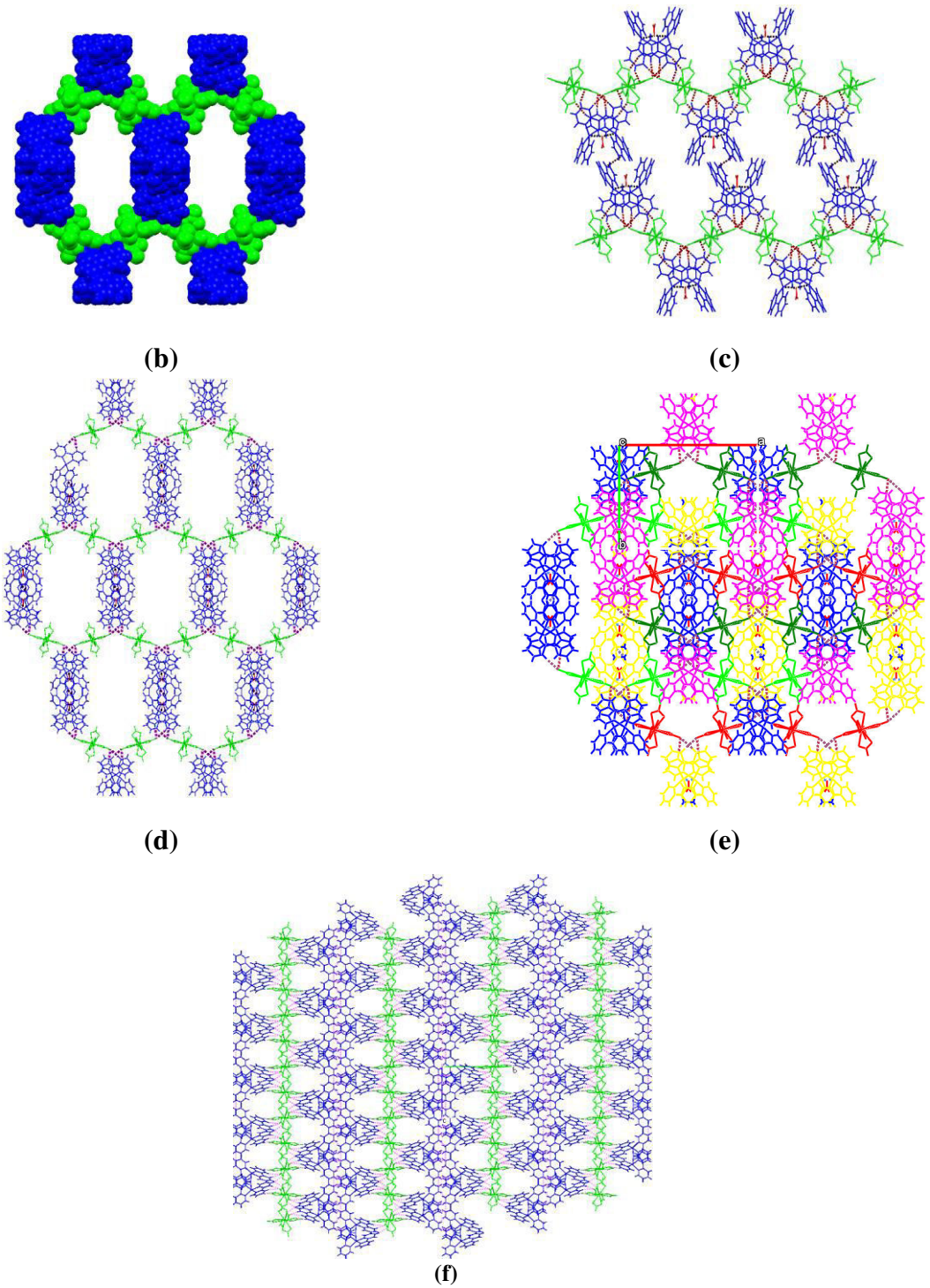

Figure 2.3. Views of (a) 1D zig-zag chain formed by H-bond interactions of cation and anion units in **1** (b) single net space-filling 2D network in **1** (c) 2D layer structure formed by π-stacking of **1** down *c*-axis (d) H-bonded 2D network in **1** down the *c*-axis (e) parallel interpenetration of identical H-bonded networks in **1** down the *c*-axis. (f) The molecular packing of **1** down *a*-axis.

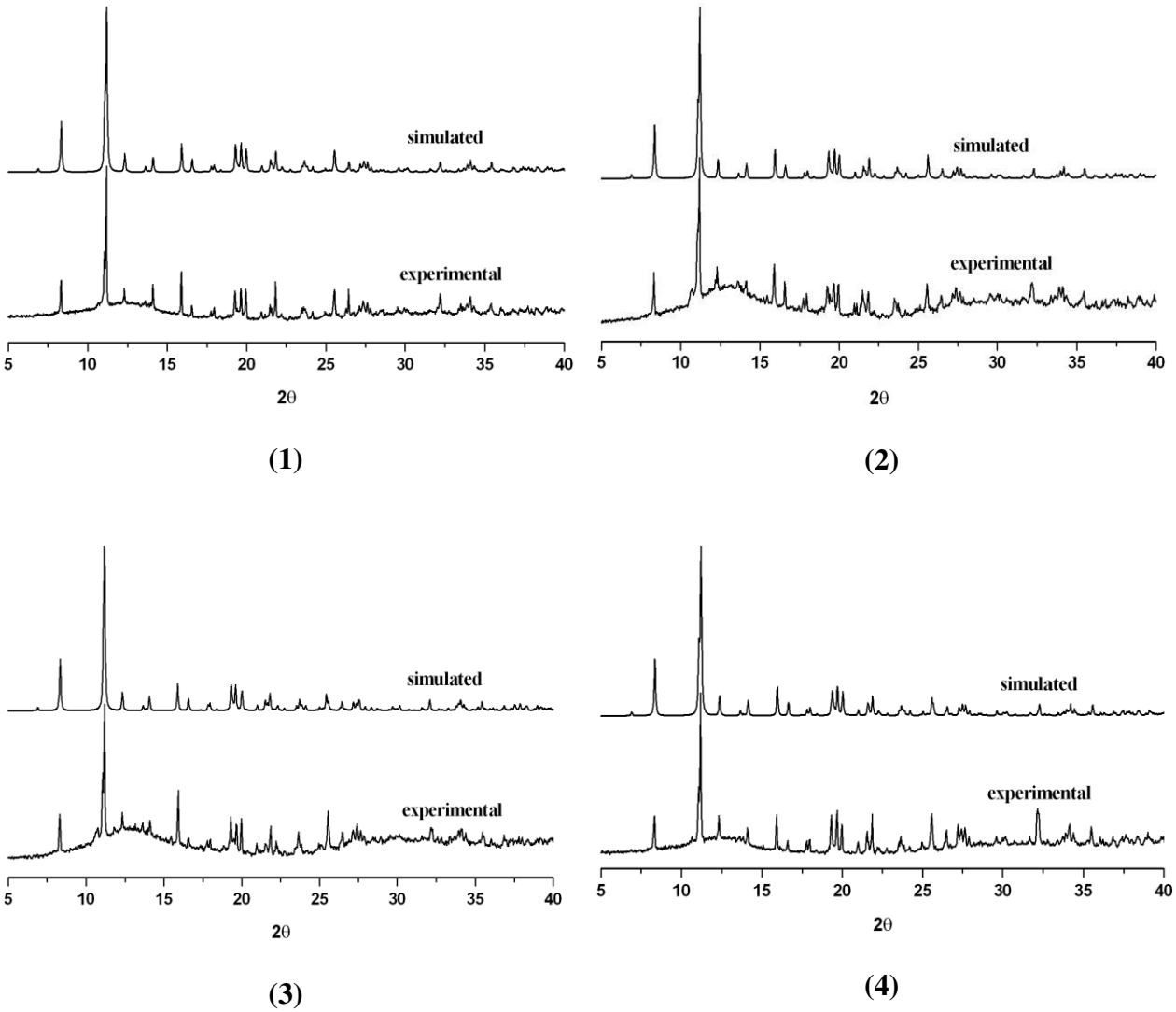

Figure 2.4. Powder X-ray diffraction computer simulated and experimental patterns of complexes **1-4**

Table 2.2: Selected bond lengths (Å) and bond angles (°) for {[$Cu_2(bpy)_4(\mu\text{-}NO_3)$][$La(NO_3)_6$]}

Cu-N(1)	1.967(5)	Cu-N(2)	1.989(4)	Cu-N(3)	1.965(4)
Cu-N(4)	1.977(5)	Cu-O(1)	2.879(1)	Cu-Cu#1	5.737(2)
La-O(3)	2.696(5)	La-O(4)	2.665(5)	La-O(9)	2.640(5)
La-O(6)	2.645(5)	La-O(7)	2.689(5)	La-O(10)	2.635(5)
N(5)-O(1)	1.208(10)	N(6)-O(5)	1.224(6)	N(8)-O(9)	1.264(6)
N(5)-O(2)	1.210(6)	N(7)-O(6)	1.255(7)	N(8)-O(10)	1.254(7)
N(6)-O(3)	1.215(7)	N(7)-O(7)	1.240(8)	N(8)-O(11)	1.206(6)

N(6)-O(4)	1.295(7)	N(7)-O(8)	1.225(7)		
N(1)-Cu-N(2)	81.91(19)	N(2)-Cu-N(3)	103.03(19)	N(3)-Cu-O(1)	85.9(2)
N(1)-Cu-N(3)	157.4(2)	N(2)-Cu-N(4)	151.9(2)	N(3)-Cu-N(4)	82.7(2)
N(1)-Cu-N(4)	103.47(19)	N(2)-Cu-O(1)	89.3(2)	N(4)-Cu-O(1)	118.7(2)
N(1)-Cu-O(1)	72.0(2)	O(1)-N(5)-O(2)	116.7(5)	Cu-O(1)-Cu#1	170.2(3)
O(3)-La-O(4)	47.20(16)	O(6)-La-O(10)	113.84(17)	O(4)-La-O(7)#1	113.78(16)
O(3)-La-O(6)	110.93(17)	O(7)-La-O(9)	108.83(17)	O(4)-La-O(9)#1	111.33(15)
O(3)-La-O(7)	110.87(17)	O(7)-La-O(10)	70.07(18)	O(4)-La-O(10)#1	112.14(16)
O(3)-La-O(9)	66.20(17)	O(9)-La-O(10)	132.13(15)	O(6)-La-O(7)#1	132.97(18)
O(3)-La-O(10)	69.97(17)	O(3)-La-O(4)#1	132.80(16)	O(6)-La-O(9)#1	112.81(17)
O(4)-La-O(6)	69.76(17)	O(3)-La-O(6)#1	69.07(17)	O(6)-La-O(10)#1	66.16(17)
O(4)-La-O(7)	66.22(16)	O(3)-La-O(7)#1	69.13(17)	O(7)-La-O(9)#1	71.17(17)
O(4)-La-O(9)	68.67(15)	O(3)-La-O(9)#1	113.80(17)	O(7)-La-O(10#1	109.93(18)
O(4)-La-O(10)	67.86(16)	O(3)-La-O(10)#1	110.03(17)	O(9)-La-O(10)#1	47.87(15)
O(6)-La-O(7)	47.03(18)	O(4)-La-O(6)#1	110.24(17)	O(2)-N(5)-O(2)#2	126.6(10)
O(6)-La-O(9)	67.19(17)	O(6)-N(7)-O(7)	117.1(5)	O(9)-N(8)-O(10)	116.4(5)
O(3)-N(6)-O(4)	117.5(5)	O(6)-N(7)-O(8)	120.3(7)	O(9)-N(8)-O(11)	122.6(5)
O(3)-N(6)-O(5)	121.0(6)	O(7)-N(7)-O(8)	122.4(7)	O(10)-N(8)-O(11)	121.0(5)
O(4)-N(6)-O(5)	121.5(6)	(#1) $-x+1/2, -y+1/2, -z+1$		(#2) $-x, y, -z+3/2$	

Table 2.3: Intermolecular interaction parameters

*H-bonding for **1***

D-H···A	**D-H(Å)**	**H···A(Å)**	**D···A(Å)**	**D-H···A(º)**
C3–H3···O10#1	0.93	2.54	3.42	158
C4–H4···O5#2	0.93	2.41	3.31	163
C7–H7···O5#2	0.93	2.48	3.40	173
C8–H8···O4#3	0.93	2.51	3.33	148
(#1) $^1/_2+x, -^1/_2+y, z$	(#2) $-x,1-y,1-z$	(#3) $x,1-y, -^1/_2+z$		

*π···π interactions for **1***

C5···C7#1	3.44(8)	C17···C17#2	3.26(1)
C14···C18#2	3.33(1)	C18···C18#3	3.10(1)
C19···C18#3	3.46(1)	(#1) $-x, 1-y, 1-z$; (#2) $-x, -y, 1-z$; (#3) $-x, y, {}^1/_2-z$	

2.6.2. Infrared spectra

The bands around 1600 and 1570 cm^{-1} were assigned to the $\nu_{C=C}$ frequency of the bpy rings. The band around 3065 cm^{-1} assigned to the ν_{C-H} frequency. This valve shifted to lower frequencies on complexation. The nitrate complexes exhibit four bands at 1490-1450 $cm^{-1}(\nu_1)$, 1280-1320 $cm^{-1}(\nu_2)$, 1020-1040 $cm^{-1}(\nu_3)$ and 810-830 cm^{-1} (ν_4) ranges which can be assigned to the vibrational modes of the coordinated (C_{2v}) nitrate groups.[21] The IR spectrum of nitrate ion is in intermediate between that of the free ion and the fully-coordinated ion. The effect of weak nitrate coordination in this case is seen in the splitting of ν_1 into bands at 1450 and 1310 cm^{-1}.

2.6.3. Electronic spectra

Diffuse reflectance spectrum of **1** (Figure 2.5) consists of a single broad band centered at 14050 cm^{-1}, is consistent with the tetrahedrally-distorted square-pyramidal stereochemistry and assigned to be the d_{z2}, d_{xy}, d_{xz}, $d_{yz} \rightarrow d_{x2-y2}$ transition.[22] Band near 33,000 cm^{-1} is due to ligand-to-metal charge transfer transition, while the band near 41,000 cm^{-1} is associated with intraligand $\pi \rightarrow \pi^*$ excitation.

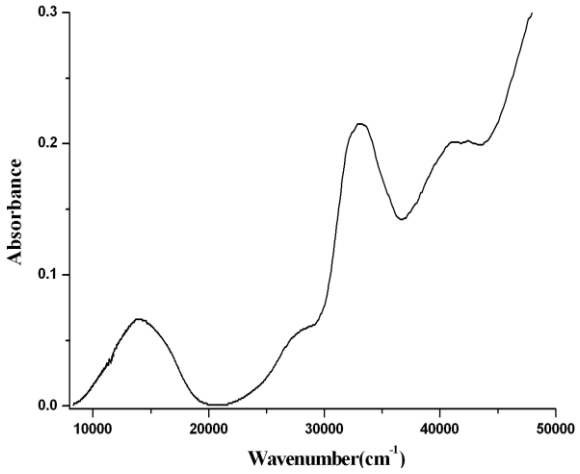

Figure 2.5. Diffuse reflectance spectrum of compound **1**

2.6.4. EPR spectra

The X-band polycrystalline EPR spectra of **1-4** were measured at room temperature as well as liquid nitrogen temperature (Figure 2.6 – 2.9). All spectra have been normalized to the same microwave frequency (ν = 9.6532 GHz). It is noteworthy that the EPR spectra of **1-4** at room temperature and liquid nitrogen temperature are almost the same. The spectra consist of a broad signal centered at g = 2.09 (width = 120 G at 300K). Zeeman anisotropy is not resolved due to exchange averaging in the dinuclear Cu(II) cation. The paramagnetic lanthanide ions, Ce(III), Pr(III) and Nd(III), in these compounds do not make any contribution to the EPR signal at the temperatures at which these samples are measured. In all four cases there is a 6-8% increase in the line width upon cooling the sample to 77K.

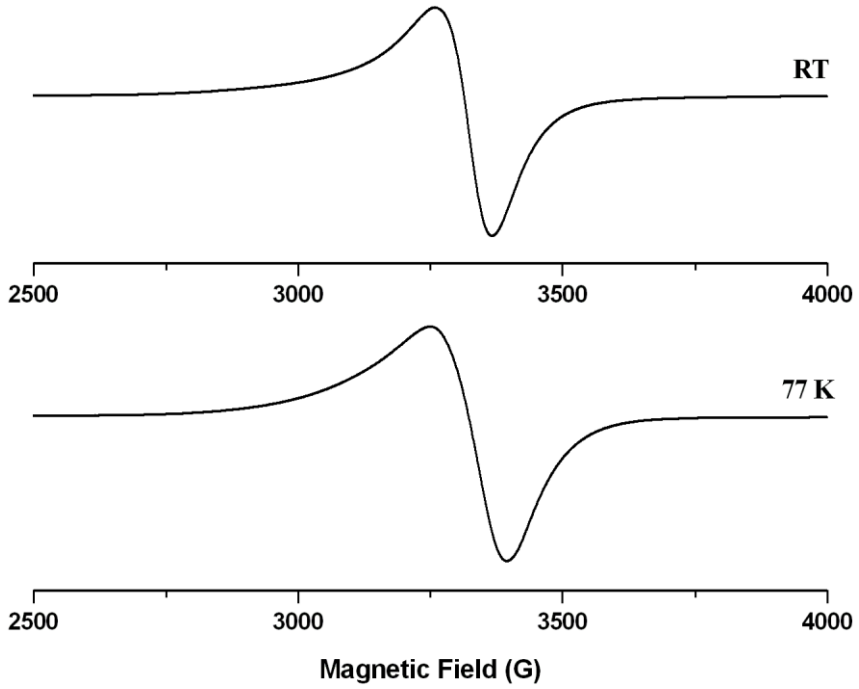

Figure 2.6. EPR spectra at two different temperatures for compound **1** (Cu_2-La)

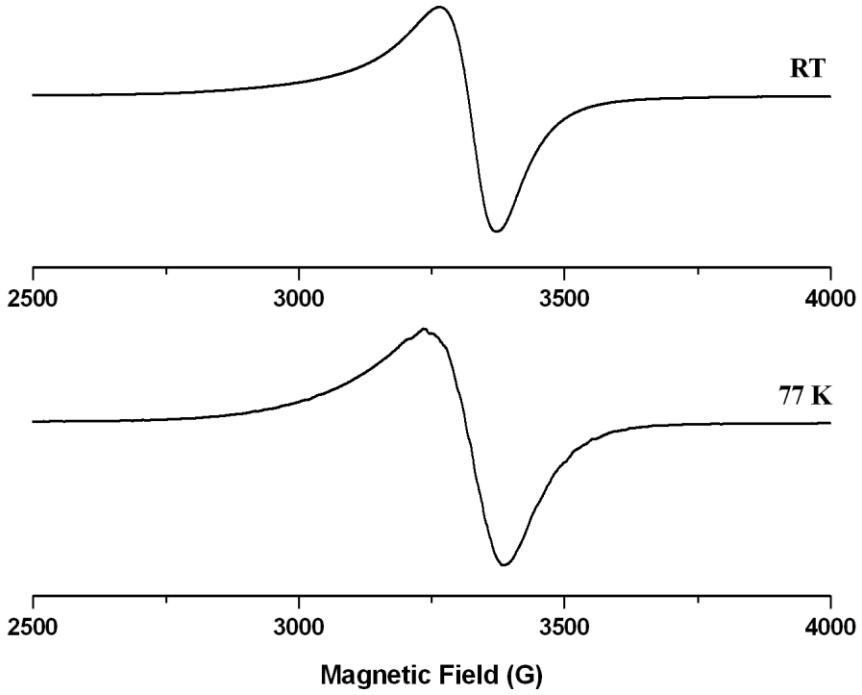

Figure 2.7. EPR spectra at two different temperatures for compound **2** (Cu_2-Ce)

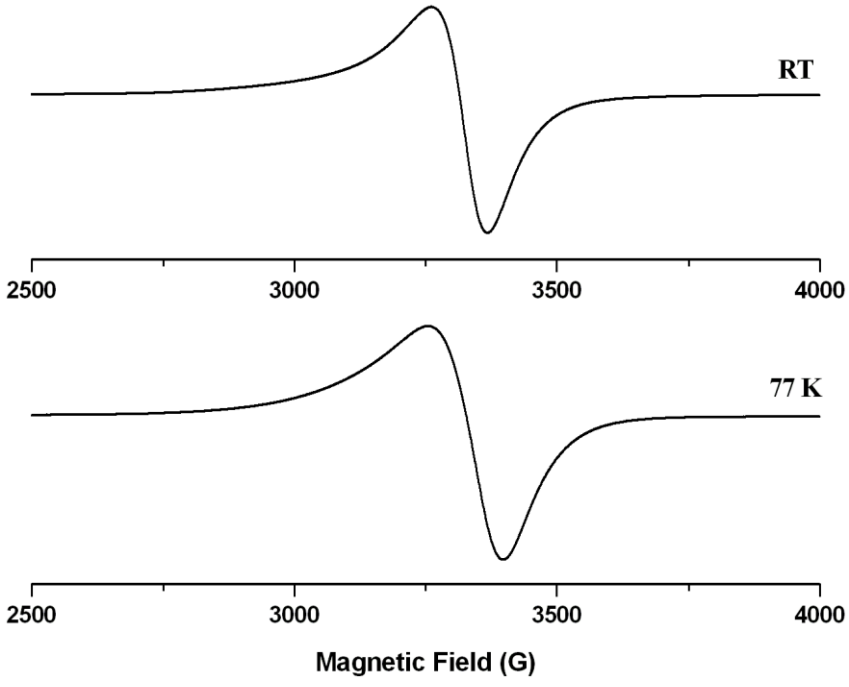

Figure 2.8. EPR spectra at two different temperatures for compound **3** (Cu_2-Pr)

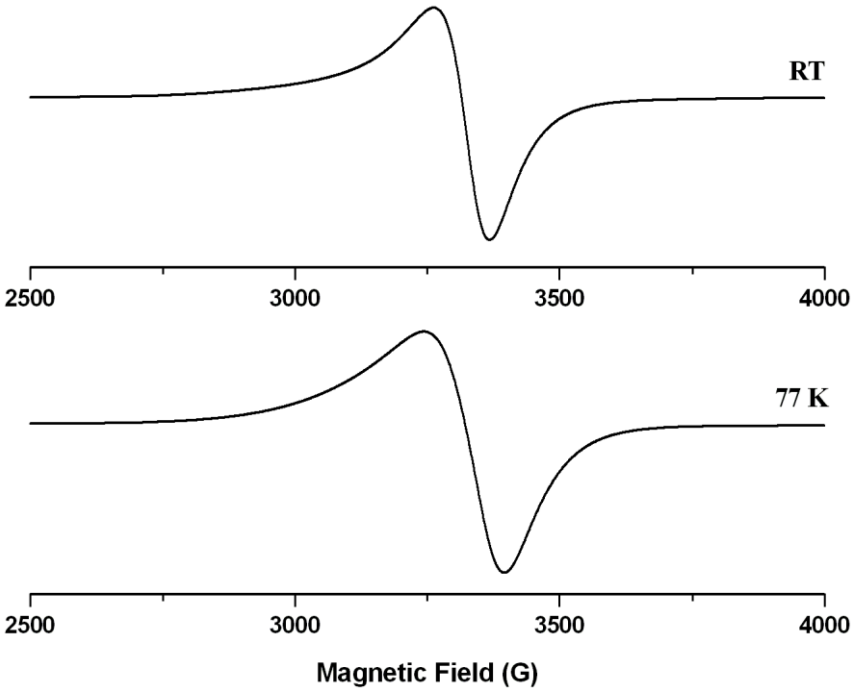

Figure 2.9. EPR spectra at two different temperatures for compound **4** (Cu_2-Nd)

2.6.5. Magnetic measurements

The temperature-dependence of the magnetic susceptibility $\chi_m T$ of compounds **1–4** were measured over the range 3-300 K (Figure 2.10).

The room temperature $\chi_m T$ ($cm^3\ mol^{-1}\ K$) value of the dinuclear compound **1** is 1.21 $cm^3\ mol^{-1}$ K, which is higher than the expected spin-only value of 0.750 $cm^3\ mol^{-1}$ K per dinuclear Cu(II) unit. While decreasing the temperature, the $\chi_m T$ value also slowly decreased and reached to 0.459 $cm^3\ mol^{-1}$ K at 3 K. The decrease is characteristic of an antiferromagnetic exchange interaction between the two Cu(II) ions. The best fit to the Bleaney–Bower equation[13] including temperature independent paramagnetism (TIP) yielded the parameters values $J = -1.12(2)\ cm^{-1}$, $zJ' = -0.30(3)\ cm^{-1}$ $g = 2.171(2)$, TIP = $100 \times 10^{-5}\ cm^3 mol^{-1}$ with a residual of 0.1831×10^{-3}.

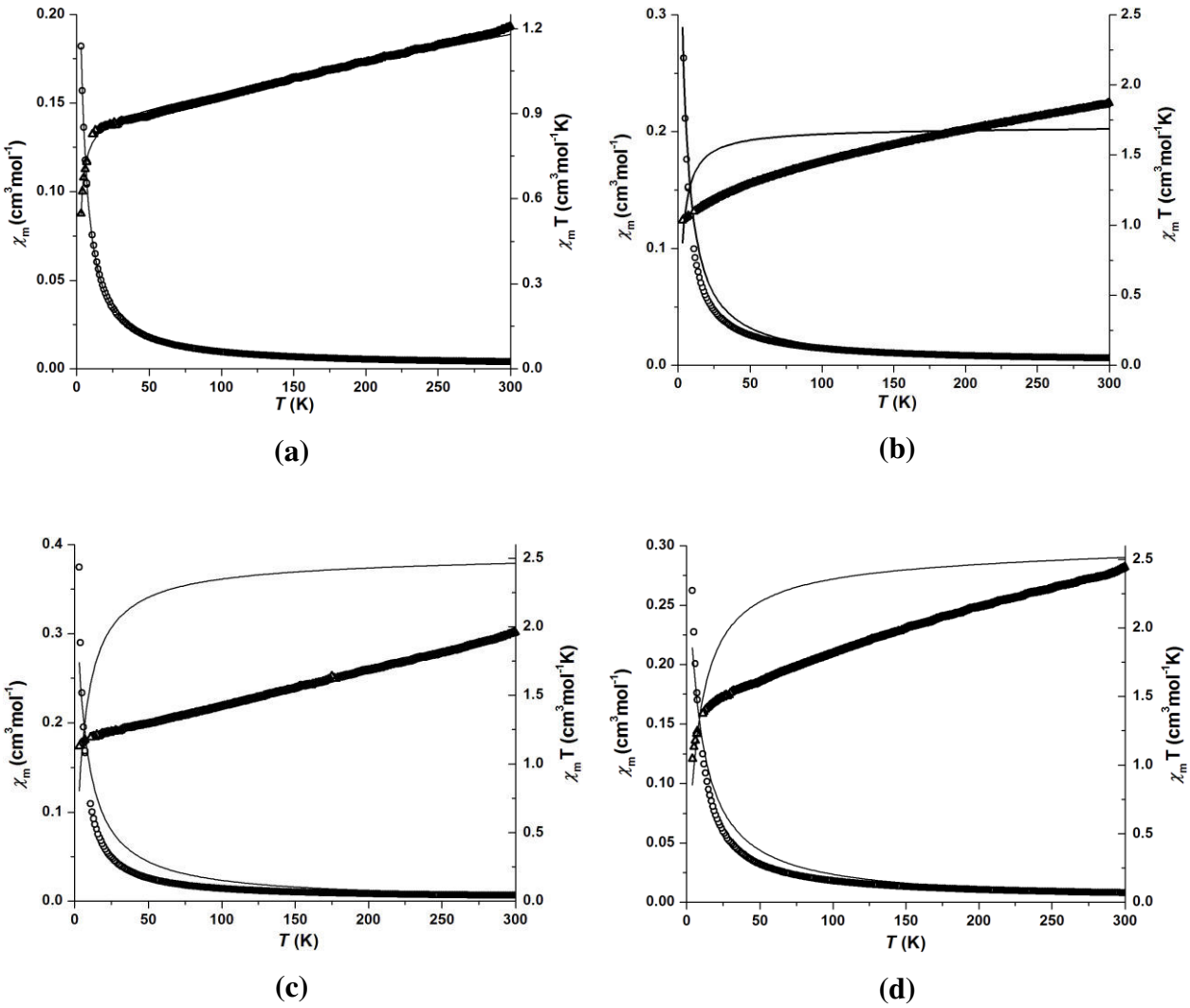

Figure 2.10. Temperature variation of magnetic susceptibility (circle) and $\chi_M T$ product (triangle) of (a) Compound **1**; The solid lines result from a least-square fit to the data of the theoretical values calculated with the Bleaney -Bowers equation including TIP. (b) Compound **2**; (c) Compound **3**; (d) Compound **4**; The solid lines are calculated by assuming free ion magnetic moment for lanthanide complex anion (including spin-orbit interaction)[23] and Bleaney-Bowers equation for the dinuclear Cu(II) complex cation. Molecular field model used for the interaction between Cu(II) and lanthanide sites.

The room temperature $\chi_m T$ (cm^3 mol^{-1} K) value of compound **2** is 1.87 cm^3 mol^{-1} K, which is higher than the expected spin-only value of 1.13 cm^3 mol^{-1} K per dinuclear Cu(II) unit

including Ce^{3+} free ion. While decreasing the temperature, the $\chi_m T$ value also slowly decreased and reached to 1.04 cm^3 mol^{-1} K at 3 K. The decrease is characteristic of an antiferromagnetic exchange interaction between the dinuclear Cu(II) units and the lanthanide ions. The best fit to the modified SUSCEP program using molecular field approximation to model Cu_2^{4+}-Ce^{3+} interaction yielded $zJ' = -0.40(1)$ cm^{-1} with a residual of 0.2833 x 10^{-1}.

The room temperature $\chi_m T$ (cm^3 mol^{-1} K) value of compound **3** is 1.96 cm^3 mol^{-1} K, which is less than the expected spin-only value of 2.25 cm^3 mol^{-1} K per dinuclear Cu(II) unit including Pr^{3+} free ion. While decreasing the temperature, the $\chi_m T$ value also slowly decreased and reached to 1.13 cm^3 mol^{-1} K at 3 K. While decreasing the temperature, the $\chi_m T$ value also slowly decreased and reached to 1.13 cm^3 mol^{-1} K at 3 K. The decrease is characteristic of an antiferromagnetic exchange interaction between the dinuclear Cu(II) units and the lanthanide ions. The best fit to the modified SUSCEP program using molecular field approximation to model Cu_2^{4+}-Pr^{3+} interaction yielded $zJ' = -0.91(3)$ cm^{-1} with a residual of 0.3868 x 10^{-1}.

The room temperature $\chi_m T$ (cm^3 mol^{-1} K) value of compound **4** is 2.45 cm^3 mol^{-1} K, which is less than the expected spin-only value of 2.63 cm^3 mol^{-1} K per dinuclear Cu(II) unit including Nd^{3+} free ion. While decreasing the temperature, the $\chi_m T$ value also slowly decreased and reached to 1.05 cm^3 mol^{-1} K at 3 K. The decrease is characteristic of an antiferromagnetic exchange interaction between the dinuclear Cu(II) units and the lanthanide ions. The best fit to the modified SUSCEP program using molecular field approximation to model Cu_2^{4+}-Nd^{3+} interaction yielded $zJ' = -0.73(4)$ cm^{-1} with a residual of 0.1147.

The fitting for Ce, Pr and Nd compounds is admittedly poor due to difficulties in modeling the exchange involving lanthanide ions.

Table 2.4: Crystallographic data and structure refinement for compounds **5−9**

Param	**5**	**6**	**7**	**8**	**9**
Formula	$C_{40}H_{36}N_{15}O_{23}Cu_2Sm$	$C_{40}H_{36}N_{15}O_{23}Cu_2Eu$	$C_{40}H_{36}N_{15}O_{23}Cu_2Gd$	$C_{40}H_{36}N_{15}O_{23}Cu_2Tb$	$C_{40}H_{36}N_{15}O_{23}Cu_2Dy$
Formula weight	1372.27	1373.88	1379.17	1380.84	1384.42
Crystal system	Triclinic	Triclinic	Triclinic	Triclinic	Triclinic
Space group	$P\bar{1}$	$P\bar{1}$	$P\bar{1}$	$P\bar{1}$	$P\bar{1}$
a (Å)	9.8650(13)	9.8993(6)	9.8975(5)	9.9008(7)	9.9011(9)
b (Å)	14.7550(4)	14.8163(9)	14.6366(7)	14.7912(11)	14.7719(13)
c (Å)	18.2220(9)	18.2885(11)	18.0289(8)	18.2723(13)	18.2502(16)
α (°)	108.420(5)	108.124(10)	107.457(10)	108.106(10)	108.058(10)
β (°)	94.500(4)	94.629(10)	94.374(10)	94.628(10)	94.628(10)
γ (°)	92.836(18)	92.918(10)	93.535(10)	92.920(10)	92.955(10)
V (Å^3)	2501.0(15)	2532.8(3)	2474.4(2)	2526.9(3)	2521.2(4)
Z	2	2	2	2	2
T(K)	298(2)	298(2)	298(2)	298(2)	298(2)
λ (Å)	0.71073	0.71073	0.71073	0.71073	0.71073
D_{cal} (g cm^{-3})	1.822	1.801	1.851	1.815	1.824
μ (mm^{-1})	2.102	2.154	2.278	2.318	2.402
F(000)	1370	1372	1374	1376	1378
Crystal size (mm)	0.24 x 0.20 x 0.16	0.28 x 0.20 x 0.16	0.24 x 0.06 x 0.04	0.28 x 0.20 x 0.12	0.32 x 0.20 x 0.16
θ Range(°)	2.59 – 25.00	1.18 – 25.91	1.19 – 25.00	1.18 – 28.26	1.18 – 28.24
h/k/l indices	-8,11/ -16,17/ -21,21	-12,12/ -18,18/ -22,22	-11,11/ -17,17/ -21,21	-12,12/ -19,19/ -23,23	-12,12/ -19,19/ -24,23
Reflection collected	16659	26210	23657	29455	29316
Unique reflect.[R_{int}]	8793 [0.0385]	9814 [0.0357]	8649 [0.0321]	11733 [0.0354]	11634 [0.0369]
GooF	1.003	1.043	1.044	1.026	1.065
R_1 [I>2σ(I)]	0.0364	0.0320	0.0309	0.0359	0.0359
wR_2	0.0761	0.0853	0.0780	0.0844	0.0844

$w = 1/[\sigma^2(F_0^2) + (AP)^2 + BP]$; where $P = [2F_C^2 + Max(F_0^2, 0)]/3$

2.7. {[Cu(bpy)$_2$(NO$_3$)]$_2$[*Ln*(NO$_3$)$_4$(OH$_2$)$_2$](NO$_3$)} (*Ln* = Sm(5), Eu(6), Gd(7), Tb(8), Dy(9))

2.7.1. Crystal structure of {[Cu(bpy)$_2$(NO$_3$)]$_2$[*Ln*(NO$_3$)$_4$(OH$_2$)$_2$](NO$_3$)} (5-9)

Compounds **5-9** form isomorphous crystals. Crystallographic data and structure refinement details are listed in Table 2.4. Since geometrical parameters of all compounds are similar the selected bond lengths and angles of compound **5** is given in Table 2.5. The asymmetric unit consists of two crystallographically independent [Cu(bpy)$_2$(NO$_3$)]$^+$ cations (Figure 2.11), accompanied by an isolated [*Ln*(NO$_3$)$_4$(OH$_2$)$_2$]$^-$ anion (Figure 2.12) and a non-coordinated NO$_3^-$ ion in the lattice. Both complex cations have the same molecular structure.

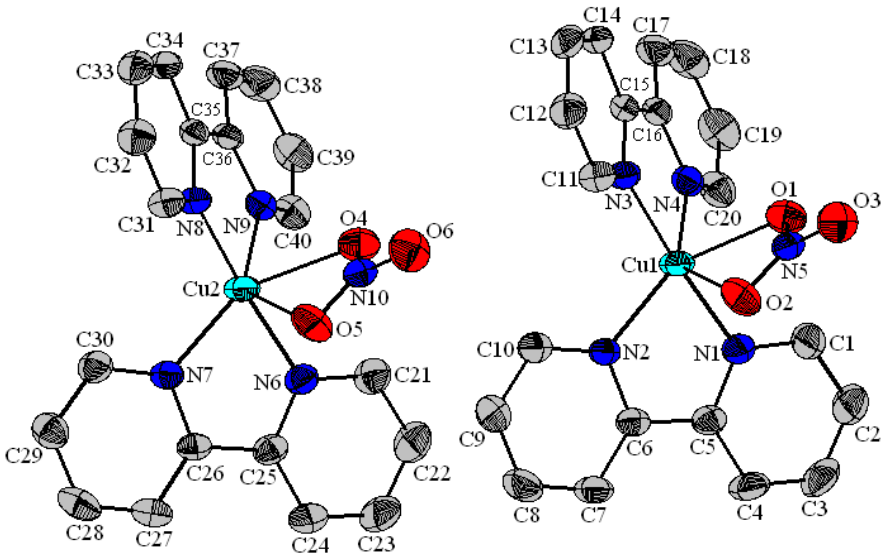

Figure 2.11. Thermal ellipsoid plot of the coordination environment of the complex cation **5**: Atoms are represented as 30% probability ellipsoids. Ring hydrogen atoms have been omitted for clarity.

The stereochemistry of the [Cu(bpy)$_2$(NO$_3$)]$^+$ cation involves *cis*-distorted bicapped square-pyramidal CuN$_4$OO* chromophore with an unsymmetrical chelated nitrato group. The geometry of the CuN$_4$O$_2$ chromophore is basically five coordinated, but with the second O atom of the nitrate ion occupying the sixth coordination position at a distance (Å) > 2.4 [2.723-2.751

(2.748-2.764) to give an unsymmetrically chelated nitrato group, and an unsymmetrical bicapped square-pyramidal (4+1+1*)[24] type coordination. The static structures of CuN_4O_2 chromophore found have been classified by Hathaway based on the types of distortions from the regular *cis*-distorted octahedral geometry.[10] As the large in-plane angles N–Cu–N >120º and the bite angle of O–Cu–O* < 50º, the following CuN_4O_2 chromophore may be described as an unsymmetrical bicapped square-pyramidal (4+1+1*) type coordination rather than *cis*-distorted octahedral geometry. The in-plane Cu-N distances (Å) differ by ΔN = 0.039 (0.042) and Cu-O distances (Å) by ΔO = 0.465 (0.400). The axial angles (º) are almost linear 173.72 (170.14). The moiety of the complex cation, $[Cu(bpy)_2(NO_3)]^+$, is similar to that of the previously reported $\{[Cu(bpy)_2(NO_3)](NO_3)\cdot H_2O\}$ compounds.[9] Molecular dimensions for $[Cu(bpy)_2(NO_3)]^+$ cation are given in Table 2.12.

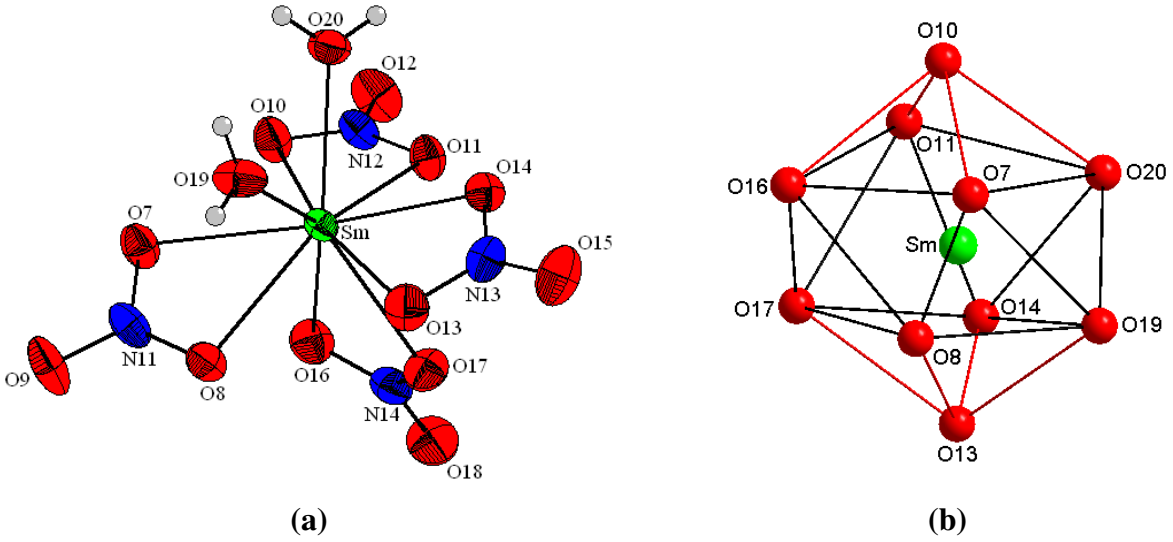

(a) **(b)**

Figure 2.12. (a) The coordination polyhedron of Sm (III) ion. (b) bicapped square antiprism coordination polyhedron of Sm (III) ion in $[Sm(NO_3)_4(OH_2)_2]^-$.

The *Ln*(III) ion is 10-coordinated with eight oxygen atoms from four chelating nitrate ligands and two oxygen atoms from water molecules, forming a distorted bicapped square

antiprism[25] shown in Figure 2.12(b). The *Ln*−O(nitrate) bond lengths (Å) lie in the range 2.452(3)-2.569(3) for **5**; 2.450(2)-2.568(2) for **6**; 2.442(2)-2.565(2) for **7**; 2.424(3)-2.555(3) for **8**; 2.408(2)-2.552(2) for **9**, implying that nitrate ions are unsymmetrically bound to *Ln*(III), probably as the result of coordinated water molecules in the inner coordination sphere. The *Ln*−O(w) bond lengths (Å), 2.398(3)-2.414(3) for **5**; 2.407(3)-2.412(2) for **6**; 2.385(2)-2.388(2) for **7**; 2.382(3)-2.383(3) for **8**; 2.362(2)-2.371(2) for **9**.

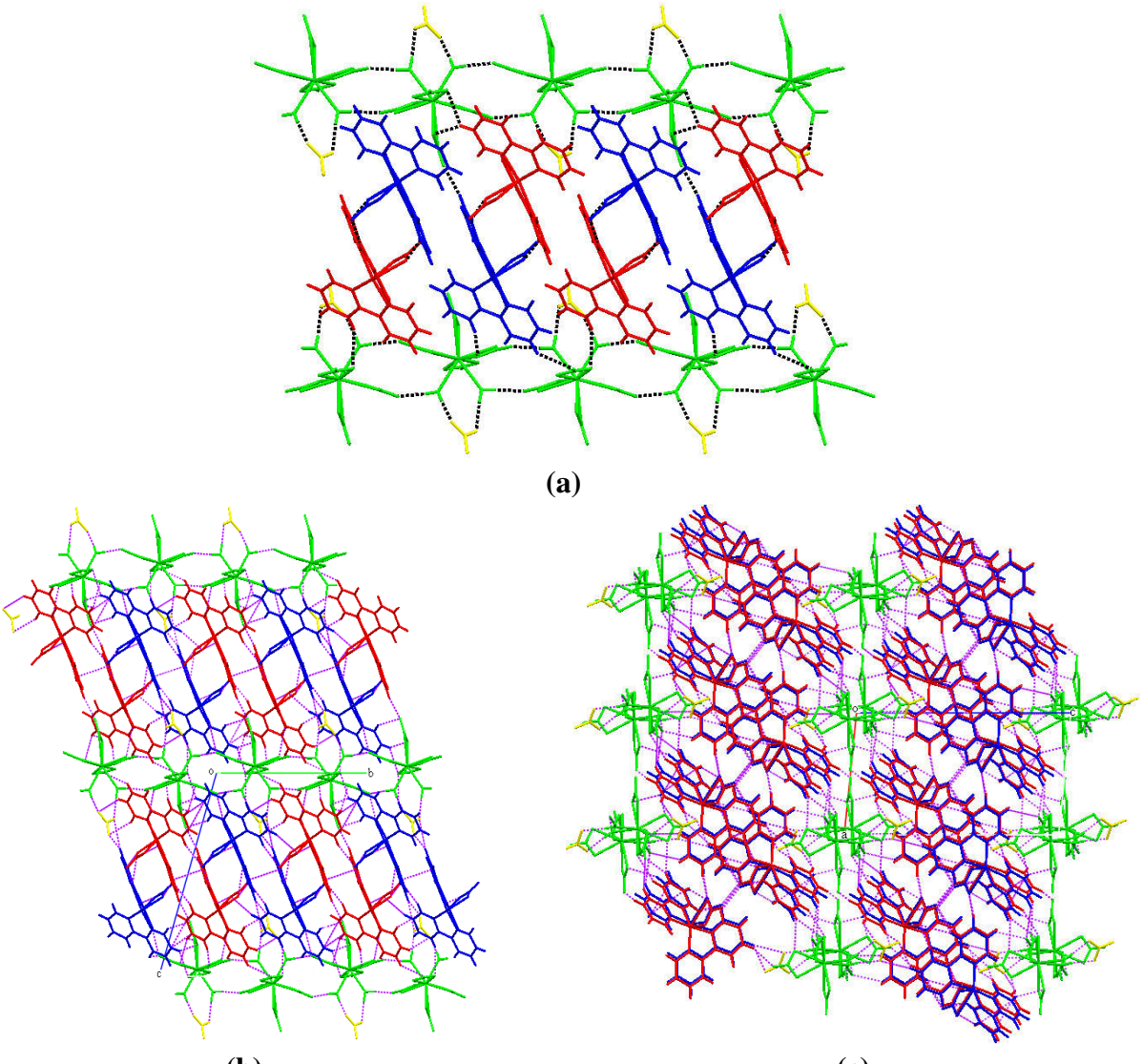

(a) **(b)** **(c)**

Figure 2.13. Views of (a) H-bond interactions of cation and anion units down the *a*-axis in **5** (b) A 3D network down the *a*-axis and (c) down the *b*-axis in **5**

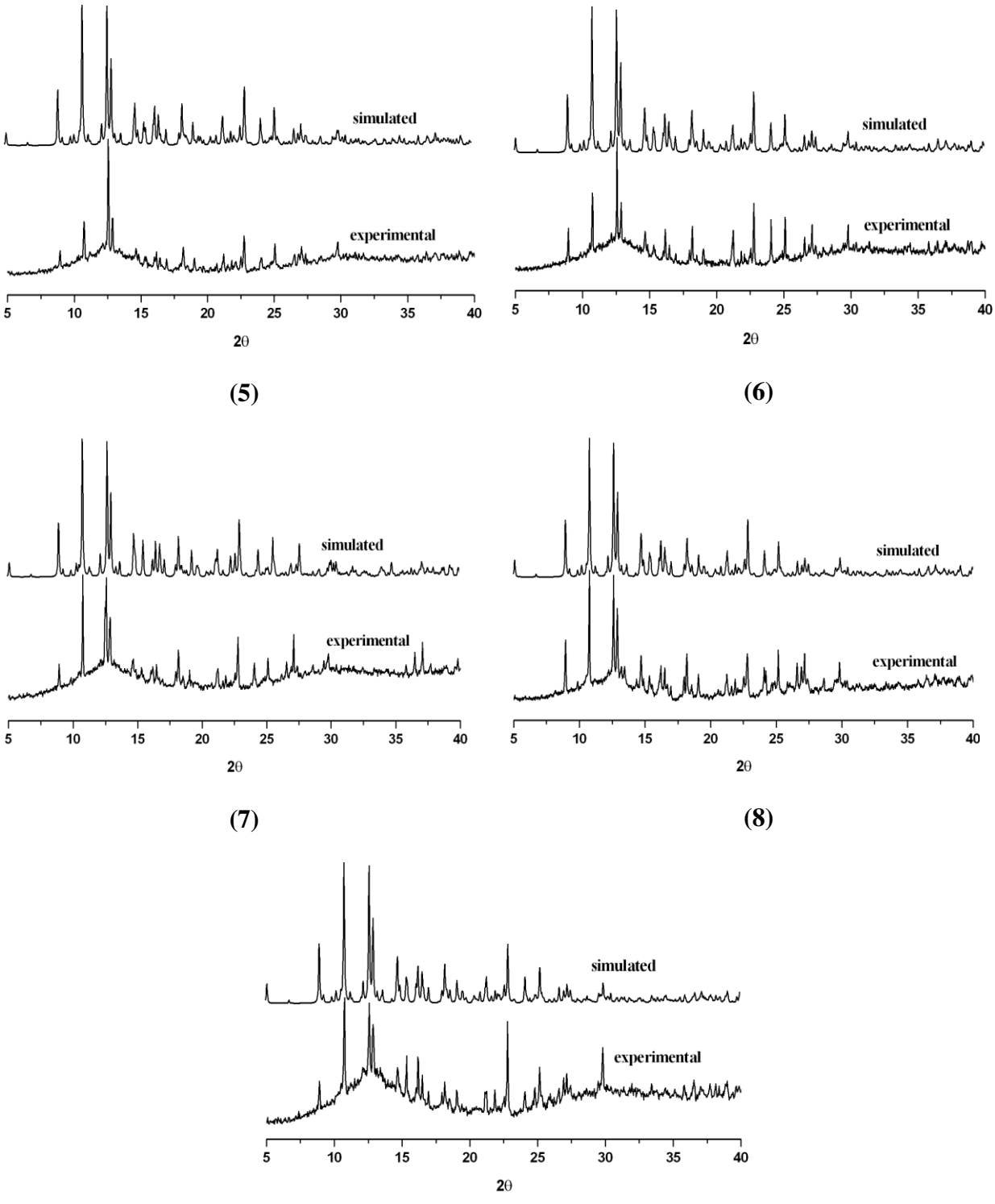

Figure 2.14. Powder X-ray diffraction computer simulated and experimental patterns of complexes **5-9**

Coming to crystal packing of **5**, (Figure 2.13), the two cations form a dimer through H-bond interactions. These dimers are further forming a chain through various C–H···O interactions. Interaction between anions and cation chain leads to a 3D network. Details of the hydrogen bonding are given in Table 2.6. The O–N distance is 1.21(4)-1.27(4) Å, and the O–N–O bond angles range is 115.9(4)-122.4(4)º.

Table 2.5: Selected bond lengths (Å) & bond angles (˚) for $\{[Cu(bpy)_2(NO_3)]_2[Sm(NO_3)_4(OH_2)_2](NO_3)\}$ (**5**)

Cu(1)-N(1)	1.955(3)	Cu(1)-O(1)	2.258(3)	Cu(2)-N(8)	1.956(3)
Cu(1)-N(2)	2.019(3)	Cu(1)-O(2)	2.723(4)	Cu(2)-N(9)	2.063(3)
Cu(1)-N(3)	1.968(3)	Cu(2)-N(6)	1.957(3)	Cu(2)-O(4)	2.348(3)
Cu(1)-N(4)	2.058(4)	Cu(2)-N(7)	2.021(3)	Cu(2)-O(5)	2.748(4)
Sm-O(7)	2.496(3)	Sm-O(11)	2.497(3)	Sm-O(14)	2.452(3)
Sm-O(8)	2.510(3)	Sm-O(19)	2.398(3)	Sm-O(16)	2.569(3)
Sm-O(10)	2.562(3)	Sm-O(13)	2.560(3)	Sm-O(17)	2.482(3)
Sm-O(20)	2.414(3)				
N(5)-O(1)	1.254(4)	N(11)-O(8)	1.257(5)	N(13)-O(15)	1.210(5)
N(5)-O(2)	1.228(4)	N(11)-O(9)	1.221(4)	N(14)-O(16)	1.255(5)
N(5)-O(3)	1.228(4)	N(12)-O(10)	1.247(4)	N(14)-O(17)	1.253(5)
N(10)-O(4)	1.252(4)	N(12)-O(11)	1.252(5)	N(14)-O(18)	1.208(4)
N(10)-O(5)	1.225(4)	N(12)-O(12)	1.225(4)	N(15)-O(21)	1.239(4)
N(10)-O(6)	1.229(4)	N(13)-O(13)	1.249(4)	N(15)-O(22)	1.223(4)
N(11)-O(7)	1.249(5)	N(13)-O(14)	1.268(4)	N(15)-O(23)	1.244(5)
N(1)-Cu(1)-N(2)	80.92(13)	N(3)-Cu(1)-N(4)	80.61(14)	N(7)-Cu(2)-N(8)	100.65(13)
N(1)-Cu(1)-N(3)	173.72(14)	N(3)-Cu(1)-O(1)	84.75(12)	N(7)-Cu(2)-N(9)	142.31(13)
N(1)-Cu(1)-N(4)	101.61(14)	N(3)-Cu(1)-O(2)	87.20(10)	N(7)-Cu(2)-O(4)	131.96(13)
N(1)-Cu(1)-O(1)	89.35(12)	N(4)-Cu(1)-O(1)	90.12(12)	N(7)-Cu(2)-O(5)	83.90(10)
N(1)-Cu(1)-O(2)	87.30(10)	N(4)-Cu(1)-O(2)	139.0(10)	N(8)-Cu(2)-N(9)	80.79(14)
N(2)-Cu(1)-N(3)	101.41(13)	N(6)-Cu(2)-N(7)	80.44(13)	N(8)-Cu(2)-O(4)	84.34(12)
N(2)-Cu(1)-N(4)	138.30(13)	N(6)-Cu(2)-N(8)	170.14(14)	N(8)-Cu(2)-O(5)	86060(10)
O(1)-Cu(1)-O(2)	49.60(10)	N(6)-Cu(2)-N(9)	104.44(14)	N(9)-Cu(2)-O(4)	85.74(12)
N(2)-Cu(1)-O(1)	131.57(13)	N(6)-Cu(2)-O(4)	87.69(13)	N(9)-Cu(2)-O(5)	133.60(10)
N(2)-Cu(1)-O(2)	82.40(10)	N(6)-Cu(2)-O(5)	83.8(10)	O(4)-Cu(2)-O(5)	48.50(10)
O(7)-Sm-O(8)	50.72(10)	O(8)-Sm-O(11)	146.15(10)	O(10)-Sm-O(16)	65.39(11)

O(7)-Sm-O(10)	69.11(10)	O(8)-Sm-O(13)	74.69(11)	O(10)-Sm-O(17)	106.56(11)
O(7)-Sm-O(11)	117.91(10)	O(8)-Sm-O(14)	124.90(11)	O(10)-Sm-O(19)	119.61(13)
O(7)-Sm-O(13)	122.25(10)	O(8)-Sm-O(16)	75.48(10)	O(10)-Sm-O(20)	71.87(13)
O(7)-Sm-O(14)	166.23(9)	O(8)-Sm-O(17)	81.24(11)	O(11)-Sm-O(13)	118.06(11)
O(7)-Sm-O(16)	74.83(11)	O(8)-Sm-O(19)	70.61(12)	O(11)-Sm-O(14)	73.22(10)
O(7)-Sm-O(17)	114.94(11)	O(8)-Sm-O(20)	135.56(12)	O(11)-Sm-O(16)	70.67(10)
O(7)-Sm-O(19)	74.98(13)	O(10)-Sm-O(11)	49.96(10)	O(11)-Sm-O(17)	77.00(11)
O(7)-Sm-O(20)	100.59(13)	O(10)-Sm-O(13)	167.98(10)	O(11)-Sm-O(19)	142.24(12)
O(8)-Sm-O(10)	114.56(11)	O(10)-Sm-O(14)	119.47(10)	O(11)-Sm-O(20)	73.57(12)
O(13)-Sm-O(14)	50.34(10)	O(17)-Sm-O(19)	132.53(13)	O(14)-Sm-O(19)	91.25(12)
O(13)-Sm-O(16)	111.90(12)	O(17)-Sm-O(20)	141.55(12)	O(14)-Sm-O(20)	73.94(13)
O(13)-Sm-O(17)	66.14(11)	O(19)-Sm-O(20)	69.06(13)	O(16)-Sm-O(17)	49.73(11)
O(13)-Sm-O(19)	69.91(13)	O(14)-Sm-O(16)	118.03(11)	O(16)-Sm-O(19)	144.18(12)
O(13)-Sm-O(20)	107.45(13)	O(14)-Sm-O(17)	74.26(10)	O(16)-Sm-O(20)	135.75(12)
O(1)-N(5)-O(2)	118.3(4)	O(7)-N(11)-O(9)	121.2(5)	O(14)-N(13)-O(15)	122.0(4)
O(1)-N(5)-O(3)	119.2(4)	O(8)-N(11)-O(9)	121.2(4)	O(16)-N(14)-O(17)	115.9(4)
O(2)-N(5)-O(3)	122.5(4)	O(10)-N(12)-O(11)	117.6(3)	O(16)-N(14)-O(18)	122.4(5)
O(4)-N(10)-O(5)	118.0(4)	O(10)-N(12)-O(12)	120.9(4)	O(17)-N(14)-O(18)	121.8(5)
O(4)-N(10)-O(6)	119.6(4)	O(11)-N(12)-O(12)	121.5(4)	O(21)-N(15)-O(22)	120.4(4)
O(5)-N(10)-O(6)	122.4(4)	O(13)-N(13)-O(14)	115.9(4)	O(21)-N(15)-O(23)	120.3(4)
O(7)-N(11)-O(8)	117.7(4)	O(13)-N(13)-O(15)	122.0(4)	O(22)-N(15)-O(23)	119.3(4)

2.7.2. Infrared spectra

The band around 3380-3420 cm^{-1} has been assigned to O-H stretching vibration of water. The $\nu_{C=C}$ frequency of the bpy rings at 1605 and 1570 cm^{-1}. The band around 3080 cm^{-1} assigned to the ν_{C-H} frequency. This valve shifted to lower frequencies on complexation. The NO_3^- ions are coordinated to Cu(II) and Ln(III) ions in a bidentate fashion. The nitrate complexes exhibit four bands at 1450-1465 $cm^{-1}(\nu_1)$, 1280-1315 $cm^{-1}(\nu_2)$, 1020-1040 $cm^{-1}(\nu_3)$ and 810-830 cm^{-1} (ν_4) ranges which can be assigned to the vibrational modes of the coordinated (C_{2v}) nitrate groups.[21] The magnitude of splitting of the two bands situated at higher wave numbers $(\nu_1-\nu_2)$ is about ~200 cm^{-1} indicating the coordinate of nitrate ion in an bidentate fashion.

Table 2.6: Intermolecular interaction parameters

*H-bonding for **5***

D-H···A	**D-H(Å)**	**H···A(Å)**	**D···A(°)**	**D-H···A(°)**
C3–H3···O15#1	0.93	2.50	3.30	145
C7–H7···O7#2	0.93	2.48	3.30	148
C18–H18···O2#2	0.93	2.44	3.25	147
C13–H13···O18#3	0.93	2.43	3.33	161
C14–H14···O4#3	0.93	2.40	3.27	155
C34–H34···O1#3	0.93	2.42	3.28	154
C37–H37···O3#3	0.93	2.49	3.33	150
C27–H27···O14#4	0.93	2.50	3.34	150
C38–H38···O5#5	0.93	2.45	3.26	146
O19–H19A···O9#6	0.81	2.04	2.83	163
O19–H19B···O23#6	0.77	190	2.66	172
O20–H20A···O12#6	0.79	2.03	2.82	176
O20–H20B···O21#6	0.78	1.92	2.69	173
C22–H22···O14	0.93	2.50	3.20	133
C22–H22···O17	0.93	2.44	3.25	146

(#1) *–x*, *–y*, 1*–z*; (#2) *–*1+*x*, *y*, *z*; (#3) 1*–x*,1*–y*, 2*–z*; (#4) *–x*, 1*–y*, 1*–z*; (#5) 1+*x*, *y*, *z*; (#6) 1*–x*, *–y*, 1*–z*

*π···π interactions for **5*** (Å)

C8···C22	3.41(8)	C14···C14#1	3.35(7)
C9···C21	3.46(7)	C14···C36#1	3.48(7)
C9···C22	3.37(8)	C34···C34#2	3.40(7)
C13···C14#1	3.49(7)		

(#1) 1*–x,* 1*–y,* 2*–z;* (#2)1*–x,* 2*–y,*2*–z*

2.7.3. Electronic spectra

The diffuse reflectance spectra of **5** (Figure 2.15) consists a broad band approximately at 13480 cm^{-1} and a lower energy shoulder peak at 10700 cm^{-1}. The highest energy band at 13480 cm^{-1} can be assigned to the d_{xy}, $d_{yz} \approx d_{zx} \rightarrow d_{x2-y2}$ where as the band at 10700 cm^{-1} to the $d_z^2 \rightarrow d_{x2-y2}$ transition.[26] Band near 33,000 cm^{-1} is due to ligand-to-metal charge transfer transition, while the band near 41,000 cm^{-1} is associated with intraligand $\pi \rightarrow \pi^*$ excitation.

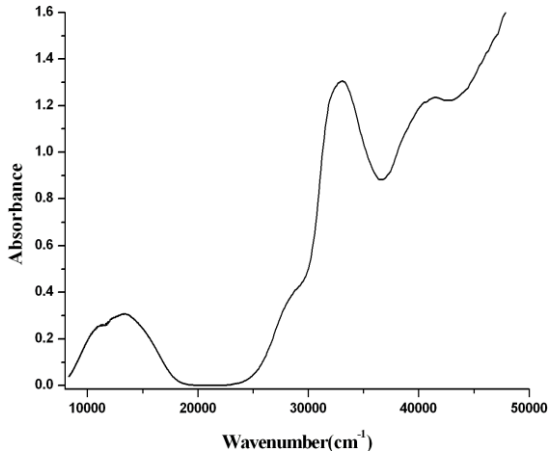

Figure 2.15. Diffuse reflectance spectrum of compound **5**

2.7.4. EPR spectra

The X-band polycrystalline powder EPR spectra of **5-9** were measured at room temperature and liquid nitrogen temperature, respectively. All spectra have been normalized to same microwave frequency (ν = 9.6532 GHz).

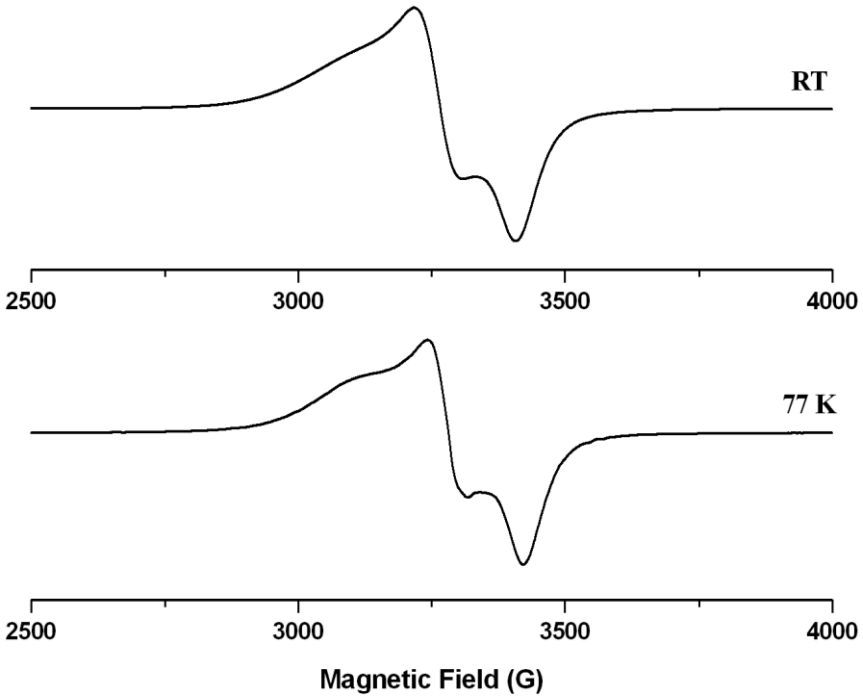

Figure 2.16. Comparison of EPR spectra in two different temperatures for compound **5** (Cu-Sm)

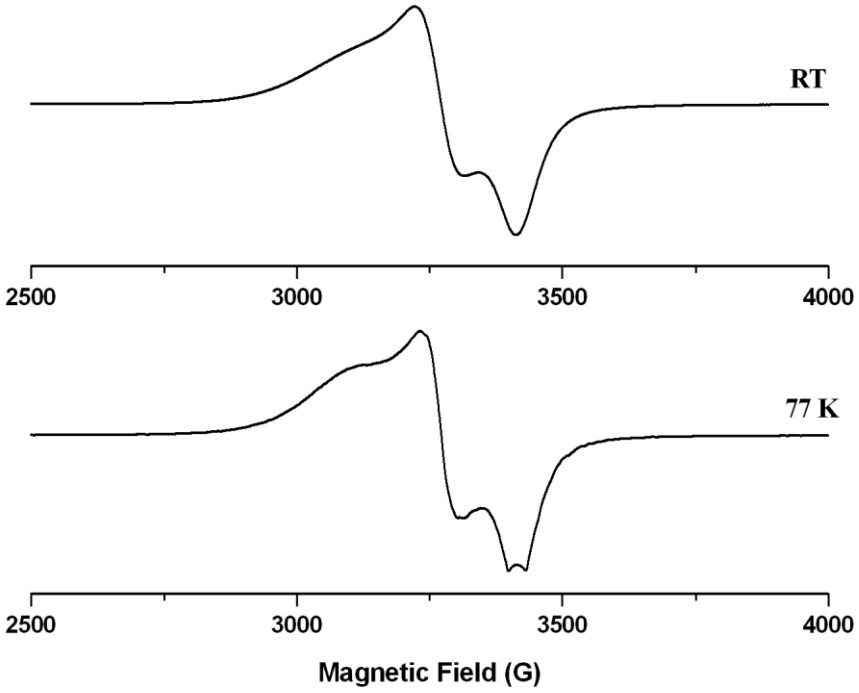

Figure 2.17. Comparison of EPR spectra in two different temperatures for compound **6** (Cu-Eu)

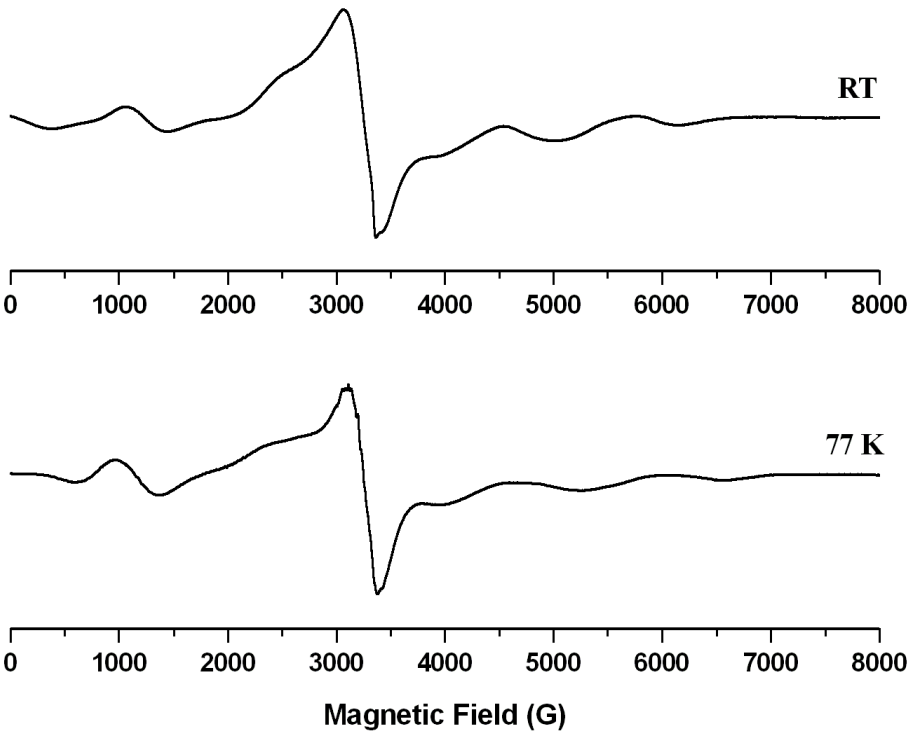

Figure 2.18. Comparison of EPR spectra in two different temperatures for compound **7** (Cu-Gd)

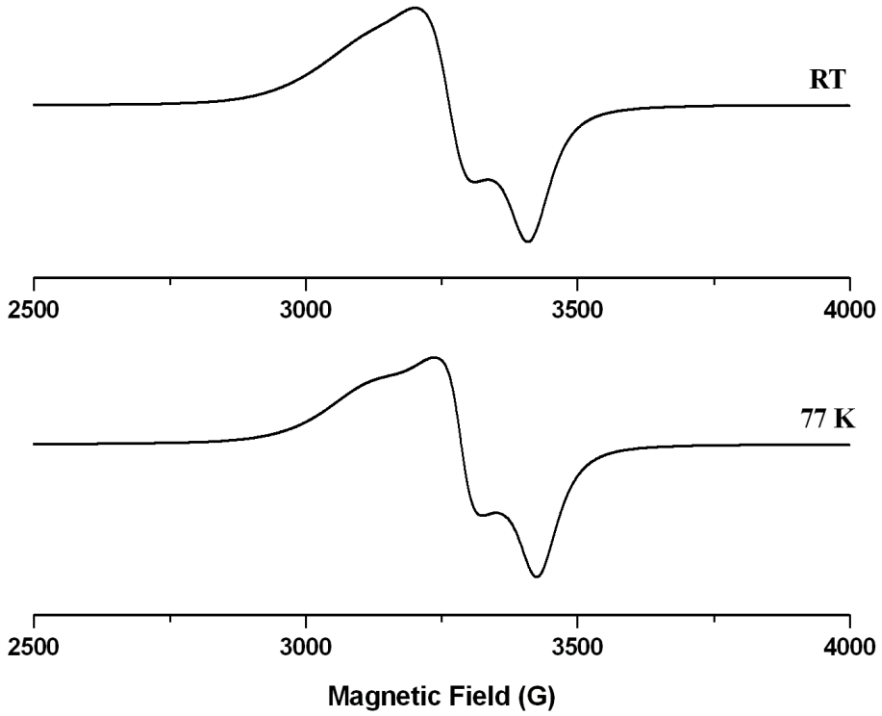

Figure 2.19. Comparison of EPR spectra in two different temperatures for compound **8** (Cu-Tb)

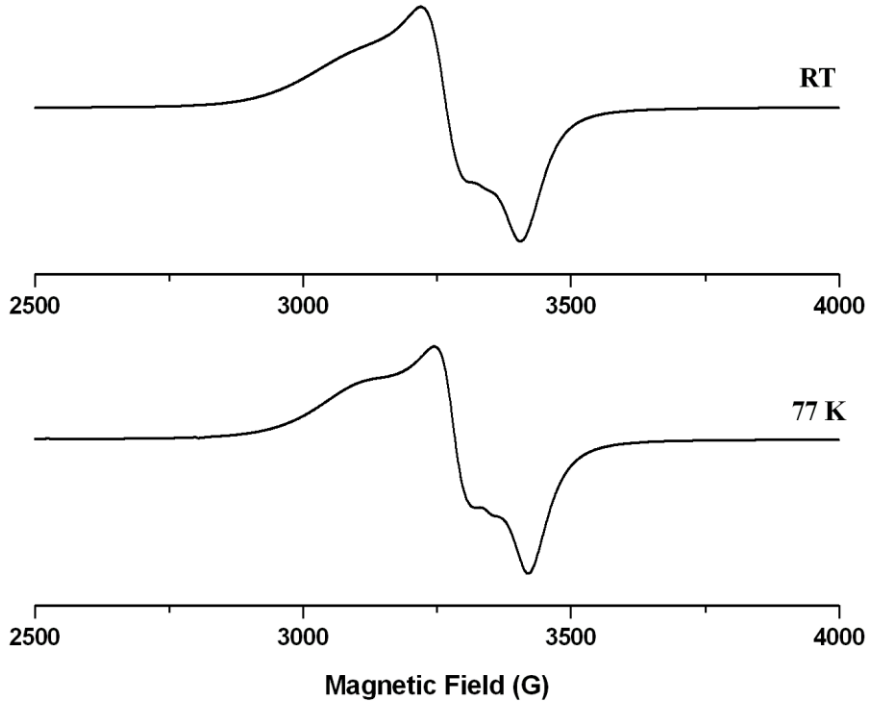

Figure 2.20. Comparison of EPR spectra in two different temperatures for compound **9** (Cu-Dy)

Due to low symmetry of the Cu(II) polyhedron, the spectra are strongly rhombic with $g_1 > g_2 > g_3 > 2.0$ suggesting a d_{x2-y2} ground state.[26] The coupling within the Cu(II) dimers are too weak to lead to exchange averaging of the *g*-values. The g parameters for compound **5** (Figure 2.16), $g_1 = 2.232$, $g_2 = 2.115$, $g_3 = 2.022$ at 298 K and $g_1 = 2.217$, $g_2 = 2.105$, $g_3 = 2.016$ at 77 K; for compound **6** (Figure 2.17), $g_1 = 2.220$, $g_2 = 2.111$, $g_3 = 2.022$ at 298 K and $g_1 = 2.217$, $g_2 = 2.109$, $g_3 = 2.022$ at 77 K; for compound **8** (Figure 2.19), $g_1 = 2.217$, $g_2 = 2.116$, $g_3 = 2.024$ at 298 K and $g_1 = 2.210$, $g_2 = 2.102$, $g_3 = 2.016$ at 77 K; for compound **9** (Figure 2.20), $g_1 = 2.224$, $g_2 = 2.115$, $g_3 = 2.025$ at 298 K and $g_1 = 2.217$, $g_2 = 2.102$, $g_3 = 2.016$ at 77 K. The paramagnetic lanthanide anions do not significantly contribute to the EPR even at 77 K except in the case of Gd^{3+}. Among the ions involved in the present set of compounds, Eu^{3+} has a non-magnetic ground state. The splitting seen at the high field line in the Cu-Eu spectrum is probably due to resolution of the g_3-value corresponding to the chemically different Cu(II) complex cations. In the Cu-Gd spectrum the Cu(II) signal overlaps with the seven line pattern expected due to zero-field splitting in the low symmetry Gd(III) anionic complex (Figure 2.18).

2.8. $[Cu(bpy)_2(NO_3)]_2[Ln(NO_3)_5]$

(*Ln* = Ho (10), Er (11) and Tm (12))

2.8.1. Crystal structure of $\{[Cu(bpy)_2(NO_3)]_2[Ln(NO_3)_5]\}$ (10-12)

Compounds **10-12** form isomorphous crystals. Crystallographic data and structure refinement details are listed in Table 2.7. Since geometrical parameters of all compounds are similar the selected bond lengths and angles of compound **10** are given in Table 2.8. The asymmetric unit consists of two crystallographically independent $[Cu(bpy)_2(NO_3)]^+$ cations (Figure 2.21)

accompanied by an isolated $[Ln(NO_3)_5]^{2-}$ anion (Figure 2.22(a)). Both complex cations have the same molecular structure. The stereochemistry of the $[Cu(bpy)_2(NO_3)]^+$ cation involves distorted octahedral CuN_4O_2 chromophore with pseudo-C_2 symmetry bisecting the nitrate group and passing between the bpy ligands.

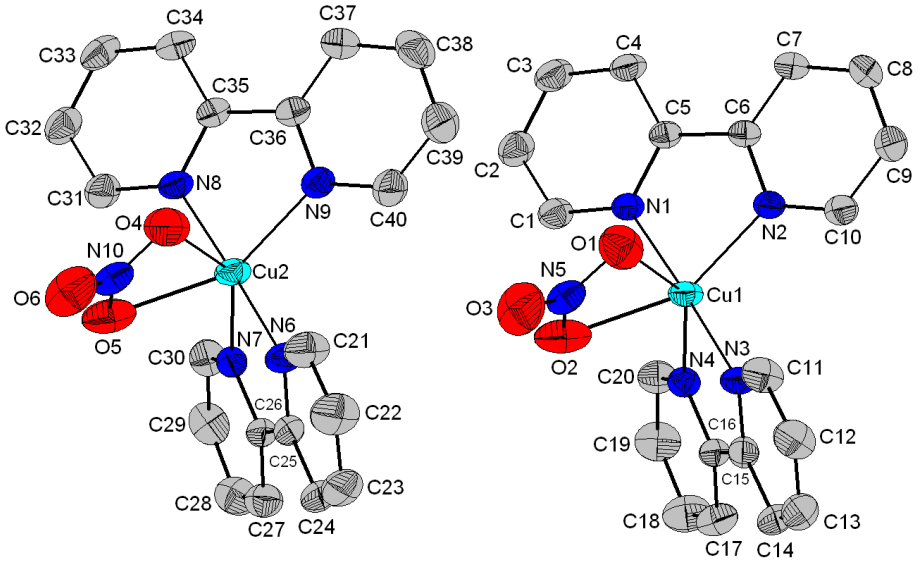

Figure 2.21. Thermal ellipsoid plot of the coordination environment of the complex molecules **10**: Atoms are represented as 30% probability ellipsoids. Ring hydrogen atoms have been omitted for clarity.

The Cu(II) ion is coordinated to the four nitrogen atoms of the two bpy ligands and two oxygen atoms of the coordinated nitrate. The mean in plane Cu-N distances (Å), 2.059 (2.062) is longer than mean out-of-plane Cu-N distance (Å), 1.971 (1.975). One oxygen of nitrate is coordinated to the copper with a distance (Å) 2.353 (2.374) while the other at 2.433 (2.418). The out-of-plane angles (º) are almost linear 176.4 (175.6). The in-plane N-Cu-N angles (º) 127.7 (126.4) and the bite angle (º) of O–Cu–O* < 50 suggesting an intermediate geometry between

the unsymmetrical *cis*-distorted octahedral and the unsymmetrical bicapped square-pyramidal (4+1+1*)[24] type coordination.

The *Ln*(III) ion is 10-coordinated with ten oxygen atoms from five chelating nitrate ligands, forming a distorted bicapped square antiprism[27] (Figure 2.22(b)). The *Ln*−O bond lengths (Å) lie in the range 2.388(4)-2.535(4) for **10**; 2.371(4)-2.527(3) for **11**; 2.360(4)-2.533(4) for **12**. Coming to crystal packing, two complex cations and anions are linked by the various C–H···O interactions to form a 2D network (C14–H14···O5, 2.528(5); C17–H17···O5, 2.596(4); C27–H27···O2, 2.506(4) Å). These are further engaged in cooperative π…π interactions (3.486-3.556 Å) leading to a 3D network structure (Figure 2.23).

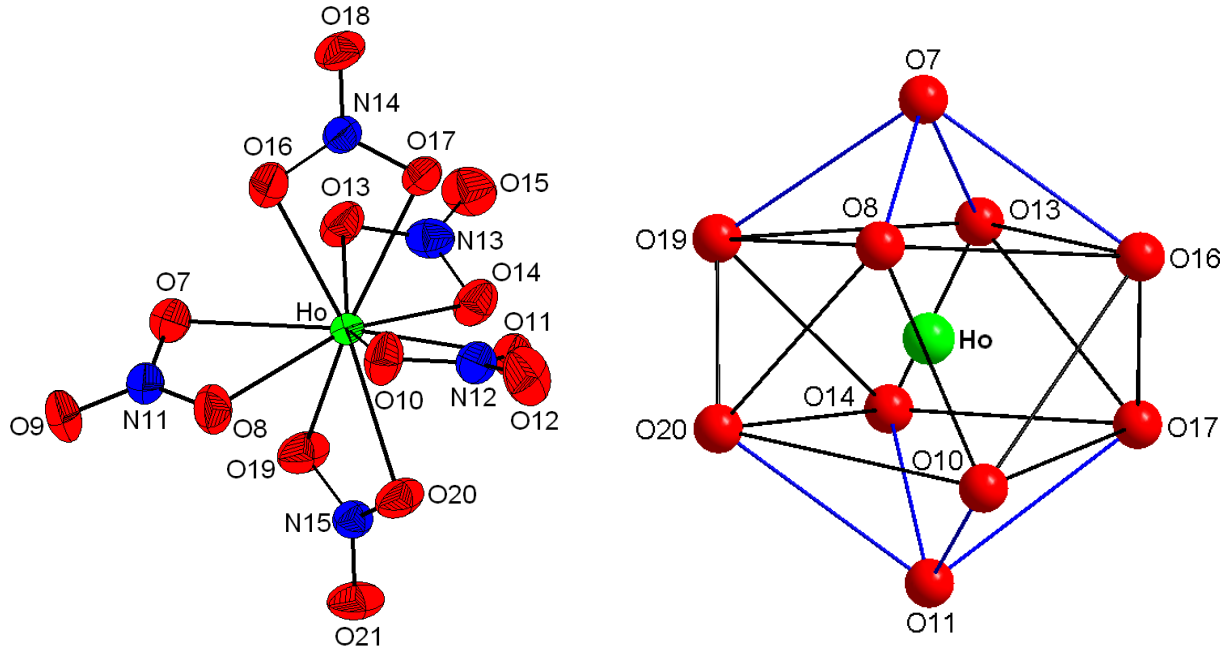

Figure 2.22. (a) The coordination polyhedron of Ho(III) ion. (b) bicapped square antiprism coordination polyhedron of Ho(III) ion in $[Ho(NO_3)_5]^{2-}$.

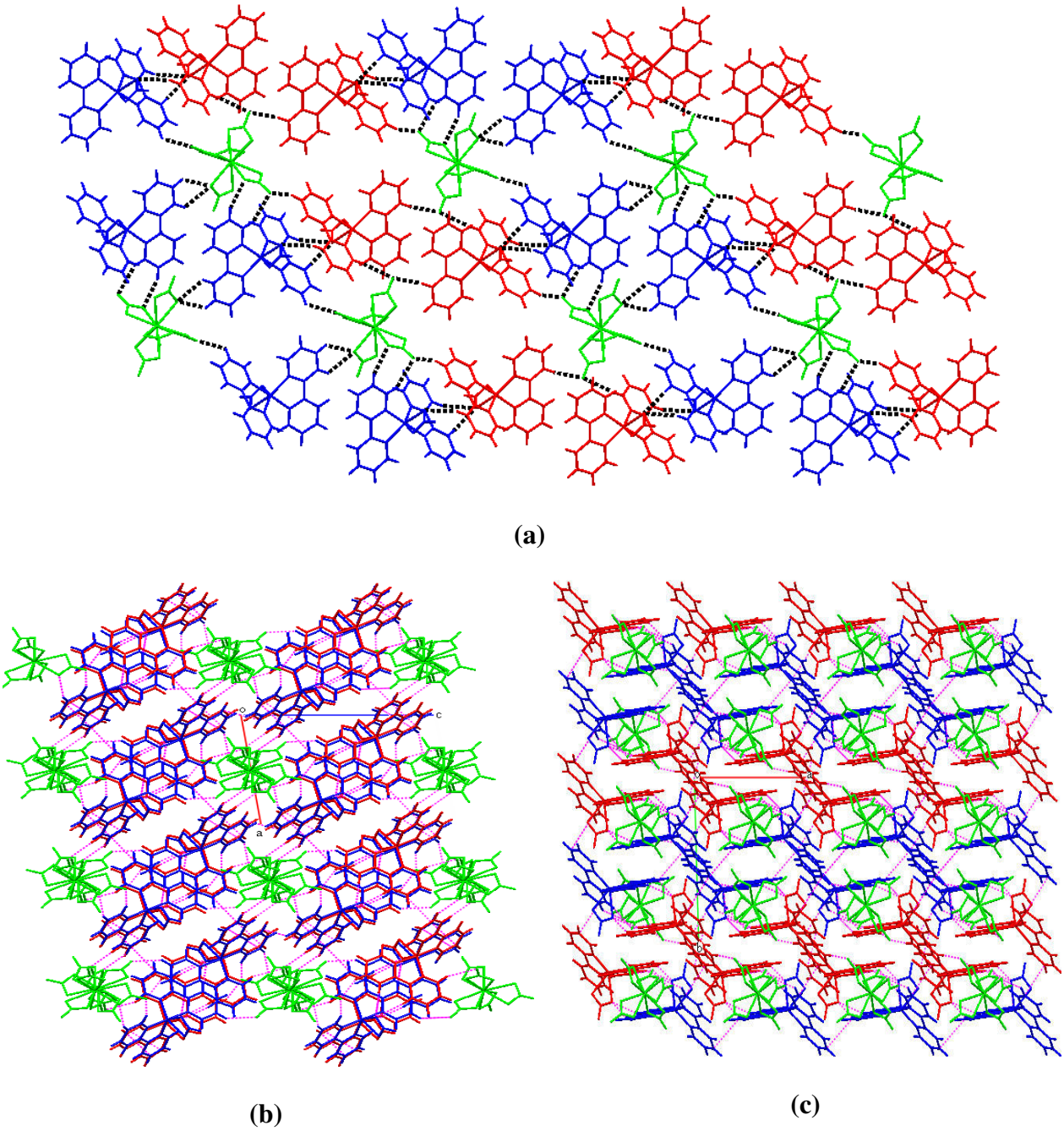

(a)

(b) **(c)**

Figure 2.23. Views of (a) H-bonded 2D network of cation and anion units in **10** (b) A 3D network down the *b*-axis and (c) down the *c*-axis in **10**

Unlike in the case of complexes in the previous section, the two Cu(II) complex cations do not form dimers through H-bond interactions. Details of the hydrogen bonding are given in

Table 2.9. The O–N distance is 1.21(6)-1.29(6) Å, and O–N–O bond angles range is 115.5(4)-123.6(5)º. The three nitrate ligands which are approximately in the same plane constitute three planar sets: O7, O8, O9, N11 and Ho (**I**); O10, O11, O12, N12 and Ho (**II**) and O13, O14, O15, N13 and Ho (**III**). The dihedral angles being 34.1° between **I** and **II**, 29° between **I** and **III**, and 33.6° between **II** and **III**. The remaining two nitrate planar sets: O16, O17, O18, N14 and Ho (**IV**); O19, O20, O21, N15 and Ho (**V**) were nearly perpendicular to these planes (the dihedral angles were 70.7-83.8°). The dihedral angle is 56.5° between **IV** and **V**.

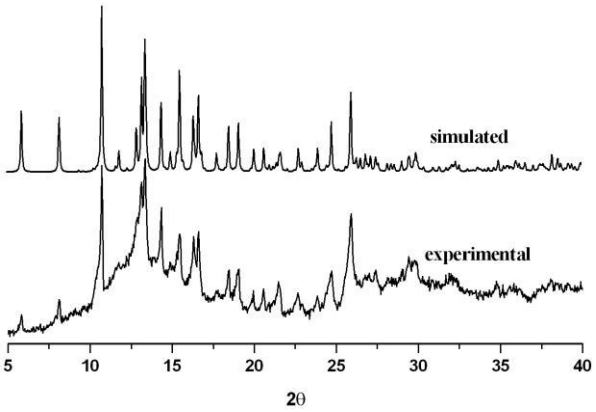

(10)

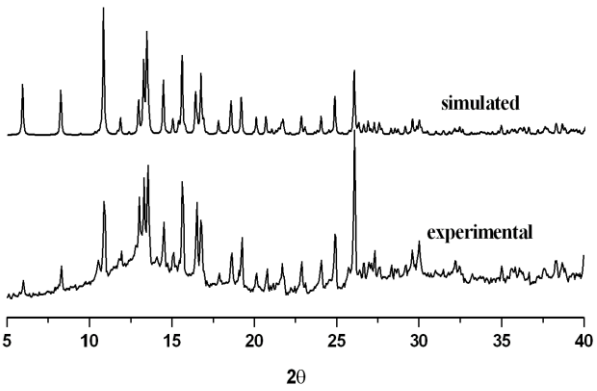

(11)

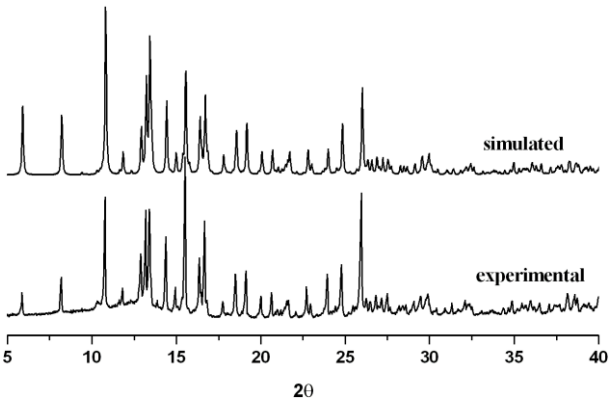

(12)

Figure 2.24. Powder X-ray diffraction computer simulated and experimental patterns of complexes **10-12**

Table 2.7: Crystallographic data and structure refinement for compounds **10−13**

Param	**10**	**11**	**12**	**13**
Formula	$C_{40}H_{32}N_{15}O_{21}Cu_2Ho$	$C_{40}H_{32}N_{15}O_{21}Cu_2Er$	$C_{40}H_{32}Cu_2N_{15}O_{21}Tm$	$C_{40}H_{40}N_{15}O_{26}Cu_2Yb$
Formula weight	1350.82	1353.15	1354.82	1446.99
Crystal system	Triclinic	Triclinic	Triclinic	Triclinic
Space group	$P\bar{1}$	$P\bar{1}$	$P\bar{1}$	$P\bar{1}$
a (Å)	10.939(2)	10.919(2)	10.910(2)	14.557(9)
b (Å)	15.308(3)	15.272(3)	15.280(3)	14.745(9)
c (Å)	16.839(4)	16.843(4)	16.830(3)	15.051(9)
α (˚)	63.808(3)	63.838(3)	63.74(3)	65.421(10)
β (˚)	79.966(3)	80.004(3)	79.95(3)	72.458(10)
γ (˚)	83.917(4)	83.906(4)	83.97(3)	66.842(10)
V (Å^3)	2490.2(9)	2481.2(9)	2476.2(8)	2664.2(3)
Z	2	2	2	2
T(K)	298(2)	298(2)	298(2)	298(2)
λ (Å)	0.71073	0.71073	0.71073	0.71073
D_{calc} (g cm^{-3})	1.802	1.811	1.817	1.804
μ (mm^{-1})	2.515	2.621	2.723	2.634
F(000)	1340	1342	1344	1442
Crystal size (mm)	0.36 x 0.28 x 0.20	0.36 x 0.20 x 0.12	0.40 x 0.28 x 0.12	0.32 x 0.20 x 0.12
θ Range(˚)	1.36 to 25.00	1.36 to 25.00	1.36 to 25.68	1.51 to 26.05
$h/k/l$ indices	-13,13/ -18,18/ -20,20	-12,12/ -18,18/ -20,20	-13,13/ -18,18/ -20,13	-17,17/ -18,18/ -18,18
Reflection collected	24030	23915	18399	27935
Unique reflect., [R_{int}]	8726 [0.0317]	8690 [0.0340]	9322 [0.0276]	10439 [0.0288]
GooF	1.059	1.061	1.093	1.045
R_1 [I>2σ(I)]	0.0513	0.0444	0.0515	0.0329
wR_2	0.1402	0.1181	0.1576	0.0860

$w = 1/[\sigma^2(F_0^2) + (AP)^2 + BP]$; where $P = [2F_C^2 + Max(F_0^2, 0)]/3$

Table 2.8: Selected bond lengths (Å) and bond angles (˚) for $\{[Cu(bpy)_2(NO_3)]_2[Ho(NO_3)_5]\}$

Cu(1)-N(1)	1.974(4)	Cu(1)-O(1)	2.433(6)	Cu(2)-N(8)	1.975(4)
Cu(1)-N(2)	2.053(4)	Cu(1)-O(2)	2.353(6)	Cu(2)-N(9)	2.065(5)
Cu(1)-N(3)	1.968(4)	Cu(2)-N(6)	1.975(4)	Cu(2)-O(4)	2.418(6)
Cu(1)-N(4)	2.066(4)	Cu(2)-N(7)	2.059(5)	Cu(2)-O(5)	2.374(6)
Ho-O(7)	2.525(4)	Ho-O(13)	2.406(4)	Ho-O(17)	2.455(4)
Ho-O(8)	2.388(4)	Ho-O(14)	2.399(4)	Ho-O(19)	2.462(4)
Ho-O(10)	2.397(4)	Ho-O(16)	2.426(4)	Ho-O(20)	2.434(4)
Ho-O(11)	2.535(4)				
N(5)-O(1)	1.237(8)	N(11)-O(8)	1.291(6)	N(13)-O(15)	1.224(6)
N(5)-O(2)	1.236(7)	N(11)-O(9)	1.210(6)	N(14)-O(16)	1.236(6)
N(5)-O(3)	1.201(7)	N(12)-O(10)	1.271(6)	N(14)-O(17)	1.272(6)
N(10)-O(4)	1.240(8)	N(12)-O(11)	1.270(6)	N(14)-O(18)	1.208(6)
N(10)-O(5)	1.238(7)	N(12)-O(12)	1.220(6)	N(15)-O(19)	1.238(6)
N(10)-O(6)	1.191(8)	N(13)-O(13)	1.269(6)	N(15)-O(20)	1.273(6)
N(11)-O(7)	1.279(6)	N(13)-O(14)	1.259(6)	N(15)-O(21)	1.205(6)
N(1)-Cu(1)-N(2)	81.48(17)	N(3)-Cu(1)-O(1)	90.1(2)	N(7)-Cu(2)-N(8)	101.73(18)
N(1)-Cu(1)-N(3)	176.4(2)	N(3)-Cu(1)-O(2)	87.74(19)	N(7)-Cu(2)-N(9)	126.40(19)
N(1)-Cu(1)-N(4)	100.85(17)	N(4)-Cu(1)-O(1)	144.22(19)	N(7)-Cu(2)-O(4)	142.59(19)
N(1)-Cu(1)-O(1)	86.61(19)	N(4)-Cu(1)-O(2)	93.09(17)	N(7)-Cu(2)-O(5)	91.81(17)
N(1)-Cu(1)-O(2)	89.19(17)	O(1)-Cu(1)-O(2)	51.74(18)	N(8)-Cu(2)-N(9)	80.99(19)
N(2)-Cu(1)-N(3)	99.69(18)	N(6)-Cu(2)-N(7)	80.97(19)	N(8)-Cu(2)-O(4)	87.60(19)
N(2)-Cu(1)-N(4)	127.72(17)	N(6)-Cu(2)-N(8)	175.6(2)	N(8)-Cu(2)-O(5)	90.06(18)
N(2)-Cu(1)-O(1)	87.86(19)	N(6)-Cu(2)-N(9)	100.24(19)	N(9)-Cu(2)-O(4)	90.7(2)
N(2)-Cu(1)-O(2)	139.12(17)	N(6)-Cu(2)-O(4)	88.2(2)	N(9)-Cu(2)-O(5)	141.74(18)
N(3)-Cu(1)-N(4)	81.14(17)	N(6)-Cu(2)-O(5)	86.4(2)	O(4)-Cu(2)-O(5)	51.63(18)
O(7)-Ho-O(8)	52.49(15)	O(10)-Ho-O(13)	151.60(17)	O(13)-Ho-O(20)	122.06(15)
O(7)-Ho-O(10)	117.82(15)	O(10)-Ho-O(14)	120.34(14)	O(17)-Ho-O(19)	154.30(16)
O(7)-Ho-O(11)	168.68(15)	O(10)-Ho-O(16)	82.67(16)	O(17)-Ho-O(20)	135.00(13)
O(7)-Ho-O(13)	74.44(16)	O(10)-Ho-O(17)	76.16(15)	O(8)-Ho-O(10)	70.59(15)
O(7)-Ho-O(14)	121.80(15)	O(10)-Ho-O(19)	126.22(15)	O(8)-Ho-O(11)	116.29(14)
O(7)-Ho-O(16)	68.48(15)	O(10)-Ho-O(20)	80.27(15)	O(8)-Ho-O(13)	126.92(15)
O(7)-Ho-O(17)	116.56(14)	O(13)-Ho-O(14)	53.27(14)	O(8)-Ho-O(14)	157.75(17)
O(7)-Ho-O(19)	67.28(15)	O(13)-Ho-O(16)	78.56(16)	O(8)-Ho-O(16)	82.49(16)
O(7)-Ho-O(20)	108.29(15)	O(13)-Ho-O(17)	75.48(15)	O(8)-Ho-O(17)	125.92(15)
O(10)-Ho-O(11)	51.65(13)	O(13)-Ho-O(19)	81.78(15)	O(8)-Ho-O(19)	77.68(17)

O(8)-Ho-O(20)	79.27(17)	O(11)-Ho-O(19)	114.20(14)	O(14)-Ho-O(20)	83.58(16)
O(11)-Ho-O(13)	116.78(14)	O(11)-Ho-O(20)	67.85(13)	O(16)-Ho-O(17)	51.52(13)
O(11)-Ho-O(14)	69.02(14)	O(14)-Ho-O(16)	116.82(15)	O(16)-Ho-O(19)	134.90(15)
O(11)-Ho-O(16)	110.90(14)	O(14)-Ho-O(17)	76.33(14)	O(16)-Ho-O(20)	158.31(18)
O(11)-Ho-O(17)	67.42(13)	O(14)-Ho-O(19)	80.56(16)	O(19)-Ho-O(20)	51.43(13)
O(1)-N(5)-O(2)	115.3(6)	O(7)-N(11)-O(9)	122.8(6)	O(14)-N(13)-O(15)	121.9(5)
O(1)-N(5)-O(3)	122.2(7)	O(8)-N(11)-O(9)	121.5(6)	O(16)-N(14)-O(17)	115.5(4)
O(2)-N(5)-O(3)	122.5(7)	O(10)-N(12)-O(11)	115.7(4)	O(16)-N(14)-O(18)	123.1(5)
O(4)-N(10)-O(5)	114.7(6)	O(10)-N(12)-O(12)	121.9(5)	O(17)-N(14)-O(18)	121.4(5)
O(4)-N(10)-O(6)	121.7(7)	O(11)-N(12)-O(12)	122.4(5)	O(19)-N(15)-O(20)	115.6(4)
O(5)-N(10)-O(6)	123.5(8)	O(13)-N(13)-O(14)	116.9(4)	O(19)-N(15)-O(21)	123.6(5)
O(7)-N(11)-O(8)	115.7(5)	O(13)-N(13)-O(15)	121.2(5)	O(20)-N(15)-O(21)	120.7(5)

Table 2.9: Intermolecular interaction parameters

*H-bonding for **10***

D-H···A	**D-H(Å)**	**H···A(Å)**	**D···A(°)**	**D-H···A(º)**
C1–H1···O9	0.93	2.56	3.39	148
C2–H2···O8	0.93	2.57	3.33	138
C7–H7···O20#1	0.93	2.60	3.18	121
C8–H8···O20#1	0.93	2.53	3.15	124
C12–H12···O12#2	0.93	2.49	3.16	130
C14–H14···O5#3	0.93	2.53	3.38	152
C17–H17···O5#3	0.93	2.60	3.43	149
C23–H23···O9#3	0.93	2.44	3.27	150
C27–H27···O2#3	0.93	2.51	3.36	152
C30–H30···O18#3	0.93	2.54	3.43	160
C37–H37···O18#4	0.93	2.55	3.47	173

(#1) –*x*, –*y*, 1–*z*; (#2) *x*, *y*, 1+*z*; (#3) 1–*x*,1–*y*, –*z*; (#4) 1+*x*, *y*, *z*

*π···π interactions for **10***

C2···C39	3.54(1)	C8···C32#2	3.56(8)
C8···C18#1	3.54(9)	C34···C34#3	3.49(7)

(#1) 1+*x*, *y*, *z*; (#2) *x*, 1+*y*, *z*; (#3) –*x*,1–*y*, 1–*z*

2.8.2. Infrared spectra

The bands around 1610 and 1570 cm^{-1} were assigned to the $\nu_{C=C}$ frequency of the bpy rings. The band around 3070 cm^{-1} assigned to the ν_{C-H} frequency. This valve shifted to lower frequencies on complexation. The NO_3^- ions are coordinated to both Cu(II) and *Ln*(III) ions in a bidentate fashion. The nitrate complexes exhibit four bands at 1440-1460 $cm^{-1}(\nu_1)$, 1270-1320 $cm^{-1}(\nu_2)$, 1020-1040 $cm^{-1}(\nu_3)$ and 810-820 cm^{-1} (ν_4) ranges which can be assigned to the vibrational modes of the coordinated (C_{2v}) nitrate groups.[21] The magnitude of splitting of the two bands situated at higher wave numbers (ν_1-ν_2) is about ~200 cm^{-1} indicating the coordinate of nitrate ion in a bidentate fashion.

2.8.3. Electronic spectra

The diffuse reflectance spectra of complex **10** (Figure 2.25) consists of two almost equally intense peaks approximately 13700 and 10650 cm^{-1} which are similar to those previously reported for [Cu(chelate)$_2$(OXO)]Y complexes involving the *cis*-distorted octahedral CuN_4O_2 chromophore.[26] The highest energy band at 13700 cm^{-1} can be assigned to the d_{xy},$d_{yz} \approx d_{zx} \rightarrow d_{x2-y2}$ transition, where as the band at 10650 cm^{-1} to the $d_z^2 \rightarrow d_{x2-y2}$ transition.

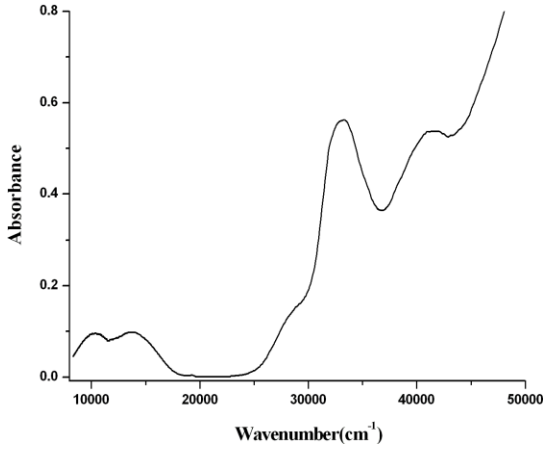

Figure 2.25. Diffuse reflectance spectrum of compound **10**

Band near 33,000 cm^{-1} is due to ligand-to-metal charge transfer transition, while the band near 41,000 cm^{-1} is associated with intraligand $\pi \rightarrow \pi^*$ excitation.

2.8.4. EPR spectra

The X-band polycrystalline powder EPR spectra of **10-12** were measured at room temperature and liquid nitrogen temperature, respectively. All spectra have been normalized to same microwave frequency (ν = 9.6532 GHz). Rhombic spectra are obtained in all cases with $g_1 > g_2 > g_3 > 2.0$ suggesting a d_{x2-y2} ground state.[26] The hyperfine splitting is not resolved. The g parameters for compound **10** (Figure 2.26), g_1 = 2.224, g_2 =2.150, g_3 = 2.016 at 298 K and g_1 = 2.217, g_2 = 2.135, g_3 = 2.011 at 77 K; For **11** (Figure 2.27), g_1 = 2.211, g_2 =2.148, g_3 = 2.014 at 298 K and g_1 = 2.213, g_2 = 2.143, g_3 = 2.019 at 77 K; For **12** (Figure 2.28), g_1 = 2.210, g_2 =2.150, g_3 = 2.017 at 298 K and g_1 = 2.217, g_2 = 2.132, g_3 = 2.008 at 77 K.

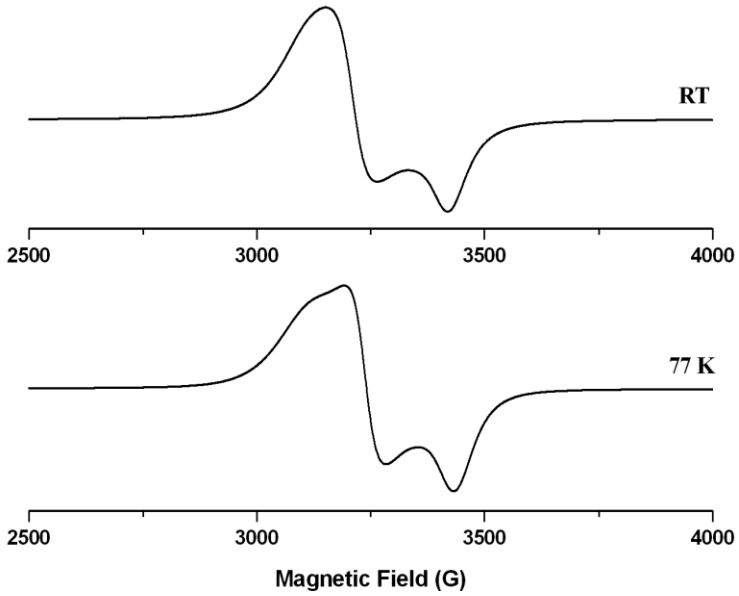

Figure 2.26. Comparison of EPR spectra in two different temperatures for compound **10** (Cu-Ho)

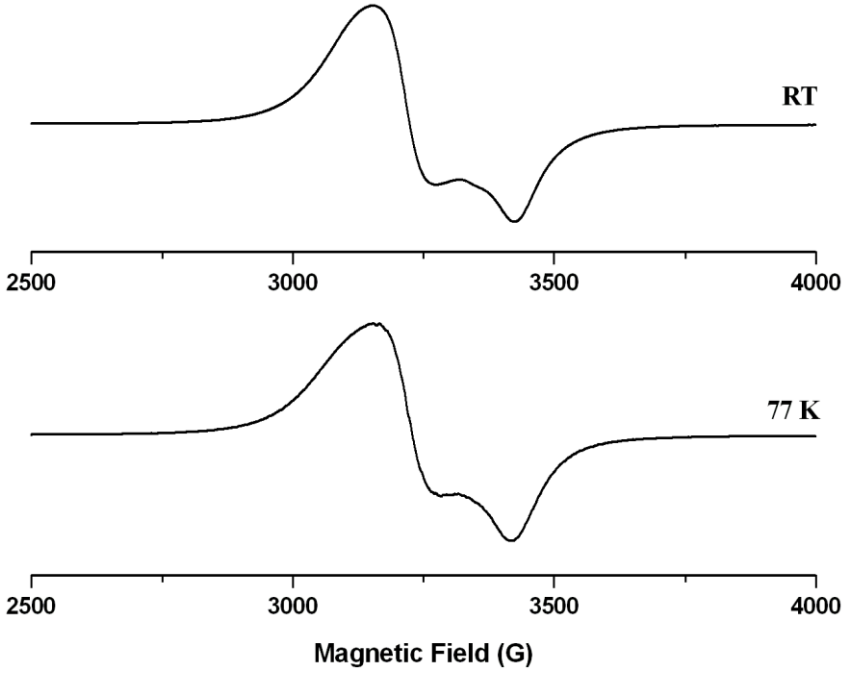

Figure 2.27. Comparison of EPR spectra in two different temperatures for compound **11** (Cu-Er)

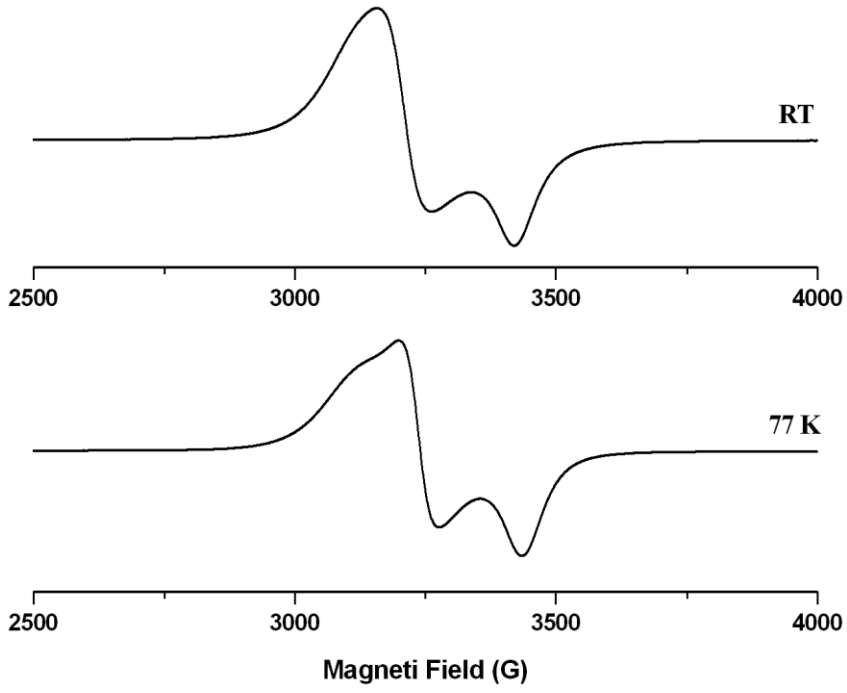

Figure 2.28. Comparison of EPR spectra in two different temperatures for compound **12** (Cu-Tm)

2.9. $[Cu(bpy)_2(NO_3)]_2[Yb(NO_3)_3(OH_2)_3](NO_3)_2{\cdot}2H_2O$

2.9.1. Crystal structure of $\{[Cu(bpy)_2(NO_3)]_2[Yb(NO_3)_3(OH_2)_3](NO_3)_2{\cdot}2H_2O\}$ (13)

The unusual and unexpected neutral molecule $Yb(NO_3)_3(OH_2)_3$ cocrystallising with $[Cu(bpy)_2(NO_3)](NO_3)$ is shown in Figure 2.29. There were two previous reports of $Yb(NO_3)_3(OH_2)_3$ cocrystallising with neutral organic molecules $\{[Yb(NO_3)_3(H_2O)_3]{\cdot}$18-crown-6$\}$[6a] and $\{[Yb(NO_3)_3(H_2O)_3]{\cdot}$TPyP$\cdot$2(benzene)$\}$ (TPyP = *meso*-tetra(4-pyridyl)porphyrin),[6b] but no reports with an inorganic salt. Crystallographic data and structure refinement details are listed in Table 2.7. Selected bond lengths and bond angles are listed in Table 2.10. The stereochemistry of the $[Cu(bpy)_2(NO_3)]$ complex salt involves a distorted octahedral CuN_4O_2 chromophore with pseudo-C_2 symmetry bisecting the nitrate ion and passing between the bpy ligand. The Cu(II) ion is coordinated to the four nitrogen atoms of the two bpy ligands and two oxygen atoms of the coordinated nitrate ion. The mean in plane Cu-N distance 2.075 (2.049) Å is longer than mean out-of-plane Cu-N distance 1.970 (1.965) Å by approximately 0.11 (0.08) Å. One oxygen atom of the nitrate ion is coordinated to copper with a distance 2.397 (2.307) Å, while the other at 2.453 (2.600) Å. The out-of-plane angles are almost linear 178.85 (174.87º). The in-plane N-Cu-N angles 122.90º (128.20º) and the bite angle of O–Cu–O is 50.66º (50.40º) suggesting an intermediate geometry between the unsymmetrical *cis*-distorted octahedral and the unsymmetrical bicapped square-pyramidal (4+1+1*)[24] type coordination.

The Yb(III) ion is 9-coordinated with six oxygen atoms from three chelating nitrate ligands and three oxygen atoms from water molecules, forming a distorted three-face centered trigonal prism[28] (Figure 2.30(b)). As the ionic radii decreases, the number of water molecules increases, and nitrate ions move outside the inner coordination sphere. The O–N distance is 1.205(4)-1.269(4) Å, and the Yb−O(nitrate) bond lengths lie in the range 2.351(2)-2.472(3) Å

(avg. 2.415(3) Å) and Yb−O(w), 2.252(3)-2.296(3) Å (avg. 2.274(3) Å). The O–N–O bond angles range is 115.3(4)-122.8(4)°, and the O–Yb–O bond angles ranging from 52.12(9)-153.77(13)°.

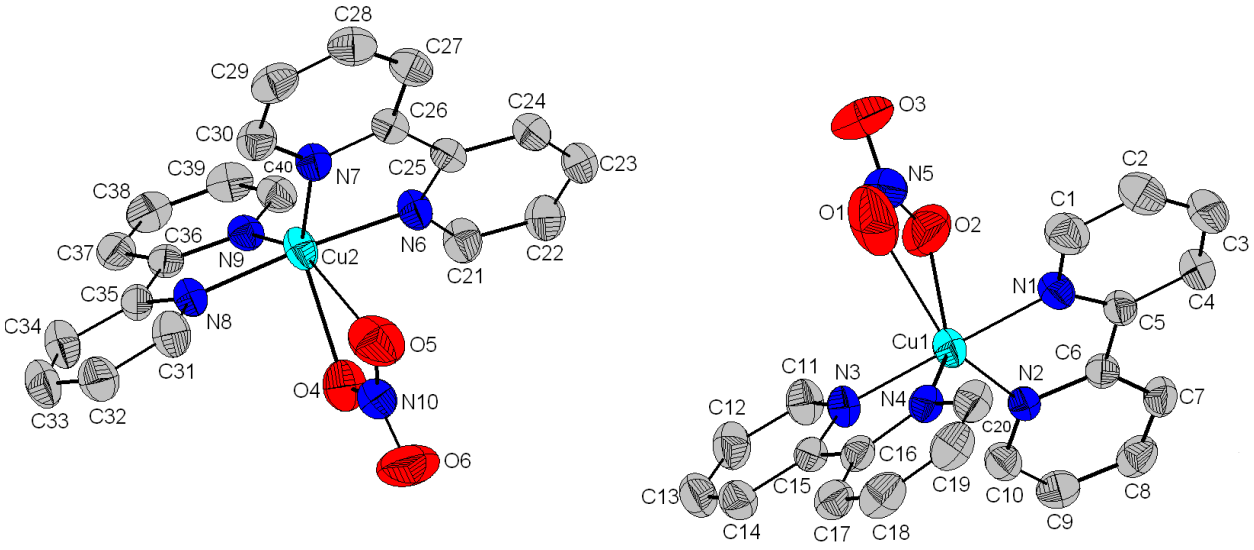

Figure 2.29. Thermal ellipsoid plot of the coordination environment of the complex cation **13**: Atoms are represented as 30% probability ellipsoids. Ring hydrogen atoms have been omitted for clarity.

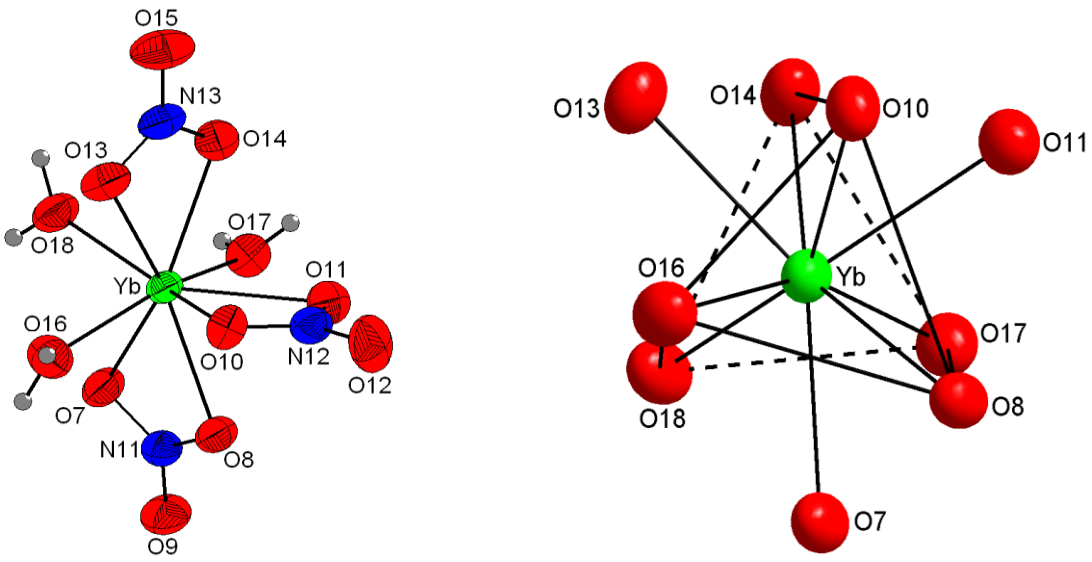

Figure 2.30. (a) The coordination polyhedron of Yb(III) ion. (b) tricapped trigonal prism coordination polyhedron of Yb(III)ion in $[Yb(NO_3)_3(OH_2)_3]$ complex salt.

Table 2.10: Selected bond lengths (Å) and bond angles (˚) for $\{[Cu(bpy)_2(NO_3)]_2[Yb(NO_3)_3(H_2O)_3](NO_3)_2 \cdot 2H_2O\}$

Cu(1)-N(1)	1.972(3)	Cu(2)-N(6)	1.965(3)
Cu(1)-N(2)	2.068(3)	Cu(2)-N(7)	2.044(3)
Cu(1)-N(3)	1.967(3)	Cu(2)-N(8)	1.964(3)
Cu(1)-N(4)	2.082(3)	Cu(2)-N(9)	2.055(3)
Cu(1)-O(1)	2.397(5)	Cu(2)-O(4)	2.307(3)
Cu(1)-O(2)	2.453(5)	Cu(2)-O(5)	2.600(3)
N(1)-Cu(1)-N(2)	80.67(12)	N(6)-Cu(2)-N(7)	80.95(12)
N(1)-Cu(1)-N(3)	178.85(13)	N(6)-Cu(2)-N(8)	174.87(13)
N(1)-Cu(1)-N(4)	100.39(12)	N(6)-Cu(2)-N(9)	100.01(12)
N(1)-Cu(1)-O(1)	90.81(14)	N(6)-Cu(2)-O(4)	90.26(12)
N(1)-Cu(1)-O(2)	83.98(10)	N(6)-Cu(2)-O(5)	83.50(10)
N(2)-Cu(1)-N(3)	98.19(12)	N(7)-Cu(2)-N(8)	102.08(12)
N(2)-Cu(1)-N(4)	122.90(11)	N(7)-Cu(2)-N(9)	128.20(11)
N(2)-Cu(1)-O(1)	138.87(13)	N(7)-Cu(2)-O(4)	131.13(11)
N(2)-Cu(1)-O(2)	88.34(10)	N(7)-Cu(2)-O(5)	80.78(10)
N(3)-Cu(1)-N(4)	80.34(12)	N(8)-Cu(2)-N(9)	81.44(12)
N(3)-Cu(1)-O(1)	89.97(14)	N(8)-Cu(2)-O(4)	84.63(12)
N(3)-Cu(1)-O(2)	95.87(10)	N(8)-Cu(2)-O(5)	92.87(10)
N(4)-Cu(1)-O(1)	98.18(13)	N(9)-Cu(2)-O(4)	100.64(11)
N(4)-Cu(1)-O(2)	148.78(10)	N(9)-Cu(2)-O(5)	151.04(10)
O(1)-Cu(1)-O(2)	50.66(2)	O(4)-Cu(2)-O(5)	50.40(10)
Yb-O(7)	2.420(2)	Yb-O(8)	2.396(2)
Yb-O(10)	2.351(2)	Yb-O(11)	2.472(3)
Yb-O(13)	2.470(3)	Yb-O(14)	2.380(3)
Yb-O(16)	2.273(3)	Yb-O(17)	2.296(3)
Yb-O(18)	2.252(3)		
O(7)-Yb-O(8)	52.75(8)	O(10)-Yb-O(11)	52.48(9)
O(7)-Yb-O(10)	126.39(9)	O(10)-Yb-O(13)	72.31(9)
O(7)-Yb-O(11)	117.57(9)	O(10)-Yb-O(14)	86.96(10)
O(7)-Yb-O(13)	138.00(9)	O(10)-Yb-O(16)	73.91(11)
O(7)-Yb-O(14)	145.79(10)	O(10)-Yb-O(17)	125.00(11)
O(7)-Yb-O(16)	77.68(11)	O(10)-Yb-O(18)	148.05(11)
O(7)-Yb-O(17)	76.22(11)	O(11)-Yb-O(13)	103.51(9)
O(7)-Yb-O(18)	72.65(10)	O(11)-Yb-O(14)	74.38(9)

O(8)-Yb-O(10)	80.05(9)	O(11)-Yb-O(16)	123.14(11)
O(8)-Yb-O(11)	70.00(9)	O(11)-Yb-O(17)	72.53(11)
O(8)-Yb-O(13)	148.15(9)	O(11)-Yb-O(18)	147.98(11)
O(8)-Yb-O(14)	142.75(9)	O(13)-Yb-O(14)	52.12(9)
O(8)-Yb-O(16)	84.91(10)	O(13)-Yb-O(16)	72.63(11)
O(8)-Yb-O(17)	81.47(10)	O(13)-Yb-O(17)	127.54(10)
O(8)-Yb-O(18)	125.21(10)	O(13)-Yb-O(18)	77.26(11)
O(14)-Yb-O(16)	124.73(11)	O(16)-Yb-O(17)	153.77(13)
O(14)-Yb-O(17)	77.80(10)	O(16)-Yb-O(18)	88.06(12)
O(14)-Yb-O(18)	81.94(11)	O(17)-Yb-O(18)	81.73(12)
N(5)-O(1)	1.204(5)	O(1)-N(5)-O(2)	116.5(5)
N(5)-O(2)	1.237(5)	O(1)-N(5)-O(3)	124.9(5)
N(5)-O(3)	1.231(5)	O(2)-N(5)-O(3)	118.5(5)
N(10)-O(4)	1.237(4)	O(4)-N(10)-O(5)	117.5(4)
N(10)-O(5)	1.226(4)	O(4)-N(10)-O(6)	122.1(4)
N(10)-O(6)	1.217(5)	O(5)-N(10)-O(6)	120.5(4)
N(11)-O(7)	1.269(4)	O(7)-N(11)-O(8)	115.3(3)
N(11)-O(8)	1.264(4)	O(7)-N(11)-O(9)	122.5(3)
N(11)-O(9)	1.205(4)	O(8)-N(11)-O(9)	122.2(3)
N(12)-O(10)	1.263(4)	O(10)-N(12)-O(11)	115.6(3)
N(12)-O(11)	1.261(4)	O(10)-N(12)-O(12)	121.6(3)
N(12)-O(12)	1.212(4)	O(11)-N(12)-O(12)	122.8(3)
N(13)-O(13)	1.254(4)	O(13)-N(13)-O(14)	115.8(3)
N(13)-O(14)	1.263(4)	O(13)-N(13)-O(15)	122.3(4)
N(13)-O(15)	1.211(4)	O(14)-N(13)-O(15)	121.9(4)
N(14)-O(19)	1.268(4)	O(19)-N(14)-O(20)	118.0(4)
N(14)-O(20)	1.229(4)	O(19)-N(14)-O(21)	119.0(3)
N(14)-O(21)	1.222(4)	O(20)-N(14)-O(21)	123.0(4)
N(15)-O(22)	1.262(4)	O(22)-N(15)-O(23)	119.8(4)
N(15)-O(23)	1.207(5)	O(22)-N(15)-O(24)	118.1(4)
N(15)-O(24)	1.235(4)	O(23)-N(15)-O(24)	122.1(4)

The two lattice water molecules and the two non-coordinated nitrate ions link the $[Yb(NO_3)_3(OH_2)_3]$ molecules to form an H-bonded tape along the *b*-axis. These negatively charged tapes are interconnected by the Cu(II) cationic complexes through hydrogen bonding

including C–H···O interactions to form a 3D-network (Figure 2.31). The complex cations form dimers via pi-stacking ("aryl embrace") between identical cations. Details of the hydrogen bonding are given in Table 2.11.

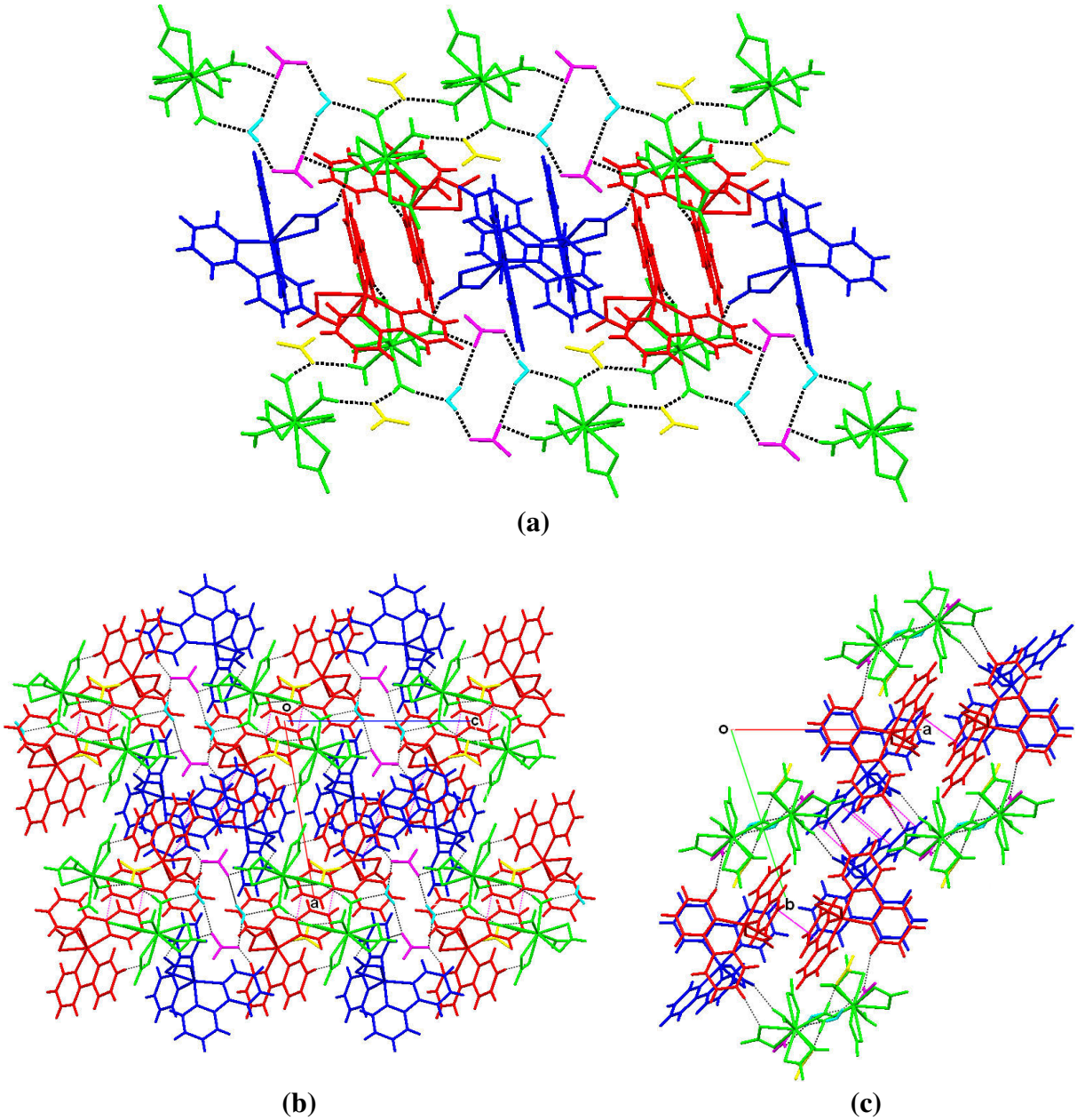

Figure 2.31. (a) H-bonded anionic tapes sandwiching the complex cations in **13** viewed in *ac*-plane (b) molecular packing of **13** in *ac*-plane and (c) molecular packing of **13** in *ab*-plane.

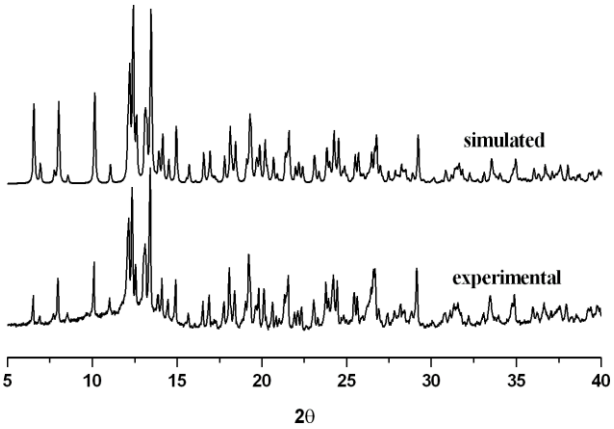

Figure 2.32. Powder X-ray diffraction computer simulated and experimental patterns of complex **13**

Table 2.11: Intermolecular interaction parameters

*H-bonding for **13***

D-H···A	**D-H(Å)**	**H···A(Å)**	**D···A(°)**	**D-H···A(º)**
O16–H16B···O3	0.77	2.15	2.89	161
O17–H17A···O19#1	0.79	1.89	2.67	169
O18–H18A···O19#2	0.84	1.83	2.66	166
O18–H18B···O25#3	0.79	1.88	2.66	168
O25–H25B···O22#3	0.92	2.35	3.22	157
O25–H25A···O24#4	0.78	2.14	2.90	167
C22–H22···O10#5	0.93	2.37	3.30	171
C30–H30···O24#6	0.93	2.38	3.25	156
O16–H16A···O22	0.82	1.88	2.67	161

(#1) *x*, *y*, 1+*z*; (#2)–*x*,1–*y*, 1–*z*; (#3) 1+*x*, *y*, *z*; (#4) 1–*x*,1–*y*, 1–*z*; (#5) 1–*x*, 1–*y*, –*z*; (#6) 1–*x*, –*y*, 1–*z*

*π···π interactions for **13***

C13···C19#1	3.460(8)	C15···C17#1	3.436(7)
C14···C19#1	3.480(9)	C36···C38#2	3.415(7)

(#1) 1–*x*, 1–*y*,1–*z*; (#2) 2–*x*, –*y*,–*z*

2.9.2. Infrared spectra

In the IR spectra the band around 3380-3420 cm^{-1} has been assigned to O-H stretching vibration of water. The $\nu_{C=C}$ frequency of the bpy rings at 1610 and 1569 cm^{-1}. The band around

2975 cm^{-1} assigned to the ν_{C-H} frequency. This valve shifted to lower frequencies on complexation. The NO_3^- ions are coordinated to both Cu(II) and Ln(III) ions in a bidentate fashion. The nitrate complexes exhibit four bands at 1440-1465 $cm^{-1}(\nu_1)$, 1278-1313 $cm^{-1}(\nu_2)$, 1016-1040 $cm^{-1}(\nu_3)$ and 810-830 cm^{-1} (ν_4) ranges which can be assigned to the vibrational modes of the coordinated (C_{2v}) nitrate groups.[21] The magnitude of splitting of the two bands situated at higher wave numbers $(\nu_1\text{-}\nu_2)$ is about ~200 cm^{-1} indicating the coordinate of nitrate ion in an bidentate fashion.

2.9.3. Electronic spectra

Diffuse reflectance spectrum of **13** (Figure 2.33) consists of two almost equally intense peaks approximately 13750 and 10250 cm^{-1}, which are similar to those previously reported for [Cu(chelate)$_2$(OXO)]Y complexes involving the *cis*-distorted octahedral CuN_4O_2 chromophore.[26]

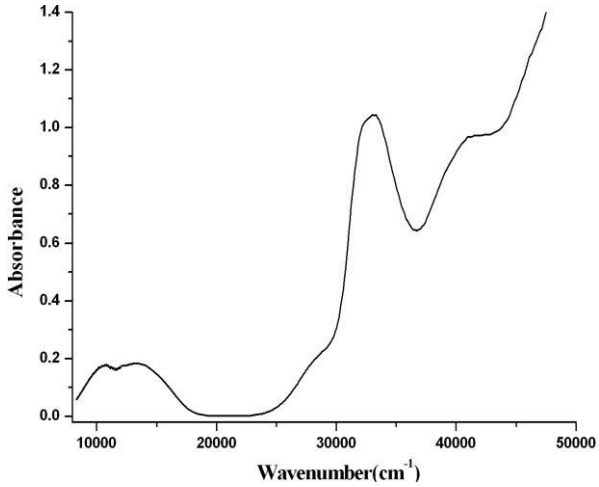

Figure 2.33. Diffuse reflectance spectrum of compound **13**

The highest energy band at 13750 cm^{-1} can be assigned to the d_{xy}, $d_{yz} \approx d_{zx} \rightarrow d_{x2-y2}$ where as the band at 10250 cm^{-1} to the $d_z^2 \rightarrow d_{x2-y2}$ transition. Band near 33,000 cm^{-1} is due to

ligand-to-metal charge transfer transition, while the band near 41,000 cm^{-1} is associated with intraligand $\pi \rightarrow \pi^*$ excitation.

Table 2.12: Molecular dimensions (Å, º) and EPR parameters for $[Cu(bpy)_2(NO_3)]^+$ cation

	5	**6**	**7**	**8**	**9**	**10**	**11**	**12**	**13**	**$[NO_3]_2$[9a]**	**$[PF_6]$[9c]**	**$[ClO_4]$[9b]**
Cu-N	1.96	1.96	1.97	1.98	1.97	1.97	1.97	1.98	1.97	1.98	1.98	1.98
	1.96	1.97	1.97	1.97	1.97	1.96	1.98	1.97	1.98	1.98		
Cu-N*	1.99	1.97	1.97	1.97	1.98	1.97	1.98	1.98	1.97	1.98	1.98	1.99
	1.96	1.98	1.98	1.98	1.97	1.98	1.98	1.97	1.97	1.98		
Cu-No	2.02	2.03	2.03	2.03	2.03	2.05	2.05	2.05	2.05	2.03	2.09	2.05
	2.02	2.03	2.03	2.03	2.03	2.06	2.05	2.05	2.05	2.01		
Cu-No*	2.06	2.07	2.08	2.07	2.06	2.07	2.06	2.06	2.06	2.05	2.03	2.04
	2.06	2.06	2.07	2.06	2.07	2.07	2.06	2.06	2.06	2.04		
Cu-O	2.26	2.36	2.30	2.36	2.27	2.35	2.35	2.36	2.35	2.21	2.15	2.38
	2.35	2.27	2.24	2.27	2.36	2.37	2.37	2.34	2.38	2.26		
Cu-O*	2.72	2.75	2.76	2.76	2.73	2.43	2.43	2.41	2.44	2.84	2.74	2.58
	2.75	2.74	2.75	2.73	2.76	2.42	2.42	2.43	2.42	2.86		
No-Cu-No*	138	142	142	142	139	128	128	127	128	136	126	136
	142	139	139	139	143	126	126	128	127	141		
O-Cu-O*	50	48	50	48	50	52	52	52	52	49	49	52
	49	49	50	49	49	52	52	51	52	48		
ΔO	0.40	0.40	0.47	0.40	0.40	0.04	0.05	0.06	0.06	0.63	0.60	0.20
	0.47	0.47	0.51	0.46	0.46	0.08	0.08	0.09	0.29	0.60		
g_1 (298 K)	2.232	2.220	-	2.217	2.224	2.224	2.211	2.210	2.239	-	-	-
(77 K)	2.217	2.217		2.210	2.217	2.217	2.213	2.217	2.217			
g_2 (298K)	2.115	2.111	-	2.116	2.115	2.150	2.148	2.150	2.137	-	-	-
(77K)	2.105	2.109		2.102	2.102	2.135	2.143	2.132	2.122			
g_3 (298 K)	2.022	2.022	-	2.024	2.025	2.016	2.014	2.017	2.031	-	-	-
(77 K)	2.016	2.022		2.016	2.016	2.011	2.019	2.008	2.019			

No denotes N trans to an O atom; * denotes the loosely coordinated axial O atom, the axial N atom trans to it and the second (equatorial) N atom within the same bpy ligand (Figure 2.35).

2.9.4. EPR spectra

The X-band polycrystalline-powder EPR spectrum of **13** was measured at room temperature and liquid nitrogen temperature, respectively. The rhombic components are poorly resolved in

this case probably because of the greater difference between the two Cu(II) complex cations (Figure 2.34).

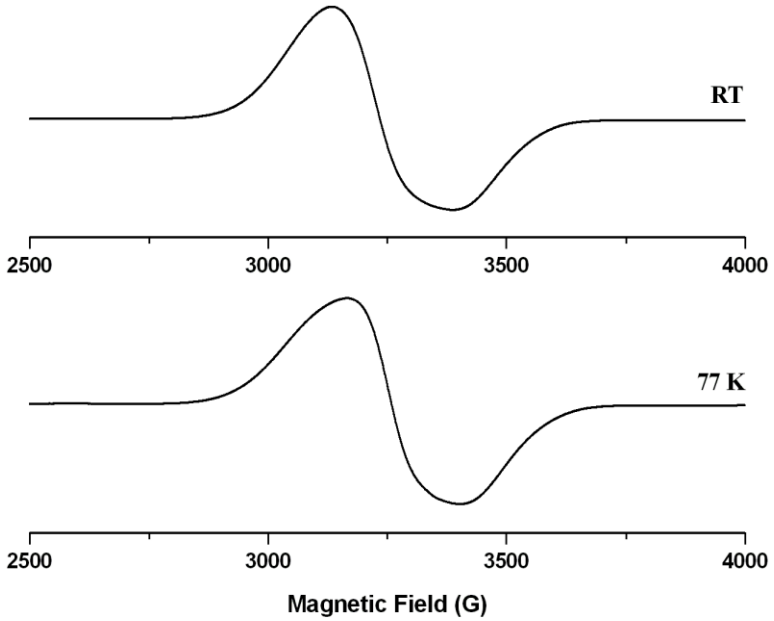

Figure 2.34. Comparison of EPR spectra in two different temperatures for compound **13** (Cu-Yb)

2.10. Nitrate coordination modes

In compounds described above, the nitrate group exhibits different types of coordinating modes, namely unidentate O bridging, unidentate, symmetrical and unsymmetrical chelating bidentate mode.

The values of Kleywegts' criteria[29] (Table 2.13) to discriminate between the various nitrate co-ordination modes. The criteria concluded that d_2-d_1 and θ_1-θ_2 yielded to a distinct and consistentent classification of nitrate ions in three groups. In the case of **5-9**, d_2-d_1 = 0.474 (0.412) Å and θ_1-θ_2 = 22.00 (18.93º) are intermediate between unidentate and unsymmetrical bidentate coordination of nitrate ions. For **10-13**, d_2-d_1 = 0.051 (0.136) Å and θ_1-θ_2 = 3.99 (2.21º) are of bidentate coordination mode.

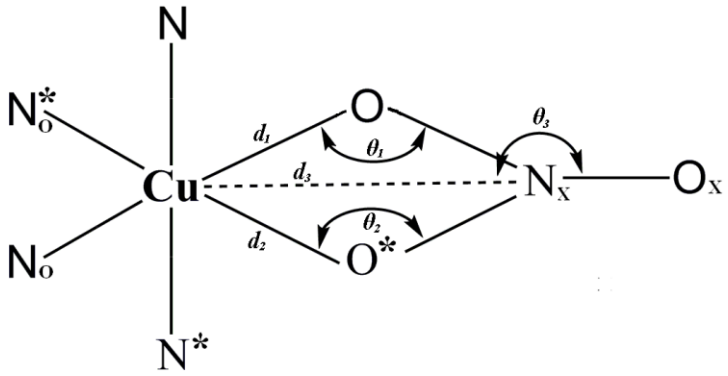

Figure 2.35. Representation of a coordination mode of nitrate ion

Table 2.13: Kleywegts criteria values (Å, º) to discriminate between various nitrate coordination modes

	unidentate	unsymmetrical bidentate	bidentate
d2-d1	> 0.6	0.3-0.6	< 0.3
d3-d2	< 0.1	0.1-0.2	> 0.2
θ_1-θ_2	> 28	14-28	< 14
θ_3	< 162	162-168	> 168

2.11. Conclusions

(1) All lanthanides (excluding Pm) are shown to form crystalline complexes of essentially the same stoichiometry (Cu^{2+} : Ln^{3+} : bpy : NO_3^- = 2 : 1 : 4 : 7, as in the preparative solution made in acetonitrile). In the case of the middle *Ln*'s, there is one free nitrate, while among the late *Ln*'s Yb has two free nitrate ions. In the case of early *Ln*'s, the *Ln* ion takes up six nitrate ions leaving only one nitrate to be shared by two Cu^{2+} ions.

(2) The coordination number shows the expected trend: early *Ln*: 12; middle *Ln*: 10; late *Ln*: 10 or 9.

(3) Regarding the number of aquo-ligands in the coordination sphere of *Ln*, no regular trend is observed: early *Ln*: nil; middle *Ln*: 2; late *Ln*: nil or 3.

(4) It is remarkable that the crystals do not incorporate any lattice water molecules (except Yb). This would mean that chelating or bridging nitrate ions are poor H-bond acceptors. In fact for both early as well as late *Ln* (exept Yb) only weak H-bonding interactions (C-H..O) are possible. In cases where there are free nitrate ions, there are water molecules: coordinated in the case of middle *Ln*; coordinated as well as lattice water molecules (in the case of Yb).

(5) The Yb complex is special in the sense that a neutral *Ln* complex is cocrystallised with a Cu(II) complex salt. It is not obvious why this does not happen with some other lanthanides as well even though several *Ln*'s (Nd, Gd, Tb, Dy, Yb) do form cocrystals of $Ln(NO_3)_3(H_2O)_{2/3}$ with neutral organic molecules like tetrapyridylporphyrin.[6]

(6) Compounds **1** – **4** (La, Ce, Pr, Nd) represent the first examples of crystals containing dinuclear Cu(II) complex having only monoatomic nitrate bridge. The exchange coupling within the dimeric unit is weakly antiferromagnetic. In the case of paramagnetic lanthanide systems the molecular field of the anions is also weakly antiferromagnetic.

(7) The EPR spectra of all the complexes (except Gd) show only signals from Cu^{2+} down to 77 K and these indicate the magnetically concentrated nature of these compounds.

2.12. References

1. (a) M. Evangelisti and E. K. Brechin, *Dalton Trans.*, **2010**, *39*, 4672; (b) M. Holynska, D. Premuzic, I. -R. Jean, W. Wernsdorfer, R. Clerac, S. Dehnen, *Chem.–Eur. J.*, **2011**, *17*, 9605; (c) G. Rigaux, R. Inglis, S. Morrison, A. Prescimone, C. Cadiou, M. Evangelisti, E. K. Brechin, *Dalton Trans.*, **2011**, *40*, 4797; (d) M. Orfanoudaki, I. Tamiolakis, M. Siczek, T. Lis, G. S. Armatas, S. A. Pergantis, C. J. Milios, *Dalton Trans.*, **2011**, *40*, 4793; (e) E. Colacio, J. Ruiz-Sanchez, F. J. White, E. K. Brechin, *Inorg. Chem.*, **2011**, *50*, 7268; (f) G.

J. Sopasis, A. B. Canaj, A. Philippidis, M. Siczek, T. Lis, J. R. O'Brien, M. M. Antonakis, S. A. Pergantis, C. J. Milios, *Inorg. Chem.*, **2012**, *51*, 5911.

2. L. Puntus, K. Lyssenko, *J. Rare Earths*, **2008**, *2*, 146; (b) D. J. Evans, P. C. Junk, M. K. Smith, *New J. Chem.*, **2002**, *26*, 1043; (c) A. G. Matveeva, Z. A. Starikova, R. R. Aysin, R. S. Skazov, S. V. Matveev, G. I. Timofeeva, M. P. Passechnik, E. E. Nifantev, *Polyhedron*, **2013**, *61*, 172.
3. (a) S. Lipstman, I. Goldberg, *Cryst. Growth Des.*, **2010**, *10*, 1823; (b) L. Zhang, Y. Zhou, L. Xu, Z. Yu, I. A. Razak, S. Chantrapromma, H. K. Fun, X. You, *Inorg. Chem. Commu*, **2001**, *4*, 368; (c) T. Otsuka, H. Cui, A. Kobayashi, Y. Misaki, H. Kobayashiz, *J. Solid State Chem.*, **2002**, *168*, 444.
4. (a) S. Nayak, G. Novitchi, M. Hołynska, S. Dehnen, *Eur. J. Inorg. Chem.,* **2014**, 3065; (b) C. -B. Ma, M. –Q. Hu, H. Chen, C. –N. Chen, Q. –T. Liu, *Eur. J. Inorg. Chem.,* **2011**, 5043; (c) F. Benetollo, P. Di Bernardo, S. Tamburini , P. A. Vigato, P. Zanonato, *Inorg. Chem. Commun.*, **2008**, *11*, 246.
5. (a) L. Jianmin, Z. Huaqianga, Z. Yugen, C. Jinhua, K. Yanxiong, W. Quanming, W. Xintao. *Cryst. Res. Technol.*, **1999**, *34*, 925; (b) J. –P. Costes, C. Duhayon, S. M. Ladeira, L. Vendier, J. G. Tojala, L. L. Banet, *Dalton Trans.*, **2014**, *43*, 11388; (c) J. –P. Costes, F. Dahan, A. Dupuis, *Inorg. Chem.*, **2000**, *39*, 5994; (d) K. S. Banu, T. Ghosh, A. Guha, T. Chattopadhyay, D. Das, E. Zangrando, *J. Coord. Chem.*, **2010**, *43*, 3714; (e) D. W. Harrison, J. –C. G. Bunzli, *Inorg. Chim. Acta*, **1985**, *109*, 185.
6. (a) C. Jones, P. C. Junk, M. K. Smith, R. C. Thomas, *Z. Anorg. Allg. Chem.*, **2000**, *626*, 2491; (b) S. Lipstman, I. Goldberg, *Cryst. Growth Des.*, **2010**, *10*, 1823.
7. I. V. Morozov, V. N. Serezhkin, S. I. Troyanov, *Russ.Chem.Bull., Int.Ed.,* **2009**, *58,* 2407.

8. (a) B. Szafranowska, J. Beck, *Eur. J. Inorg. Chem.,* **2013**, 3167; (b) Z. Shi, X. Tang, X. Zhou, J. Cheng, Q. Han, J. Zhou, B. Wang, Y. Yang, W. Liu, D. Bai, *Inorg. Chem.,* **2013**, *52*, 12668; (c) Z. -Yi Liu, Y. –H. Su, E. –C. Yang, X. –J. Zhao, *Inorg. Chem. Commun.*, **2012**, *26*, 56; (d) S. –P. Tang, S. –H. Zhang, Y. –Q. Yang, *Chin. J. Inorg. Chem.*, **2013**, *29*, 2465; (e) K. Koga, M. Ohtsubo, Y. Yamada, M. Koikawa, T. Tokii, *Chem. Lett.*, **2004**, *33*, 1606.

9. (a) A. S. Potapov, G. A. Domina, T. V. Petrenko, A. I. Khlebnikov, *Polyhedron*, **2012**, *33*, 150; (b) Y. Zhu, Y. –L. Wu, C. –X. Huang, J. –M. Xie, *Acta Cryst.*, **2011**, *E67*, m306; (c) G. Beobide, O. Castillo, U. Garcia-Couceiro, J. P. Garcia-Teran, A. Luque, *Acta Cryst.,* **2006**, *E62*, m1353; (d) K. Marjani, S. C. Davies, M. C. Durrant, D. L. Hughes, N. Khodamorada, A. Samodia, *Acta Cryst.*, **2005**, *E61*, m11; (e) P. Y. Zavalij, B. L. Burton, W. E. Jones Jr, *Acta Cryst.,* **2002**, *C58*, m330; (f) B. L. V. Prasad, H. Sato, T. Enoki, S. Cohen, T. P. Radhakrishnan, *J. Chem. Soc*., *Dalton Trans*., **1999**, 25; (g) K. J. Catalan, S. Jackson, J. D. Zubkowski, D. L. Perry, E. J. Valente, L. A. Feliu, A. Polanco, *Polyhedron*, **1995**, *14*, 2165; (h) H. Nakai, *Bull. Chem. Soc. Jpn.*, **1980**, *53*, 1321; (i) J. Sletten, A. Sorensen, *Acta Chemica Scandinavica*, **1990**, *44*, 1018.

10. (a) R. J. Fereday, P. Hodgson, S. Tyagi, B. J. Hathaway, *J. Chem. Soc.*, *Dalton Trans.*, **1981**, 2070; (b) R. J. Fereday, P. Hodgson, S. Tyagi, B. J. Hathaway, *Inorg. Nucl. Chem. Letters*, **1981**, *17*, 243.

11. P. Pascal, *Ann. Chim. Phys.*, **1910**, *19*, 5.

12. G. V. R. Chandramouli, C. Balagopalakrishna, M. V. Rajasekharan, P. T. Manoharan, *Comput. Chem.*, **1996**, *20*, 353.

13. B. Bleaney, K. D. Bowers, *Proc. R. Soc. London, Ser. A.*, **1952**, *214*, 451.

14. *CrysAlisPro* version 1.171.33, Oxford Diffraction Ltd., Abingdon, Oxfordshire, UK, **2007**.

15. *SAINTPLUS*, Bruker AXS Inc., Madison, Wisconsin, USA **2003**.

16. G. M. Sheldrick, *SADABS, Program for empirical absorption correction* (University of Gottingen, Gottingen, Germany) **1996**.

17. G. M. Sheldrick, *Acta Crystallogr.*, **2008**, *A64*, 112.

18. L. J. Farrugia, *J. Appl. Crystallogr.,* **1999**, *32***,** 837.

19. (a) I. M. Procter, B. J. Hathaway, P. Nicholls, *J. Chem. Soc., A*, **1968**, 1678; (b) J. Foley, S. Tyagi, B. J. Hathaway, *J. Chem. Soc., Dalton Trans.,***1984**, 1; (c) W. D. Harrison, B. J. Hathaway, *Acta Crystallogr.,* **1979**, *B35*, 2910.

20. (a) G. L. Guillet, I. F. Dempsey Hyatt, P. C. Hillesheim, K. A. Abboud, M. J. Scott, *New J. Chem.,* **2013**, *37*, 119; (b) S. -P. Ji, M. Tang, L. He, G. -H. Tao, *Chem. Eur. J.,* **2013**, *19*, 4452; (c)Y. Zhu, W. S. Liu, M. Tan, T. Jiao, *Polyhedron*, **1993**, *12*, 939; (d) W. J. Lu, L. P. Zhang, H. S. Chan, T. L. Chan, T. C. W. Mak, *Polyhedron*, **2004**, *23*, 1089; (e) X. Li, W. Liu, Z. Guo, M. Tan, *Inorg. Chem.,* **2003**, *42*, 8735; (f) C. D. Polyzou, H. Nikolaou, C. Papatriantafyllopoulou, V. Psycharis, A. Terzis, C. P. Raptopoulou, A. Escuer, S. P. Perlepes, *Dalton Trans.,* **2012**, *41*,13755; (g) M. G. B. Drew, P. B. Iveson, M. J. Hudson, J. O. Liljenzin, L. Spjuth, P. -Y. Cordier, A. Enarsson, C. Hill, C. Madic, *J. Chem. Soc., Dalton Trans.,* **2000**, 821; (h) M. G. B. Drew, M. J. Hudson, P. B. Iveson, M. L. Russell, J.-O. Liljenzin, M. Skalberg, L. Spjuth, C. Madic, *J. Chem. Soc., Dalton Trans.,* **1998**, 2973.

21. (a) B. Keshavan, Ramalingaiah, *Asian J. Chem.*, **1997**, *9*, 283; (b) K. Nakamoto, *Infrared Spectra of Inorganic and Coordination Compounds*, 4th Ed. (J. Wiley and Sons, New York), **1986**, 256.

22. S. Youngme, J. Phatchimkun, N. Wannarit, N. Chaichit, S. Meejoo, G. A. van Albada, J. Reedijk, *Polyhedron,* **2008**, *27*, 304.

23. R. L. Datta, A. Shyamal, *Elements of Magnetochemistry*, 2nd Edn., East-West Press Pvt Ltd., New Delhi, India, **2004**.

24. B. J. Hathaway, *Struct. Bonding (Berlin)*, **1973**, *14*, 49.

25. (a) Z. Xu, L. K. Thompson, D. O. Miller, *Chem. Commun.*, **2001**, 1170; (b) J. Mao, Z. Jin, J. Ni, L. Yu, *Polyhedron,* **1994**, *13*, 313.

26. S. Youngme, P. Phuengphai, S. Booncoon, N. Chaichit, *Polyhedron*, **2004**, *23*, 1685.

27. (a) W. Urland, E. Warkentin, *Z. Naturforsch*. **1983**, *88b*, 299; (b) H. Cui, T. Otsuka, A. Kobayashi, N. Takeda, M. Ishikawa, Y. Misaki, H. Kobayashi, *Inorg. Chem.*, **2003**, *42*, 6114; (c) E. B. Dhoot, J. Fawcett, R. A. Kresinski, A. W. G. Platt, *Polyhedron*, **2009**, *28*, 1497.

28. (a) C. Jones, P. C. Junk, M. K. Smith, R. C. Thomas, *Z. Anorg. Allg. Chem.*, **2000**, *626*, 2491; (b) S. Lipstman, I. Goldberg, *Cryst. Growth Des.*, **2010**, *10*, 1823.

29. J. G. Kleywegt, W. G. R. Wiesmeijer, G. J. van Driel, W. L. Driessen, J. Reedijk, J. H. Noordik, *Dalton Trans*., **1985**, 2177.

CHAPTER III

Synthesis, structural and spectral characterization of the lanthanide nitrato complex anions crystallised with Cu(2,2'-bipyridine)$_3^{2+}$

3.1. Introduction

In chapter 2, we studied a series of heterometallic Cu(II)/*Ln*(III) complexes in order to probe the possible cation-anion networks as well as the influence of lanthanide anions on the composition of the complex cations using bpy as a co-ligand. Herein, by varying the molar ratio of the initial reactants (*Ln*$(NO_3)_3$:$Cu(NO_3)_2$:bpy/1:1:3), we have obtained a series of novel heterometallic tris-chelated Cu(II) complexes containing bpy ligand accompanied by lanthanide anions with the general formula, {[$Cu(bpy)_3$][$La(NO_3)_5(OH_2)$]} (**1**), {[$Cu(bpy)_3$][*Ln*$(NO_3)_5(OH_2)$]·$2CH_3CN$} [*Ln* = Ce (**2**) and Pr (**3**)] and {[$Cu(bpy)_3$][*Ln*$(NO_3)_5$]} [*Ln* = Nd (**4**), Sm (**5**), Eu (**6**), Gd (**7**), Tb (**8**), Dy (**9**), Ho (**10**), Er (**11**), Tm (**12**), Yb (**13**) and Lu (**14**)].

Only a few examples of deformation of $[Cu(bpy)_3]^{2+}$ crystallized with various anions such as NO_3^-, ClO_4^-, PF_6^-, BF_4^-, BPh_4, SO_4^{2-}, CrO_4^{2-}, Br^-, I^- have been reported in the literature.[1] No compound was reported with lanthanide anions. The counter ion could be a suitable structural factor for determining the distortion of $[Cu(bpy)_3]^{2+}$ cation. To classify the structure of cationic distortion as dynamic or static, the value of tetragonality parameter *T* is often used.[2] *T* is defined as $T = d_{eq}/d_{ax}$, where the d_{eq} is the mean of the four equatorial bond distances and d_{ax} is the mean of two axial bond distances. For the CuX6 chromophore, it was suggested that $T = 1$ for the dynamic system, where as $T < 0.9$ for the static systems. Fluxional stereochemistry is characterized by *T* values within the range 1.0 and 0.9.

In this chapter, we report further investigation of cation deformation of $Cu(bpy)_3^{2+}$ in presence of lanthanide anions. In addition, polycrystalline EPR spectra of all samples were measured at different temperature and the results are discussed.

3.2. Experimental

3.2.1. Reagents

All the chemicals were of reagent grade obtained from commercial sources and were used without further purification.

3.2.2. Synthesis

Preparation of {[Cu(bpy)$_3$][La(NO$_3$)$_5$(OH$_2$)]} (1)

To 2,2'–bipyridine (0.094 g, 0.60 mmol) dissolved in acetonitrile (10 mL), $Cu(NO_3)_2 \cdot 3H_2O$ (0.048 g, 0.20 mmol) and $La(NO_3) \cdot 6H_2O$ (0.086 g, 0.20 mmol) dissolved in acetonitrile (10 mL) was added slowly while stirring. The resulting blue solution, kept at 6 ºC for crystallization. On standing for 5 days, plate shaped blue crystals of **1** were obtained. Crystals were washed with acetonitrile and air dried. Yield : 0.146 g, (0.146 mmol, 73%). *Anal.* Calc. for $C_{30}H_{26}N_{11}O_{16}CuLa$ (M.W. 999.07 g): C, 36.07; H, 2.62; N, 15.42. Found: C, 36.18; H, 2.21; N, 15.32. Important IR absorptions (KBr disk, cm^{-1}): 3369, 3106, 1602, 1575, 1482, 1444, 1382, 1308, 1162, 1028, 812, 763 and 656.

Preparation of {[Cu(bpy)$_3$][*Ln*(NO$_3$)$_5$(OH$_2$)]·2CH$_3$CN} (2-3)

To 2,2'–bipyridine (0.094 g, 0.60 mmol) dissolved in acetonitrile (10 mL), $Cu(NO_3)_2 \cdot 3H_2O$ (0.048 g, 0.20 mmol) and $Ln(NO_3) \cdot 6H_2O$ (0.200 mmol) where *Ln* = Ce (0.086 g) (**2**) and Pr (0.087 g) (**3**) dissolved in acetonitrile (10 mL) was added slowly while stirring. The resulting

dark blue solution, kept at 6 ºC for crystallization. On standing for 5 days, block shaped blue crystals of the compound **2-3** were obtained. Crystals were washed with acetonitrile and air dried.

Yield of **2**: 0.128 g, (0.118 mmol, 59%). *Anal.* Calc. for $C_{34}H_{32}N_{13}O_{16}CuCe$ (M.W. 1082.39 g): C, 37.73; H, 2.98; N, 16.82. Found: C, 37.63; H, 2.91; N, 16.72. Important IR absorptions (KBr disk, cm^{-1}): 3390, 3080, 1600, 1562, 1480, 1446, 1380, 1320, 1156, 1024, 821, 761 and 647.

Yield of **3**: 0.134 g, (0.124 mmol, 62%). *Anal.* Calc. for $C_{34}H_{32}N_{13}O_{16}CuPr$ (M.W. 1083.18 g): C, 37.70; H, 2.98; N, 16.81. Found: C, 37.61; H, 3.06; N, 16.91. Important IR absorptions (KBr disk, cm^{-1}): 3390, 3100, 1600, 1567, 1484, 1452, 1382, 1304, 1156, 1035, 816, 756 and 646.

Preparation of {[Cu(bpy)$_3$][*Ln*(NO$_3$)$_5$]} (4-14)

To 2,2'–bipyridine (0.094 g, 0.60 mmol) dissolved in acetonitrile (10 mL), $Cu(NO_3)_2 \cdot 3H_2O$ (0.048 g, 0.20 mmol) and $Ln(NO_3) \cdot 6H_2O$ (0.200 mmol) where *Ln* = Nd (0.088 g) (**4**), Sm (0.088 g) (**5**), Eu (0.086 g) (**6**), Gd (0.090 g) (**7**), Tb (0.087 g) (**8**), Dy (0.088 g) (**9**), Ho (0.088 g) (**10**), Er (0.088 g) (**11**), Tm (0.089 g) (**12**), Yb (0.090 g) (**13**) and Lu (0.072 g) (**14**) dissolved in acetonitrile (10 mL) was added slowly while stirring. The resulting clear blue solution, kept at 6 ºC for crystallization. On standing for 5 days, plate shape blue crystals were obtained. Crystals were washed with acetonitrile and air dried.

For **4**: Yield 0.154 g, (0.156 mmol, 78%). *Anal.* Calc. for $C_{30}H_{24}N_{11}O_{15}CuNd$ (M.W. 986.38 g): C, 36.53; H, 2.45; N, 15.62. Found: C, 36.45; H, 2.39; N, 15.56. Important IR absorptions (KBr disk, cm^{-1}): 3106, 1605, 1572, 1474, 1435, 1385, 1304, 1172, 1024, 816, 756 and 646.

For **5**: Yield 0.162 g, (0.163 mmol, 82%). *Anal.* Calc. for $C_{30}H_{24}N_{11}O_{15}CuSm$ (M.W. 992.49 g): C, 36.30; H, 2.44; N, 15.52. Found: C, 36.18; H, 2.36; N, 15.42. Important IR absorptions (KBr disk, cm^{-1}): 3092, 1784, 1602, 1568, 1474, 1430, 1326, 1154, 1034, 816 and 763.

For **6**: Yield 0.142 g, (0.143 mmol, 72%). *Anal.* Calc. for $C_{30}H_{24}N_{11}O_{15}CuEu$ (M.W. 994.08 g): C, 36.25; H, 2.43; N, 15.50. Found: C, 36.15; H, 2.49; N, 15.39. Important IR absorptions (KBr disk, cm^{-1}): 3102, 1610, 1572, 1468, 1435, 1386, 1304, 1172, 1030, 816, 756 and 646.

For **7**: Yield 0.138 g, (0.138 mmol, 69%). *Anal.* Calc. for $C_{30}H_{24}N_{11}O_{15}CuGd$ (M.W. 999.39 g): C, 36.06; H, 2.42; N, 15.42. Found: C, 36.15; H, 2.26; N, 15.53. Important IR absorptions (KBr disk, cm^{-1}): 3096, 1784, 1600, 1574, 1479, 1432, 1324, 1155, 1038, 814 and 762.

For **8**: Yield 0.156 g, (0.156 mmol, 78%). *Anal.* Calc. for $C_{30}H_{24}N_{11}O_{15}CuTb$ (M.W. 1001.06 g): C, 36.00; H, 2.42; N, 15.39. Found: C, 35.89; H, 2.34; N, 15.28. Important IR absorptions (KBr disk, cm^{-1}): 3100, 1590, 1572, 1480, 1446, 1384, 1310, 1164, 1025, 810, 766 and 652.

For **9**: Yield 0.134 g, (0.133 mmol, 67%). *Anal.* Calc. for $C_{30}H_{24}N_{11}O_{15}CuDy$ (M.W. 1004.64 g): C, 35.87; H, 2.41; N, 15.34. Found: C, 35.72; H, 2.48; N, 15.21. Important IR absorptions (KBr disk, cm^{-1}): 3096, 1784, 1602, 1570, 1478, 1432, 1324, 1158, 1038, 812 and 760.

For **10**: Yield 0.156 g, (0.155 mmol, 78%). *Anal.* Calc. for $C_{30}H_{24}N_{11}O_{15}CuHo$ (M.W. 1007.07 g): C, 35.78; H, 2.40; N, 15.30. Found: C, 35.63; H, 2.35; N, 15.21. Important IR absorptions (KBr disk, cm^{-1}): 3100, 1595, 1570, 1480, 1445, 1386, 1302, 1164, 1024, 814, 762 and 650.

For **11**: Yield 0.170 g, (0.169 mmol, 84%). *Anal.* Calc. for $C_{30}H_{24}N_{11}O_{15}CuEr$ (M.W. 1009.41 g): C, 35.70; H, 2.40; N, 15.26. Found: C, 35.46; H, 2.16; N, 15.32. Important IR absorptions (KBr disk, cm^{-1}): 3380, 3090, 1780, 1600, 1572, 1479, 1435, 1320, 1150, 1035, 816 and 767.

For **12**: Yield 0.174 g, (0.172 mmol, 86%). *Anal.* Calc. for $C_{30}H_{24}N_{11}O_{15}CuTm$ (M.W. 1011.07 g): C, 35.64; H, 2.39; N, 15.24. Found: C, 35.52; H, 2.27; N, 15.46. Important IR absorptions (KBr disk, cm^{-1}): 3369, 3106, 1599, 1577, 1484, 1440, 1380, 1308, 1160, 1029, 810, 760 and 656.

For **13**: Yield 0.140 g, (0.140 mmol, 70%). *Anal.* Calc. for $C_{30}H_{24}N_{11}O_{15}CuYb$ (M.W. 1015.18 g): C, 35.49; H, 2.38; N, 15.18. Found: C, 35.48; H, 2.41; N, 15.25. Important IR absorptions (KBr disk, cm^{-1}): 3094, 1780, 1602, 1570, 1474, 1430, 1330, 1140, 1030, 812 and 762.

For **14**: Yield 0.125 g, (0.123 mmol, 62%). *Anal.* Calc. for $C_{30}H_{24}N_{11}O_{15}CuLu$ (M.W. 1017.11 g): C, 35.43; H, 2.38; N, 15.15. Found: C, 35.52; H, 2.31; N, 15.25. Important IR absorptions (KBr disk, cm^{-1}): 3090, 1597, 1570, 1474, 1420, 1390, 1304, 1160, 1020, 812, 760 and 650.

3.3. Physical measurements

IR spectra were obtained for KBr pellets on a Jasco FT-IR 5300 spectrometer in the range 4000-400 cm^{-1}. Elemental analysis for C, H and N was performed on a Perkin-Elmer 240C elemental analyzer. Diffuse reflectance spectra were measured by using a Shimadzu UV-3100 spectrometer. EPR spectra were recorded on Bruker Xenon EMX-ER-073 spectrometer. Powder X-ray diffraction patterns were recorded on a Bruker D8-Advance diffractometer using graphite monochromated $CuK_{\alpha 1}$ (1.5406 Å) and $K_{\alpha 2}$ (1.54439 Å) radiations. Simulation of the P-XRD patterns was carried out using the Mercury.

3.4. X-ray crystallography

The unit cell parameters and intensity data at 100 K for **1** and 298 K for **2-14** were obtained on a Bruker-Nonius SMART APEX CCD 1000 area detector, using graphite-monochromated Mo-Kα radiation (λ = 0.71073 Å). Data were reduced using SAINTPLUS[3] and a multi-scan absorption correction using SADABS[4] was performed. The structure of complexes were solved by direct methods and refined on F^2 by full-matrix least-squares procedures. The non-hydrogen atoms were refined using anisotropic thermal parameters. The hydrogen atoms

were included in the structure factor calculations at idealized positions using a riding model, and the hydrogen atoms attached to oxygen atoms were located from the difference maps. The structures were solved using SHELXS-97 and refined using SHELXL-97.[5] Drawings were made using Mercury.[6] Three of the nitrate ions in compound **1** were greatly disordered. Since the disorder could not be modeled, some of the atoms were restricted to isotropic thermal motion in order to prevent them from becoming non-positive definite. Crystallographic data and structure refinement parameters are given in Table 3.1, Table 3.7 and Table 3.8. Selected bond lengths and bond angles of compounds **2** and **5** are listed in Table 3.2, Table 3.4 and Table 3.9. Intermolecular interaction parameters and π-stacking interactions of compounds **2** and **5** are listed in Table 3.3, Table 3.5 and Table 3.10.

3.5. Crystal structures

3.5.1. Crystal structure of $[Cu(bpy)_3][La(NO_3)_5(OH_2)]$ (1)

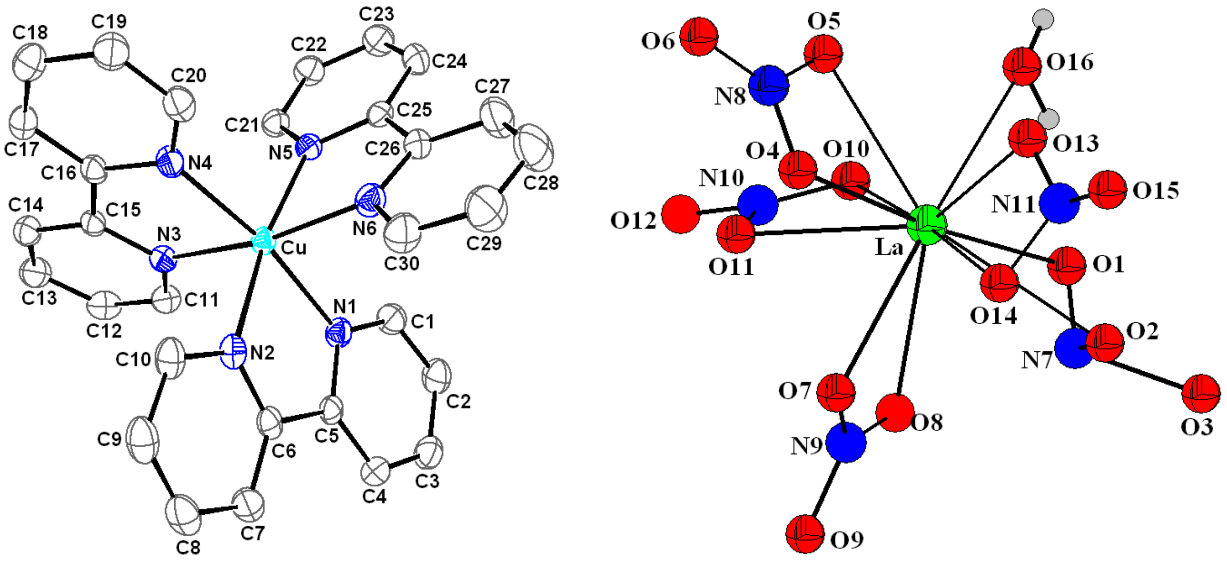

(a) **(b)**

Figure 3.1. Thermal ellipsoid plot of the coordination environment of the (a) complex cation (b) complex anion of **1**: Atoms are represented as 30% probability ellipsoids. Ring hydrogen atoms have been omitted for clarity.

The molecular structure of **1** consisted of a $[Cu(bpy)_3]^{2+}$ cation and one $[La(NO_3)_5(OH_2)_2]^{2-}$ anion per asymmetric unit shown in Figure 3.1. Crystallographic data and structure refinement parameters are given in Table 3.1. Selected bond lengths and angles are given in Table 3.2. The Cu(II) ion adopts a CuN_6 chromophore with a regular elongated octahedral (REO) stereochemistry and rhombic in-plane bond lengths. The four in-plane bond lengths (Å) Cu–N(2), 2.039(5) Cu–N(3), 2.019(4) Cu–N(4) 2.044(5) and Cu–N(5) 2.035(4) are very similar (mean value of $Cu–N_{in}$ = 2.034(5) (Å)). The axial bond lengths differ significantly, with values of Cu–N(6) = 2.229(5), and Cu–N(1) = 2.361(5) (Å) (mean value of $Cu–N_{out}$ = 2.295(5) (Å)) are in good agreement with the previously reported values for analogous complexes.[1a-e]

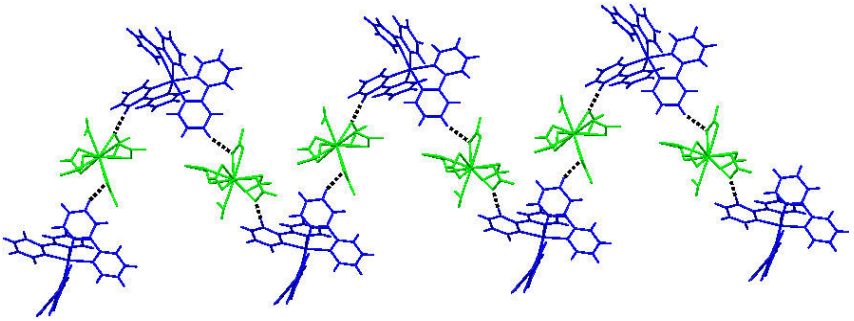

(a)

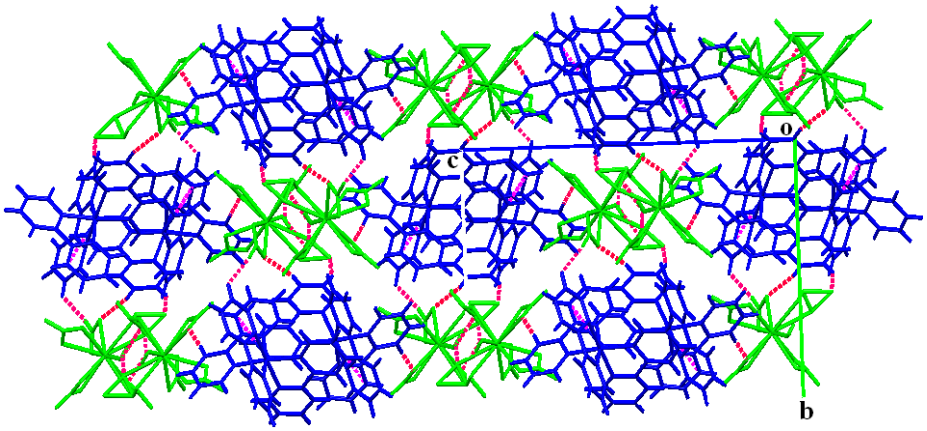

(b)

Figure 3.2. (a) H-bonded 1D zig-zag chain network in **1** (b) molecular packing of **1** viewed down the *a*-axis.

Table 3.1: Crystallographic data and structure refinement of **1-4**

Param	**1**	**2**	**3**	**4**
Formula	$C_{30}H_{26}N_{11}O_{16}CuLa$	$C_{34}H_{32}N_{13}O_{16}CuCe$	$C_{34}H_{32}N_{13}O_{16}CuPr$	$C_{30}H_{24}N_{11}O_{15}CuNd$
Formula weight	999.07	1082.39	1083.18	986.38
Crystal system	Orthorhombic	Triclinic	Triclinic	Triclinic
Space group	$P2_12_12_1$	$P\,\bar{1}$	$P\,\bar{1}$	$P\,\bar{1}$
a (Å)	15.315(3)	10.560(4)	10.525(2)	9.326(11)
b (Å)	12.447(3)	13.078(5)	13.090(3)	12.886(15)
c (Å)	19.822(4)	16.240(6)	16.196(3)	16.634(19)
α (°)	90.000	85.501(6)	85.471(3)	79.643(2)
β (°)	90.000	78.564(6)	78.599(3)	78.961(2)
γ (°)	90.000	87.666(6)	87.895(3)	75.978(2)
V (Å^3)	3778.6(14)	2190.9(14)	2180.0(7)	1884.7(4)
Z	4	2	2	2
T(K)	100(2)	298(2)	298(2)	298(2)
λ (Å)	0.71073	0.71073	0.71073	0.71073
D_{calc} (g cm^{-3})	1.756	1.641	1.650	1.738
μ (mm^{-1})	1.765	1.594	1.676	2.010
F(000)	1988	1084	1086	980
Crystal size (mm)	0.28 x 0.20 x 0.12	0.32 x 0.24 x 0.20	0.32 x 0.24 x 0.20	0.24 x 0.20 x 0.08
θ Range(°)	1.68 – 26.07	1.28 – 25.68	1.29 – 25.68	1.26 to 25.00
h/k/l indices	–15, 15/ –18, 18/ –24, 24	–11, 12/ –15, 15/ –14, 19	–12, 12/ –15,15/ –19,19	–11, 11/ –15, 15/ –19, 19
Refl^n collected	37843	10522	22129	18282
Unique refl^n [R_{int}]	7465 [0.0587]	7427 [0.0198]	8243 [0.0309]	6617 [0.0255]
GooF	1.044	1.123	1.059	1.032
R_1 [I>2σ(I)]	0.0744	0.0396	0.0256	0.0400
wR_2	0.2068	0.1507	0.0660	0.1067

$w = 1/[\sigma^2(F_0^2) + (AP)^2 + BP]$; where $P = [2F_C^2 + Max(F_0^2, 0)]/3$

The tetragonality value, *T* is 0.886, which indicates that the JT distortion is static. Moreover, it is very close to reported values for the analogous complexes (Table 3.12) and shows typical static JT distortion. The bite angle of the N(3)N(4) bpy ligand, is 80.84(2)º and has two similar bond lengths of 2.019(4) and 2.044(5) Å respectively. For the N(5)N(6) bpy ligand,

there is a significantly smaller bite angle, 77.74(2)º, due to the intermediate bond lengthening of Cu–N(6) to 2.29(5) (Å). The N(1)N(2) bpy ligand has the longest Cu–N bond, Cu–N(1) = 2.361(5) (Å), and the bite angle decreases to 75.18(2)º, giving a total variation in the bite angles of 5.74(2)º. A definite pattern was clearly observed *i.e.* when one of the Cu–N bond distance lengthens, the bite angle of the related bpy ligand decreases.

The La(III) ion is 11-coordinated with ten oxygen atoms from five chelating nitrate ligands and one oxygen atom from a water molecule, forming a distorted monocapped pentagonal antiprismatic geometry.[7b] The cations and anions are linked by the C-H···O interactions to form a 1D chain along *b*-axis. These are further interconnect with π-stacking interactions to form a 3D network (Figure 3.2).

Table 3.2: Selected bond lengths (Å) and bond angles (˚) for {[$Cu(bpy)_3$][$La(NO_3)_5(OH_2)$]}

Cu-N(1)	2.032(8)	Cu-N(3)	2.353(9)	Cu-N(5)	2.038(8)
Cu-N(2)	2.018(8)	Cu-N(4)	2.050(9)	Cu-N(6)	2.238(9)
La-O(1)	2.629(7)	La-O(13)	2.566(12)	La-O(8)	2.662(15)
La-O(4)	2.620(8)	La-O(16)	2.573(7)	La-O(11)	2.637(8)
La-O(7)	2.709(11)	La-O(2)	2.790(15)	La-O(14)	2.769(13)
La-O(10)	2.613(10)	La-O(5)	2.623(7)		
N(7)-O(1)	1.081(19)	N(8)-O(6)	1.216(12)	N(10)-O(11)	1.222(13)
N(7)-O(2)	1.42(6)	N(9)-O(7)	1.246(13)	N(10)-O(12)	1.243(19)
N(7)-O(3)	1.80(8)	N(9)-O(8)	1.276(13)	N(11)-O(13)	1.131(12)
N(8)-O(4)	1.272(13)	N(9)-O(9)	1.29(2)	N(11)-O(14)	1.303(12)
N(8)-O(5)	1.273(12)	N(10)-O(10)	1.270(13)	N(11)-O(15)	1.194(12)
N(1)-Cu-N(2)	81.1(3)	N(2)-Cu-N(3)	90.3(3)	N(3)-Cu-N(6)	174.0(3)
N(1)-Cu-N(3)	88.3(3)	N(2)-Cu-N(4)	93.2(3)	N(4)-Cu-N(5)	91.7(3)
N(1)-Cu-N(4)	162.7(3)	N(2)-Cu-N(5)	169.9(4)	N(4)-Cu-N(6)	99.7(3)
N(1)-Cu-N(5)	96.6(3)	N(3)-Cu-N(4)	75.4(3)	N(5)-Cu-N(6)	77.1(3)
N(1)-Cu-N(6)	96.9(3)	N(3)-Cu-N(5)	99.5(3)	N(2)-Cu-N(6)	93.4(3)
O(1)-La-O(2)	40.3(8)	O(8)-La-O(11)	71.1(4)	O(5)-La-O(7)	113.4(3)
O(1)-La-O(4)	174.9(3)	O(8)-La-O(13)	139.1(5)	O(5)-La-O(8)	138.4(4)
O(1)-La-O(5)	129.1(2)	O(8)-La-O(14)	97.7(4)	O(5)-La-O(10)	75.7(3)

O(1)-La-O(7)	114.6(3)	O(8)-La-O(16)	132.1(4)	O(5)-La-O(11)	67.4(2)
O(1)-La-O(8)	70.3(4)	O(10)-La-O(11)	48.9(4)	O(5)-La-O(13)	77.3(5)
O(1)-La-O(10)	71.6(3)	O(10)-La-O(13)	139.8(4)	O(5)-La-O(14)	105.9(3)
O(1)-La-O(11)	113.2(3)	O(10)-La-O(14)	176.0(4)	O(5)-La-O(16)	68.1(2)
O(1)-La-O(13)	104.7(7)	O(10)-La-O(16)	71.4(4)	O(7)-La-O(8)	49.3(4)
O(1)-La-O(14)	109.4(4)	O(14)-La-O(16)	112.6(3)	O(7)-La-O(10)	112.2(5)
O(1)-La-O(16)	65.1(2)	O(2)-La-O(4)	139.2(8)	O(7)-La-O(11)	72.2(5)
O(4)-La-O(5)	48.5(3)	O(2)-La-O(5)	155.1(4)	O(7)-La-O(13)	105.6(5)
O(4)-La-O(7)	69.4(3)	O(2)-La-O(7)	87.7(6)	O(7)-La-O(14)	63.8(5)
O(4)-La-O(8)	114.6(4)	O(2)-La-O(8)	65.3(4)	O(7)-La-O(16)	176.3(4)
O(4)-La-O(10)	110.4(3)	O(2)-La-O(10)	109.5(8)	O(11)-La-O(13)	139.1(6)
O(4)-La-O(11)	70.7(4)	O(2)-La-O(11)	134.9(4)	O(11)-La-O(14)	128.1(4)
O(4)-La-O(13)	70.6(7)	O(2)-La-O(13)	84.6(7)	O(11)-La-O(16)	111.4(3)
O(4)-La-O(14)	69.0(4)	O(2)-La-O(14)	70.7(8)	O(13)-La-O(14)	44.0(4)
O(4)-La-O(16)	110.7(3)	O(2)-La-O(16)	90.1(6)	O(13)-La-O(16)	71.2(5)
O(8)-La-O(10)	78.9(5)				
O(1)-N(7)-O(2)	96(4)	O(5)-N(8)-O(6)	124.8(10)	O(10)-N(10)-O(12)	129.3(15)
O(1)-N(7)-O(3)	116(5)	O(7)-N(9)-O(8)	125.2(17)	O(11)-N(10)-O(12)	108.8(13)
O(2)-N(7)-O(3)	60(3)	O(7)-N(9)-O(9)	118.1(16)	O(13)-N(11)-O(14)	111.0(13)
O(4)-N(8)-O(5)	115.5(8)	O(8)-N(9)-O(9)	116.6(16)	O(13)-N(11)-O(15)	123.3(11)
O(4)-N(8)-O(6)	119.4(9)	O(10)-N(10)-O(11)	121.5(13)	O(14)-N(11)-O(15)	117.7(11)

Table 3.3: Intermolecular interaction parameters

*H-bonding for **1***

D-H···A	***d*(D-H)(Å)**	***d*(H···A)(Å)**	***d*(D···A)(Å)**	**<(D-H···A)(º)**
C7–H7···O5#1	0.95	2.38	3.33	175
C12–H12···O9#2	0.95	2.46	2.94	111
C28–H28···O8#3	0.95	2.34	3.25	161
C29–H29···O3#3	0.95	2.44	3.24	141
O16–H16B···O2#3	0.85	2.50	3.19	143
O16–H16B···O14#3	0.85	2.40	3.06	133
(#1) 1–*x*, ½+*y*, 1.5–*z*; (#2) *x*, 1+*y*, *z*; (#3) ½+*x*, 1.5–*y*, 2–*z*				
*π···π interactions for **1** (Å)*				
C3···C23#1	3.50(2)	C14···C24#1	3.55(2)	
C4···C23#1	3.44(2)	C17···C23#1	3.59(2)	
(#1) ½+*x*, ½–*y*, 2–*z*				

3.5.2. Crystal structure of {[Cu(bpy)$_3$][*Ln*(NO$_3$)$_5$(OH$_2$)]·2CH$_3$CN} (2-3)

Compound **2** and **3** form isomorphous crystals. The main difference with previous compound **1** was the two acetonitrile molecules present in the lattice. Since geometrical parameters of compounds **1-3** are similar the selected bond lengths and angles of compound **2** are given in Table 3.4. The asymmetric unit consisted of a $[Cu(bpy)_3]^{2+}$ cation, one $[Ln(NO_3)_5(OH_2)_2]^{2-}$ anion [*Ln* = Ce (**2**) and Pr (**3**)] and two acetonitrile molecules in the lattice shown in Figure 3.3. The Cu(II) ion adopts a CuN_6 chromophore with a regular elongated octahedral (REO) stereochemistry and rhombic in-plane bond lengths. The four in-plane Cu–N bond lengths (Å) are in the range 2.0184(4)-2.115(5) (mean Cu–N_{in} = 2.053(4) for **2**); 2.0177(2)-2.093(2) (mean Cu–N_{in} = 2.047(2) for **3**). The axial Cu–N bond lengths (Å) differ significantly, with values of 2.250(5) and 2.346(5) (mean Cu–N_{out} = 2.298(5) for **2**); 2.263(2) and 2.343(2) (mean Cu–N_{out} = 2.303(2) for **3**) are in good agreement with the previously reported values for analogous complexes.[1a-e] The tetragonality value, *T* is 0.893 for **2** and 0.889 for **3** indicating that the JT distortion is static. Moreover, it is very close to reported values for the analogous complexes (Table 3.12) and shows typical static JT distortion. The bite angle (º) of the bpy1 ligand is 80.5(2) for **2**; 79.9(7) for **3**, has two similar bond lengths (Å) of 2.040(4), 2.018(4) for **2**; 2.017(2), 2.046(2) for **3**. For the bpy2 ligand, there is a significantly smaller bite angle (º) is 76.9(2) for **2**; 76.8(8) for **3**, due to the intermediate bond lengthening (Å) to 2.250(5) for **2**; 2.263(2) for **3**. The bpy3 ligand has the longest Cu–N bond, 2.346(5) for **2**; 2.343(2) for **3**, and the bite angle (º) decreases to 74.5(2) for **2**; 74.4(8) for **3**, giving a total variation in the bite angles (º) of 6.0(2) for **2**; 5.5(2) for **3**.

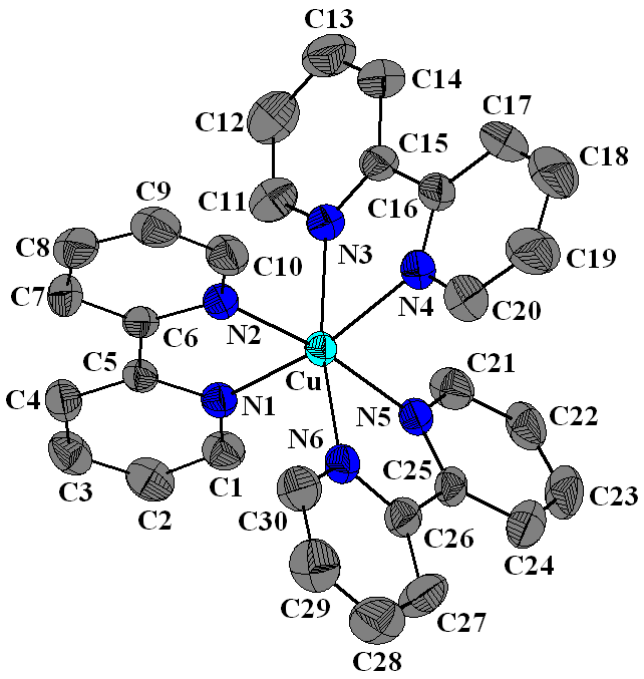

(a)

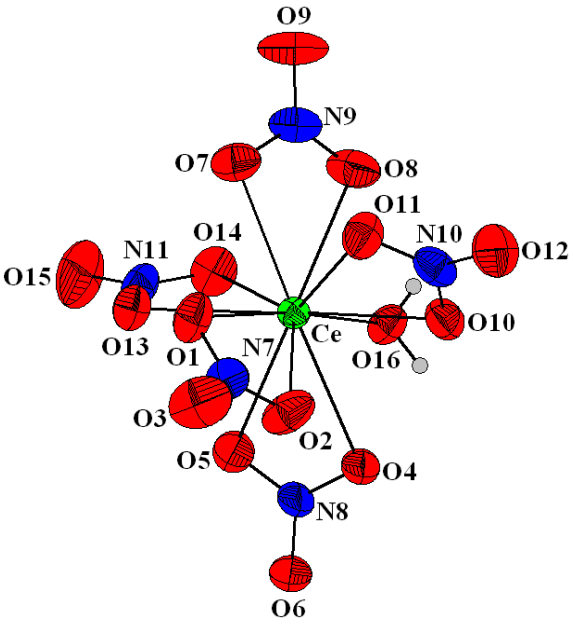

(b)

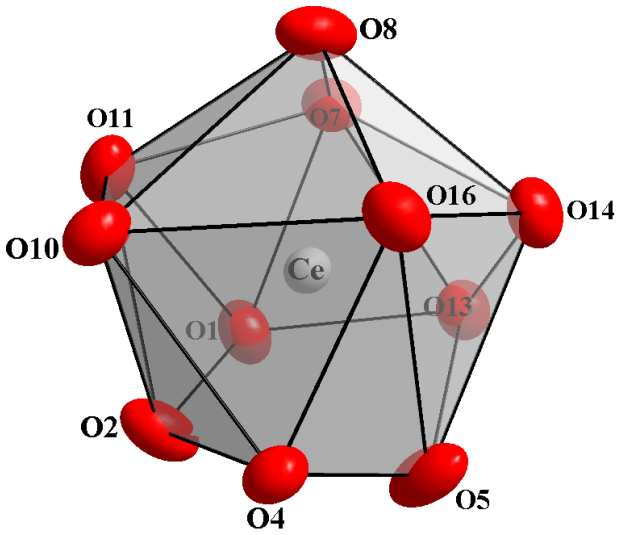

(c)

Figure 3.3. Thermal ellipsoid plot of the coordination environment of the (a) complex cation (b) complex anion of **2** (c) monocapped pentagonal antiprism coordination polyhedron of Ce(III) ion in $[Ce(NO_3)_5(OH_2)]^{2-}$: Atoms are represented as 30% probability ellipsoids. Ring hydrogen atoms and acetonitrile have been omitted for clarity.

The *Ln*(III) ion is 11-coordinated with ten oxygen atoms from five chelating nitrate ligands and one oxygen atom from water molecule, forming a distorted monocapped pentagonal antiprismatic geometry[7] (Figure 3.3(c)). The *Ln*−O(nitrate) bond lengths (Å) lie in the range 2.583(5)-2.691(4) for **2**; 2.552(2)-2.691(2) for **3** and *Ln*−O(w), 2.524(4) for **2**; 2.504(2) for **3**.

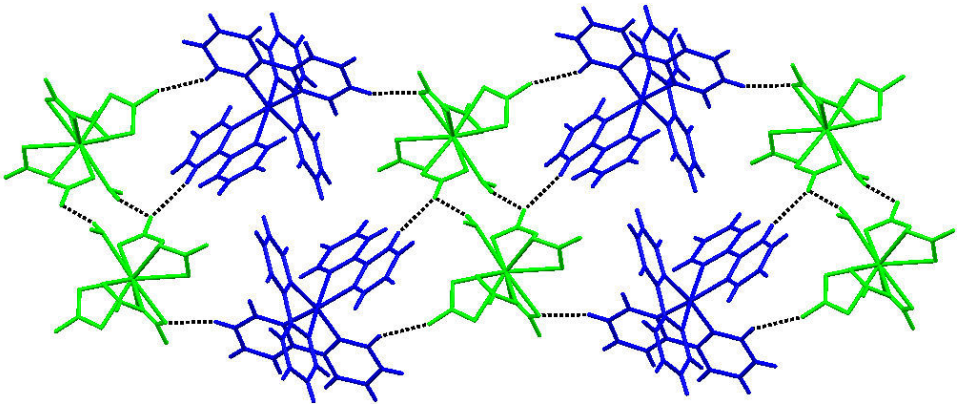

(a)

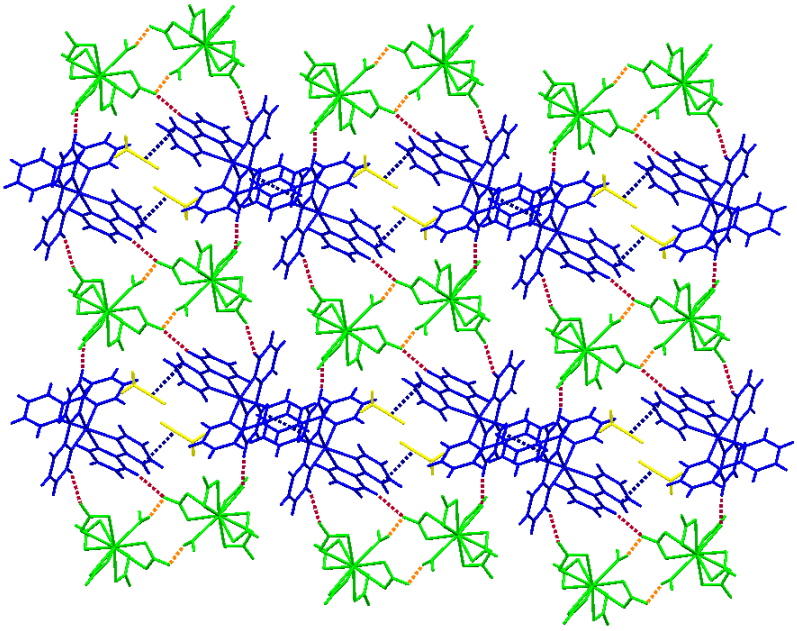

(b)

Figure 3.4. (a) H-bonded 2D network in **2** (b) molecular packing of **2** viewed down the *a*-axis

In crystal packing **2**, the presence of water molecule enables each $[Ce(NO_3)_5(OH_2)]^{2-}$ moiety to link to another $[Ce(NO_3)_5(OH_2)]^{2-}$ moiety through the intermolecular H-bonding gives a dimeric moiety. These form a 2D network with the help of C-H···O interactions (C2–H2···O1, 2.399(4); C10–H10···O12, 2.361(4); C17–H17···O6, 2.360(4); O16–H16B···O6, 1.960(4) Å) (Figure 3.4(a)). These are further interconnected with the lattice acetonitrile and π-stacking interactions (3.445-3.598 Å) to build the above network into a 3D network (Figure 3.4(b)).

Table 3.4: Selected bond lengths (Å) and bond angles (°) for $\{[Cu(bpy)_3][Ce(NO_3)_5(OH_2)]\cdot 2CH_3CN\}$

Cu-N(1)	2.040(4)	Cu-N(3)	2.346(5)	Cu-N(5)	2.039(4)
Cu-N(2)	2.018(4)	Cu-N(4)	2.115(5)	Cu-N(6)	2.250(5)
Ce-O(1)	2.596(4)	Ce-O(4)	2.691(4)	Ce-O(7)	2.584(4)
Ce-O(2)	2.613(5)	Ce-O(5)	2.591(4)	Ce-O(8)	2.583(5)
Ce-O(10)	2.586(4)	Ce-O(13)	2.645(4)	Ce-O(16)	2.524(4)
Ce-O(11)	2.623(4)	Ce-O(14)	2.601(4)		
N(7)-O(1)	1.271(7)	N(7)-O(2)	1.246(6)	N(7)-O(3)	1.216(6)
N(8)-O(4)	1.234(6)	N(8)-O(5)	1.260(6)	N(8)-O(6)	1.214(6)
N(9)-O(7)	1.268(7)	N(9)-O(8)	1.244(7)	N(9)-O(9)	1.224(7)
N(10)-O(10)	1.270(7)	N(10)-O(11)	1.261(7)	N(10)-O(12)	1.237(6)
N(11)-O(13)	1.245(6)	N(11)-O(14)	1.267(7)	N(11)-O(15)	1.204(6)
N(1)-Cu-N(2)	80.53(17)	N(2)-Cu-N(3)	91.54(17)	N(3)-Cu-N(6)	169.26(17)
N(1)-Cu-N(3)	93.19(18)	N(2)-Cu-N(4)	96.27(17)	N(4)-Cu-N(5)	88.86(17)
N(1)-Cu-N(4)	167.25(19)	N(2)-Cu-N(5)	170.25(18)	N(4)-Cu-N(6)	95.85(19)
N(1)-Cu-N(5)	96.19(17)	N(3)-Cu-N(4)	74.5(2)	N(5)-Cu-N(6)	76.98(17)
N(1)-Cu-N(6)	96.69(17)	N(3)-Cu-N(5)	97.83(17)	N(2)-Cu-N(6)	94.21(17)
O(1)-Ce-O(2)	48.58(14)	O(7)-Ce-O(10)	109.04(15)	O(5)-Ce-O(7)	134.39(15)
O(1)-Ce-O(4)	109.47(15)	O(7)-Ce-O(11)	67.90(15)	O(5)-Ce-O(8)	142.04(18)
O(1)-Ce-O(5)	92.11(18)	O(7)-Ce-O(13)	69.38(15)	O(5)-Ce-O(10)	116.57(14)
O(1)-Ce-O(7)	73.11(16)	O(7)-Ce-O(14)	71.93(15)	O(5)-Ce-O(11)	147.57(18)
O(1)-Ce-O(8)	118.29(16)	O(7)-Ce-O(16)	112.25(15)	O(5)-Ce-O(13)	65.39(14)
O(1)-Ce-O(10)	107.19(15)	O(11)-Ce-O(13)	124.41(13)	O(5)-Ce-O(14)	73.99(17)
O(1)-Ce-O(11)	70.57(15)	O(11)-Ce-O(14)	137.29(15)	O(5)-Ce-O(16)	81.96(17)
O(1)-Ce-O(13)	64.17(14)	O(11)-Ce-O(16)	113.85(15)	O(8)-Ce-O(10)	77.68(17)
O(1)-Ce-O(14)	110.91(14)	O(14)-Ce-O(16)	69.09(14)	O(8)-Ce-O(11)	69.09(16)

O(1)-Ce-O(16)	173.85(16)	O(2)-Ce-O(4)	65.14(13)	O(8)-Ce-O(13)	106.05(16)
O(4)-Ce-O(5)	47.45(13)	O(2)-Ce-O(5)	76.69(19)	O(8)-Ce-O(14)	74.09(17)
O(4)-Ce-O(7)	177.15(13)	O(2)-Ce-O(7)	116.84(14)	O(8)-Ce-O(16)	67.79(15)
O(4)-Ce-O(8)	127.91(14)	O(2)-Ce-O(8)	140.20(18)	O(10)-Ce-O(11)	49.10(13)
O(4)-Ce-O(10)	69.24(13)	O(2)-Ce-O(10)	73.81(16)	O(10)-Ce-O(13)	171.37(13)
O(4)-Ce-O(11)	111.56(13)	O(2)-Ce-O(11)	71.30(17)	O(10)-Ce-O(14)	140.03(15)
O(4)-Ce-O(13)	112.68(13)	O(2)-Ce-O(13)	99.10(16)	O(10)-Ce-O(16)	74.34(14)
O(4)-Ce-O(14)	107.81(14)	O(2)-Ce-O(14)	143.26(17)	O(13)-Ce-O(14)	48.26(14)
O(4)-Ce-O(16)	65.24(14)	O(2)-Ce-O(16)	127.71(14)	O(13)-Ce-O(16)	114.24(14)
O(7)-Ce-O(8)	49.24(15)				
O(1)-N(7)-O(2)	116.7(5)	O(1)-N(7)-O(3)	120.4(5)	O(2)-N(7)-O(3)	122.9(6)
O(4)-N(8)-O(5)	117.0(4)	O(4)-N(8)-O(6)	123.4(5)	O(5)-N(8)-O(6)	119.6(5)
O(7)-N(9)-O(8)	117.9(5)	O(7)-N(9)-O(9)	120.4(7)	O(8)-N(9)-O(9)	121.6(6)
O(10)-N(10)-O(11)	117.5(5)	O(10)-N(10)-O(12)	119.3(6)	O(11)-N(10)-O(12)	123.1(6)
O(13)-N(11)-O(14)	117.3(5)	O(13)-N(11)-O(15)	121.5(6)	O(14)-N(11)-O(15)	121.2(6)

Table 3.5: Intermolecular interaction parameters

*H-bonding for **2***

D-H···A	***d*(D-H)(Å)**	***d*(H···A)(Å)**	***d*(D···A)(Å)**	**<(D-H···A)(º)**
C2–H2···O1#1	0.93	2.39	3.23	153
C10–H10···O12#2	0.93	2.36	3.07	133
C17–H17···O6#3	0.93	2.36	3.24	157
C22–H22···O14#4	0.93	2.48	3.36	159
C30–H30···O3#5	0.93	2.46	3.19	137
O16–H16B···O6#6	0.85	1.96	2.77	159

(#1) 1+*x*, *y*, *z*; (#2) *x*, 1+*y*, *z*; (#3)1–*x*, 1–*y*, 1–*z*; (#4) –*x*, 1–*y*, 1–*z*; (#5)1–*x*, 1–*y*, –*z*; (#6)1–*x*, –*y*, 1–*z*

*π···π interactions for **2** (Å)*

C3···C4#1	3.520(9)	C3···C5#1	3.598(9)
C4···C4#1	3.445(8)	(#1) –*x*, 1–*y*, –*z*	

3.5.3. Infrared spectra

The band around 3300-3450 cm^{-1} has been assigned to O-H stretching vibration of water for **1-3**. The $\nu_{C=C}$ frequency of the bpy rings at 1610 and 1570 cm^{-1}. The band around 3100 cm^{-1}

assigned to the ν_{C-H} frequency. This valve shifted to lower frequencies on complexation. The stretching vibrations corresponding to those typical of coordinated bpy occur around at 760, 810, 1030, 1180 and 1600 cm^{-1}.

3.5.4. Electronic spectra

The electronic spectra of **1-3** consist of a broad band centered at 14700 cm^{-1} ($d_z^2 \approx d_{xy} \rightarrow d_{x2-y2}$) can be assigned to a d-d transition, which is similar to those previously reported $[Cu(bpy)_3]Y$ complexes.[1] The lower energy band maximum (about 6000 cm^{-1}) is too low to be seen in the present measurement. Band near 33,000 cm^{-1} is due to ligand-to-metal charge transfer transition, while the band near 41,000 cm^{-1} is associated with intraligand $\pi \rightarrow \pi^*$ excitation (Figure 3.5).

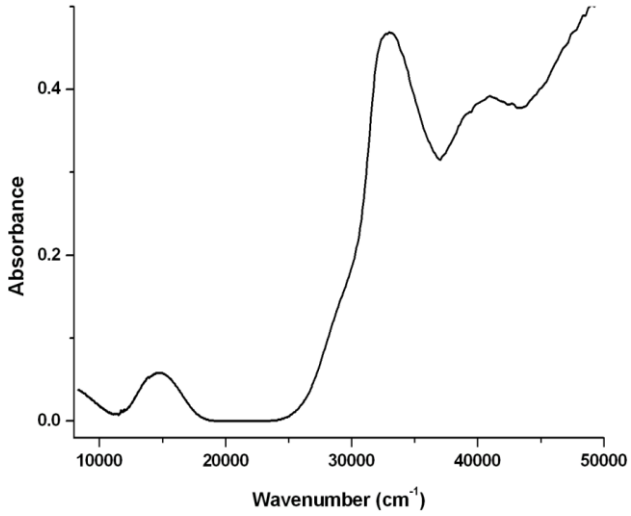

Figure 3.5. Diffuse reflectance spectrum of compound **2**

3.5.5. EPR spectra

The X-band polycrystalline-powder electron paramagnetic resonance (EPR) spectra of **1-3** were measured at room temperature and 77 K (Figure 3.6 - Figure 3.8). All spectra have been normalized to same microwave frequency (ν = 9.6528 GHz). The spectra **2** and **3** show well

resolved EPR signals at both temperatures, the corresponding g, A values were given in Table 3.6. The parameters are consistent with tetragonally elongated $Cu(bpy)_3^{2+}$. The resolution of hyperfine splittings in these pure (magnetically concentrated) samples indicate that lanthanide anions serve to magnetically isolate the $Cu(bpy)_3^{2+}$ ions. The paramagnetic lanthanide ions do not make any significant contribution to the EPR spectrum down to 77K (except in the case of Gd^{3+}). Temperature dependence of the EPR parameters arises as a consequence of the change in Jahn-Teller distortion. There could also be some contribution from dynamic Jahn-Teller effect which can be probed only by variable temperature measurements to much lower temperatures. Remarkably, the temperature dependent changes do not lead to disorder which would have caused broadening of the spectrum as in the case of strain-broadening.[8] The spectrum of **1** is less resolved at room temperature. The resulting g, A values at 300 K: ($g_{\|}$, $A_{\|}$) not resolved, $g_{\perp}$ = 2.096, $A_{\perp} \leq 65$ G; at 77 K: $g_{\|} = 2.276$, $g_{\perp} = 2.071$, $A_{\|} = 151$ G, $A_{\perp} \leq 50$ G.

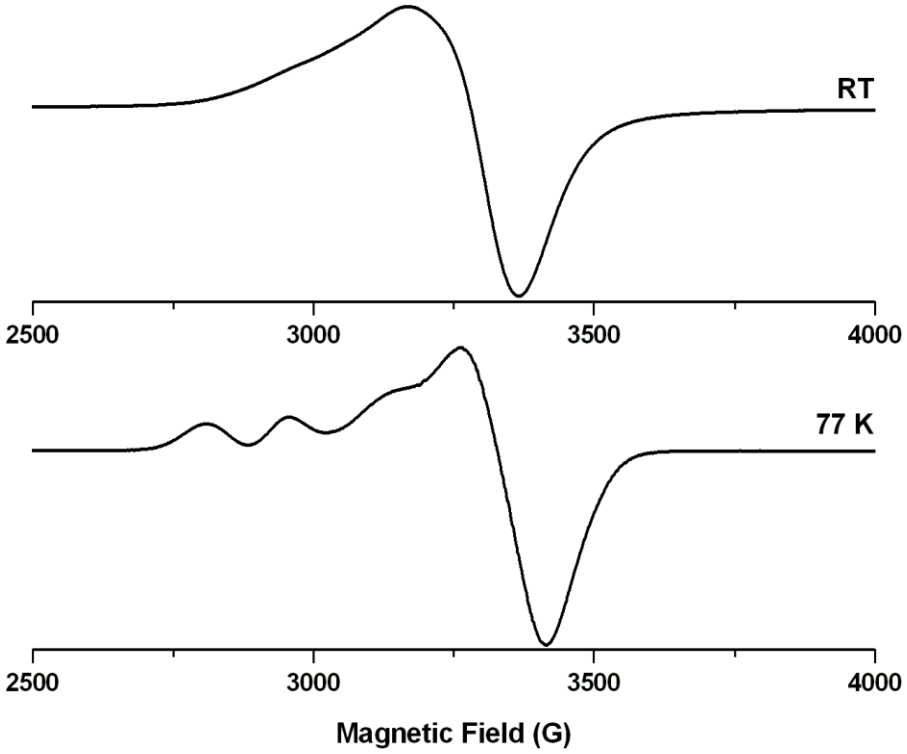

Figure 3.6. Comparison of EPR spectra collected at two different temperatures for compound **1** (Cu-La)

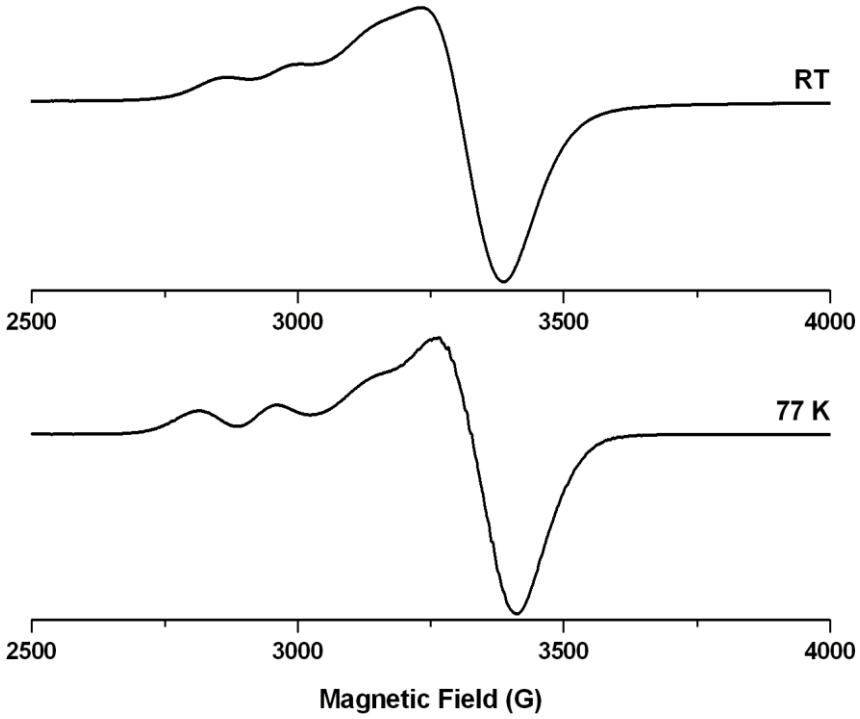

Figure 3.7. Comparison of EPR spectra collected at two different temperatures for compound **2** (Cu-Ce)

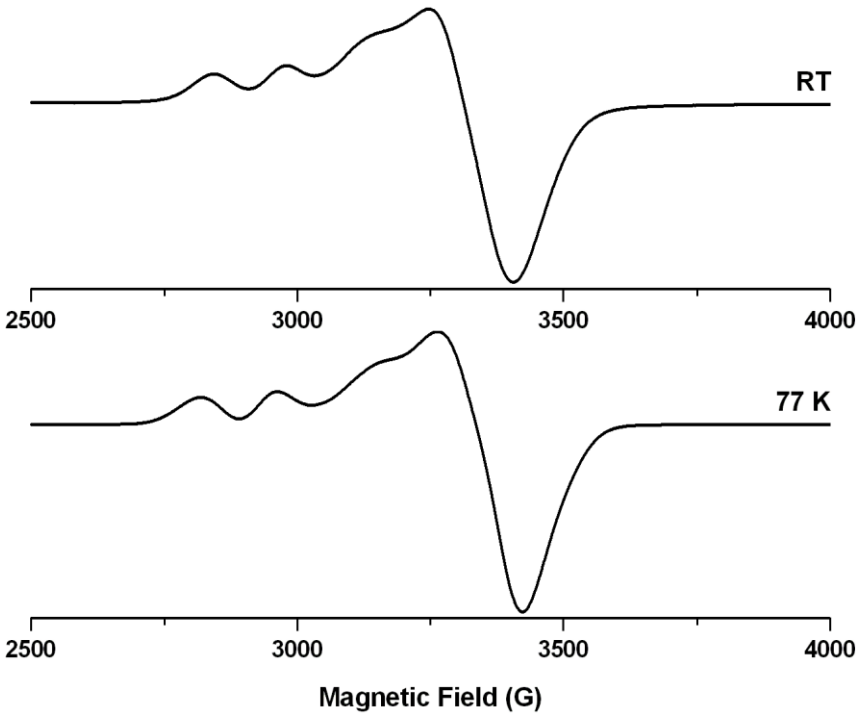

Figure 3.8. Comparison of EPR spectra collected at two different temperatures for compound **3** (Cu-Pr)

Table 3.6. EPR parameters for **1 − 3**

	300 K				77 K			
Comp.	$g_{\|}$	$g_{\perp}$	$A_{\|}$ (G)	$A_{\perp}$ (G)	$g_{\|}$	$g_{\perp}$	$A_{\|}$ (G)	$A_{\perp}$ (G)
1	-	2.096	-	≤ 65	2.276	2.071	151	≤ 50
2	2.268	2.083	127	≤ 52	2.272	2.068	148	≤ 50
3	2.264	2.077	137	≤ 50	2.268	2.058	148	≤ 50

Table 3.7: Crystallographic data and structure refinement of **5-9**

Param	**5**	**6**	**7**	**8**	**9**
Formula	$C_{30}H_{24}N_{11}O_{15}CuSm$	$C_{30}H_{24}N_{11}O_{15}CuEu$	$C_{30}H_{24}N_{11}O_{15}CuGd$	$C_{30}H_{24}N_{11}O_{15}CuTb$	$C_{30}H_{24}N_{11}O_{15}CuDy$
Formula weight	992.49	994.10	999.39	1001.06	1004.64
Crystal system	Triclinic	Triclinic	Triclinic	Triclinic	Triclinic
Space group	$P\,\bar{1}$	$P\,\bar{1}$	$P\,\bar{1}$	$P\,\bar{1}$	$P\,\bar{1}$
a (Å)	9.338(2)	9.342(7)	9.339(12)	9.336(2)	9.344(3)
b (Å)	12.866(3)	12.892(10)	12.863(16)	12.864(3)	12.822(4)
c (Å)	16.587(4)	16.581(13)	16.522(2)	16.516(4)	16.483(5)
α (°)	79.766(4)	79.852(14)	79.995(2)	80.009(4)	79.947(4)
β (°)	78.956(4)	79.104(14)	78.925(2)	78.948(4)	79.214(5)
γ (°)	76.054(4)	75.913(14)	76.090(2)	76.187(4)	76.007(5)
V (Å^3)	1880.1(7)	1884.1(3)	1873.6(4)	1873.4(7)	1864.9(9)
Z	2	2	2	2	2
T(K)	298(2)	298(2)	298(2)	298(2)	298(2)
λ (Å)	0.71073	0.71073	0.71073	0.71073	0.71073
D_{cal} (g cm^{-3})	1.753	1.752	1.772	1.775	1.789
μ (mm^{-1})	2.196	2.297	2.406	2.524	2.643
F(000)	984	986	988	990	992
Crystal size (mm)	0.24 x 0.20 x 0.12	0.28 x 0.12 x 0.08	0.36 x 0.32 x 0.16	0.36 x 0.24 x 0.12	0.28 x 0.20 x 0.08
θ Range(°)	1.26 – 25.00	1.26 – 24.41	1.27 – 25.00	1.27 – 25.00	1.27 – 25.00
h/k/l indices	–11, 11/ –15, 15/ –19, 19	–10, 10/ –14, 14/ –18, 18	–11, 11/ –15, 15/ –19, 19	–11, 11/ –15, 15/ –19, 19	–11, 11/ –15, 15/ –19, 19
Refl^n collected	18205	8497	18138	18143	17882
Unique refl^n [R_{int}]	6597 [0.0335]	5677 [0.0409]	6576 [0.0290]	6579 [0.0308]	6558 [0.0361]
GooF	1.027	1.015	1.011	1.036	1.029
R_1 [I>2σ(I)]	0.0416	0.0653	0.0394	0.0383	0.0454
wR_2	0.1147	0.1599	0.1061	0.1068	0.1147

Table 3.8: Crystallographic data and structure refinement of **10-14**

Param	**10**	**11**	**12**	**13**	**14**
Formula	$C_{30}H_{24}N_{11}O_{15}CuHo$	$C_{30}H_{24}N_{11}O_{15}CuEr$	$C_{30}H_{24}N_{11}O_{15}CuTm$	$C_{30}H_{24}N_{11}O_{15}CuYb$	$C_{30}H_{24}N_{11}O_{15}CuLu$
Formula weight	1007.07	1009.40	1011.07	1015.18	1017.11
Crystal system	Triclinic	Triclinic	Triclinic	Triclinic	Triclinic
Space group	$P\bar{1}$	$P\bar{1}$	$P\bar{1}$	$P\bar{1}$	$P\bar{1}$
a (Å)	9.3361(6)	9.3473(3)	9.3400(15)	9.3383(7)	9.3353(19)
b (Å)	12.8314(8)	12.8213(4)	12.795(2)	12.8072(10)	12.791(3)
c (Å)	16.4690(11)	16.4648(7)	16.424(3)	16.4190(13)	16.421(3)
α (˚)	80.0180(10)	79.949(3)	79.805(2)	80.0810(10)	80.167(3)
β (˚)	79.0640(10)	79.179(3)	79.496(2)	79.1580(10)	79.128(3)
γ (˚)	76.0960(10)	76.029(3)	75.968(2)	76.0410(10)	76.008(3)
V (Å^3)	1863.4(2)	1854.0(5)	1854.0(5)	1855.0(2)	1852.3(7)
Z	2	2	2	2	2
T(K)	298(2)	298(2)	298(2)	298(2)	298(2)
λ (Å)	0.71073	0.71073	0.71073	0.71073	0.71073
D_{calc} (g cm^{-3})	1.795	1.799	1.811	1.818	1.824
μ (mm^{-1})	2.763	5.511	3.036	3.164	3.309
F(000)	994	996	998	1000	1002
Crystal size (mm)	0.36 x 0.28 x 0.16	0.28 x 0.20 x 0.16	0.28 x 0.20 x 0.08	0.36 x 0.20 x 0.12	0.40 x 0.36 x 0.32
θ Range(˚)	1.27 – 25.00	3.59 – 71.58	1.66 – 25.96	1.27 – 25.00	1.66 – 25.00
h/k/l indices	–11, 11/ –15, 15/ –19, 19	–11, 11/ –15, 10/ –20, 20	–11, 11/ –15, 15/ –20, 20	–11, 11/ –15, 15/ –19, 19	–11, 11/ –15, 10/ –19, 19
Refl^n collected	18063	11795	19204	17944	17888
Unique refl^n [R_{int}]	6549 [0.0313]	7088 [0.0198]	7183 [0.0281]	6521 [0.0280]	6513 [0.0263]
GooF	1.030	1.033	1.022	1.048	1.029
R_1 [I>2σ(I)]	0.0381	0.0467	0.0360	0.0361	0.0341
wR_2	0.1039	0.1364	0.0973	0.0988	0.0940

3.6. $[Cu(bpy)_3][Ln(NO_3)_5]$ (*Ln* = Nd (4), Sm (5), Eu (6), Gd (7), Tb (8), Dy (9), Ho (10), Er (11), Tm (12), Yb (13) and Lu (14))

3.6.1. Crystal structure of $\{[Cu(bpy)_3][Ln(NO_3)_5]\}$ (4-14)

Compounds **4-14** form isomorphous crystals. Since geometrical parameters of all compounds are similar the selected bond lengths and angles of compound **5** are given in Table

3.9. The asymmetric unit consisted of a discrete $[Cu(bpy)_3]^{2+}$ cation and $[Ln(NO_3)_5]^{2-}$ anion in a 1:1 ratio is shown in Figure 3.9.

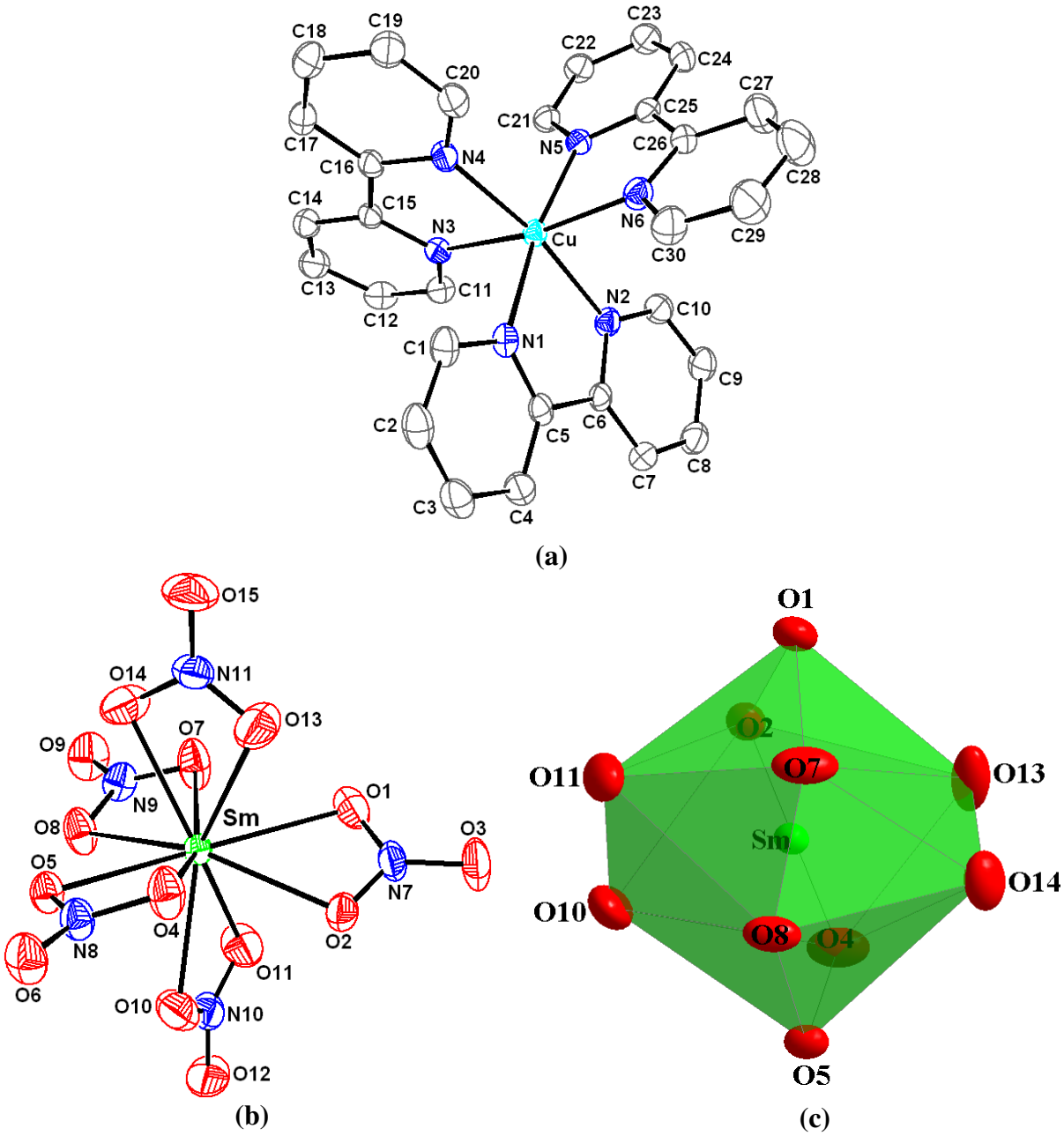

Figure 3.9: Thermal ellipsoid plot of the coordination environment of the (a) complex cation and (b) complex anion of **5** (c) bicapped square antiprism coordination polyhedron of Sm(III) ion in $[Sm(NO_3)_5)]^{2-}$: Atoms are represented as 30% probability ellipsoids. Ring hydrogen atoms have been omitted for clarity.

The Cu(II) ion adopts a distorted octahedral environment, coordinated by six nitrogen atoms from three bpy ligands. Cu–N bond lengths (Å) are in the range 2.085(3)–2.157(4) in good agreement with the previously reported values for analogous complexes.[1f-h] At room temperature for **4-14**, the *T* value is 0.98 indicating that the JT distortion is disordered (Table 3.11). In agreement with $1.0 \leq T \geq 0.9$ range this disorder is fluxional, but the 0.98 value could be representative of almost dynamic geometry of Cu(II) centre, which is very close to reported values for the analogous complexes (Table 3.12). The pyridine rings of three bpy ligands are not coplanar with the dihedral angels of 3.05 (4)º, 8.90 (3)º and 5.11 (3)º. The cation charge is balanced by a $Ln(NO_3)_5]^{2-}$ counter anion.

The *Ln*(III) ion is 10-coordinated with ten oxygen atoms from five chelating nitrate ions, forming a distorted bicapped square antiprism[9] (Figure 3.9(c)). *Ln*–O bond lengths (Å) lie in the range 2.472(4)-2.542(4) for **4**; 2.448(4)-2.515(4) for **5**; 2.420(4)-2.521(4) for **6**; 2.429(4)-2.498(4) for **7**; 2.414(4)-2.490(4) for **8**; 2.395(5)-2.477(5) for **9**; 2.385(4)-2.468(4) for **10**; 2.385(5)-2.468(4) for **11**; 2.371(4)-2.454(4) for **12**; 2.355(4)-2.455(4) for **13**; 2.344(4)-2.456(4) for **14**.

The crystal packing of **5** (Figure 3.10) forms 1D network with the help of C-H···O interactions (C3–H3···O5, 2.580(4); C22–H22···O13, 2.589(8); C28–H28···O3, 2.595(7) Å). These are further interconnect with the π-stacking interactions (3.470-3.580 Å) build the above network into a 2D network. The O–N distances (Å) are 1.18(7)-1.32(8) (avg. 1.23(4)) and O–N–O bond angles (º) range is 112.7(5)-125.4(8). The three nitrate ions were approximately in the same plane constitute three planar sets: O1, O2, O3, N7 and Sm (plane **I**); O4, O5, O6, N8 and Sm (plane **II**), and O7, O8, O9, N9 and Sm (plane **III**). The dihedral angles being 28.6º between plane **I** and plane **II**, 15.0º between plane **II** and plane **III**, and 18.3° between plane **I** and plane

III. The remaining two nitrate planar sets: O10, O11, O12, N10 and Sm (plane **IV**); O13, O14, O15, N11 and Sm (plane **V**) were nearly perpendicular to these planes (the dihedral angles were 74.72-85.95°). The dihedral angles being 87.95° between plane **IV** and plane **V**.

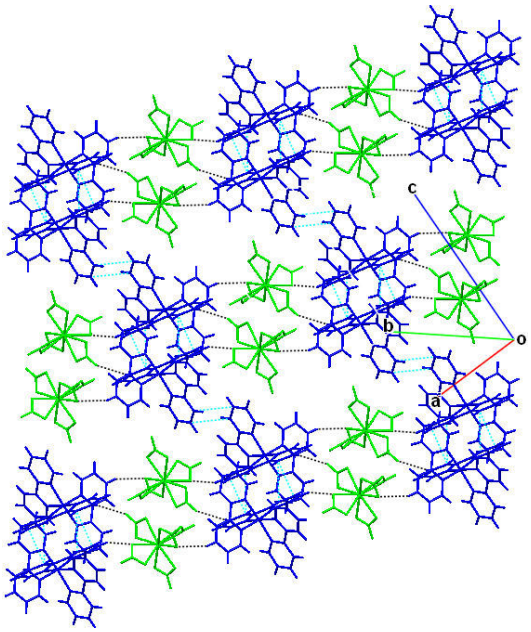

Figure 3.10. The molecular packing of **5**

Table 3.9: Selected bond lengths (Å) and bond angles (˚) for {[Cu(bpy)$_3$][Sm(NO$_3$)$_5$]}

Cu-N(1)	2.082(4)	Cu-N(3)	2.120(4)	Cu-N(5)	2.097(4)
Cu-N(2)	2.126(4)	Cu-N(4)	2.114(4)	Cu-N(6)	2.158(4)
Sm-O(1)	2.515(4)	Sm-O(13)	2.480(5)	Sm-O(8)	2.461(4)
Sm-O(4)	2.456(4)	Sm-O(2)	2.494(4)	Sm-O(11)	2.475(5)
Sm-O(7)	2.448(4)	Sm-O(5)	2.505(3)	Sm-O(14)	2.504(5)
Sm-O(10)	2.475(5)				
N(7)-O(1)	1.255(7)	N(8)-O(6)	1.197(6)	N(10)-O(11)	1.181(7)
N(7)-O(2)	1.242(7)	N(9)-O(7)	1.249(6)	N(10)-O(12)	1.208(7)
N(7)-O(3)	1.199(6)	N(9)-O(8)	1.245(6)	N(11)-O(13)	1.187(7)
N(8)-O(4)	1.272(6)	N(9)-O(9)	1.209(6)	N(11)-O(14)	1.242(7)
N(8)-O(5)	1.233(5)	N(10)-O(10)	1.316(8)	N(11)-O(15)	1.189(6)
N(1)-Cu-N(2)	77.96(15)	N(2)-Cu-N(3)	97.77(16)	N(3)-Cu-N(6)	170.58(14)
N(1)-Cu-N(3)	92.65(15)	N(2)-Cu-N(4)	170.73(15)	N(4)-Cu-N(5)	90.79(15)
N(1)-Cu-N(4)	94.35(15)	N(2)-Cu-N(5)	97.49(15)	N(4)-Cu-N(6)	96.91(16)
N(1)-Cu-N(5)	171.33(14)	N(3)-Cu-N(4)	77.21(16)	N(5)-Cu-N(6)	77.28(15)

N(1)-Cu-N(6)	95.15(14)	N(3)-Cu-N(5)	95.29(15)	N(2)-Cu-N(6)	89.02(16)
O(1)-Sm-O(2)	50.09(16)	O(2)-Sm-O(13)	74.47(16)	O(5)-Sm-O(7)	117.50(14)
O(1)-Sm-O(4)	117.37(16)	O(2)-Sm-O(14)	122.84(15)	O(5)-Sm-O(8)	68.62(13)
O(1)-Sm-O(5)	167.13(14)	O(10)-Sm-O(11)	49.7(2)	O(5)-Sm-O(10)	72.18(17)
O(1)-Sm-O(7)	73.76(17)	O(10)-Sm-O(13)	140.5(3)	O(5)-Sm-O(11)	113.24(17)
O(1)-Sm-O(8)	123.68(16)	O(10)-Sm-O(14)	148.2(2)	O(5)-Sm-O(13)	100.93(19)
O(1)-Sm-O(10)	109.06(18)	O(11)-Sm-O(13)	144.0(2)	O(5)-Sm-O(14)	76.10(17)
O(1)-Sm-O(11)	74.72(18)	O(11)-Sm-O(14)	149.9(2)	O(7)-Sm-O(8)	50.75(14)
O(1)-Sm-O(13)	69.70(19)	O(13)-Sm-O(14)	48.38(17)	O(7)-Sm-O(10)	117.8(2)
O(1)-Sm-O(14)	102.22(18)	O(4)-Sm-O(5)	49.93(12)	O(7)-Sm-O(11)	74.5(2)
O(2)-Sm-O(4)	74.11(15)	O(4)-Sm-O(7)	158.87(19)	O(7)-Sm-O(13)	100.1(2)
O(2)-Sm-O(5)	119.88(14)	O(4)-Sm-O(8)	118.26(14)	O(7)-Sm-O(14)	75.89(19)
O(2)-Sm-O(7)	122.36(15)	O(4)-Sm-O(10)	77.1(2)	O(8)-Sm-O(10)	91.1(2)
O(2)-Sm-O(8)	160.14(16)	O(4)-Sm-O(11)	124.6(2)	O(8)-Sm-O(11)	81.34(19)
O(2)-Sm-O(10)	76.05(18)	O(4)-Sm-O(13)	70.0(2)	O(8)-Sm-O(13)	123.34(19)
O(2)-Sm-O(11)	78.80(18)	O(4)-Sm-O(14)	83.92(19)	O(8)-Sm-O(14)	75.69(18)
O(1)-N(7)-O(2)	116.3(5)	O(5)-N(8)-O(6)	124.0(5)	O(10)-N(10)-O(12)	120.6(8)
O(1)-N(7)-O(3)	121.2(7)	O(7)-N(9)-O(8)	115.0(5)	O(11)-N(10)-O(12)	125.4(8)
O(2)-N(7)-O(3)	122.5(7)	O(7)-N(9)-O(9)	123.0(6)	O(13)-N(11)-O(14)	114.4(5)
O(4)-N(8)-O(5)	113.4(5)	O(8)-N(9)-O(9)	121.9(6)	O(13)-N(11)-O(15)	123.6(7)
O(4)-N(8)-O(6)	122.1(5)	O(10)-N(10)-O(11)	112.7(5)	O(14)-N(11)-O(15)	121.7(7)

Table 3.10: Intermolecular interaction parameters

*H-bonding for **5***

D-H···A	***d*(D-H)(Å)**	***d*(H···A)(Å)**	***d*(D···A)(Å)**	**<(D-H···A)(º)**
C3–H3···O5#1	0.93	2.58	3.42	151
C22–H22···O13#2	0.93	2.59	3.42	148
C28–H28···O3#3	0.93	2.59	3.18	121

(#1) *x*, –1+*y*, *z***;** (#2) 1+*x*, *y*, *z*; (#3)2–*x*, 1–*y*, 1–*z*

*π···π interactions for **5** (Å)*

C17···C18#1	3.580(9)	C23···C27#2	3.470(8)
C24···C27#2	3.561(7)	(#1) 1–*x*, 1–*y*, –*z***;** (#2) 1–*x*, 1–*y*, 1–*z*	

Table 3.11: Cu-N equatorial and axial bond distances (Å) and Tetragonality (*T*) values for **1-14**

	Cu-N(1) equa	Cu-N(2) equa	Cu-N(3) **axial**	Cu-N(4) equa	Cu-N(5) equa	Cu-N(6) **axial**	*T*
1	2.044(5)	2.019(4)	**2.361(5)**	2.039(5)	2.035(4)	**2.229(5)**	0.8863
2	2.040(4)	2.018(4)	**2.346(5)**	2.115(5)	2.039(4)	**2.250(5)**	0.8933
3	2.047(2)	2.018(2)	**2.343(2)**	2.093(2)	2.034(2)	**2.263(2)**	0.8891
4	2.085(3)	2.129(4)	**2.149(4)**	2.094(4)	2.117(4)	**2.123(4)**	0.9859
5	2.082(4)	2.126(4)	**2.120(4)**	2.097(4)	2.114(4)	**2.158(4)**	0.9840
6	2.100(8)	2.120(8)	**2.163(8)**	2.096(8)	2.129(8)	**2.124(8)**	0.9848
7	2.080(4)	2.119(4)	**2.156(4)**	2.095(4)	2.113(4)	**2.125(4)**	0.9817
8	2.082(4)	2.121(4)	**2.158(4)**	2.095(4)	2.110(4)	**2.124(4)**	0.9817
9	2.085(4)	2.119(5)	**2.156(5)**	2.101(5)	2.108(5)	**2.114(5)**	0.9850
10	2.084(4)	2.120(4)	**2.162(4)**	2.098(4)	2.111(4)	**2.126(4)**	0.9808
11	2.080(4)	2.121(4)	**2.133(4)**	2.104(4)	2.108(4)	**2.160(4)**	0.9798
12	2.084(3)	2.119(4)	**2.153(4)**	2.103(4)	2.109(4)	**2.121(4)**	0.9845
13	2.087(4)	2.118(4)	**2.156(4)**	2.102(4)	2.106(4)	**2.127(4)**	0.9822
14	2.085(4)	2.110(4)	**2.160(4)**	2.099(4)	2.102(4)	**2.125(4)**	0.9796

Table 3.12: Structural data for the $[Cu(bpy)_3]Y$ series of complexes

Comp.	*T*	*JT* distortion	Ref.
$[Cu(bpy)_3][CrO_4]\cdot 7.5H_2O$	0.9830/0.9876	fluxional	[1g]
$[Cu(bpy)_3][PF_6]_2$	0.9608	fluxional	[1f]
$[Cu(bpy)_3][SO_4]\cdot 7.5H_2O$	0.958	fluxional	[1h]
4-14	0.9796-0.9859	fluxional	pw
$[Cu(bpy)_3][SO_4]_{0.5}(7.8\cdot H_2O)$	0.9435	fluxional	[1a]
$[Cu(bpy)_3][BPh_4]_2$	0.8868	static	[1a]
$[Cu(bpy)_3][BF_4]_2$	0.8699	static	[1b]
$[Cu(bpy)_3][ClO_4]_2$	0.8636-0.8695	static	[1c-e]
1-3	0.8863-0.8933	static	pw

3.6.2. Infrared spectra

The $\nu_{C=C}$ frequency of the bpy rings at 1600 and 1570 cm^{-1}. The band around 3100 cm^{-1} assigned to the ν_{C-H} frequency. This valve shifted to lower frequencies on complexation. The

stretching vibrations corresponding to those typical of coordinated bpy occur around at 760, 810, 1030, 1160 and 1600 cm^{-1}.

3.6.3. Electronic spectra

The electronic spectra of **4-14** consist of a broad band centered at 14500 cm^{-1} ($d_z^2 \approx d_{xy} \rightarrow d_{x2-y2}$) may be assigned to metal centered d-d transition, which is similar to those previously reported $[Cu(bpy)_3]Y$ complexes.[1] The lower energy band maximum (about 6000 cm^{-1}) is too low to be seen in the present measurement. Band near 33,000 cm^{-1} is due to ligand-to-metal charge transfer transition, while the band near 40,600 cm^{-1} is associated with intraligand $\pi \rightarrow \pi^*$ excitation (Figure 3.11).

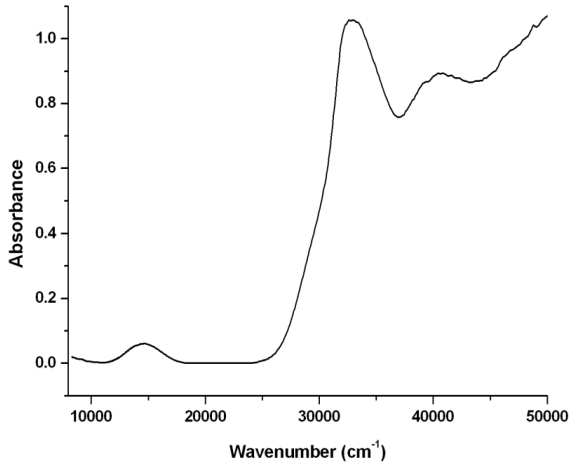

Figure 3.11. Diffuse reflectance spectrum of compound **5**

3.6.4. EPR spectra

The X-band polycrystalline-powder electron paramagnetic resonance (EPR) spectra of **4-14** were measured at room temperature and 77 K (Figure 3.12-Figure 3.22). All spectra have been normalized to same microwave frequency (ν = 9.6528 GHz). The room temperature spectra consisting of a broad signal centered at about ~3240 G, as expected for Cu(II) system. The liquid

nitrogen temperature spectra of all compounds have shown better resolved EPR signals and corresponding g, A values were given in Table 3.13. In complex **7** the Cu(II) signals overlap with Gd^{3+} signals and therefore not included in the Table. The EPR parameters are, as expected, comparable to the previous set of compounds. However, the resolution is greatly reduced. This is the case even for the Lu^{3+} complex indicating that the reduced efficiency of the 10-coordinate lanthanide ions for magnetically isolating $Cu(bpy)_3^{2+}$. Another factor responsible for the difference in RT and 77K spectra is the greatly enhanced value of *T* in these complexes leading to dynamic effects.

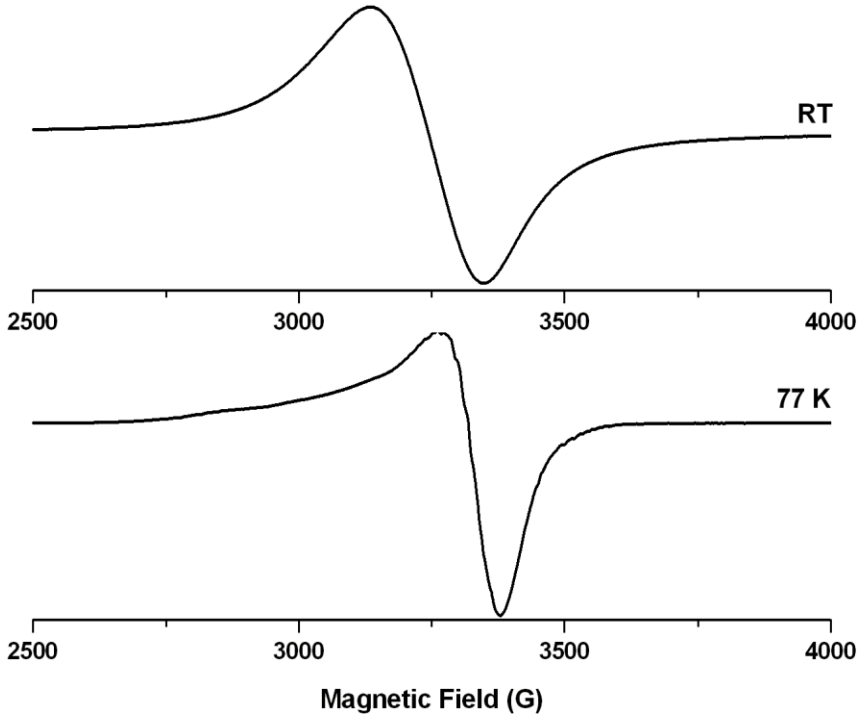

Figure 3.12. Comparison of EPR spectra collected at two different temperatures for compound **4** (Cu-Nd)

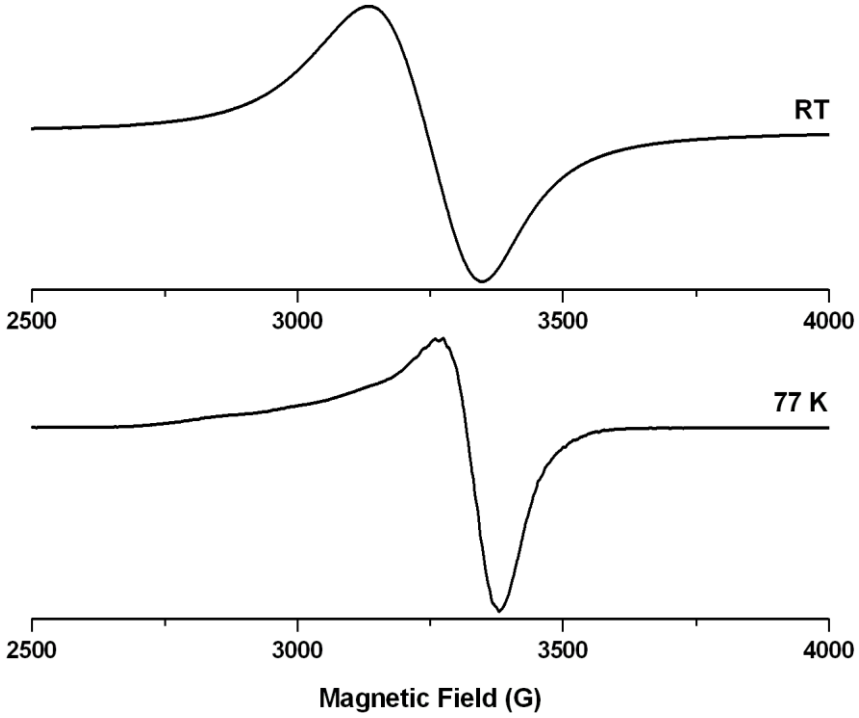

Figure 3.13. Comparison of EPR spectra collected at two different temperatures for compound **5** (Cu-Sm)

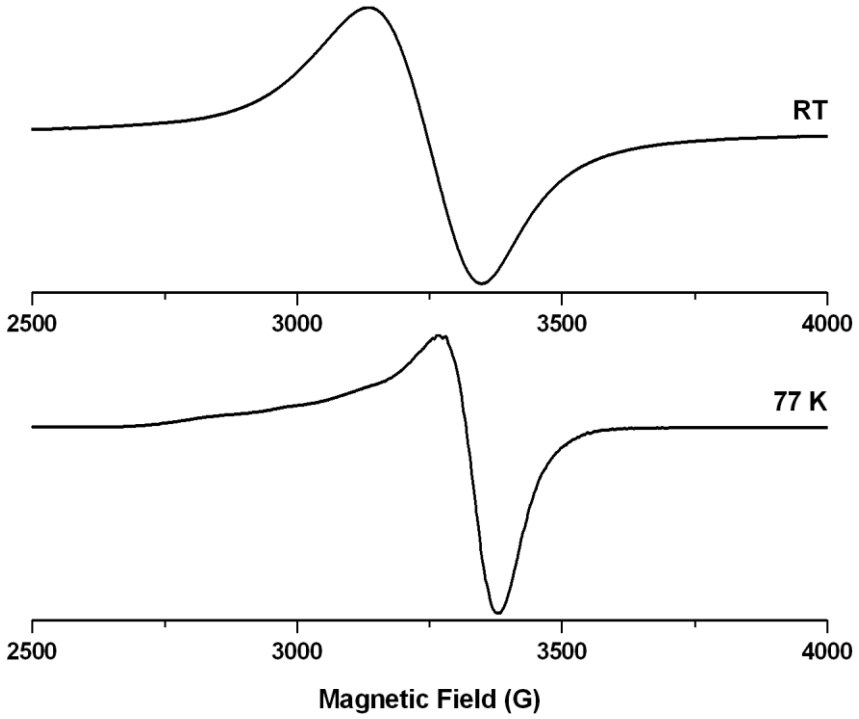

Figure 3.14. Comparison of EPR spectra collected at two different temperatures for compound **6** (Cu-Eu)

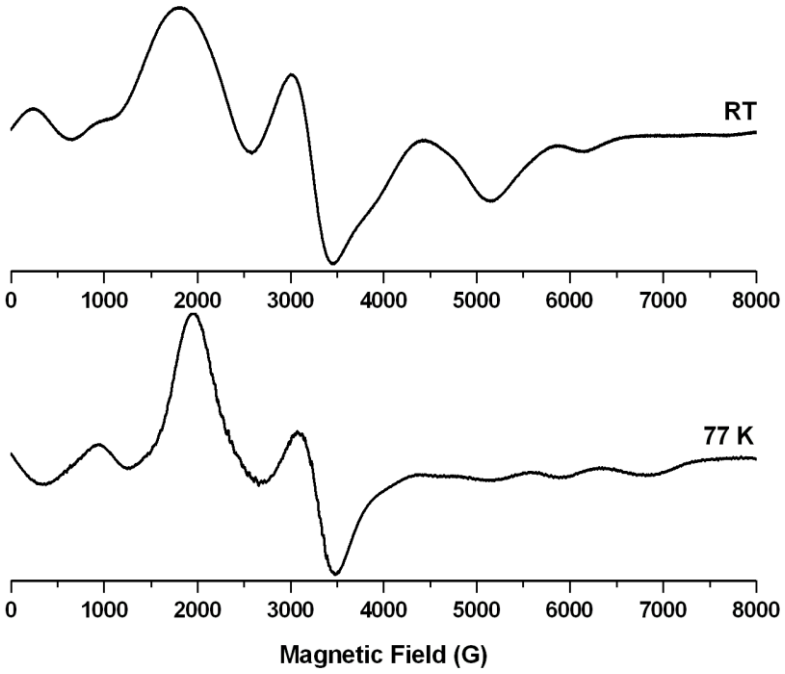

Figure 3.15. Comparison of EPR spectra collected at two different temperatures for compound **7** (Cu-Gd)

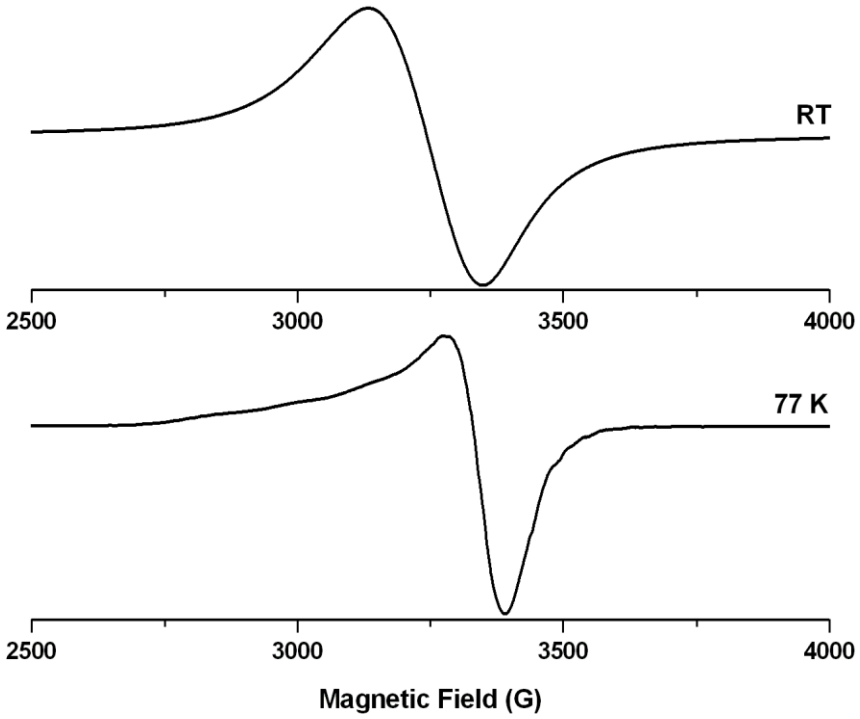

Figure 3.16. Comparison of EPR spectra collected at two different temperatures for compound **8** (Cu-Tb)

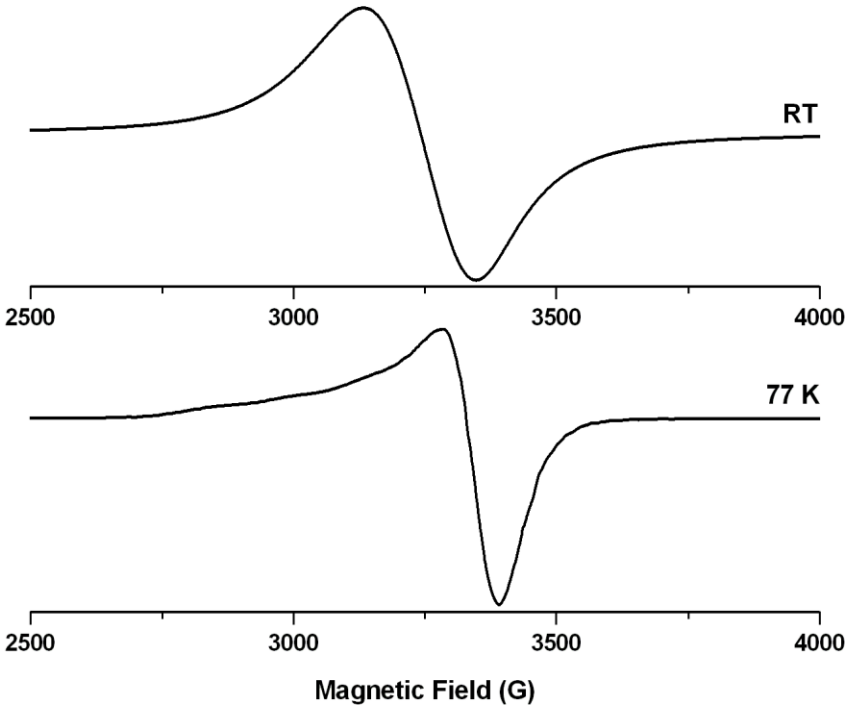

Figure 3.17. Comparison of EPR spectra collected at two different temperatures for compound **9** (Cu-Dy)

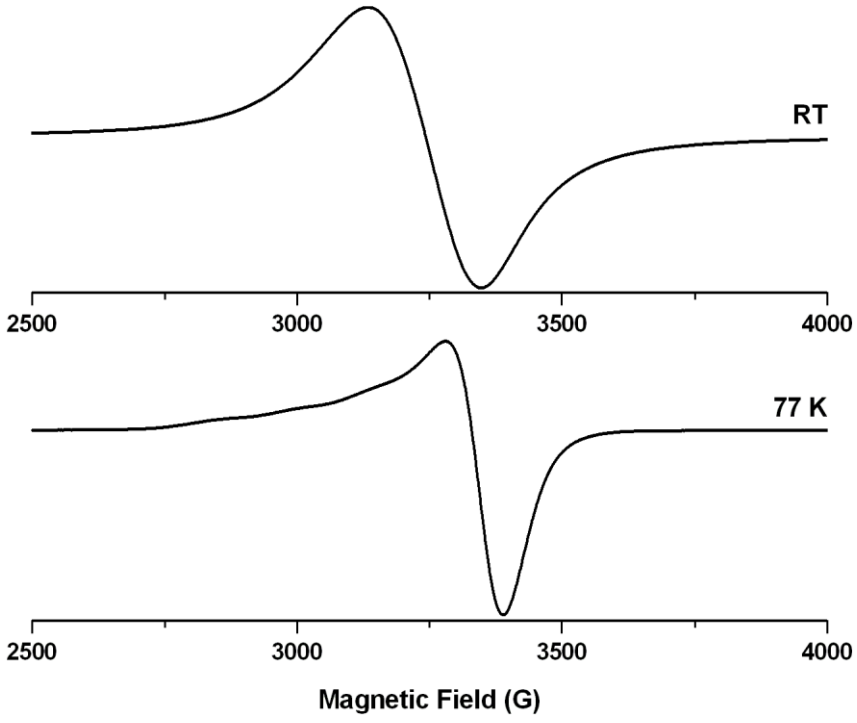

Figure 3.18. Comparison of EPR spectra collected at two different temperatures for compound **10** (Cu-Ho)

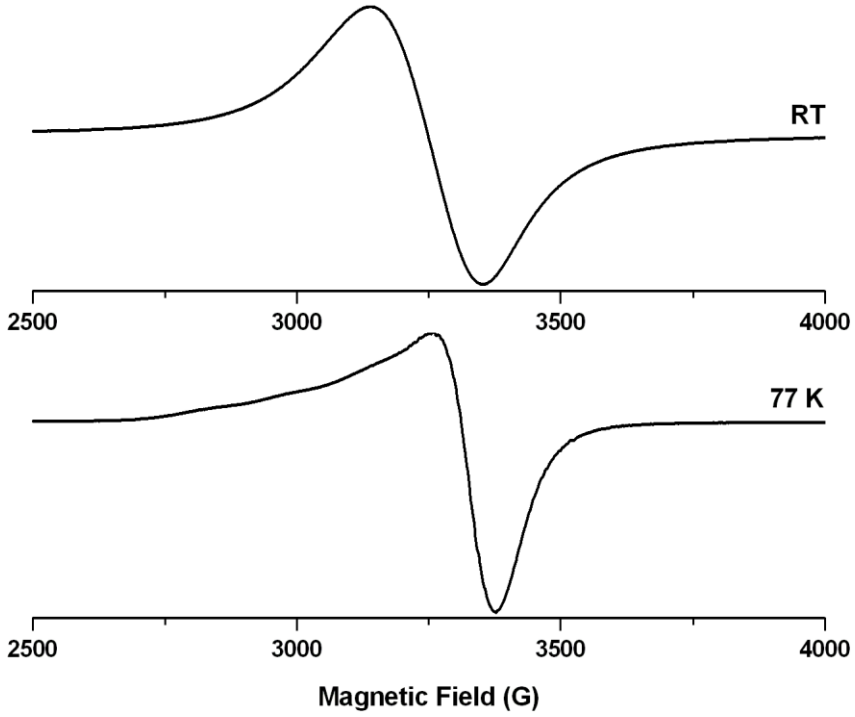

Figure 3.19. Comparison of EPR spectra collected at two different temperatures for compound **11** (Cu-Er)

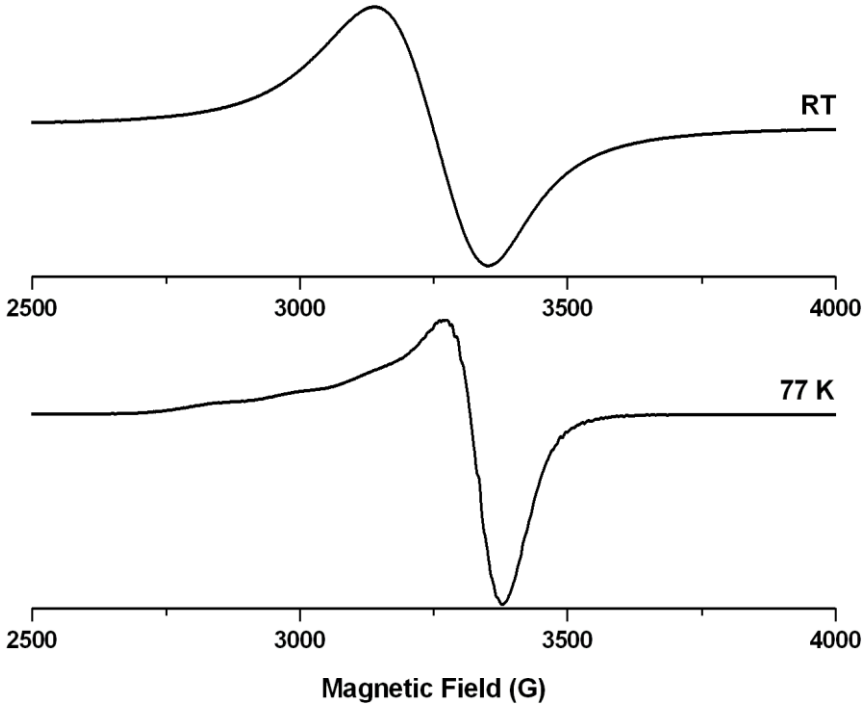

Figure 3.20. Comparison of EPR spectra collected at two different temperatures for compound **12** (Cu-Tm)

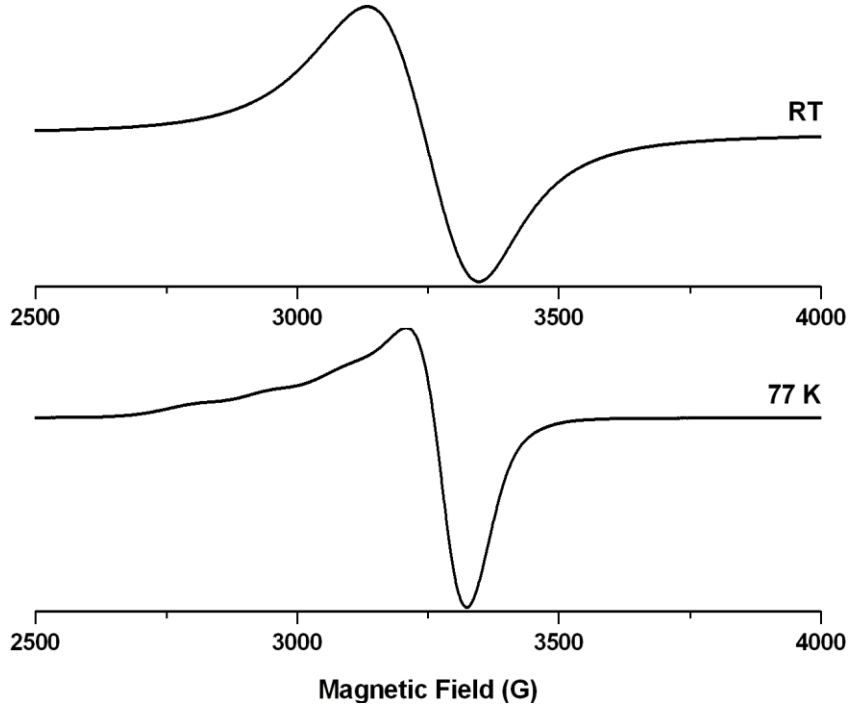

Figure 3.21. Comparison of EPR spectra collected at two different temperatures for compound **13** (Cu-Yb)

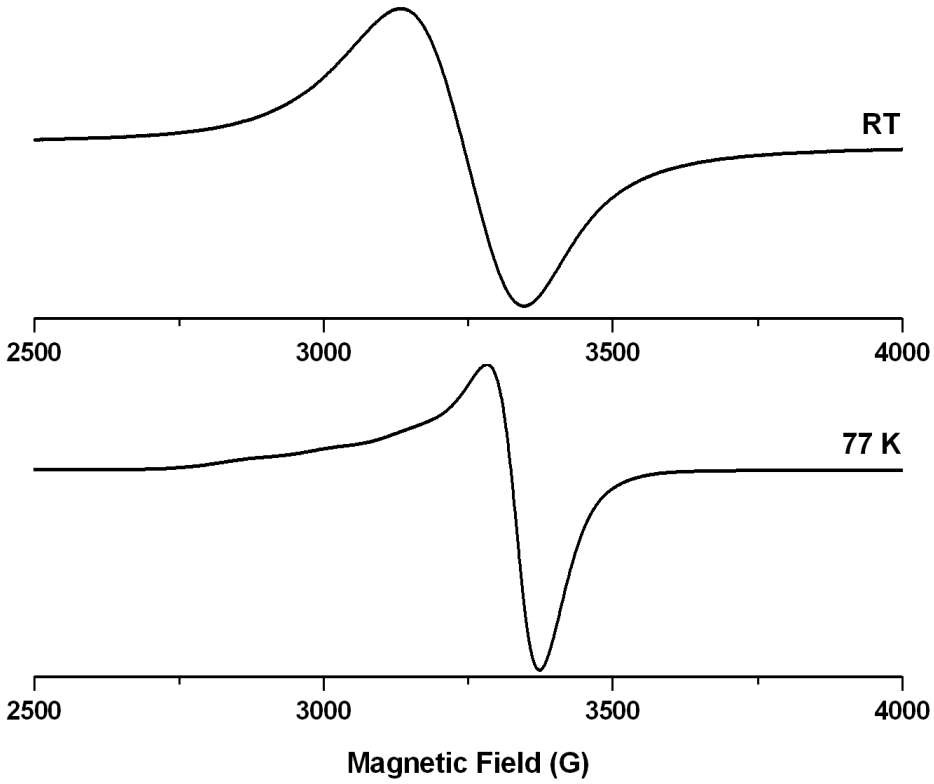

Figure 3.22. Comparison of EPR spectra collected at two different temperatures for compound **14** (Cu-Lu)

Table 3.13. EPR parameters for **4-14** at 77 K (except **7**)

Comp.	$g_{\|}$	$g_{\perp}$	$A_{\|}$ (G)	$A_{\perp}$ (G)
4	2.247	2.071	130	≤ 39
5	2.253	2.073	139	≤ 38
6	2.248	2.071	135	≤ 36
8	2.253	2.071	142	≤ 38
9	2.253	2.068	145	≤ 37
10	2.246	2.068	141	≤ 36
11	2.246	2.077	140	≤ 41
12	2.253	2.077	141	≤ 35
13	2.291	2.108	137	≤ 38
14	2.246	2.071	139	≤ 30

3.7. Conclusions

(1) All lanthanides (excluding Pm) are shown to form crystalline complexes of essentially the same stoichiometry (Cu^{2+} : Ln^{3+} : bpy : NO_3^- = 1 : 1 : 3 : 5, as in the preparative solution made in acetonitrile). The $Cu(bpy)_3^{2+}$ is less dicriminatory than $Cu(bpy)_2(NO_3)^+$ (Chapter 2) in bringing out the structural trends in the *Ln*-NO_3^--H_2O system. The cation and anion are isovalent and results in $Ln(NO_3)_5(OH_2)^{2-}$ for the first three early *Ln*'s and $Ln(NO_3)_5^{2-}$ for all other *Ln*(III) ions. Ce and Pr crystals incorporate two solvent molecules (acetonitrile). The La compound has no solvent, and unlike all other compounds discussed here it crystallises in a chiral space group ($P2_12_12_1$).

(2) The $Cu(bpy)_3^{2+}$ ion in the series Nd-Lu has a *T*-value (measure of tetragonality) of 0.98, higher than reported for $[Cu(bpy)_3](SO_4)_{0.5}\cdot(7.8\ H_2O)$[1a] which has a *T* of 0.94. This implies possible dynamic Jahn-Teller coupling operating in these crystals. In the case of La-Pr, the *T* value is less than 0.9 indicating a static distortion in these crystals.

(3) The EPR spectra are in agreement with the expectation from differing tetragonalities mentioned above. The Cu-trischelate ion is magnetically isolated by the lanthanide anions leading to resolution of Cu-nuclear hyperfine splitting at 77K in all cases. The Nd-Lu series show enhanced temperature dependence as expected from dynamic vibronic effects.

3.8. References

1. (a) B. Murphy, M. Aljabri, A. Mohamed Ahmed, G. Murphy, B. J. Hathaway, M. E. Light, T. Geilbrich, M. Hursthouse, *J. Chem. Soc., Dalton Trans*., **2006**, 357; (b) A. –C. Chamayou, C. Biswas, C. Janiaka, A. Ghosh, *Acta Cryst.,* **2007**, *E63*, m1936; (c) V. V. Pavlishchuk, A. V. Kalaida, E. A. Goreshnik, *Koord. Khim.*, **1999**, *25*, 542; (d) P. Majumdar, A. K. Ghosh, L. R. Falvello, S. -M. Peng, S. Goswami, *Inorg. Chem.*, **1998**, *37*, 1651; (e) Z. -M. Liu, Z. -H. Jiang, D. -Z. Liao, G. -L.Wang, *Polyhedron*, **1991**, *10*, 101; (f) J. M. Seco, M. J. Garmendia, M. Quitros, *J. Coord. Chem.*, **2002**, *55*, 345; (g) A. Wojciechowska, A. Pietraszko, W. Bronowska, Z. Staszak, J. Jezierska, M. C. Golonka, *Polyhedron*, **2010**, *29*, 2574; (h) A. Wojciechowska, J. Jezierska, A. Bienko, M. Daszkiewicz, *Polyhedron*, **2011**, *30*, 1547
2. A. Murphy, B. J. Hathaway, *J. Chem. Soc.,Dalton Trans.*, **1979**, 1646.
3. SAINTPLUS, Bruker AXS Inc., Madison, Wisconsin, USA **2003**.
4. G. M. Sheldrick, SADABS, Program for empirical absorption correction (University of Gottingen, Gottingen, Germany) **1996**.
5. G. M. Sheldrick, *Acta Crystallogr*., **2008**, *A64*, 112.
6. C. F. Macrae, I. J. Bruno, J. A. Chisholm, P. R. Edgington, P. McCabe, E. Pidcock, L. Rodriguez-Monge, R. Taylor, J. van de Streek, P. A. Wood, *J. Appl. Cryst*., **2008**, *41*, 466.

7. (a) D. J. Evans, P. C. Junk, M. K. Smith, *New J. Chem.*, **2002**, *26*, 1043; (b) G. Novitskii, A. Borta, D. Ganzhu, S. Shova, I. G. Filippova, Yu. A. Simonov, *Koord. Khim.(Russ.)*, **2009**, *35*, 386; (c) G. -L. Xue, Y. -X. Yang, H. -X. Li, S. -Y. He, J. Li, *Chin. J. Inorg. Chem.*, **2001**, *3*, 423; (d) C. -B. Ma, M. -Q. Hu, H. Chen, C. -N. Chen, Q. -T. Liu, *Eur. J. Inorg. Chem.*, **2011**, 5043; (e) G. Y. S. Chan, M. G. B. Drew, M. J. Hudson, N. S. Isaacs, P. Byers, *Polyhedron*, **1996**, *15*, 3385.

8. (a) B. Hathaway, *Struct. Bonding*, **1984**, *57*, 55; (b) B. J. Hathaway, A. A. G. Tomlinson, *Coord. Chem. Rev.*, **1970**, *5*, 1; (c) H. Elliott, B. J. Hathaway, *Inorg. Chem.*, **1966**, *5*, 885; (d) F. Clifford, E. Counihan, W. Fitzgerald, K. Seff, Ch. Simmons, S. Tyagi, B. Hathaway, *J. Chem. Soc., Chem. Commun.*, **1982**, 196.

9. (a) M. W. Chorab, A. Gorczynski, M. Kubicki, Z. Hnatejko, V. Patroniak, *Polyhedron*, **2012**, *31,* 51; (b) E. B. Dhoot, J. Fawcett, R. A. Kresinski, A. W. G. Platt, *Polyhedron*, **2009**, *28,* 1497; (c) A. N. Georgopoulou, R. Adam, C. P. Raptopoulou, V. Psycharis, R. Ballesteros, B. Abarca, A. K. Boudalis, *Dalton Trans*., **2011**, *40*, 8199; (d) T. Otsuka, H. Cui, A. Kobayashi, Y. Misaki, H. Kobayashiz, *J. Solid State Chem.*, **2002**, *168*, 444; (e) C. G. Efthymiou, A. N. Georgopoulou, C. Papatriantafyllopoulou, A. Terzis, C. P. Raptopoulou, A. Escuer, S. P. Perlepes, *Dalton Trans*., **2010**, *39*, 8603; (f) H. Cui, T. Otsuka, A. Kobayashi, N. Takeda, M. Ishikawa, Y. Misaki, H. Kobayashi, *Inorg. Chem.*, **2003**, *42*, 6114; (g) W. Urland, E. Warkentin, *Z. Naturforsch*. **1983**, *88b*, 299.

CHAPTER IV

Synthesis, structural and spectral properties of the lanthanide nitrato complex anions crystallized using Cu(II) nitrate and 5,5'-dimethyl-2,2'-bipyridine

4.1. Introduction

Earlier studies, chapter II and chapter III have been focused on the synthesis of heterometallic Cu(II)/*Ln*(III) compounds using 2,2'-bipyridine (bpy) as a co-ligand, exploring the possible networks using Cu(II)-complex cations and lanthanide complex anions and also the influence of lanthanide anions on the composition of the Cu(II) complex cations. Herein, we present our further investigation of Cu(II) complex cation distortion using 5,5'-dimethyl-2,2'-bipyridine (dmbpy) in octahedral environments involving lanthanide anions. Therefore, we report a series of novel heterometallic Cu(II)/*Ln*(III) compounds containing 5,5'-dimethyl-2,2'-bipyridine (dmbpy). Depending upon the size of the *Ln*(III) ion and the molar ratio of intial reactants, we obtained three types of compounds, $\{[Cu(dmbpy)_2(NO_3)]_2[Ln(NO_3)_5(OH_2)]\cdot CH_3CN\}$ [*Ln* = La (**1**), Ce (**2**), Pr (**3**), Nd (**4**), Sm (**5**), Eu (**6**), Gd (**7**) and Tb (**8**)] (Type **I**), $\{[Cu(dmbpy)_3][Ln(NO_3)_5(OH_2)]\cdot 2CH_3CN\}$ [*Ln* = La (**9**) and Ce (**10**)] (Type **II**) and $\{[Cu(dmbpy)_3][Ln(NO_3)_5]\}$ [*Ln* = Pr (**11**), Nd (**12**), Sm (**13**), Eu (**14**), Gd (**15**), Tb (**16**), Dy (**17**), Ho (**18**), Er (**19**), Tm (**20**), Yb (**21**) and Lu (**22**) (Type **III**). The ligand 5,5'-dimethyl-2,2'-bipyridine (dmbpy) has been selected due to the presence of two methyl groups introduce a steric influence in the structural behavior of the compounds. Only one Cu(II) complex with the formula $[Cu(dmbpy)_2(NO_3)](NO_3)$[1] has been reported and described as distorted square-pyramidal geometry. Two tris-chelated Cu(II) complexes with the formula $[Cu(dmbpy)_3](PF_6)_2\cdot CH_3CN$[2] and $[Cu(dmbpy)_3](BF_4)_2\cdot EtOH$[1] have been described as distorted,

elongated octahedral geometry. No compounds have been reported with rare earth anions. In our studies on the geometries of lanthanide anions, we have isolated and characterized two forms of anions such as $[Ln(NO_3)_5(OH_2)]^{2-}$ and $[Ln(NO_3)_5]^{2-}$. Polycrystalline EPR spectra of all samples were measured at different temperature and the results are discussed.

4.2. Experimental

4.2.1. Reagents

All the chemicals were of reagent grade obtained from commercial sources and were used without further purification.

4.2.2. Synthesis

Preparation of $\{[Cu(dmbpy)_2(NO_3)]_2[Ln(NO_3)_5(OH_2)]\cdot CH_3CN\}$ (1-8)

To 5,5'-dimethyl-2,2'-bipyridine (0.074 g, 0.400 mmol) dissolved in acetonitrile (10 mL), $Cu(NO_3)_2\cdot 3H_2O$ (0.048 g, 0.200 mmol) and $Ln(NO_3)\cdot 6H_2O$ (0.100 mmol) where *Ln* = La (0.043 g) (**1**), Ce (0.043 g) (**2**), Pr (0.044 g) (**3**), Nd (0.044 g) (**4**), Sm (0.044 g) (**5**), Eu (0.043 g) (**6**), Gd (0.045 g) (**7**) and Tb(0.045 g) (**8**) dissolved in acetonitrile (10 mL) was added slowly while stirring. The resulting clear blue solution was kept at 6 ºC temperature for crystallization. Plate shaped blue crystals were obtained after 5 days.

For **1**: Yield 0.110 g, (0.074 mmol, 74%). *Anal.* Calc. for $C_{50}H_{53}N_{16}O_{22}Cu_2La$ (M.W. 1496.09 g): C, 40.14; H, 3.57; N, 14.98. Found: C, 40.26; H, 3.51; N, 15.07. Important IR absorptions (KBr disk, cm^{-1}): 3457, 2356, 1742, 1610, 1578, 1454, 1386, 1320, 1252, 1156, 1032, 1001, 838, 816, 780, 738 and 645.

For **2**: Yield 0.108 g, (0.072 mmol, 72%). *Anal.* Calc. for $C_{50}H_{53}N_{16}O_{22}Cu_2Ce$ (M.W. 1497.30 g): C, 40.11; H, 3.57; N, 14.97. Found: C, 40.26; H, 3.49; N, 14.85. Important IR absorptions (KBr disk, cm^{-1}): 3463, 1610, 1572, 1463, 1262, 1150, 1052, 1033, 1010, 840, 816, 781, 723 and 646.

For **3**: Yield 0.110 g, (0.073 mmol, 73%). *Anal.* Calc. for $C_{50}H_{53}N_{16}O_{22}Cu_2Pr$ (M.W. 1498.09 g): C, 40.09; H, 3.57; N, 14.96. Found: C, 40.21; H, 3.51; N, 14.85. Important IR absorptions (KBr disk, cm^{-1}): 3454, 2352, 1748, 1612, 1573, 1458, 1320, 1254, 1156, 1056, 1038, 839, 811, 782, 732 and 649.

For **4**: Yield 0.114 g, (0.076 mmol, 76%). *Anal.* Calc. for $C_{50}H_{53}N_{16}O_{22}Cu_2Nd$ (M.W. 1501.42 g): C, 40.00; H, 3.56; N, 14.93. Found: C, 39.85; H, 3.48; N, 14.82. Important IR absorptions (KBr disk, cm^{-1}): 3462, 1616, 1575, 1468, 1276, 1150, 1046, 1031, 1002, 838, 810, 781, 728 and 646.

For **5**: Yield 0.116 g, (0.077 mmol, 77%). *Anal.* Calc. for $C_{50}H_{53}N_{16}O_{22}Cu_2Sm$ (M.W. 1507.54 g): C, 39.84; H, 3.54; N, 14.87. Found: C, 39.92; H, 3.51; N, 14.76. Important IR absorptions (KBr disk, cm^{-1}): 3452, 2350, 1744, 1616, 1572, 1456, 1325, 1252, 1158, 1039, 998, 842, 814, 782, 726 and 645.

For **6**: Yield 0.125 g, (0.083 mmol, 83%). *Anal.* Calc. for $C_{50}H_{53}N_{16}O_{22}Cu_2Eu$ (M.W. 1509.12 g): C, 39.80; H, 3.54; N, 14.85. Found: C, 39.68; H, 3.65; N, 14.72. Important IR absorptions (KBr disk, cm^{-1}): 3459, 1609, 1572, 1462, 1269, 1156, 1052, 1039, 1001, 839, 815, 779, 725 and 646.

For **7**: Yield 0.122 g, (0.081 mmol, 81%). *Anal.* Calc. for $C_{50}H_{53}N_{16}O_{22}Cu_2Gd$ (M.W. 1514.43 g): C, 39.66; H, 3.53; N, 14.80. Found: C, 39.56; H, 3.48; N, 14.71. Important IR absorptions (KBr disk, cm^{-1}): 3456, 2351, 1749, 1614, 1576, 1452, 1326, 1256, 1158, 1034, 841, 814, 728 694 and 644.

For **8**: Yield 0.110 g, (0.073 mmol, 73%). *Anal.* Calc. for $C_{50}H_{53}N_{16}O_{22}Cu_2Tb$ (M.W. 1516.11 g): C, 39.61; H, 3.52; N, 14.78. Found: C, 39.72; H, 3.48; N, 14.65. Important IR absorptions (KBr disk, cm^{-1}): 3460, 1610, 1578, 1479, 1386, 1298, 1256, 1156, 1046, 1024, 838, 810, 745, 726 and 652.

Preparation of {[Cu(dmbpy)$_3$][*Ln*(NO$_3$)$_5$(OH$_2$)]·2CH$_3$CN} (9-10)

To 5,5'-dimethyl-2,2'-bipyridine (0.055 g, 0.300 mmol) dissolved in acetonitrile (10 mL), $Cu(NO_3)_2 \cdot 3H_2O$ (0.024 g, 0.100 mmol) and $Ln(NO_3) \cdot 6H_2O$ (0.100 mmol) where *Ln* = La (0.043 g) (**9**) and Ce (0.043 g) (**10**) dissolved in acetonitrile (10 mL) was added slowly while stirring. The resulting clear blue solution was kept at 6 ºC temperature for crystallization. Plate shaped blue crystals were obtained after 5 days.

For **9**: Yield 0.082 g, (0.070 mmol, 70%). *Anal.* Calc. for $C_{40}H_{44}N_{13}O_{16}CuLa$ (M.W. 1165.33 g): C, 41.23; H, 3.81; N, 15.62. Found: C, 41.32; H, 3.86; N, 15.56. Important IR absorptions (KBr disk, cm^{-1}): 3454, 1616, 1572, 1479, 1304, 1156, 1046, 1004, 839, 812, 789, 735 and 645.

For **10**: Yield 0.076 g, (0.065 mmol, 65%). *Anal.* Calc. for $C_{40}H_{44}N_{13}O_{16}CuCe$ (M.W. 1166.53 g): C, 41.19; H, 3.80; N, 15.61. Found: C, 41.06; H, 3.71; N, 15.52. Important IR absorptions (KBr disk, cm^{-1}): 3468, 1605, 1567, 1480, 1380, 1304, 1249, 1156, 1041, 998, 838, 816, 783, 739 and 646.

Preparation of [Cu(dmbpy)$_3$][*Ln*(NO$_3$)$_5$] (11-22)

To 5,5'-dimethyl-2,2'-bipyridine (0.055 g, 0.300 mmol) dissolved in acetonitrile (10 mL), $Cu(NO_3)_2 \cdot 3H_2O$ (0.024 g, 0.100 mmol) and $Ln(NO_3) \cdot 5H_2O$ (0.100 mmol) where *Ln* = Pr (0.044 g) (**11**), Nd (0.044 g) (**12**), Sm (0.044 g) (**13**), Eu (0.043 g) (**14**) and Gd (0.045 g) (**15**), Tb(0.045 g) (**16**), Dy (0.044 g) (**17**), Ho (0.044 g) (**18**), Er (0.044 g) (**19**), Tm (0.045 g) (**20**), Yb (0.045 g) (**21**) and Lu (0.036 g) (**22**) dissolved in acetonitrile solution (10 mL) was added slowly while

stirring. The resulting clear blue solution was kept at 6 ºC temperature for crystallization. Block shaped blue crystals were obtained after 5 days.

For **11**: Yield 0.086 g, (0.081 mmol, 81%). *Anal.* Calc. for $C_{36}H_{36}N_{11}O_{15}CuPr$ (M.W. 1067.21 g): C, 40.52; H, 3.40; N, 14.44. Found: C, 40.38; H, 3.48; N, 14.52. Important IR absorptions (KBr disk, cm^{-1}): 1600, 1578, 1484, 1386, 1301, 1287, 1156, 1046, 1024, 838, 816, 778, 728 and 652.

For **12**: Yield 0.091 g, (0.085 mmol, 85%). *Anal.* Calc. for $C_{36}H_{36}N_{11}O_{15}CuNd$ (M.W. 1070.54 g): C, 40.39; H, 3.39; N, 14.39. Found: C, 40.45; H, 3.32; N, 14.29. Important IR absorptions (KBr disk, cm^{-1}): 1601, 1572, 1484, 1304, 1156, 1046, 1006, 839, 814, 786, 740 and 640.

For **13**: Yield 0.086 g, (0.080 mmol, 80%). *Anal.* Calc. for $C_{36}H_{36}N_{11}O_{15}CuSm$ (M.W. 1076.68 g): C, 40.16; H, 3.37; N, 14.31. Found: C, 40.06; H, 3.32; N, 14.21. Important IR absorptions (KBr disk, cm^{-1}): 1604, 1568, 1483, 1298, 1154, 1042, 1003, 837, 810 and 808.

For **14**: Yield 0.080 g, (0.074 mmol, 74%). *Anal.* Calc. for $C_{36}H_{36}N_{11}O_{15}CuEu$ (M.W. 1078.26 g): C, 40.10; H, 3.37; N, 14.29. Found: C, 40.26; H, 3.34; N, 14.35. Important IR absorptions (KBr disk, cm^{-1}): 1616, 1572, 1512, 1391, 1304, 1161, 1046, 1019, 838, 805, 734 and 641

For **15**: Yield 0.085 g, (0.078 mmol, 78%). *Anal.* Calc. for $C_{36}H_{36}N_{11}O_{15}CuGd$ (M.W. 1083.55 g): C, 39.91; H, 3.35; N, 14.22. Found: C, 39.85; H, 3.29; N, 14.12. Important IR absorptions (KBr disk, cm^{-1}): 1600, 1567, 1479, 1386, 1298, 1249, 1156, 1134, 1046, 1024, 843, 810, 781, 745 and 645.

For **16**: Yield 0.082 g, (0.076 mmol, 76%). *Anal.* Calc. for $C_{36}H_{36}N_{11}O_{15}CuTb$ (M.W. 1085.22 g): C, 39.84; H, 3.34; N, 14.20. Found: C, 39.76; H, 3.23; N, 14.15. Important IR absorptions (KBr disk, cm^{-1}): 1604, 1570, 1482, 1296, 1154, 1040, 998, 842, 811, 790, 740 and 651.

For **17**: Yield 0.078 g, (0.072 mmol, 72%). *Anal.* Calc. for $C_{36}H_{36}N_{11}O_{15}CuDy$ (M.W. 1088.80 g): C, 39.71; H, 3.33; N, 14.15. Found: C, 39.71; H, 3.33; N, 14.15. Important IR absorptions (KBr disk, cm^{-1}): 1602, 1572, 1483, 1298, 1158, 1048, 1001, 839, 812, 790, 740 and 642.

For **18**: Yield 0.092 g, (0.084 mmol, 84%). *Anal.* Calc. for $C_{36}H_{36}N_{11}O_{15}CuHo$ (M.W. 1091.23 g): C, 39.63; H, 3.33; N, 14.12. Found: C, 39.51; H, 3.38; N, 14.06. Important IR absorptions (KBr disk, cm^{-1}): 1610, 1578, 1490, 1380, 1304, 1249, 1156, 1046, 1002, 838, 810, 791, 739 and 645.

For **19**: Yield 0.086 g, (0.079 mmol, 79%). *Anal.* Calc. for $C_{36}H_{36}N_{11}O_{15}CuEr$ (M.W. 1093.57 g): C, 39.54; H, 3.32; N, 14.09. Found: C, 39.71; H, 3.33; N, 14.15. Important IR absorptions (KBr disk, cm^{-1}): 1602, 1572, 1483, 1304, 1156, 1044, 1005, 842, 812, 791, 741 and 642.

For **20**: Yield 0.092 g, (0.084 mmol, 84%). *Anal.* Calc. for $C_{36}H_{36}N_{11}O_{15}CuTm$ (M.W. 1095.23 g): C, 39.48; H, 3.31; N, 14.07. Found: C, 39.71; H, 3.33; N, 14.15. Important IR absorptions (KBr disk, cm^{-1}): 1604, 1569, 1484, 1306, 1156, 1048, 1006, 842, 807, 792, 742 and 647.

For **21**: Yield 0.088 g, (0.080 mmol, 80%). *Anal.* Calc. for $C_{36}H_{36}N_{11}O_{15}CuYb$ (M.W. 1099.35 g): C, 39.33; H, 3.30; N, 14.01. Found: C, 39.71; H, 3.33; N, 14.15. Important IR absorptions (KBr disk, cm^{-1}): 1780, 1742, 1572, 1484, 1380, 1304, 1156, 1046, 1019, 838, 810, 739, 657 and 586.

For **22**: Yield 0.078 g, (0.071 mmol, 71%). *Anal.* Calc. for $C_{36}H_{36}N_{11}O_{15}CuLu$ (M.W. 1101.28 g): C, 39.26; H, 3.30; N, 13.99. Found: C, 39.71; H, 3.33; N, 14.15. Important IR absorptions (KBr disk, cm^{-1}): 1605, 1566, 1484, 1302, 1156, 1048, 1001, 848, 812, 792, 742 and 642.

4.3. Physical measurements

IR spectra were obtained for KBr pellets on a Jasco FT-IR 5300 spectrometer in the range 4000-400cm^{-1}. Diffuse reflectance spectra were measured by using a Shimadzu UV-3100 spectrometer. Elemental analysis for C, H and N was performed on a Perkin-Elmer 240C elemental analyzer. EPR spectra were recorded on Bruker Xenon EMX-ER-073 spectrometer.

4.4. X-ray crystallography

The unit cell parameters and the intensity data at 298 K were obtained on an Oxford Diffraction Xcalibur Gemini single crystal X-ray diffractometer using graphite-monochromated Cu-Kα radiation (k= 1.54184 Å) for **10**, **11, 13** and **21**, Mo-Kα radiation (λ = 0.71073 Å) for **1-3, 7, 17, 19-20**. The CrysAlisPro software[3] was used for data collection, reduction and absorption correction. The unit cell parameters and intensity data at 100 K for **4, 8, 9** and 298 K for **5-6, 12, 14-16, 18** and **22** were obtained on a Bruker-Nonius SMART APEX CCD 1000 area detector, using graphite-monochromated Mo-Kα radiation (λ = 0.71073 Å). Data were reduced using SAINTPLUS[4] and a multi-scan absorption correction using SADABS[5] was performed. The structure of complexes were solved by direct methods and refined on F^2 by full-matrix least-squares procedures. The non-hydrogen atoms were refined using anisotropic thermal parameters. The hydrogen atoms were included in the structure factor calculations at idealized positions using a riding model, and the hydrogen atoms attached to oxygen atoms were located from the difference maps. The structures were solved using SHELXS-97 and refined using SHELXL-97.[6] Drawings were made using Mercury.[7] Crystallographic data and structure refinement are given in Table 4.1, Table 4.2, Table 4.6, Table 4.8 and Table 4.9. Selected bond lengths and bond angles are listed in Table 4.3, Table 4.7 and Table 4.11.

Table 4.1: Crystallographic data and structure refinement for compounds **1-4**

Param	**1**	**2**	**3**	**4**
Formula	$C_{50}H_{53}N_{16}O_{22}Cu_2La$	$C_{50}H_{53}N_{16}O_{22}Cu_2Ce$	$C_{50}H_{53}N_{16}O_{22}Cu_2Pr$	$C_{50}H_{53}N_{16}O_{22}Cu_2Nd$
Formula weight	1496.07	1497.28	1498.07	1501.40
Crystal system	Monoclinic	Monoclinic	Monoclinic	Monoclinic
Space group	$P2_1/n$	$P2_1/c$	$P2_1/n$	$P2_1/n$
a (Å)	8.8338(4)	8.8445(5)	8.8306(4)	8.6436(4)
b (Å)	35.402(2)	35.3936(16)	35.300(2)	35.2311(17)
c (Å)	19.4090(10)	21.4089(10)	19.3951(7)	19.2196(9)
α (˚)	90	90	90	90
β (˚)	90.318(4)	114.710(6)	90.290(4)	90.7680(10)
γ (˚)	90	90	90	90
V (Å^3)	6069.7(5)	6088.2(5)	6045.9(5)	5852.3(5)
Z	4	4	4	4
T (K)	298(2)	298(2)	298(2)	100(2)
λ (Å)	0.71073	0.71073	0.71073	0.71073
D_{cal} (g cm^{-3})	1.637	1.634	1.646	1.704
μ (mm^{-1})	1.476	1.517	1.581	1.688
F(000)	3024	3028	3032	3036
Crystal size (mm)	0.20 x 0.16 x 0.10	0.24 x 0.20 x 0.16	0.20 x 0.16 x 0.12	0.28 x 0.16 x 0.08
θ Range(˚)	2.58 – 24.71	2.71 – 24.71	2.72 – 24.41	1.16 – 25.00
h/k/l indices	–10, 10/ –41, 32/ –22,22	–10, 10/ –41, 39/ –25,24	–10, 8/ –41, 34/ –9, 22	–10, 10/ –41, 41/ –22, 22
Refl^n collected	22140	18103	14662	56258
Unique refl^n [R_{int}]	10344 [0.1012]	10203 [0.0340]	8968 [0.0431]	10303 [0.0711]
GooF	0.740	1.087	1.063	1.060
R_1 [I>2σ(I)]	0.0575	0.0514	0.0572	0.0566
wR_2	0.0997	0.1006	0.1133	0.1367

$w = 1 / [\sigma^2(F_0^2) + (AP)^2 + BP]$; where $P = [2F_C^2 + Max(F_0^2, 0)]/3$

Table 4.2: Crystallographic data and structure refinement for compounds **5-8**

Param	**5**	**6**	**7**	**8**
Formula	$C_{50}H_{53}N_{16}O_{22}Cu_2Sm$	$C_{50}H_{53}N_{16}O_{22}Cu_2Eu$	$C_{50}H_{53}N_{16}O_{22}Cu_2Gd$	$C_{50}H_{53}N_{16}O_{22}Cu_2Tb$
Formula weight	1507.51	1509.12	1514.41	1516.08
Crystal system	Monoclinic	Monoclinic	Monoclinic	Monoclinic
Space group	$P2_1/c$	$P2_1/n$	$P2_1/c$	$P2_1/n$
a (Å)	8.857(3)	8.844(3)	8.8348(3)	8.6375(5)
b (Å)	35.358(13)	35.320(12)	35.3969(13)	35.090(2)
c (Å)	21.217(7)	19.373(6)	19.4266(10)	19.0478(11)
α (˚)	90	90	90	90
β (˚)	114.272(12)	90.528(6)	90.315(3)	90.909(10)
γ (˚)	90	90	90	90
V (Å^3)	6057(4)	6051(3)	6075.1(4)	5772.5(6)
Z	4	4	4	4
T (K)	298(2)	298(2)	298(2)	100(2)
λ (Å)	0.71073	0.71073	0.71073	0.71073
D_{cal} (g cm^{-3})	1.653	1.657	1.656	1.744
μ (mm^{-1})	1.743	1.811	1.863	2.037
F(000)	3044	3048	3052	3056
Crystal size (mm)	0.22 x 0.20 x 0.12	0.24 x 0.16 x 0.12	0.20 x 0.16 x 0.12	0.32 x 0.24 x 0.12
θ Range(˚)	1.15 – 24.74	1.20 – 20.81	2.79 – 24.71	1.16 – 25.00
h/k/l indices	–10, 10/ –41, 41/ –24, 24	–8, 8/ –35, 35/ –19, 19	–10, 10/ –41, 22/ –22, 19/	–10, 10/ –41, 41/ –22, 22
Refl^n collected	42626	39133	19267	55221
Unique refl^n [R_{int}]	10348 [0.0452]	6334 [0.0492]	10180 [0.0367]	10166 [0.0381]
GooF	1.042	1.048	1.086	1.047
R_1 [I>2σ(I)]	0.0520	0.0507	0.0662	0.0584
wR_2	0.1391	0.1269	0.1690	0.1491

$w = 1 / [\sigma^2(F_0^2) + (AP)^2 + BP]$; where $P = [2F_C^2 + Max(F_0^2, 0)]/3$

4.5. {[Cu(dmbpy)$_2$(NO$_3$)]$_2$[*Ln*(NO$_3$)$_5$(OH$_2$)]·CH$_3$CN} (1-8)

[*Ln* = La (**1**), Ce (**2**), Pr (**3**), Nd (**4**), Sm (**5**), Eu (**6**), Gd (**7**) and Tb (**8**)]

4.5.1. Crystal structure of {[Cu(dmbpy)$_2$(NO$_3$)]$_2$[*Ln*(NO$_3$)$_5$(OH$_2$)]·CH$_3$CN} (1-8)

Compounds **1-8** form isomorphous crystals. Crystallographic data and structure refinement details are listed in Table 4.1 and Table 4.2. Since geometrical parameters of all compounds are similar the selected bond lengths and angles of compound **1** are given in Table 4.3. The asymmetric unit consisted of two crystallographically independent $[Cu(dmbpy)_2(NO_3)]^+$ cations, one $[Ln(NO_3)_5(OH_2)_2]^{2-}$ anion and one acetonitrile solvent molecule in the lattice shown in Figure 4.1. Both complex cations have the same molecular structure.

The geometry of the $[Cu(dmbpy)_2(NO_3)]^+$ cation involves a *cis*-distorted octahedral CuN_4O_2 chromophore with an unsymmetrical chelated nitrate ion. The CuN_4O_2 chromophore has a pseudo-C_2 symmetry bisecting the nitrate ion and passing between the two dmbpy ligands. The Cu(II) ion is coordinated to the four nitrogen atoms of the two dmbpy ligands and two oxygen atoms of a chelated nitrate ion. Two nitrogen atoms are axially coordinated with N-Cu-N approximately linear angles (178.5(3), 176.9(3)º). Nitrate ion bonds in an approximately symmetrical mode. One oxygen of nitrate ion is coordinated to the copper with a distance 2.335 (2.286) Å, while the other at 2.357 (2.385) Å. For six-coordinate $[Cu(bpy)_2X]Y$ complexes, the specific distorted octahedral geometry can be obtained by the two types of coordination of X anions: *cis*-chelated ($X = NO_2^-$, $RCOO^-$) or *trans*-coordinated ($X = SO_4^{2-}$, $S_3O_6^{2-}$, $S_4O_6^{2-}$, ClO_4^-, NO_3^-). The present structures are clearly different from the equally elongated *trans*-octahedral (4+2) chromophore in $[Cu(bpy)_2(S_3O_6)]$,[8a] $[Cu(bpy)_2(S_4O_6)]$[8b] and $\{[Cu(bpy)_2(NO_3)](NO_3)\}_n$[8c] unequally elongated *trans*-octahedral (4+1+1*) chromophore of $[Cu(bpy)_2(ClO_4)](ClO_4)$[9] and

have some similarity to the pseudo-symmetric *cis*-distorted octahedral geometries of $[Cu(phen)_2(CH_3COO)](ClO_4)\cdot 2H_2O$,[10a] $[Cu(phen)_2(HCOO)](ClO_4)$[10b] and $[Cu(bpy)_2(SO_4)]\cdot CH_3OH$[10c] with two Cu-O distances of 2.26-2.36 Å. The unsymmetrical chelated nitrate ion has no unusual bond lengths, the N(5)-O(2) distance of 1.247(9) is longer than N(5)-O(1) distance of 1.224(7), consistent with stronger Cu(1)-O(1) bond than Cu(1)-O(2) bond. The mean N-O distance of 1.235(1), of the nitrate ion is not significantly different from the 1.245 Å for the free nitrate ion, but O(1)-N(5)-O(2) angle of 114.3(9)º is significantly smaller than the 119.9º of the free ion. The O(1)–Cu(1)–O(2) bond angle of 52.5(2)º is good agreement with the value previously reported $[Cu(chelate)_2(ONO)]Y$ complexes.[11] The Cu(1)–O(1)–N(5) angle (96.2(6)º) is within the range of 93–100º for the purely bidentate nitrite ion. The binding mode of the nitrate ion is independent of the O(1)–Cu(1)–O(2) and O(1)–N(5)–O(2) angles, but dependent to the Cu(1)–O(1)–N(5) angle.

The *Ln*(III) ion is 11-coordinated with ten oxygen atoms from five chelating nitrate ligands and one oxygen atom from water molecule, forming a distorted monocapped pentagonal antiprismatic geometry[12] (Figure 4.1(c)). The structural data for La(III) anion can explain the structure of $[Ln(NO_3)_5(OH_2)]^{2-}$. The *Ln*–O(nitrate) bond lengths (Å) lie in the range 2.585-2.670 and *Ln*–O(w), 2.521 (Table 4.5). The crystal packing analysis indicates that both intermolecular H-bonding and π-stacking interactions combine to stabilize the extended structure. The coordinated water molecule of the $[La(NO_3)_5(OH_2)_2]^{2-}$ anionic units form 1D chains by H-bonding interactions. These are further inter connect with various C-H···O interactions of cationic units (C27-H27···O9, 2.475(4); C8-H8···O21, 2.448(4); C44-H44···O11, 2.463(4); O22-H22B···O15, 1.97(7) Å) give a 2D sandwich layer structure along *c*-axis (Figure 4.2).

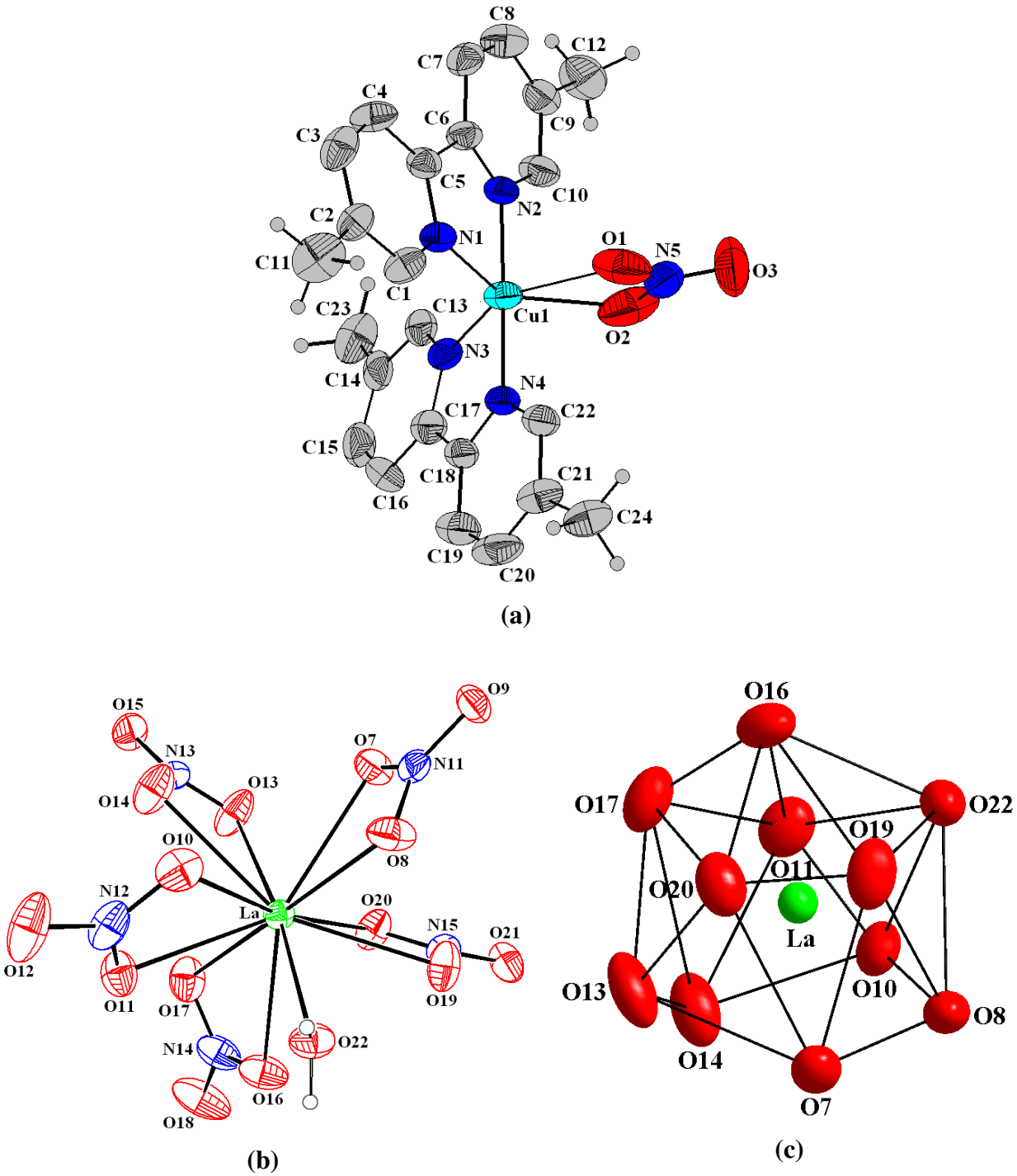

Figure 4.1. Thermal ellipsoid plot of the coordination environment of the (a) complex cation (b) complex anion of **1** (c) monocapped pentagonal antiprism coordination polyhedron of La(III) ion in $[La(NO_3)_5(OH_2)]^{2-}$: Atoms are represented as 30% probability ellipsoids. One of the crystallographic independent cation, ring hydrogen atoms and acetonitrile solvent molecule have been omitted for clarity.

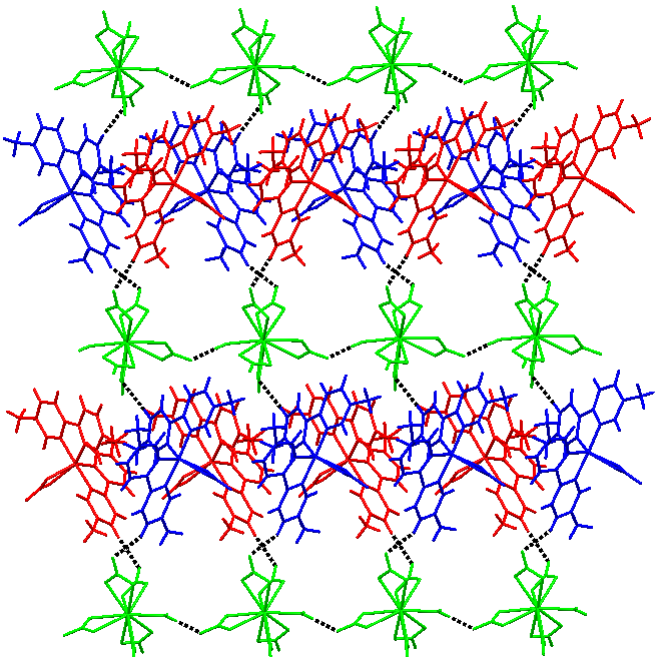

(a)

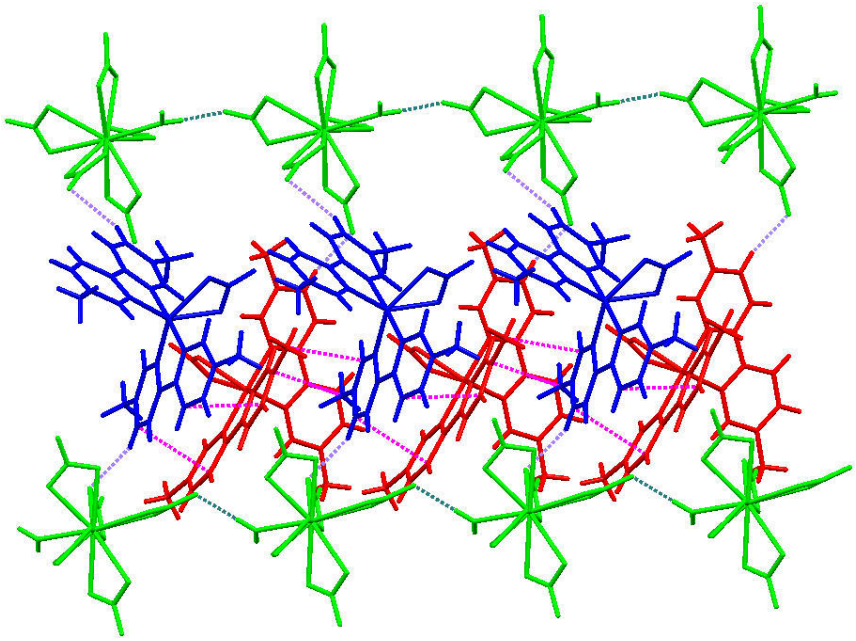

(b)

Figure 4.2. (a) 2D layer structure formed by the H-bonding interactions in **1** down *c*-axis (b) a view of cationic layer sandwiched between the anionic layer in **1**.

Table 4.3: Selected bond lengths(Å) and bond angles(°) for **1**

Cu(1)-N(1)	2.102(5)	Cu(2)-N(6)	1.983(6)	Cu(1)-O(1)	2.357(7)
Cu(1)-N(2)	1.985(6)	Cu(2)-N(7)	2.080(5)	Cu(1)-O(2)	2.335(7)
Cu(1)-N(3)	2.088(6)	Cu(2)-N(8)	1.985(6)	Cu(2)-O(4)	2.286(6)
Cu(1)-N(4)	1.976(6)	Cu(2)-N(9)	2.077(6)	Cu(2)-O(5)	2.385(8)
N(5)-O(1)	1.224(7)	N(5)-O(3)	1.185(9)	N(10)-O(5)	1.214(7)
N(5)-O(2)	1.247(9)	N(10)-O(4)	1.266(8)	N(10)-O(6)	1.176(8)
La-O(7)	2.599(6)	La-O(13)	2.664(5)	La-O(19)	2.604(6)
La-O(8)	2.646(6)	La-O(14)	2.670(6)	La-O(20)	2.634(6)
La-O(10)	2.641(6)	La-O(16)	2.585(6)	La-O(22)	2.521(6)
La-O(11)	2.595(6)	La-O(17)	2.599(6)		
N(1)-Cu(1)-N(2)	80.4(2)	O(2)-Cu(1)-N(1)	143.0(2)	N(8)-Cu(2)-N(9)	80.5(3)
N(1)-Cu(1)-N(3)	118.3(2)	O(2)-Cu(1)-N(2)	86.5(2)	O(4)-Cu(2)-N(6)	87.7(2)
N(1)-Cu(1)-N(4)	99.2(2)	O(2)-Cu(1)-N(3)	97.6(2)	O(4)-Cu(2)-N(7)	146.6(2)
N(2)-Cu(1)-N(3)	98.1(2)	O(2)-Cu(1)-N(4)	94.6(2)	O(4)-Cu(2)-N(8)	94.6(2)
N(2)-Cu(1)-N(4)	178.5(3)	O(2)-Cu(1)-O(1)	52.5(2)	O(4)-Cu(2)-N(9)	98.1(2)
N(3)-Cu(1)-N(4)	80.8(3)	N(6)-Cu(2)-N(7)	80.7(2)	O(5)-Cu(2)-N(6)	90.9(2)
O(1)-Cu(1)-N(1)	92.9(2)	N(6)-Cu(2)-N(8)	176.9(3)	O(5)-Cu(2)-N(7)	95.5(2)
O(1)-Cu(1)-N(2)	90.3(2)	N(6)-Cu(2)-N(9)	97.2(2)	O(5)-Cu(2)-N(8)	92.1(2)
O(1)-Cu(1)-N(3)	148.6(2)	N(7)-Cu(2)-N(8)	98.4(2)	O(5)-Cu(2)-N(9)	150.03(19)
O(1)-Cu(1)-N(4)	91.2(2)	N(7)-Cu(2)-N(9)	114.3(2)	O(5)-Cu(2)-O(4)	53.24(19)
O(1)-N(5)-O(2)	114.3(9)	O(2)-N(5)-O(3)	122.8(9)	O(4)-N(10)-O(6)	120.5(9)
O(1)-N(5)-O(3)	122.8(10)	O(4)-N(10)-O(5)	115.3(8)	O(5)-N(10)-O(6)	124.2(10)
O(7)-La-O(8)	48.11(18)	O(10)-La-O(11)	48.71(18)	O(13)-La-O(17)	63.1(2)
O(7)-La-O(10)	94.9(2)	O(10)-La-O(13)	109.84(19)	O(13)-La-O(19)	110.6(2)
O(7)-La-O(11)	138.62(18)	O(10)-La-O(14)	64.00(19)	O(13)-La-O(20)	66.61(19)
O(7)-La-O(13)	68.4(2)	O(10)-La-O(16)	117.1(2)	O(13)-La-O(22)	172.7(2)
O(7)-La-O(14)	77.8(2)	O(10)-La-O(17)	113.9(2)	O(14)-La-O(16)	123.8(2)
O(7)-La-O(16)	146.5(2)	O(10)-La-O(19)	130.3(2)	O(14)-La-O(17)	79.0(2)
O(7)-La-O(17)	129.4(2)	O(10)-La-O(20)	171.2(2)	O(14)-La-O(19)	149.8(2)
O(7)-La-O(19)	74.70(19)	O(10)-La-O(22)	70.7(2)	O(14)-La-O(20)	112.68(19)
O(7)-La-O(20)	76.34(19)	O(20)-La-O(22)	113.9(2)	O(14)-La-O(22)	133.0(2)
O(7)-La-O(22)	118.9(2)	O(11)-La-O(13)	102.3(2)	O(16)-La-O(17)	47.6(2)
O(8)-La-O(10)	68.2(2)	O(11)-La-O(14)	69.0(2)	O(16)-La-O(19)	76.8(2)
O(8)-La-O(11)	114.5(2)	O(11)-La-O(16)	74.7(2)	O(16)-La-O(20)	71.6(2)
O(8)-La-O(13)	114.9(2)	O(11)-La-O(17)	67.9(2)	O(16)-La-O(22)	67.6(2)

O(8)-La-O(14)	100.73(19)	O(11)-La-O(19)	141.2(2)	O(17)-La-O(19)	109.50(19)
O(8)-La-O(16)	133.4(2)	O(11)-La-O(20)	139.0(2)	O(17)-La-O(20)	72.3(2)
O(8)-La-O(17)	177.3(2)	O(11)-La-O(22)	72.3(2)	O(17)-La-O(22)	109.9(2)
O(8)-La-O(19)	69.42(19)	O(13)-La-O(14)	46.10(17)	O(19)-La-O(20)	48.43(18)
O(8)-La-O(20)	105.5(2)	O(13)-La-O(16)	106.4(2)	O(19)-La-O(22)	72.8(2)
O(8)-La-O(22)	72.3(2)				
N(11)-O(7)	1.261(8)	N(14)-O(17)	1.262(8)	O(11)-N(12)-O(12)	120.5(11)
N(11)-O(8)	1.262(8)	N(14)-O(18)	1.204(8)	O(13)-N(13)-O(14)	116.9(7)
N(11)-O(9)	1.223(8)	N(15)-O(19)	1.237(8)	O(13)-N(13)-O(15)	120.8(8)
N(12)-O(10)	1.262(10)	N(15)-O(20)	1.283(8)	O(14)-N(13)-O(15)	122.0(8)
N(12)-O(11)	1.247(8)	N(15)-O(21)	1.221(8)	O(16)-N(14)-O(17)	113.8(8)
N(12)-O(12)	1.232(9)	O(7)-N(11)-O(8)	115.9(8)	O(16)-N(14)-O(18)	124.6(10)
N(13)-O(13)	1.206(7)	O(7)-N(11)-O(9)	121.7(9)	O(17)-N(14)-O(18)	121.3(10)
N(13)-O(14)	1.244(8)	O(8)-N(11)-O(9)	122.4(8)	O(19)-N(15)-O(20)	117.0(8)
N(13)-O(15)	1.241(7)	O(10)-N(12)-O(11)	118.7(9)	O(19)-N(15)-O(21)	120.8(9)
N(14)-O(16)	1.237(9)	O(10)-N(12)-O(12)	120.8(10)	O(20)-N(15)-O(21)	121.9(8)

Table 4.4: Molecular geometries of $[Cu(5,5'\text{-dmbpy})_2(NO_3)]^+$ cation

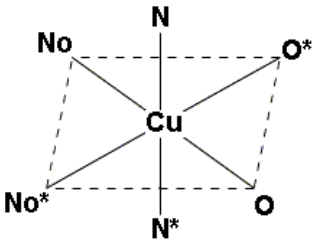

	1	2	3	4	5	6	7	8
Cu-N	1.985(6)	1.978(4)	1.975(5)	1.980(4)	1.990(4)	1.980(6)	1.986(6)	1.973(4)
	1.983(6)	1.980(4)	1.977(5)	1.982(4)	1.992(4)	1.988(6)	1.990(6)	1.975(4)
Cu-N*	1.976(6)	1.981(4)	1.969(5)	1.985(4)	1.981(4)	1.985(6)	1.986(6)	1.972(4)
	1.985(6)	1.979(4)	1.979(5)	1.975(4)	1.986(4)	1.985(6)	1.983(6)	1.976(4)
Cu-No	2.102(5)	2.103(4)	2.100(5)	2.067(5)	2.110(4)	2.107(5)	2.092(6)	2.069(4)
	2.080(5)	2.107(4)	2.088(5)	2.090(4)	2.100(4)	2.110(6)	2.108(6)	2.071(4)
Cu-No*	2.088(6)	2.084(4)	2.072(5)	2.114(4)	2.082(4)	2.096(6)	2.078(6)	2.106(4)
	2.077(6)	2.073(4)	2.081(5)	2.076(4)	2.084(4)	2.097(6)	2.085(6)	2.114(5)
Cu-O	2.335(7)	2.296(4)	2.330(6)	2.336(6)	2.313(6)	2.297(7)	2.299(8)	2.127(4)
	2.286(6)	2.340(5)	2.299(6)	2.286(6)	2.287(6)	2.303(8)	2.332(8)	2.108(4)
Cu-O*	2.357(7)	2.377(5)	2.352(6)	2.371(6)	2.358(6)	2.406(8)	2.379(9)	2.659(4)

	2.385(8)	2.356(5)	2.374(7)	2.403(7)	2.378(7)	2.403(8)	2.350(8)	2.675(4)
ΔO	0.045(1)	0.103(1)	0.056(0)	0.087(1)	0.082(1)	0.109(8)	0.094(1)	0.570(0)
	0.104(1)	0.051(0)	0.084(1)	0.138(1)	0.113(1)	0.100(8)	0.048(1)	0.611(0)
N-Cu-N*	178.5(3)	176.4(15)	178.8(2)	178.6(18)	178.1(2)	177.6(3)	176.6(2)	178.5(19)
	176.9(3)	178.6(16)	176.7(2)	176.8(18)	177.0(2)	177.8(2)	178.8(2)	177.7(18)
No-Cu-O	143.0(2)	146.5(15)	142.7(2)	148.6(16)	142.9(2)	146.4(2)	145.7(2)	144.5(16)
	146.6(2)	142.7(16)	146.3(2)	146.4(16)	146.4(2)	143.5(2)	142.6(2)	142.0(16)
No*-Cu-O*	148.6(2)	149.9(14)	148.9(2)	142.0(16)	149.3(2)	148.9(2)	149.8(2)	147.7(16)
	150.0(2)	149.0(14)	149.5(2)	149.4(16)	149.3(2)	149.4(2)	148.8(2)	149.8(17)
No-Cu-No*	118.3(2)	114.4(14)	118.6(2)	119.6(16)	117.8(2)	115.1(2)	114.6(2)	117.9(17)
	114.3(2)	118.6(14)	114.5(2)	115.1(16)	114.8(2)	117.5(2)	118.5(2)	118.5(17)
O-Cu-O*	52.5(2)	53.2(14)	52.7(2)	53.2(15)	52.6(17)	52.8(2)	52.5(2)	52.2(16)
	53.2(2)	52.8(14)	52.7(2)	53.4(15)	52.7(17)	52.7(2)	52.1(2)	52.2(16)
No*-Cu-O	97.6(2)	98.1(14)	97.7(2)	91.6(16)	98.3(17)	97.4(2)	98.7(2)	96.9(16)
	98.1(2)	97.7(15)	98.2(2)	97.4(16)	97.8(17)	98.1(2)	98.1(2)	99.1(16)
No-Cu-O*	92.9(2)	95.5(14)	92.3(2)	97.1(16)	92.6(17)	95.8(2)	95.4(2)	94.0(16)
	95.5(2)	92.1(14)	95.8(2)	95.3(16)	95.8(17)	92.9(2)	92.5(2)	91.2(16)
N-Cu-No	80.4(2)	80.2(15)	80.5(2)	80.8(18)	80.1(17)	80.5(2)	80.0(2)	80.8(17)
	80.7(2)	80.4(15)	79.9(2)	80.2(17)	80.1(16)	80.3(2)	80.6(2)	80.9(17)
N-Cu-No*	98.1(2)	97.3(15)	98.5(2)	99.5(17)	98.6(18)	97.7(2)	97.4(2)	98.6(17)
	97.2(2)	98.4(16)	97.4(2)	97.4(17)	97.5(17)	98.3(2)	98.5(2)	99.3(18)
N-Cu-O	86.5(2)	88.2(15)	86.3(2)	91.3(17)	86.9(18)	87.7(2)	88.0(2)	88.5(17)
	87.7(2)	86.6(15)	88.1(2)	87.7(17)	88.2(18)	87.0(2)	86.7(2)	88.5(17)
N-Cu-O*	90.3(2)	91.1(15)	89.9(2)	95.5(17)	89.9(17)	90.5(2)	90.8(2)	90.7(16)
	90.9(2)	89.8(15)	91.0(2)	90.9(17)	90.7(17)	90.2(2)	89.8(2)	89.8(17)
No-Cu-N*	99.2(2)	98.5(15)	99.4(2)	98.3(17)	98.9(17)	98.8(2)	98.7(2)	99.15(17)
	98.4(2)	99.1(15)	98.9(2)	98.4(17)	98.9(16)	98.5(2)	98.8(2)	97.55(17)
N*-Cu-No*	80.8(3)	80.2(15)	80.5(2)	80.1(17)	80.4(18)	80.5(2)	80.3(2)	80.2(17)
	80.5(3)	80.7(17)	80.2(2)	80.5(17)	80.3(17)	80.6(3)	81.0(3)	79.9(18)
N*-Cu-O	94.6(2)	94.7(14)	94.5(2)	90.1(16)	94.8(18)	97.4(2)	94.7(2)	92.3(16)
	94.6(2)	94.6(15)	94.5(2)	94.9(17)	94.1(17)	98.1(2)	94.3(2)	93.8(17)
N*-Cu-O*	91.2(2)	92.3(15)	91.3(2)	85.6(17)	91.8(18)	91.8(2)	92.5(2)	90.7(16)
	92.1(2)	91.5(16)	92.2(2)	92.1(17)	92.3(17)	91.7(2)	91.2(2)	91.9(17)

No denotes N trans to an O atom; * denotes the loosely coordinated axial O atom, the axial N atom trans to it and the second (equatorial) N atom within the same 5-dmbpy ligand.

Table 4.5: Bond lengths (Å) *Ln*–O and bond angles (º) O–*Ln*–O of $[Ln(NO_3)_5(OH_2)_2]^{2-}$ anion

	Ln							
	La	**Ce**	**Pr**	**Nd**	**Sm**	**Eu**	**Gd**	**Tb**
Ln–O7	2.599(6)	2.661(4)	2.554(5)	2.531(4)	2.764(7)	2.473(8)	2.600(6)	2.459(4)
Ln–O8	2.646(6)	2.653(4)	2.608(5)	2.556(4)	2.606(6)	2.420(9)	2.582(6)	2.524(4)
Ln–O10	2.641(6)	2.572(4)	2.571(5)	2.531(4)	2.512(5)	2.523(8)	2.619(6)	2.543(4)
Ln–O11	2.595(6)	2.627(4)	2.588(5)	2.599(4)	2.507(5)	3.040(1)	2.578(6)	2.462(4)
Ln–O13	2.664(5)	2.577(4)	2.563(5)	2.538(4)	2.503(5)	2.551(10)	2.652(6)	2.480(4)
Ln–O14	2.670(6)	2.637(4)	2.565(5)	2.586(4)	2.588(6)	2.491(8)	2.653(6)	2.447(4)
Ln–O16	2.585(6)	2.591(4)	2.637(5)	2.548(4)	2.545(5)	2.543(7)	2.630(6)	2.470(4)
Ln–O17	2.599(6)	2.589(4)	2.648(5)	2.582(4)	2.511(4)	2.487(6)	2.576(6)	2.472(4)
Ln–O19	2.604(6)	2.589(4)	2.551(5)	2.604(4)	2.554(6)	2.474(6)	2.570(6)	2.415(4)
Ln–O20	2.634(6)	2.619(4)	2.604(5)	2.647(4)	2.505(5)	2.565(9)	2.599(6)	3.535(4)
Ln–Ow	2.521(6)	2.504(4)	2.482(5)	2.452(4)	2.435(4)	2.424(6)	2.507(6)	2.372(4)
O7–*Ln*–O8	48.11(18)	46.32(12)	48.91(15)	49.70(14)	43.51(18)	50.1(4)	48.59(19)	50.97(13)
O10–*Ln*–O11	48.71(18)	48.71(12)	49.03(15)	49.02(14)	50.35(17)	40.2(3)	48.50(19)	50.44(14)
O13–*Ln*–O14	46.10(17)	48.62(14)	48.87(17)	49.87(12)	48.92(18)	49.7(3)	46.1(2)	52.08(14)
O16–*Ln*–O17	47.6(2)	48.41(14)	46.22(16)	49.55(13)	49.51(15)	49.0(2)	48.2(2)	51.69(13)
O19–*Ln*–O20	48.43(18)	48.75(12)	49.05(17)	47.85(12)	48.3(2)	44.3(3)	48.1(2)	37.4(1)

4.5.2. Infrared spectra

In the IR spectra the band around 3400-3470 cm^{-1} has been assigned to O-H stretching vibration of water for **1-8**. The $\nu_{C=C}$ frequency of the bpy rings at 1610 and 1570 cm^{-1}. In IR spectra there are 4 bands assigned to NO_3^- ion bound to Cu(II) center: 1450-1460 $cm^{-1}(\nu_1)$, 1250-1260 $cm^{-1}(\nu_2)$, 1030-1040 $cm^{-1}(\nu_3)$ and 810-820 cm^{-1} (ν_4) ranges which can be assigned to the vibrational modes of the coordinated (C_{2v}) nitrate groups.[13] The splitting of the bands situated at higher wave numbers (ν_1-ν_2) is about ~200 cm^{-1} indicating the coordinate of nitrate ion in a bidentate fashion.

4.5.3. Electronic spectra

Diffuse reflectance spectrum of **1** (Figure 4.3) exhibits an asymmetric broad band with two clearly marked maxima at 9,800 and 13,830 cm^{-1}. The energy level sequence is $d_{x2-y2} > d_{z2} > d_{xy} > d_{xz} > d_{yz}$ similar to those previously reported $[Cu(chelate)_2(OXO)]Y$ complexes involving the *cis*-distorted octahedral CuN_4O_2 chromophore.[11] The low energy band at 9,800 cm^{-1} can be assigned to the $d_{z2} \approx dxy \rightarrow d_{x2-y2}$ transition, whereas the high energy absorption with a maximum at 13,830 cm^{-1} arises from $dxz \approx dyz \rightarrow d_{x2-y2}$ electronic transition.[14] Band near 32,000 cm^{-1} is due to ligand-to-metal charge transfer transition, while the band near 39,000 cm^{-1} is associated with intraligand $\pi \rightarrow \pi^*$ excitation.

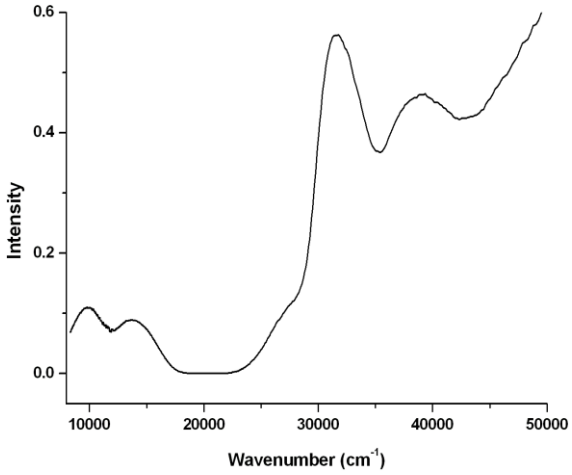

Figure 4.3. Diffuse reflectance spectrum of compound **1**

4.5.4. EPR spectra

The X-band polycrystalline-powder electron paramagnetic resonance (EPR) spectra of **1-8** were measured at room temperature (Figure 4.4 – Figure 4.11). There was no significant change in the spectra with decreasing temperature to 77K. The spectra consist of a broad signal centered at about ~3260 G, as expected for Cu(II) system except the Gd^{3+} complex (**7**). All

spectra have been normalized to same microwave frequency (ν = 9.6844 GHz). The broad isotropic signal is consistent with exchange-averaging due to coupling between the two $[Cu(dmbpy)_2(NO_3)]^+$ ions in the crystals.

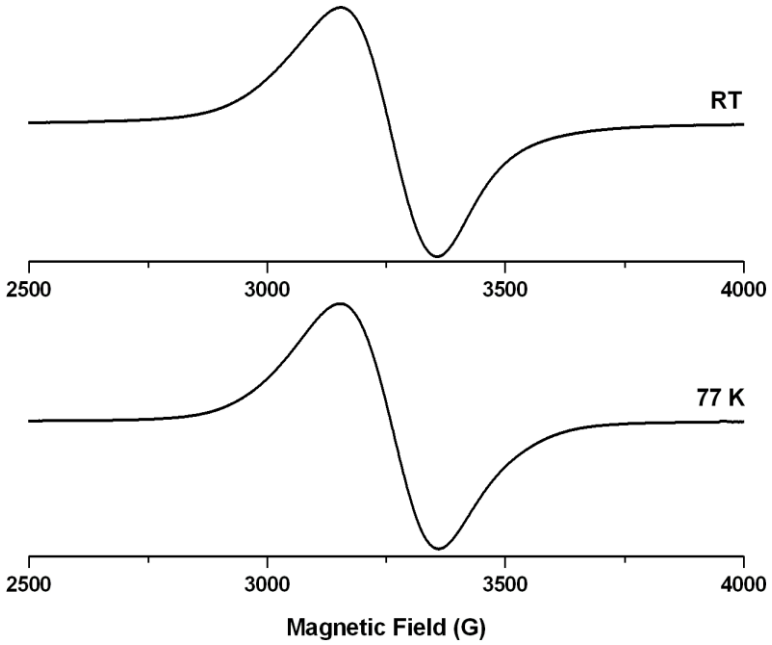

Figure 4.4. Comparison of EPR spectra collected at two different temperatures for compound **1** (Cu-La)

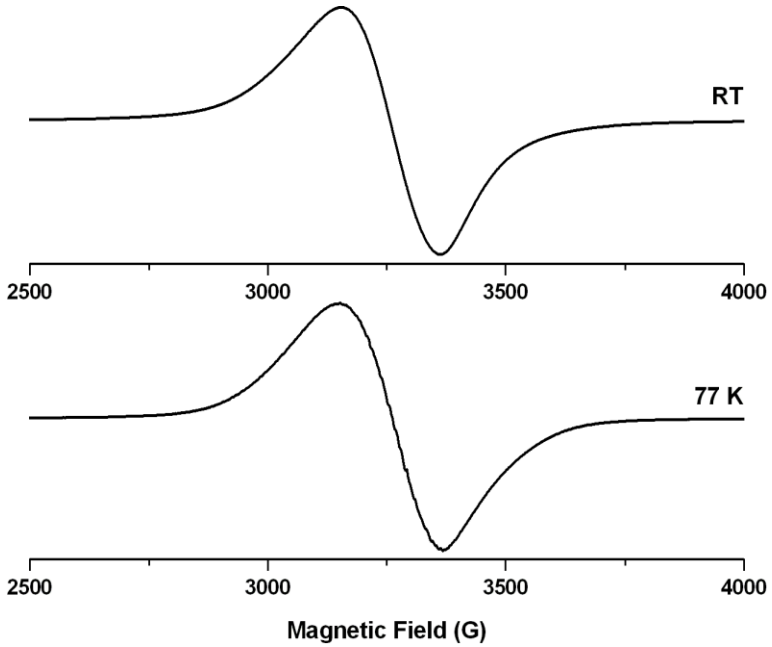

Figure 4.5. Comparison of EPR spectra collected at two different temperatures for compound **2** (Cu-Ce)

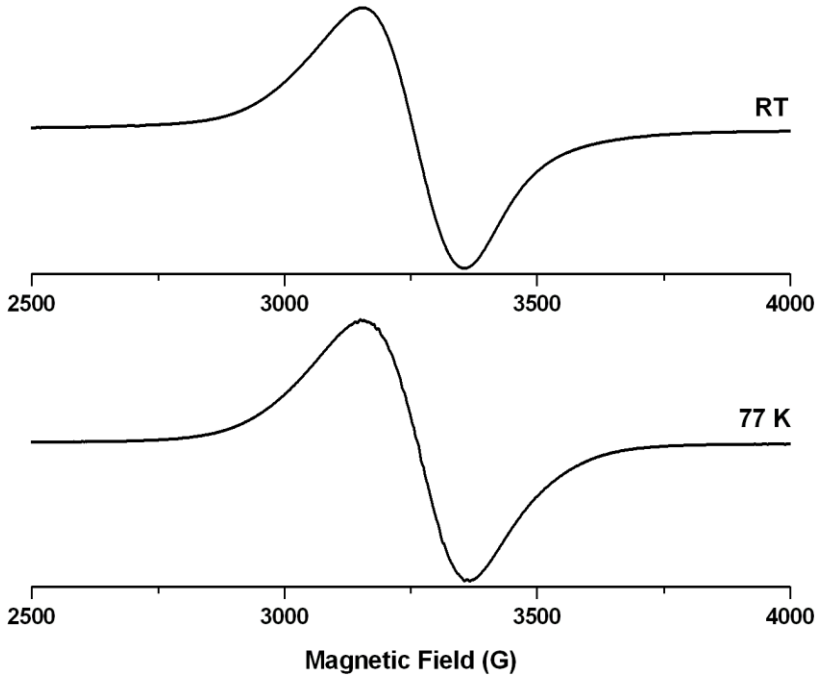

Figure 4.6. Comparison of EPR spectra collected at two different temperatures for compound **3** (Cu-Pr)

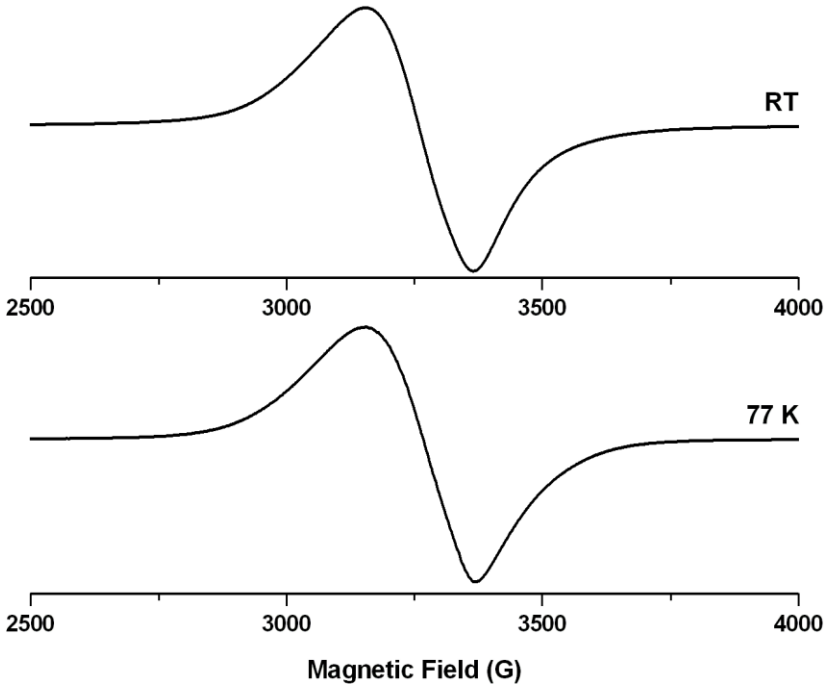

Figure 4.7. Comparison of EPR spectra collected at two different temperatures for compound **4** (Cu-Nd)

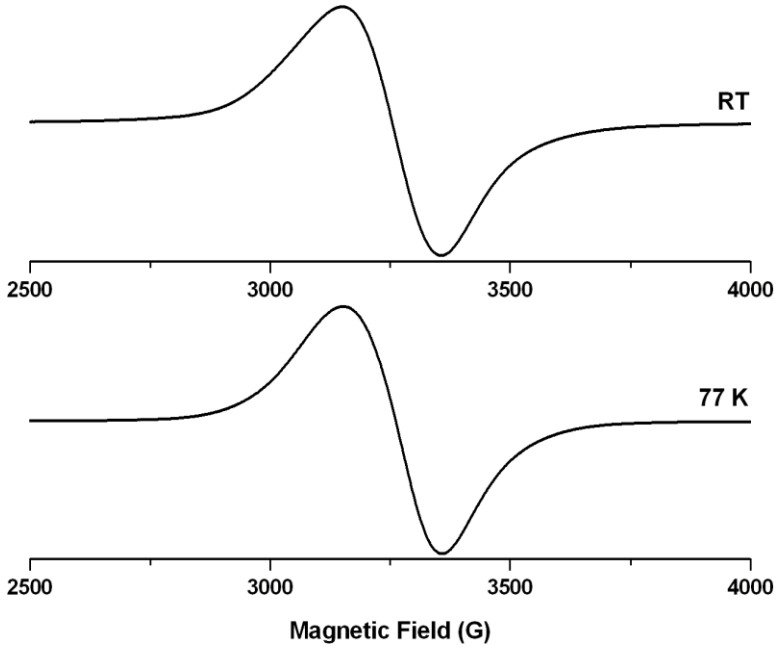

Figure 4.8. Comparison of EPR spectra collected at two different temperatures for compound **5** (Cu-Sm)

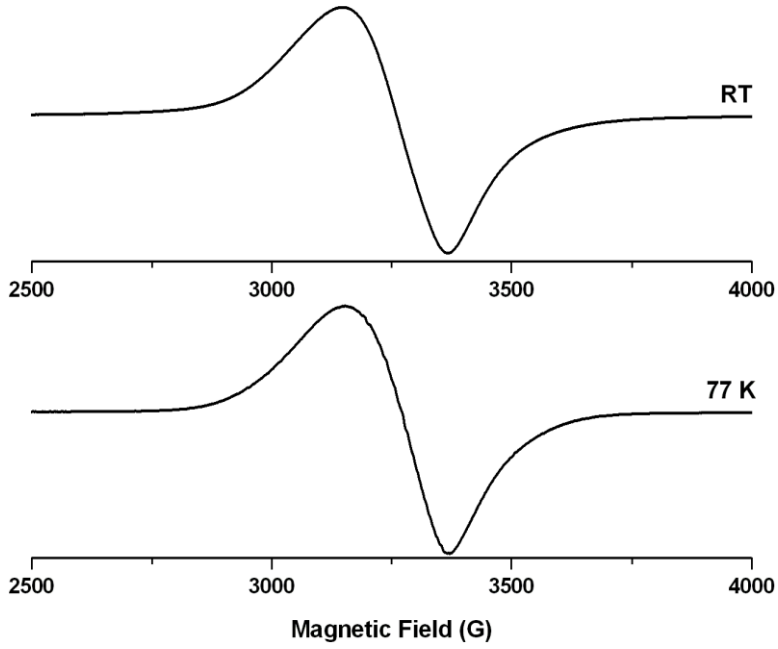

Figure 4.9. Comparison of EPR spectra collected at two different temperatures for compound **6** (Cu-Eu)

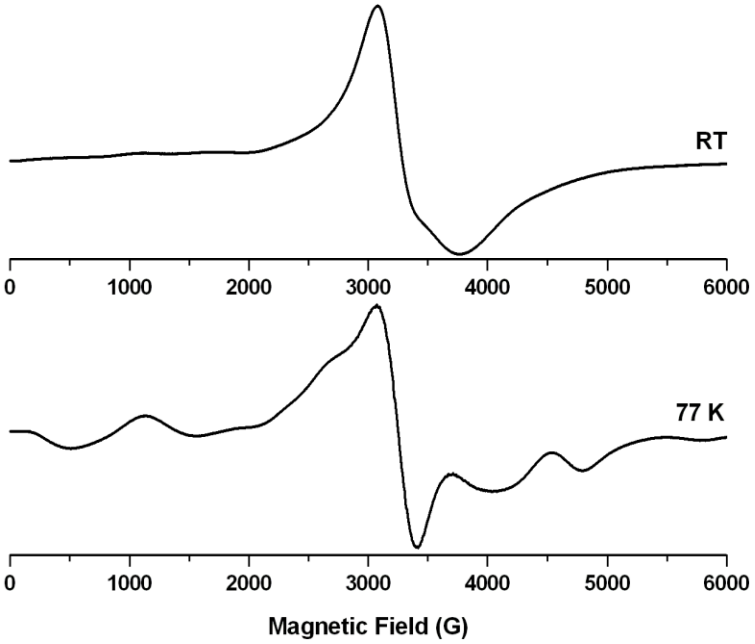

Figure 4.10. Comparison of EPR spectra collected at two different temperatures for compound **7** (Cu-Gd)

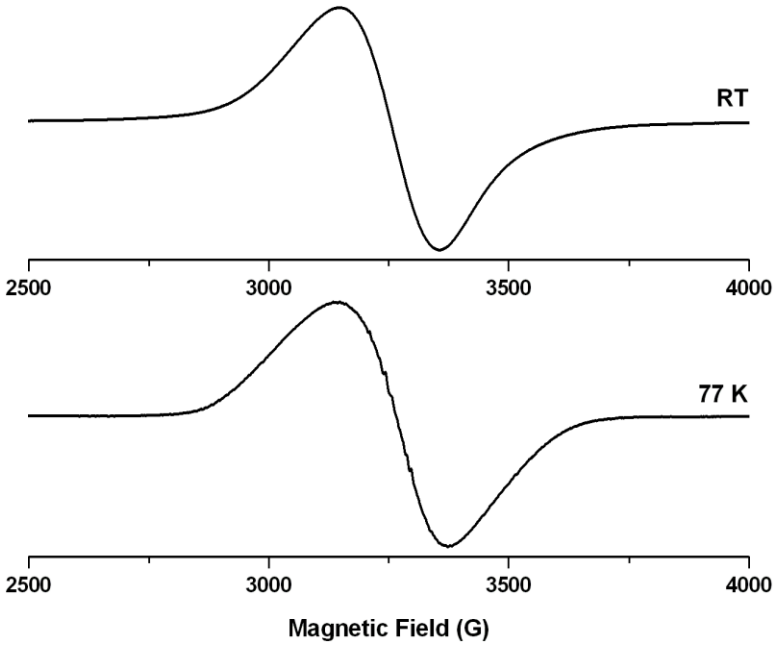

Figure 4.11. Comparison of EPR spectra collected at two different temperatures for compound **8** (Cu-Tb)

Table 4.6: Crystallographic data and structure refinement for compounds **9-14**

	9	**10**	**11**	**12**	**13**
Formula	$C_{40}H_{44}N_{13}O_{16}CuLa$	$C_{40}H_{44}N_{13}O_{16}CuCe$	$C_{36}H_{36}N_{11}O_{15}CuPr$	$C_{36}H_{36}N_{11}O_{15}CuNd$	$C_{36}H_{36}N_{11}O_{15}CuSm$
Formula weight	1165.33	1166.54	1067.21	1070.54	1076.65
Crystal system	Triclinic	Triclinic	Monoclinic	Monoclinic	Monoclinic
Space group	$P\bar{1}$	$P\bar{1}$	$P2_1/c$	$P2_1/c$	$P2_1/c$
a (Å)	13.6013(16)	13.875(8)	10.0568(3)	9.9436(6)	10.0298(2)
b (Å)	13.8408(16)	13.987(4)	21.2709(4)	21.0815(13)	21.2626(6)
c (Å)	14.7160(17)	14.846(8)	20.7955(5)	20.4629(12)	20.7374(6)
α (˚)	78.488(2)	78.836(4)	90	90	90
β (˚)	63.335(2)	62.996(6)	99.766(3)	100.019(10)	99.753(2)
γ (˚)	82.854(2)	82.465(4)	90	90	90
V (Å^3)	2424.0(5)	2515.4(2)	4384.05(19)	4224.1(4)	4358.5(2)
Z	2	2	4	4	4
T (K)	100(2)	298(2)	298(2)	100(2)	298(2)
λ (Å)	0.71073	1.54184	1.54184	0.71073	1.54184
D_{cal} (g cm^{-3})	1.597	1.540	1.617	1.683	1.641
μ (mm^{-1})	1.390	8.103	9.707	1.801	11.306
F(000)	1178	1180	2148	2152	2160
Crystal size (mm)	0.52 x 0.36 x 0.12	0.32 x 0.24 x 0.20	0.32 x 0.28 x 0.20	0.36 x 0.32 x 0.20	0.40 x 0.28 x 0.20
θ Range (˚)	1.50 – 25.68	3.22 – 71.96	2.99 – 71.73	1.40 – 26.04	3.00 – 71.81
$h/k/l$ indices	–16, 16/ –16, 16/ –-17, 17	–17, 16/ –17, 10/ –18, 17	-10, 12/ -23, 26/ -25, 15	-12, 12/ -26, 26/ -25, 25	-12, 7/ -24, 25/ -24, 25
Reflection collected	16973	19037	16574	43438	19836
Unique reflect. [R_{int}]	8519 [0.0214]	9623 [0.0719]	7945 [0.0552]	8314 [0.0293]	8382 [0.0699]
GooF	1.156	1.033	1.055	1.054	1.038
R_1 [I>2σ(I)]	0.0300	0.0639	0.0538	0.0228	0.0574
wR_2	0.1015	0.1766	0.1475	0.0599	0.1502

$w = 1 / [\sigma^2(F_0^2) + (AP)^2 + BP]$; where $P = [2F_C^2 + Max(F_0^2, 0)]/3$

4.6. {[Cu(dmbpy)$_3$][*Ln*(NO$_3$)$_5$(OH$_2$)]·2CH$_3$CN} (9-10)

[*Ln* = La (**9**) and Ce (**10**)]

4.6.1. Crystal structure of {[Cu(dmbpy)$_3$][*Ln*(NO$_3$)$_5$(OH$_2$)]·2CH$_3$CN} (9-10)

Compound **9** and **10** form isomorphous crystals. Crystallographic data and structure refinement details are listed in Table 4.6. Since geometrical parameters of both compounds are similar the selected bond lengths and angles of compound **9** are given in Table 4.7. The molecular structure of **9** consisted of a $[Cu(dmbpy)_3]^{2+}$ cation and one $[La(NO_3)_5(OH_2)_2]^{2-}$ anion per asymmetric unit (Figure 4.12). The Cu(II) ion adopts a distorted elongated-octahedral environment, with the equatorial plane comprised of four nitrogen atoms from three chelating dmbpy ligands. The Cu–N bond distances (Å) lie in the range of 2.012(3)–2.108(3). The angle of equatorial planes are 167.27(1), 168.24(1)º. The axial positions are occupied by the nitrogen atoms of the two different bis-chelating dmbpy ligands [Cu–N distances of 2.233(3), 2.265(3) Å with an angle of 170.18(1)º]. The structure of cationic distortion as dynamic or static disorder can be described by the value of tetragonality parameter *T*.[15] The tetragonality value, *T* is 0.9128, which indicating that the JT distortion is disordered. In agreement with the range $1.0 \leq T \geq 0.9$ this disorder is fluxional. The bite angle of the N(1)N(2) dmbpy ligand, is 79.90(12)º, has two reasonably similar bond lengths of 2.012(3) and 2.072(3) (Å) respectively. For the N(5)N(6) dmbpy ligand, there is a significantly smaller bite angle, 77.61(1)º, due to the intermediate bond lengthening of Cu–N(6) to 2.233(3) (Å). The N(1)N(2) dmbpy ligand has the longest Cu–N bond, Cu–N(3) = 2.265(3) (Å), and the bite angle decreases to 75.55(1)º, giving a total variation in the bite angles of 4.4(1)º. When one of the Cu–N bond distance lengthens, the bite angle of the

related dmbpy ligand decreases. The pyridine rings of three dmbpy ligands are not coplanar with the dihedral angels of 7.61 (5)º, 5.72 (2)º and 9.30 (14)º.

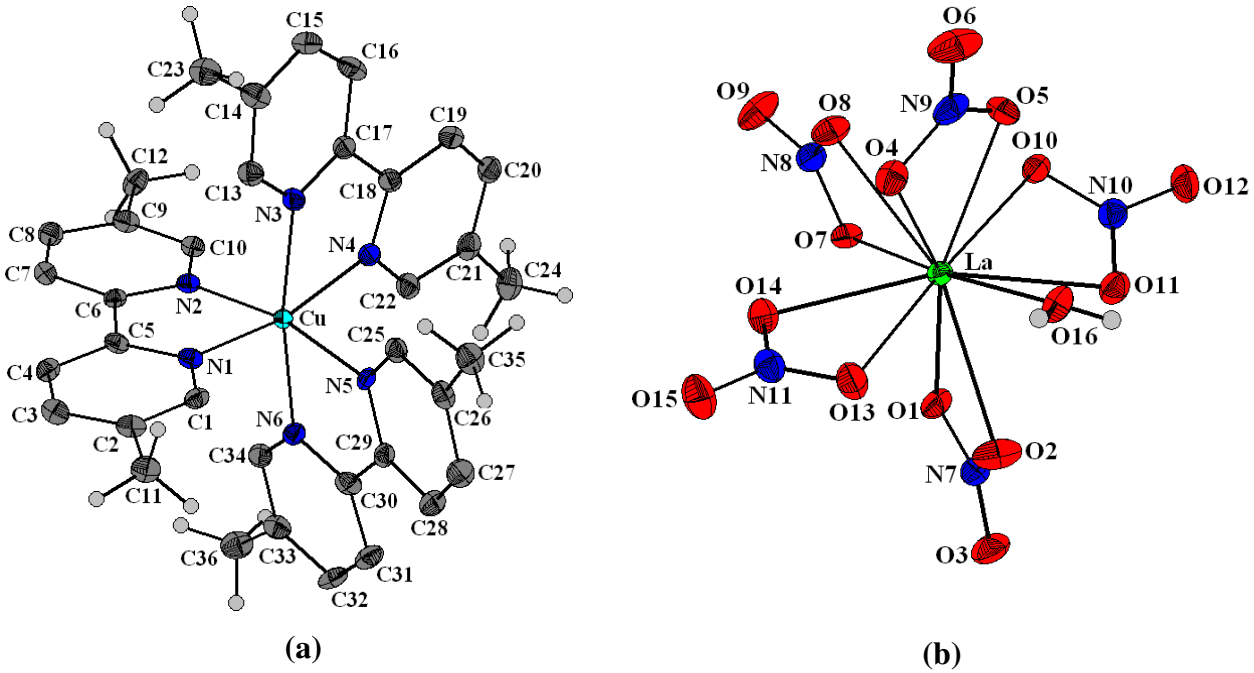

(a) **(b)**

Figure 4.12. Thermal ellipsoid plot of the coordination environment of the (a) complex cation and (b) complex anion of **9**: Atoms are represented as 30% probability ellipsoids. Ring hydrogen atoms and acetonitrile solvent molecules have been omitted for clarity.

The La(III) ion is 11-coordinated with ten oxygen atoms from five chelating nitrate ligands and one oxygen atom from water molecule, forming a distorted monocapped pentagonal antiprismatic geometry[12] (Figure 4.12(b)). The La–O(nitrate) bond lengths (Å) lie in the range 2.589-2.668 and La–O(w), 2.542(2). Coming to crystal packing of **9**, the $[La(NO_3)_5(OH_2)]^{2-}$ anion forms 1D chain with cation by H-bonding interactions (C31-H31···O10, 2.430(4); C19-H19···O8, 2.483(4); O16-H16B···O12, 2.03(4) Å) along *a*-axis. These are further interconnected with various π-stacking interactions (3.085-3.472 Å) forming a 2D network structure. However, the voids are blocked by the $[La(NO_3)_5(OH_2)]^{2-}$ anions (Figure 4.13).

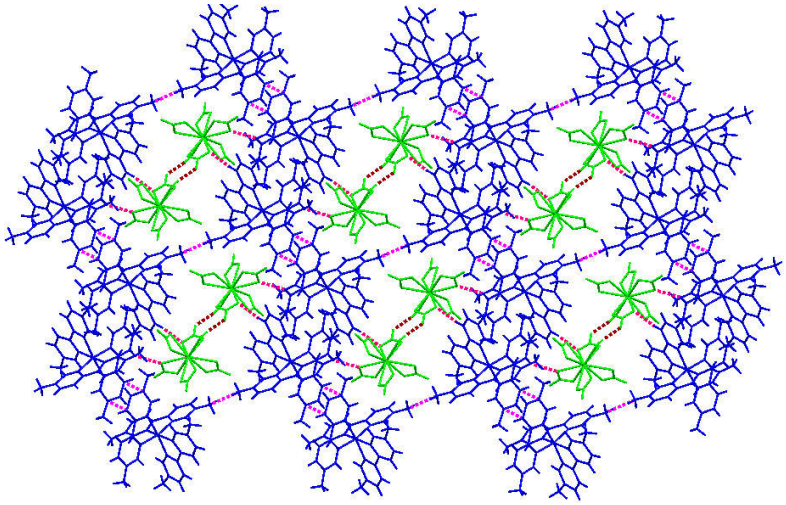

Figure 4.13. A view of the 2D structure formed by the H-bonding interactions in **9** down *a*-axis.

Table 4.7: Selected bond lengths(Å) and bond angles (˚) for {[Cu(dmbpy)$_3$][La(NO$_3$)$_5$(OH$_2$)]·2CH$_3$CN}

Cu-N(1)	2.072(3)	Cu-N(3)	2.265(3)	Cu-N(5)	2.020(3)
Cu-N(2)	2.012(3)	Cu-N(4)	2.108(3)	Cu-N(6)	2.233(3)
La-O(1)	2.609(2)	La-O(7)	2.656(2)	La-O(13)	2.668(3)
La-O(2)	2.671(3)	La-O(8)	2.624(2)	La-O(14)	2.589(2)
La-O(4)	2.595(2)	La-O(10)	2.652(3)	La-O(16)	2.542(2)
La-O(5)	2.642(3)	La-O(11)	2.653(2)		
N(7)-O(1)	1.271(4)	N(8)-O(6)	1.221(4)	N(10)-O(11)	1.254(4)
N(7)-O(2)	1.253(4)	N(9)-O(7)	1.267(4)	N(10)-O(12)	1.239(4)
N(7)-O(3)	1.225(4)	N(9)-O(8)	1.262(4)	N(11)-O(13)	1.259(4)
N(8)-O(4)	1.286(4)	N(9)-O(9)	1.231(4)	N(11)-O(14)	1.272(4)
N(8)-O(5)	1.255(4)	N(10)-O(10)	1.255(4)	N(11)-O(15)	1.220(4)
N(1)-Cu-N(2)	79.90(11)	N(2)-Cu-N(3)	93.53(10)	N(3)-Cu-N(5)	97.30(10)
N(1)-Cu-N(3)	93.66(10)	N(2)-Cu-N(4)	95.90(10)	N(3)-Cu-N(6)	170.18(10)
N(1)-Cu-N(4)	168.24(11)	N(2)-Cu-N(5)	167.27(10)	N(4)-Cu-N(5)	93.26(10)
N(1)-Cu-N(5)	92.72(11)	N(2)-Cu-N(6)	92.60(10)	N(4)-Cu-N(6)	96.20(10)
N(1)-Cu-N(6)	94.96(10)	N(3)-Cu-N(4)	75.55(10)	N(5)-Cu-N(6)	77.61(10)
O(1)-La-O(2)	48.01(7)	O(4)-La-O(5)	48.80(9)	O(7)-La-O(11)	99.82(7)
O(1)-La-O(4)	159.49(9)	O(4)-La-O(7)	116.85(7)	O(7)-La-O(13)	116.95(8)
O(1)-La-O(5)	151.43(8)	O(4)-La-O(8)	70.19(8)	O(7)-La-O(14)	70.70(7)
O(1)-La-O(7)	62.07(7)	O(4)-La-O(10)	112.35(9)	O(7)-La-O(16)	169.01(8)

O(1)-La-O(8)	109.93(7)	O(4)-La-O(11)	125.66(8)	O(8)-La-O(10)	72.92(8)
O(1)-La-O(10)	86.42(8)	O(4)-La-O(13)	67.67(9)	O(8)-La-O(11)	120.83(8)
O(1)-La-O(11)	72.81(8)	O(4)-La-O(14)	76.57(8)	O(8)-La-O(13)	109.70(8)
O(1)-La-O(13)	94.04(9)	O(4)-La-O(16)	70.32(8)	O(8)-La-O(14)	69.10(8)
O(1)-La-O(14)	84.32(8)	O(14)-La-O(16)	120.03(8)	O(8)-La-O(16)	135.25(8)
O(1)-La-O(16)	114.46(8)	O(5)-La-O(7)	107.85(8)	O(10)-La-O(11)	47.94(8)
O(2)-La-O(4)	125.32(8)	O(5)-La-O(8)	68.51(8)	O(10)-La-O(13)	176.93(7)
O(2)-La-O(5)	136.44(8)	O(5)-La-O(10)	65.57(8)	O(10)-La-O(14)	134.81(8)
O(2)-La-O(7)	109.66(7)	O(5)-La-O(11)	83.65(8)	O(10)-La-O(16)	104.04(9)
O(2)-La-O(8)	154.91(8)	O(5)-La-O(13)	113.62(9)	O(11)-La-O(13)	129.35(8)
O(2)-La-O(10)	111.73(8)	O(5)-La-O(14)	119.01(8)	O(11)-La-O(14)	156.98(8)
O(2)-La-O(11)	68.94(9)	O(5)-La-O(16)	69.95(9)	O(11)-La-O(16)	69.36(8)
O(2)-La-O(13)	66.62(9)	O(7)-La-O(8)	48.19(7)	O(13)-La-O(14)	48.25(8)
O(2)-La-O(14)	93.96(9)	O(7)-La-O(10)	65.92(8)	O(13)-La-O(16)	73.00(9)
O(2)-La-O(16)	68.97(8)				
O(1)-N(7)-O(2)	116.7(3)	O(5)-N(8)-O(6)	122.5(4)	O(10)-N(10)-O(12)	119.9(3)
O(1)-N(7)-O(3)	121.4(3)	O(7)-N(9)-O(8)	116.9(3)	O(11)-N(10)-O(12)	121.7(3)
O(2)-N(7)-O(3)	121.9(3)	O(7)-N(9)-O(9)	121.4(3)	O(13)-N(11)-O(14)	116.3(3)
O(4)-N(8)-O(5)	116.7(3)	O(8)-N(9)-O(9)	121.6(3)	O(13)-N(11)-O(15)	122.1(3)
O(4)-N(8)-O(6)	120.7(4)	O(10)-N(10)-O(11)	118.4(3)	O(14)-N(11)-O(15)	121.6(3)

4.6.2. Infrared spectra

In the IR spectra the band around 3450-3470 cm^{-1} has been assigned to O-H stretching vibration of water for **9** and **10**. The $\nu_{C=C}$ frequency of the bpy rings at 1610 and 1570 cm^{-1}. The stretching vibrations corresponding to those typical of the lanthanide anions occur around at 1480, 1300, 1040 and 810 cm^{-1}.

4.6.3. Electronic spectra

Diffuse reflectance spectrum of **9** is similar to the spectra of $[Cu(bpy)_3](Y)_2$ as reported previously (Figure 4.14). A broad band centered at 14840 cm^{-1} ($d_z^2 \approx d_{xy} \rightarrow d_{x2-y2}$) can be

assigned to metal centered d-d transition.[16] The lower energy band maximum (about 6000 cm^{-1}) is too low to be seen in the present measurement. Band near 32,000 cm^{-1} is due to ligand-to-metal charge transfer transition, while the band near 39,000 cm^{-1} is associated with intra-ligand $\pi \rightarrow \pi^*$ excitation.

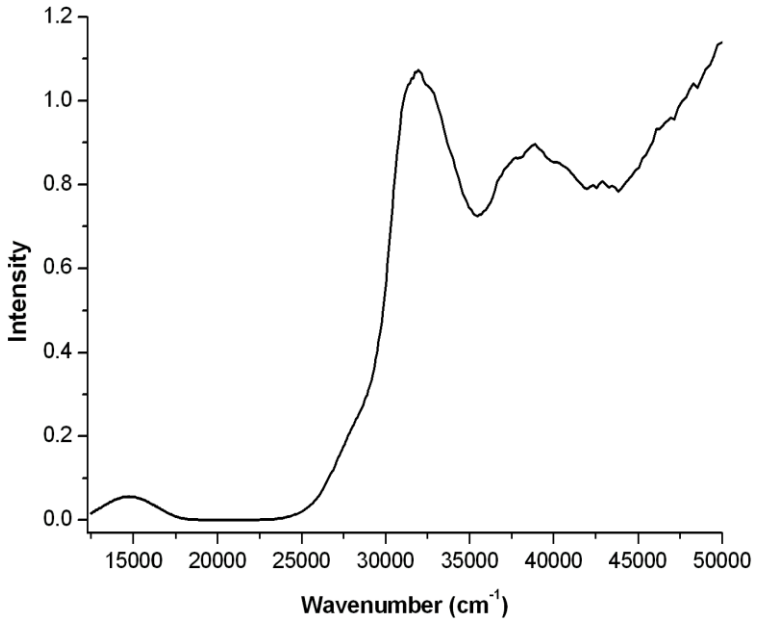

Figure 4.14. Diffuse reflectance spectrum of compound **9**

4.6.4. EPR spectra

The X-band polycrystalline-powder electron paramagnetic resonance (EPR) spectra of **9** and **10** were measured at room temperature and 77 K (Figure 4.15 and Figure 4.16). Both have shown resolved EPR signals and corresponding g, A values at 300 K: $g_{\|} = 2.321$, $g_{\perp} = 2.103$, $A_{\|} =$ 130 G, $A_{\perp} = 64$ G; at 77 K: $g_{\|} = 2.261$, $g_{\perp} = 2.068$, $A_{\|} = 150$ G, $A_{\perp} = 40$ G. Both spectra have been normalized to same microwave frequency (ν = 9.684055 GHz). As in the case of $Cu(bpy)_3^{2+}$ complexes described in chapter 3, here again the temperature dependent changes in distortion is responsible for the variation of the EPR parameters.

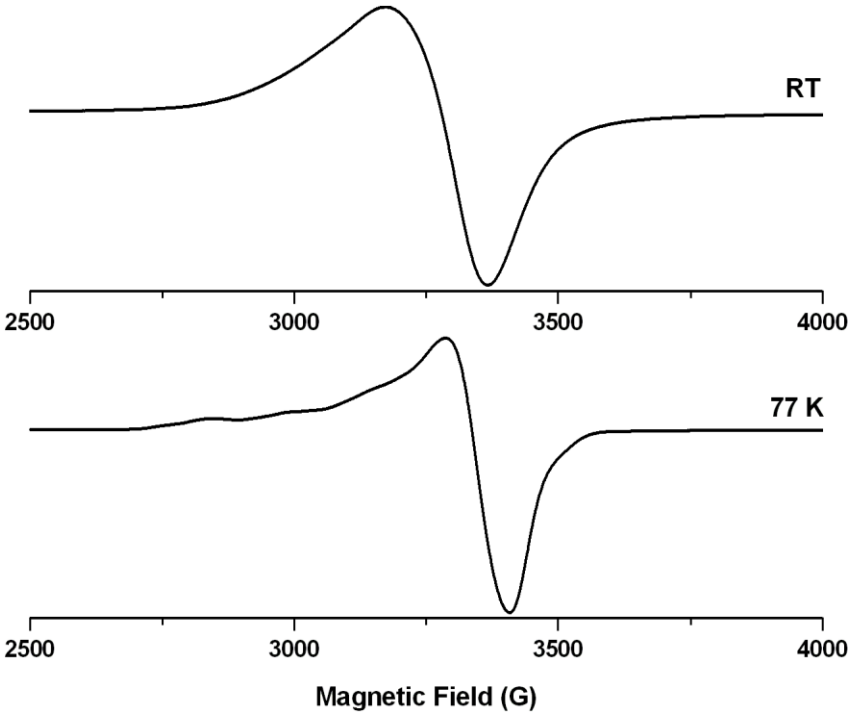

Figure 4.15. Comparison of EPR spectra collected at two different temperatures for compound **9** (Cu-La)

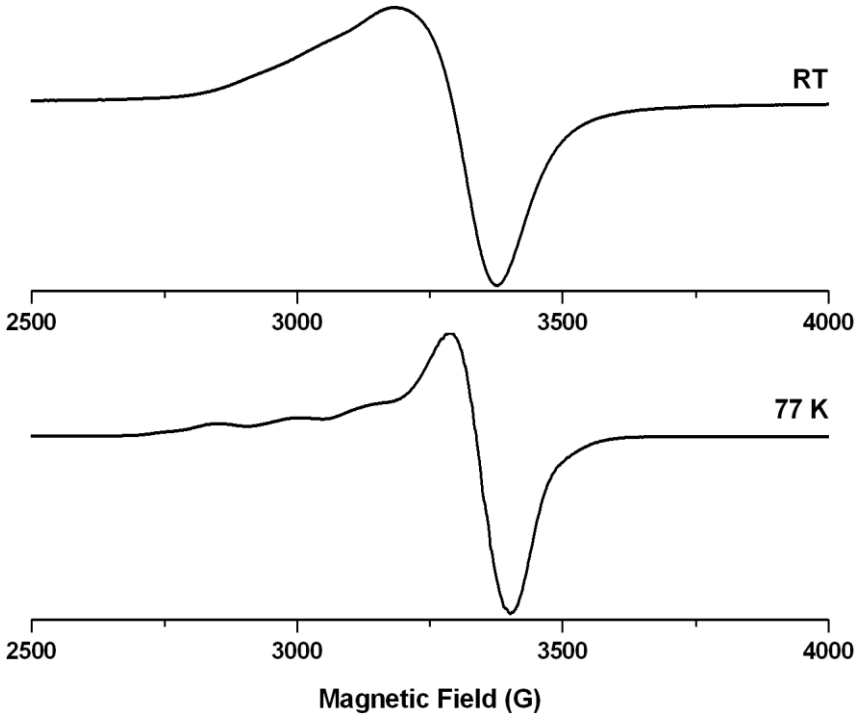

Figure 4.16. Comparison of EPR spectra collected at two different temperatures for compound **10** (Cu-Ce)

Table 4.8: Crystallographic data and structure refinement for compounds **14-18**

	14	**15**	**16**	**17**	**18**
Formula	$C_{36}H_{36}N_{11}O_{15}CuEu$	$C_{36}H_{36}N_{11}O_{15}CuGd$	$C_{36}H_{36}N_{11}O_{15}CuTb$	$C_{36}H_{36}N_{11}O_{15}CuDy$	$C_{36}H_{36}N_{11}O_{15}CuHo$
Formula weight	1078.26	1083.55	1085.22	1088.80	1091.23
Crystal system	Monoclinic	Monoclinic	Monoclinic	Monoclinic	Monoclinic
Space group	$P2_1/c$	$P2_1/c$	$P2_1/c$	$P2_1/c$	$P2_1/c$
a (Å)	10.022(11)	10.024(4)	10.007(2)	10.0191(5)	10.0001(8)
b (Å)	21.245(2)	21.265(9)	21.262(5)	21.2615(8)	21.2165(18)
c (Å)	20.714(2)	20.756(9)	20.706(5)	20.7082(8)	20.6652(18)
β (˚)	99.779(2)	99.632(7)	99.859(3)	99.798(4)	99.787(10)
V (Å^3)	4346.2(8)	4362(3)	4340.4(16)	4346.9(3)	4320.7(6)
Z	4	4	4	4	4
T(K)	298(2)	298(2)	298(2)	298(2)	298(2)
λ (Å)	0.71073	0.71073	0.71073	0.71073	0.71073
D_{calc} (g cm^{-3})	1.648	1.650	1.661	1.664	1.678
μ (mm^{-1})	1.999	2.074	2.186	2.275	2.390
F(000)	2164	2168	2172	2176	2180
Crystal size (mm)	0.40 x 0.28 x 0.20	0.64 x 0.42 x 0.28	0.48 x 0.32 x 0.20	0.24 x 0.20 x 0.12	0.52 x 0.24 x 0.16
θ Range(˚)	1.38 – 26.04	1.38 – 25.70	1.38 – 25.71	2.79 – 26.02	1.39 – 26.07
$h/k/l$ indices	–12, 12/ –25,25/ –25,25	–12, 12/ –25, 25/ –25, 24	–12, 11/ –24, 25/ –19,25	–12, 11/ –26, 26/ –25, 25	–12, 12/ –26, 26 / –25,25
Reflection collected	44798	32563	21740	19391	44564
Unique reflect. [R_{int}]	8553 [0.0321]	8289 [0.0386]	8093 [0.0436]	8555 [0.0470]	8543 [0.0333]
GooF	1.042	1.030	1.040	1.039	1.037
R_1 [I>2σ(I)]	0.0275	0.0283	0.0319	0.0479	0.0267
wR_2	0.0708	0.0732	0.0801	0.0935	0.0687

$w = 1 / [\sigma^2(F_0^2) + (AP)^2 + BP]$; where $P = [2F_C^2 + Max(F_0^2, 0)]/3$

4.7. {[Cu(dmbpy)$_3$][*Ln*(NO$_3$)$_5$]} (11-22)

[*Ln* = Pr (**10**), Nd(**12**), Sm(**13**), Eu(**14**), Gd(**15**), Tb(**16**), Dy(**17**), Ho(**18**), Er(**19**), Tm(**20**), Yb(**21**), Lu(**22**)]

4.7.1. Crystal structure of {[Cu(dmbpy)$_3$][*Ln*(NO$_3$)$_5$]} (11-22)

Compounds **11-22** form isomorphous crystals. Crystallographic data and structure refinement details are listed in Table 4.6, Table 4.8 and Table 4.9. Since geometrical parameters of all compounds are similar the selected bond lengths and angles of compound **19** are given in Table 4.11. The asymmetric unit consisted of a discrete $[Cu(dmbpy)_3]^{2+}$ cation and $[Ln(NO_3)_5]^{2-}$ anion is shown in Figure 4.17. The Cu(II) ion adopts a distorted elongated-octahedral environment, with the equatorial plane comprised of four nitrogen atoms from three chelating dmbpy ligands. The Cu–N bond distances (Å) lie in the range of 2.024(4)–2.064(4). The angle of equatorial planes are 162.34(1), 171.07(1)°. The axial positions are occupied by the nitrogen atoms of the two different bis-chelating dmbpy ligands [Cu–N distances of 2.249(3), 2.433(4) Å with an angle of 174.94(13)°]. The tetragonality value(*T*) lie in the range 0.8675–0.8761 indicating that the JT distortion is disordered. Moreover, it is close to reported values for the analogous complexes (Table 4.10) and shows typical static JT distortion. The bite angle of the dmbpy1 ligand is 80.2(14)º, has two reasonably similar bond lengths (Å) of 2.024(3), 2.064(4). For the dmbpy2 ligand, there is a significantly smaller bite angle 76.86(13)º, due to the intermediate bond lengthening to 2.249(3) (Å). The dmbpy3 ligand has the longest Cu–N bond, 2.433(4), and the bite angle decreases to 75.52(14)º, giving a total variation in the bite angle of 4.7(1)º. The pyridine rings of three dmbpy ligands are not coplanar with the dihedral angels of 7.10 (3)°, 5.64 (3)° and 29.04 (1)°.

Table 4.9: Crystallographic data and structure refinement for compounds **19-22**

	19	**20**	**21**	**22**
Formula	$C_{36}H_{36}N_{11}O_{15}CuEr$	$C_{36}H_{36}N_{11}O_{15}CuTm$	$C_{36}H_{36}N_{11}O_{15}CuYb$	$C_{36}H_{36}N_{11}O_{15}CuLu$
Formula weight	1093.56	1095.23	1099.34	1101.27
Crystal system	Monoclinic	Monoclinic	Monoclinic	Monoclinic
Space group	$P2_1/c$	$P2_1/c$	$P2_1/c$	$P2_1/c$
a (Å)	9.9816(3)	9.9123(11)	9.99250(10)	9.9813(15)
b (Å)	21.1959(9)	21.0756(17)	21.2125(2)	21.209(3)
c (Å)	20.6406(8)	20.4942(18)	20.6575(3)	20.649(3)
β (°)	99.775(3)	99.984(9)	99.846(10)	99.880(2)
V (Å^3)	4303.5(3)	4216.6(7)	4314.19(9)	4306.4(11)
Z	4	4	4	4
T(K)	298(2)	298(2)	298(2)	298(2)
λ (Å)	0.71073	0.71073	1.54184	0.71073
D_{calc} (g cm^{-3})	1.688	1.725	1.693	1.699
μ (mm^{-1})	2.511	2.677	5.210	2.853
F(000)	2184	2188	2192	2196
Crystal size (mm)	0.20 x 0.16 x 0.12	0.24 x 0.20 x 0.12	0.22 x 0.20 x 0.08	0.20 x 0.18 x 0.08
θ Range(°)	2.80 to 26.02	2.65 to 26.37	3.01 to 71.72	1.39 to 26.09
$h/k/l$ indices	–12,12/ –22,26/ –16,25	–10,12/ –25,26/ –22,25	–8,12/ –25,24/ –25,25	–12,12/ –26,26/ –25,25
Reflection collected	17759	18071	16883	44397
Unique reflect. [R_{int}]	8477 [0.0333]	8613 [0.0458]	8280 [0.0250]	8523 [0.0480]
GooF	1.047	1.023	1.033	1.040
R_1 [I>2σ(I)]	0.0398	0.0466	0.0345	0.0353
wR_2	0.0927	0.0920	0.0921	0.0883

$w = 1 / [\sigma^2(F_0^2) + (AP)^2 + BP]$; where $P = [2F_C^2 + Max(F_0^2, 0)]/3$

In $[Cu(bpy)_3]Y$ complexes the counter ions position can be occupied by various anions such as NO_3^-, ClO_4^-, PF_6^-, BF_4^-, BPh_4, SO_4^{2-}, CrO_4^{2-}, Br^-, I^-, $[Ln(NO_3)_5]^{2-}$ and $[Ln(NO_3)_5(OH_2)]^{2-}$.[17] The counter ion (Y) could be a suitable structural factor determining the dynamic or static Jahn–Teller distortion for the $[Cu(bpy)_3]^{2+}$ cations. The influence of Y anions

is clearly seen on the values of *T* parameter for $[Cu(dmbpy)_3]^{2+}$ cations in other $[Cu(bpy)_3]Y$ complexes collected in Table 4.13. The $[Cu(bpy)_3]^{2+}$ cations exhibit the fluxional character of JT distortion in complexes containing anions such as SO_4^{2-}, CrO_4^{2-}, Br^-, PF_6^- and $[Ln(NO_3)_5]^{2-}$. On the contrary, the *T* values are less than 0.9 and the $[Cu(bpy)_3]^{2+}$ cations exhibit a typical static JT distortion for the compounds with other anions such as BF_4^-, BPh_4^-, ClO_4^- and $[Ln(NO_3)_5(OH_2)]^{2-}$.

The *Ln*(III) ion is 10-coordinated with ten oxygen atoms from five chelating nitrate ligands, forming a distorted bicapped square antiprism[18] (Figure 4.17(b)). The structural data for Er(III) anion can explain the structure of $[Ln(NO_3)_5]^{2-}$. The three nitrate ions which are approximately in the same plane constitute three planar sets: O1, O2, O3, N7 and Er (plane **I**); O4, O5, O6, N8 and Er (plane **II**) and O7, O8, O9, N9 and Er (plane **III**). The dihedral angles being 20.2º between the plane **I** and plane **II**, 26.7º between the plane **I** and plane **III**, and 26.3° between the plane **II** and plane **III**. The remaining two nitrate ion planar sets: O10, O11, O12, N10 and Er (plane **IV**); O13, O14, O15, N11 and Er (plane **V**) were nearly perpendicular to these planes (the dihedral angles were 73.3-86.9º). The dihedral angle between the plane **IV** and plane **V** is 72.3º. The O–N distance (Å) is 1.20(5)-1.27(5), and the *Ln*–O(nitrate) bond lengths (Å) lie in the range 2.374-2.485 (Table 4.12). The O–N–O bond angles (º) range is 114.1(4)-124.0(5) and O–*Ln*–O bond angles (º) lie in the range 50.7(13)-52.5(12) (Table 4.12). The crystal packing analysis indicates that both intermolecular H-bonding and π-stacking interactions combine to stabilize the extended structure. The $[Er(NO_3)_5]^{2-}$ anionic units form 1D zig-zag chain with cation by C-H···O interactions (C16-H16···O2, 2.445(5); C24-H24B···O11, 2.482(5) Å) along *a*-axis. These are further interconnected with other C-H···O interactions (C24-H24A···O15, 2.584(5) Å) of cationic units to form 2D network (Figure 4.18).

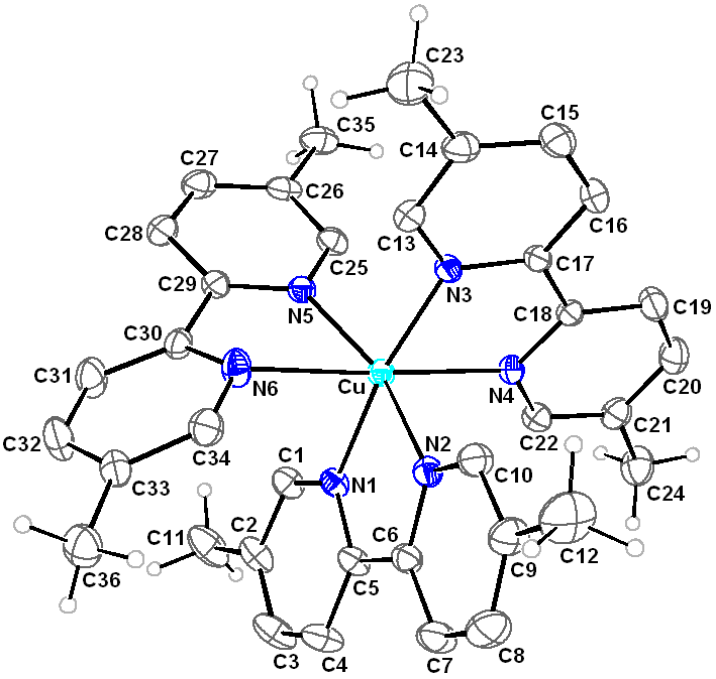

(a)

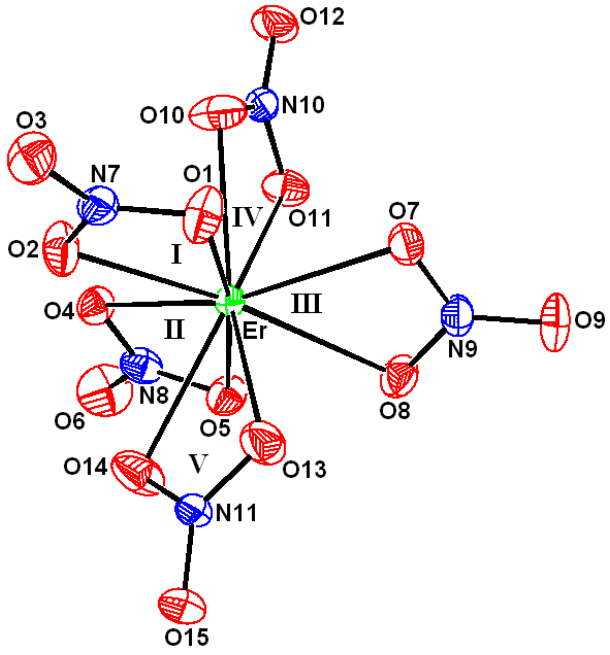

(b)

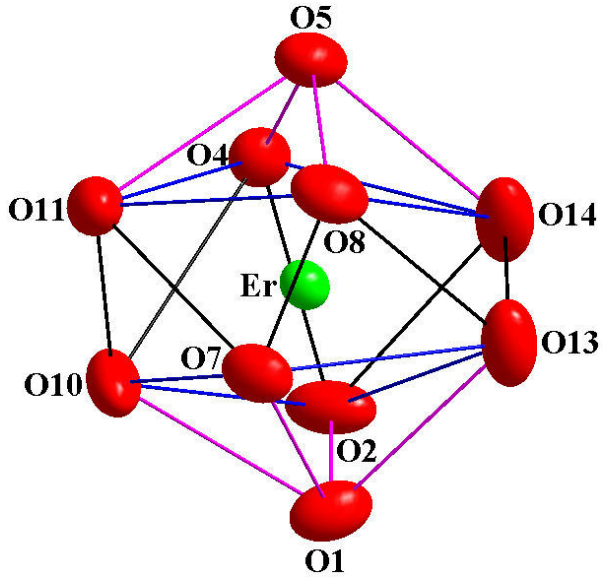

(c)

Figure 4.17. Thermal ellipsoid plot of the coordination environment of the (a) complex cation (b) complex anion of **19** (c) bicapped square antiprism coordination polyhedron of Er(III) ion in $[Er(NO_3)_5]^{2-}$: Atoms are represented as 30% probability ellipsoids. Ring hydrogen atoms have been omitted for clarity.

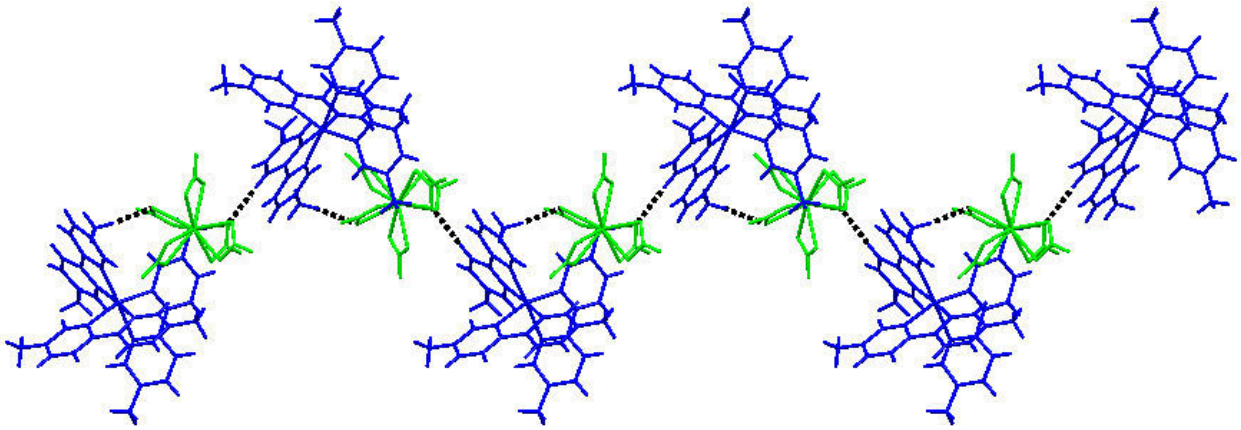

(a)

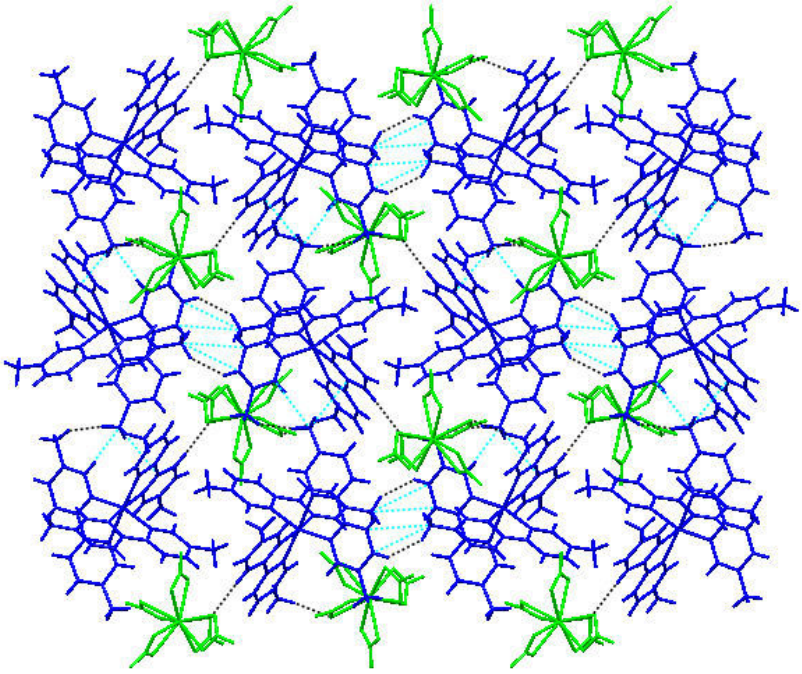

(b)

Figure 4.18. Views of (a) 1D zig-zag chain formed by H-bond interactions of cation and anion units in **19** (b) 2D structure formed by H-bonding contacts of **19** down *c*-axis.

Table 4.10: Cu-N equatorial and axial bond distances (Å) and Tetragonality (*T*) values for **9-22**

	Cu-N(A) equa	Cu-N(B) equa	Cu-N(C) **axial**	Cu-N(D) equa	Cu-N(E) equa	Cu-N(F) **axial**	*T*
9	2.012(3)	2.072(3)	**2.233(3)**	2.020(3)	2.108(3)	**2.265(3)**	0.9128
10	2.032(4)	2.080(4)	**2.222(5)**	2.030(4)	2.120(4)	**2.242(5)**	0.9252
11	2.026(4)	2.077(4)	**2.249(5)**	2.028(4)	2.052(4)	**2.421(5)**	0.8761
12	2.018(16)	2.058(16)	**2.251(17)**	2.019(16)	2.040(16)	**2.438(17)**	0.8675
13	2.021(5)	2.069(5)	**2.244(5)**	2.023(4)	2.048(5)	**2.428(5)**	0.8734
14	2.019(2)	2.070(2)	**2.250(2)**	2.025(2)	2.049(2)	**2.432(2)**	0.8717
15	2.021(2)	2.073(2)	**2.257(2)**	2.027(2)	2.050(2)	**2.438(3)**	0.8702
16	2.020(2)	2.073(2)	**2.253(3)**	2.027(2)	2.054(2)	**2.435(3)**	0.8718
17	2.020(4)	2.065(4)	**2.256(4)**	2.023(4)	2.052(4)	**2.439(4)**	0.8690
18	2.021(2)	2.066(2)	**2.254(2)**	2.025(2)	2.048(2)	**2.439(2)**	0.8694
19	2.024(3)	2.064(4)	**2.249(3)**	2.027(3)	2.050(4)	**2.433(4)**	0.8719
20	2.007(4)	2.058(4)	**2.234(4)**	2.016(4)	2.038(4)	**2.412(4)**	0.8737
21	2.023(3)	2.073(3)	**2.254(3)**	2.025(2)	2.049(2)	**2.428(3)**	0.8725
22	2.021(3)	2.068(3)	**2.252(3)**	2.024(3)	2.053(3)	**2.439(3)**	0.8704

Table 4.11: Selected bond lengths (Å) and bond angles (˚) for {[Cu(dmbpy)$_3$][Er(NO$_3$)$_5$]}

Cu-N(1)	2.024(3)	Cu-N(3)	2.027(3)	Cu-N(5)	2.050(4)
Cu-N(2)	2.064(4)	Cu-N(4)	2.249(3)	Cu-N(6)	2.433(4)
Er-O(1)	2.485(3)	Er-O(7)	2.393(3)	Er-O(11)	2.464(4)
Er-O(2)	2.395(4)	Er-O(8)	2.405(3)	Er-O(13)	2.428(4)
Er-O(4)	2.404(3)	Er-O(10)	2.374(3)	Er-O(14)	2.442(4)
Er-O(5)	2.449(3)				
N(7)-O(1)	1.233(5)	N(8)-O(6)	1.210(6)	N(10)-O(11)	1.256(5)
N(7)-O(2)	1.255(5)	N(9)-O(7)	1.252(5)	N(10)-O(12)	1.203(5)
N(7)-O(3)	1.217(5)	N(9)-O(8)	1.251(5)	N(11)-O(13)	1.245(5)
N(8)-O(4)	1.271(5)	N(9)-O(9)	1.206(5)	N(11)-O(14)	1.226(5)
N(8)-O(5)	1.256(5)	N(10)-O(10)	1.237(6)	N(11)-O(15)	1.220(5)
N(1)-Cu-N(2)	80.20(14)	N(2)-Cu-N(3)	93.21(14)	N(3)-Cu-N(6)	98.21(13)
N(1)-Cu-N(3)	171.07(15)	N(2)-Cu-N(4)	91.75(13)	N(4)-Cu-N(5)	105.72(14)
N(1)-Cu-N(4)	97.19(13)	N(2)-Cu-N(5)	162.34(14)	N(4)-Cu-N(6)	174.94(13)
N(1)-Cu-N(5)	94.78(14)	N(3)-Cu-N(4)	76.86(13)	N(5)-Cu-N(6)	75.52(14)
N(1)-Cu-N(6)	87.55(13)	N(3)-Cu-N(5)	93.26(13)	N(2)-Cu-N(6)	87.30(14)

O(1)-Er-O(2)	51.12(12)	O(2)-Er-O(13)	89.77(15)	O(7)-Er-O(8)	52.04(12)
O(1)-Er-O(4)	122.33(12)	O(2)-Er-O(14)	76.59(16)	O(7)-Er-O(10)	77.65(15)
O(1)-Er-O(5)	169.10(15)	O(4)-Er-O(5)	52.47(12)	O(7)-Er-O(11)	78.57(13)
O(1)-Er-O(7)	72.08(13)	O(4)-Er-O(7)	153.19(13)	O(7)-Er-O(13)	79.66(13)
O(1)-Er-O(8)	117.52(12)	O(4)-Er-O(8)	120.14(12)	O(7)-Er-O(14)	128.31(13)
O(1)-Er-O(10)	68.99(15)	O(4)-Er-O(10)	86.70(15)	O(8)-Er-O(10)	116.21(16)
O(1)-Er-O(11)	117.47(13)	O(4)-Er-O(11)	74.66(13)	O(8)-Er-O(11)	79.63(14)
O(1)-Er-O(13)	70.08(14)	O(4)-Er-O(13)	125.33(13)	O(8)-Er-O(13)	74.25(15)
O(1)-Er-O(14)	99.14(16)	O(4)-Er-O(14)	74.75(13)	O(8)-Er-O(14)	95.61(15)
O(2)-Er-O(4)	72.27(13)	O(5)-Er-O(7)	116.92(13)	O(10)-Er-O(11)	51.21(13)
O(2)-Er-O(5)	120.82(13)	O(5)-Er-O(8)	68.40(13)	O(10)-Er-O(13)	137.55(15)
O(2)-Er-O(7)	122.12(12)	O(5)-Er-O(10)	117.72(15)	O(10)-Er-O(14)	148.12(16)
O(2)-Er-O(8)	163.54(14)	O(5)-Er-O(11)	71.80(13)	O(11)-Er-O(13)	152.87(14)
O(2)-Er-O(10)	73.11(15)	O(5)-Er-O(13)	104.49(14)	O(11)-Er-O(14)	141.07(13)
O(2)-Er-O(11)	115.58(14)	O(5)-Er-O(14)	70.61(15)	O(13)-Er-O(14)	50.71(13)
O(1)-N(7)-O(2)	115.8(4)	O(5)-N(8)-O(6)	122.5(5)	O(10)-N(10)-O(12)	122.4(5)
O(1)-N(7)-O(3)	123.2(5)	O(7)-N(9)-O(8)	114.4(4)	O(11)-N(10)-O(12)	123.4(5)
O(2)-N(7)-O(3)	121.0(5)	O(7)-N(9)-O(9)	123.1(5)	O(13)-N(11)-O(14)	115.1(4)
O(4)-N(8)-O(5)	116.2(4)	O(8)-N(9)-O(9)	122.5(5)	O(13)-N(11)-O(15)	120.7(5)
O(4)-N(8)-O(6)	121.3(5)	O(10)-N(10)-O(11)	114.1(4)	O(14)-N(11)-O(15)	124.0(5)

Table 4.12: Bond lengths (Å) of *Ln*–O and bond angles (°) of O–*Ln*–O

	Ln													
	La	**Ce**	**Pr**	**Nd**	**Sm**	**Eu**	**Gd**	**Tb**	**Dy**	**Ho**	**Er**	**Tm**	**Yb**	**Lu**
Ln–O1	2.609(2)	2.624(6)	2.545(6)	2.575(15)	2.464(5)	2.448(2)	2.523(2)	2.444(2)	2.415(4)	2.399(2)	2.485(3)	2.415(4)	2.385(3)	2.364(3)
Ln–O2	2.671(3)	2.632(5)	2.544(4)	2.498(15)	2.483(5)	2.461(2)	2.452(2)	2.475(3)	2.501(4)	2.418(2)	2.395(4)	2.375(4)	2.438(3)	2.380(3)
Ln–O4	2.595(2)	2.588(5)	2.511(5)	2.506(14)	2.491(5)	2.493(2)	2.468(2)	2.440(2)	2.418(3)	2.460(2)	2.404(3)	2.365(4)	2.382(3)	2.477(3)
Ln–O5	2.642(3)	2.648(5)	2.516(5)	2.529(15)	2.489(5)	2.474(2)	2.493(2)	2.427(2)	2.433(4)	2.421(2)	2.449(3)	2.460(4)	2.368(3)	2.365(3)
Ln–O7	2.656(2)	2.585(5)	2.529(5)	2.490(15)	2.526(5)	2.521(2)	2.445(2)	2.431(3)	2.433(3)	2.494(2)	2.393(3)	2.363(4)	2.479(3)	2.378(3)
Ln–O8	2.624(2)	2.625(7)	2.573(5)	2.500(15)	2.486(5)	2.463(2)	2.456(2)	2.502(3)	2.469(4)	2.410(2)	2.405(3)	2.383(4)	2.371(3)	2.435(3)
Ln–O10	2.652(3)	2.583(5)	2.562(5)	2.552(15)	2.465(6)	2.505(2)	2.492(3)	2.467(3)	2.474(4)	2.454(2)	2.374(3)	2.417(4)	2.455(3)	2.400(3)
Ln–O11	2.653(2)	2.660(7)	2.552(5)	2.538(15)	2.523(5)	2.495(2)	2.484(3)	2.474(3)	2.454(4)	2.443(2)	2.464(4)	2.398(4)	2.355(3)	2.415(3)
Ln–O13	2.668(3)	2.627(6)	2.568(5)	2.482(15)	2.519(5)	2.442(2)	2.430(3)	2.497(3)	2.411(4)	2.388(2)	2.428(4)	2.439(4)	2.415(3)	2.341(3)
Ln–O14	2.589(2)	2.573(5)	2.518(6)	2.558(15)	2.532(6)	2.522(2)	2.509(2)	2.415(3)	2.485(4)	2.475(2)	2.442(4)	2.352(4)	2.428(3)	2.448(3)
O1–*Ln*–O2	48.01(7)	47.79(19)	49.92(18)	50.18(5)	50.64(18)	50.95(8)	50.24(8)	51.88(9)	50.74(12)	51.95(8)	51.12(12)	52.98(14)	52.96(1)	53.03(1)
O4–*Ln*–O5	48.80(9)	48.37(14)	49.3(2)	50.95(5)	51.48(18)	51.42(8)	51.49(8)	51.52(9)	51.80(14)	52.24(8)	52.47(12)	50.83(13)	52.74(1)	51.31(1)
O7–*Ln*–O8	48.19(7)	47.8(2)	49.18(16)	51.19(5)	49.96(17)	50.02(7)	51.16(8)	50.40(9)	52.17(13)	50.93(7)	52.04(12)	52.44(15)	51.01(9)	52.82(1)
O10–*Ln*–O11	47.94(8)	47.68(18)	48.74(18)	49.98(5)	49.34(19)	49.84(8)	50.10(8)	50.41(9)	50.41(13)	50.74(8)	51.21(13)	50.92(14)	51.74(1)	51.31(1)
O13–*Ln*–O14	48.25(8)	48.5(2)	48.6(2)	50.47(5)	49.83(18)	49.94(8)	50.28(9)	50.58(9)	50.74(15)	51.12(8)	50.71(13)	51.50(16)	51.24(1)	52.11(1)

Table 4.13: Structural data for the $[Cu(bpy)_3][Y]_2$ series of complexes

Comp.	***T***	***JT* distortion**	**Ref.**
$[Cu(bpy)_3][CrO_4]\cdot 7.5H_2O$	0.9830/0.9876	fluxional	[17g]
$[Cu(bpy)_3][PF_6]_2$	0.9608	fluxional	[17f]
$[Cu(bpy)_3][SO_4]\cdot 7.5H_2O$	0.9580	fluxional	[17h]
$[Cu(bpy)_3][Ln(NO_3)_5]$	0.9796-0.9859	fluxional	Chapter 3
$[Cu(bpy)_3][SO_4]_{0.5}(7.8\cdot H_2O)$	0.9435	fluxional	[17a]
$[Cu(dmbpy)_3](PF_6)_2\cdot CH_3CN$	0.9705	fluxional	[2]
9-**10**	0.9128-0.9252	fluxional	Present work
$[Cu(dmbpy)_3](BF_4)_2\cdot EtOH$	0.8999	static	[1]
$[Cu(bpy)_3][BPh_4]_2$	0.8868	static	[17a]
$[Cu(bpy)_3][BF_4]_2$	0.8699	static	[17b]
$[Cu(bpy)_3][ClO_4]_2$	0.8636-0.8695	static	[17c-e]
$[Cu(bpy)_3][Ln(NO_3)_5(OH_2)]\cdot 2CH_3CN$	0.8863-0.8933	static	Chapter 3
11-**22**	0.8675-0.8761	static	Present work

4.7.2. Infrared spectra

The $\nu_{C=C}$ frequency of the dmbpy rings at 1620 and 1570 cm^{-1}. The stretching vibrations corresponding to those typical of the lanthanide anions occur around at 1480, 1300, 1040 and 810 cm^{-1}.

4.7.3. Electronic spectra

Diffuse reflectance spectrum of **11** is shown in Figure 4.19. A broad band centered at 14800 cm^{-1} ($d_z^2 \approx d_{xy} \rightarrow d_{x2-y2}$) can be assigned to metal centered d-d transition.[16] The lower energy band maximum (about 6000 cm^{-1}) is too low to be seen in the present measurement. Band near 32,000 cm^{-1} is due to ligand-to-metal charge transfer transition, while the band near 39,000 cm^{-1} is associated with intraligand $\pi \rightarrow \pi^*$ excitation.

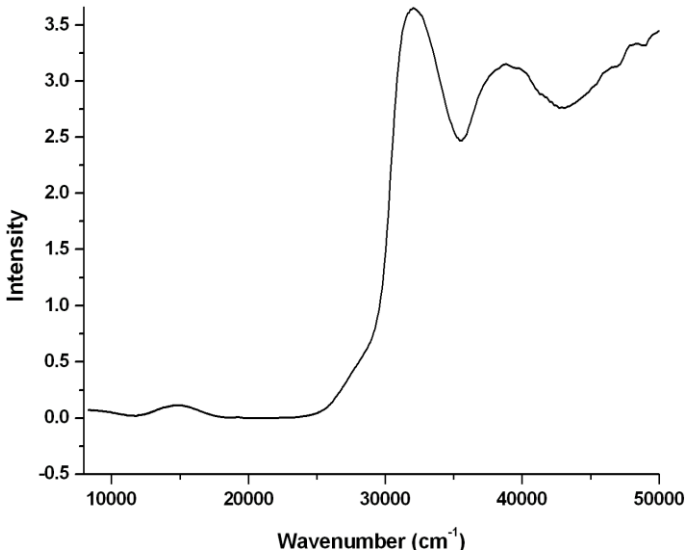

Figure 4.19. Diffuse reflectance spectrum of compound **11**

4.7.4. EPR spectra

The X-band polycrystalline-powder electron paramagnetic resonance (EPR) spectra of **11-22** were measured at room temperature (Figure 4.20 – 4.31). All spectra have been normalized to same microwave frequency (ν = 9.684055 GHz). All spectra have shown well resolved EPR signals and corresponding g, A values at both temperature were given in Table 4.14. Unlike in the case of the complexes described in chapter 3, the reduction in the size of the *Ln*-coordination polyhedron from 11 to 10 does not seriously affect the resolution of the Cu(II) EPR. The effect of reduction in the anion size appears to have been offset by the increase in cation size. Moreover, the low teragonality (T = 0.87-0.88) of Pr-Lu compounds imply static distortion giving rise to well resolved EPR at 77K.

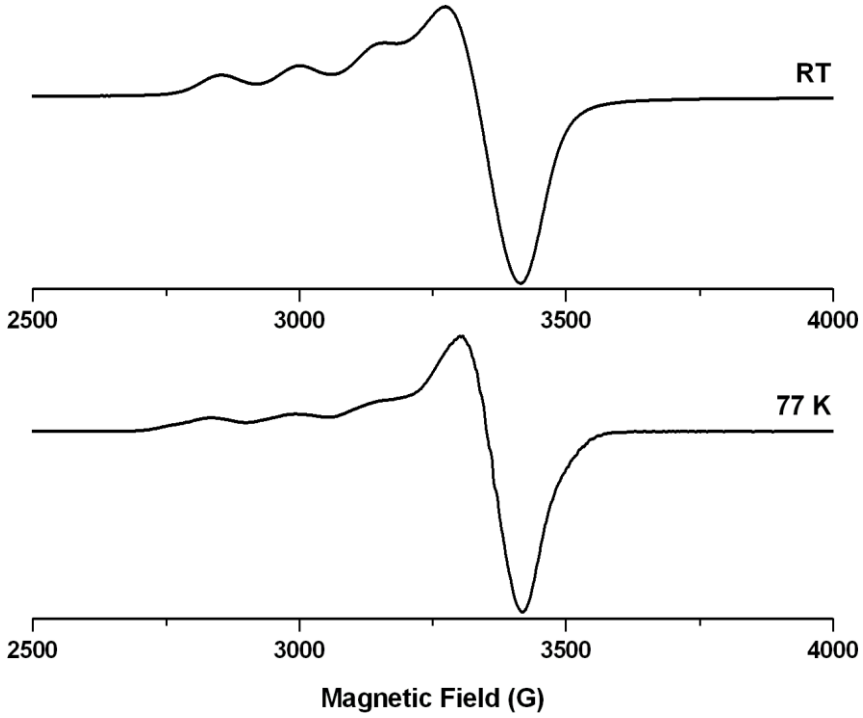

Figure 4.20. Comparison of EPR spectra collected at two different temperatures for compound **11** (Cu-Pr)

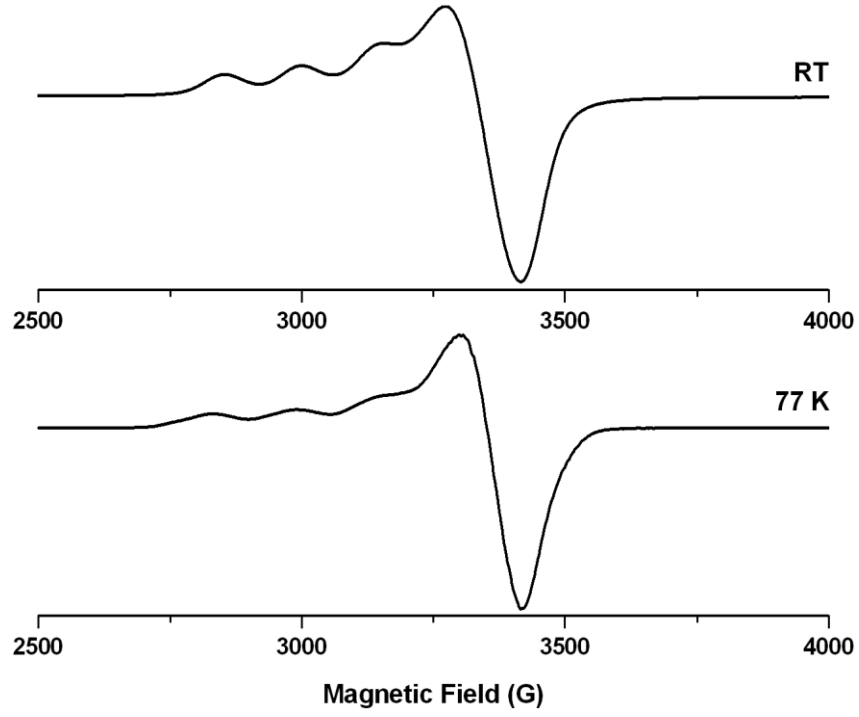

Figure 4.21. Comparison of EPR spectra collected at two different temperatures for compound **12** (Cu-Nd)

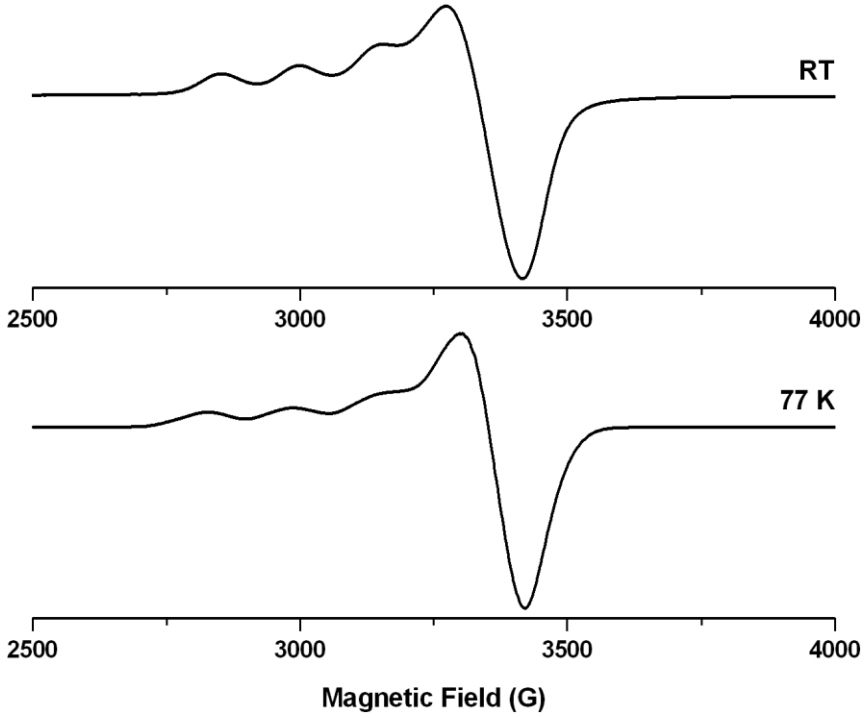

Figure 4.22. Comparison of EPR spectra collected at two different temperatures for compound **13** (Cu-Sm)

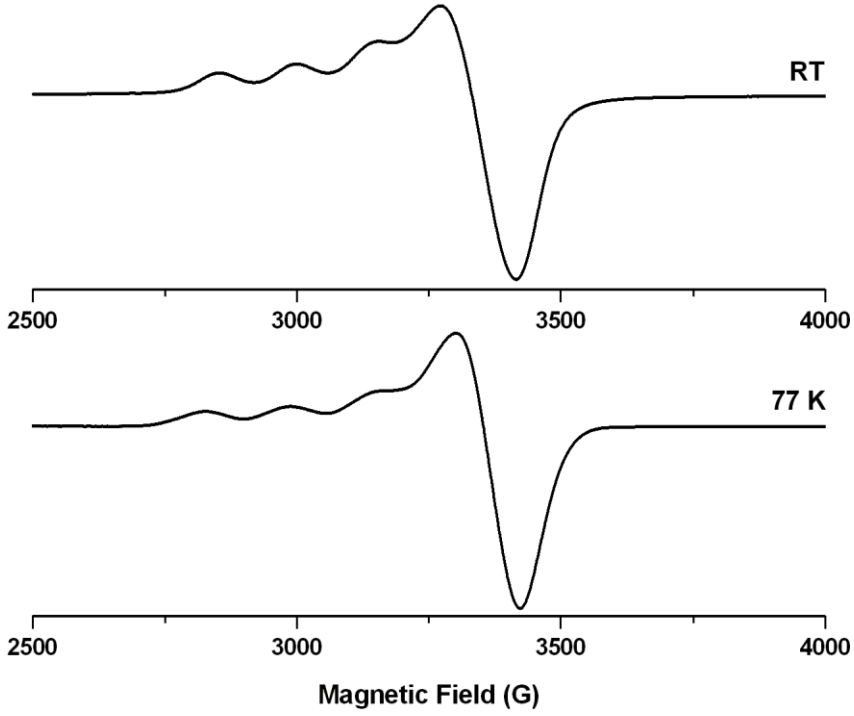

Figure 4.23. Comparison of EPR spectra collected at two different temperatures for compound **14** (Cu-Eu)

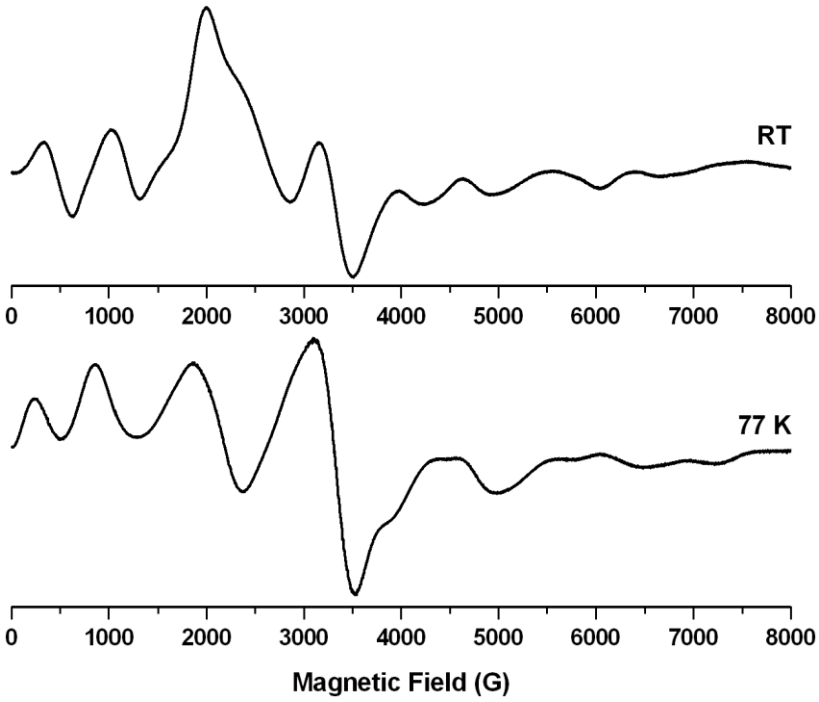

Figure 4.24. Comparison of EPR spectra collected at two different temperatures for compound **15** (Cu-Gd)

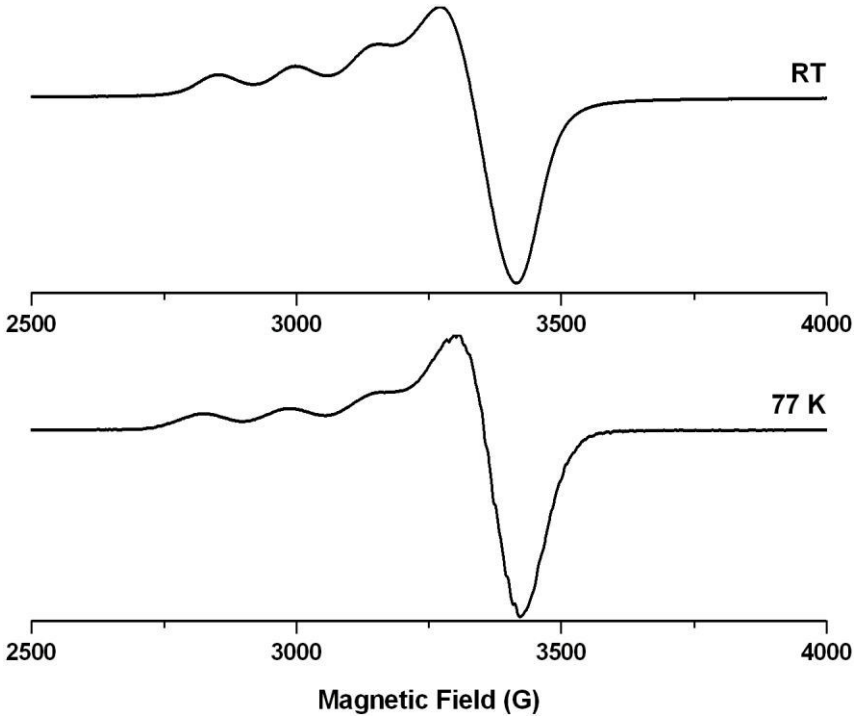

Figure 4.25. Comparison of EPR spectra collected at two different temperatures for compound **16** (Cu-Tb)

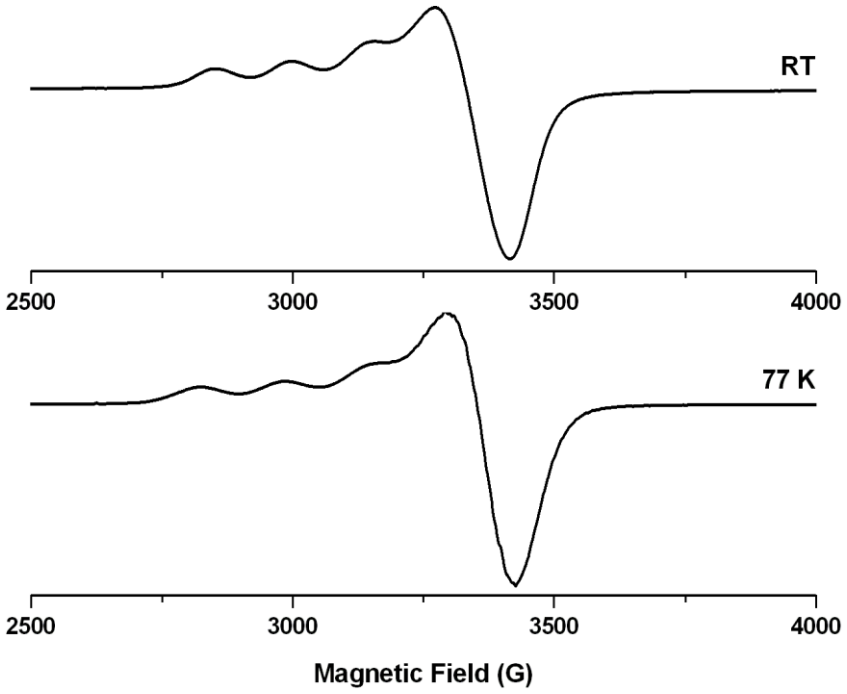

Figure 4.26. Comparison of EPR spectra collected at two different temperatures for compound **17** (Cu-Dy)

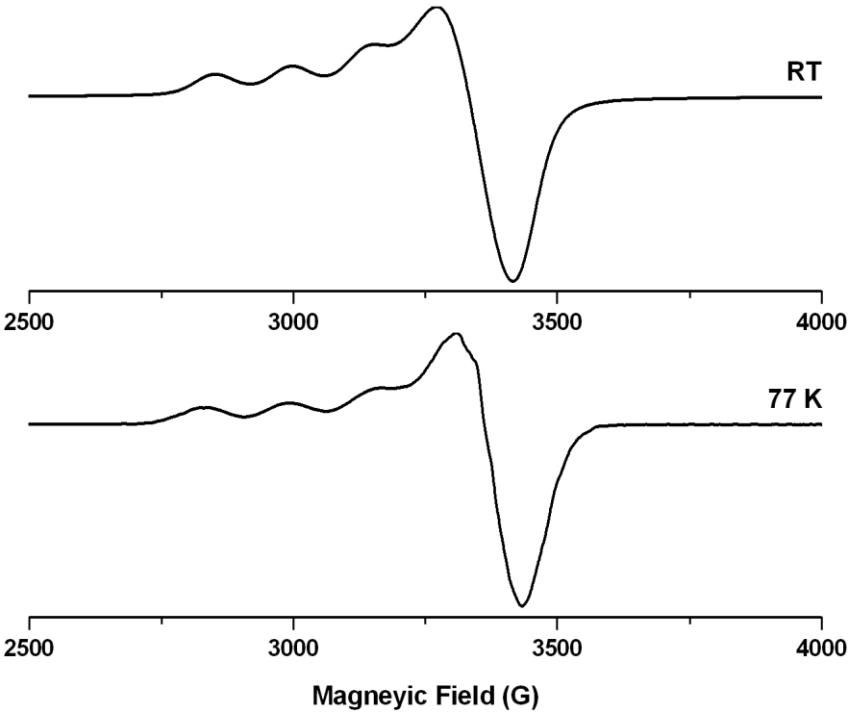

Figure 4.27. Comparison of EPR spectra collected at two different temperatures for compound **18** (Cu-Ho)

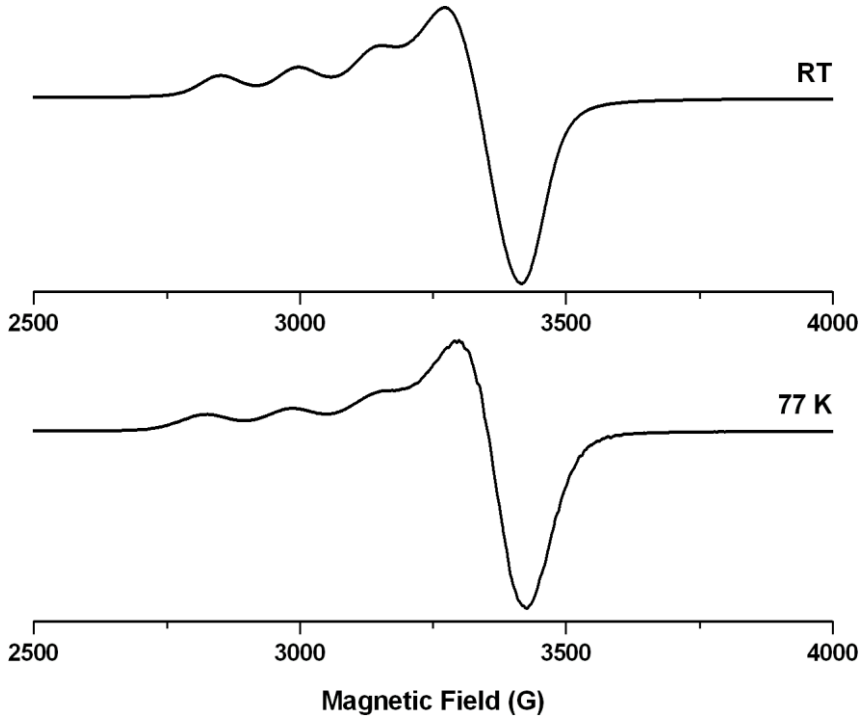

Figure 4.28. Comparison of EPR spectra collected at two different temperatures for compound **19** (Cu-Er)

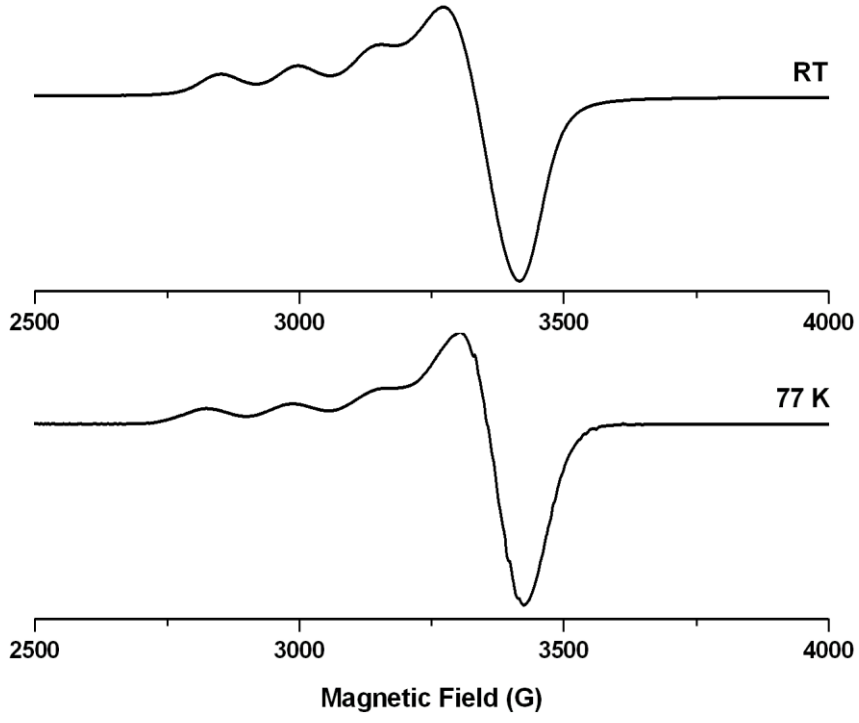

Figure 4.29. Comparison of EPR spectra collected at two different temperatures for compound **20** (Cu-Tm)

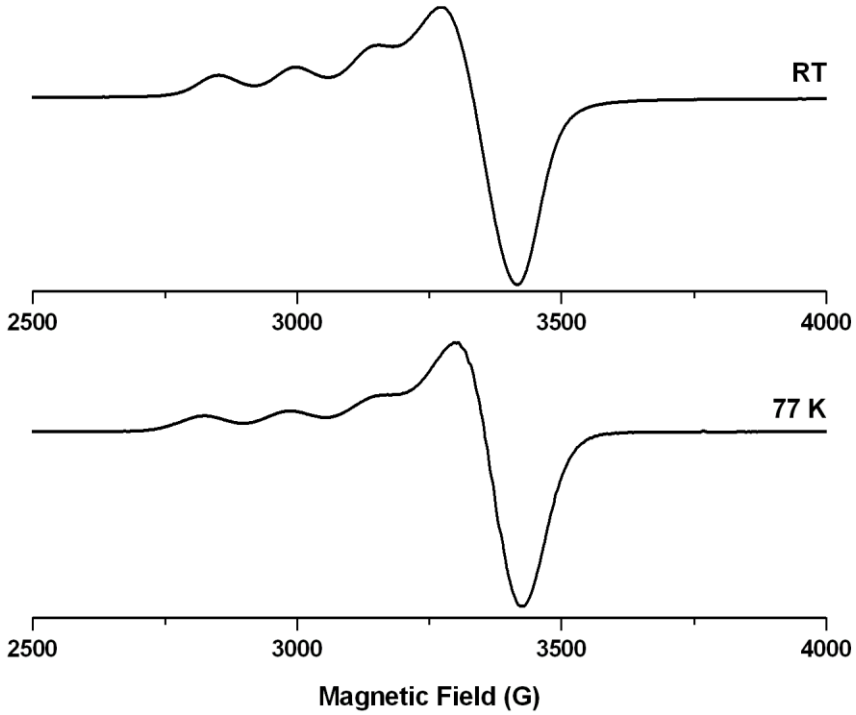

Figure 4.30. Comparison of EPR spectra collected at two different temperatures for compound **21** (Cu-Yb)

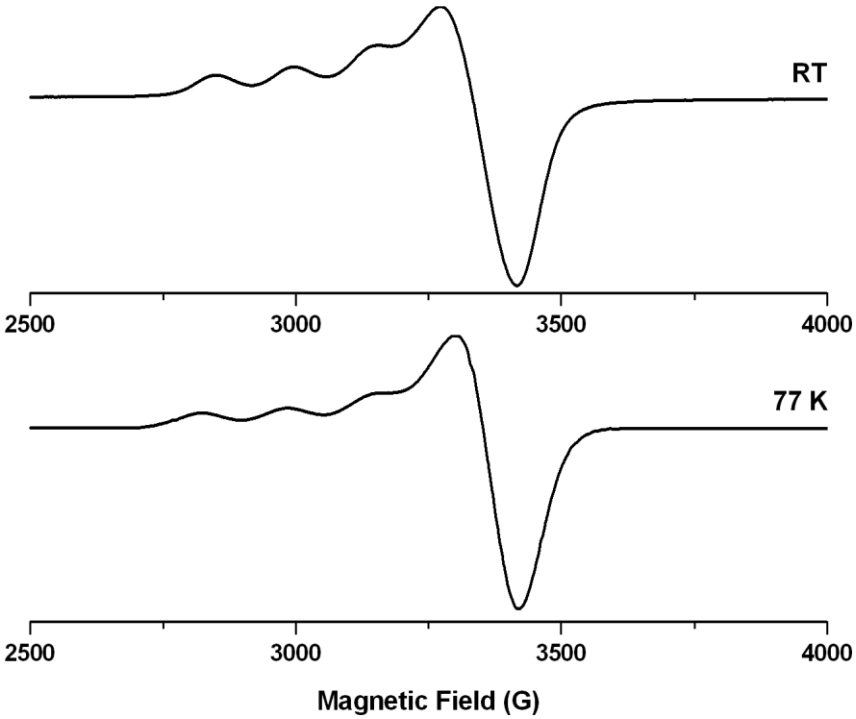

Figure 4.31. Comparison of EPR spectra collected at two different temperatures for compound **22** (Cu-Lu)

Table 4.14. EPR parameters for 9-22

	300 K				77 K			
Comp.	$g_{\|}$	$g_{\perp}$	$A_{\|}$ (G)	$A_{\perp}$ (G)	$g_{\|}$	$g_{\perp}$	$A_{\|}$ (G)	$A_{\perp}$ (G)
9	2.321	2.103	130	64	2.261	2.068	150	40
10	2.329	2.097	147	62	2.255	2.071	146	38
11	2.261	2.071	140	47	2.256	2.059	155	40
12	2.259	2.071	140	46	2.257	2.059	157	40
13	2.258	2.071	140	47	2.261	2.059	159	40
14	2.258	2.071	140	46	2.259	2.059	158	40
16	2.261	2.071	140	47	2.259	2.059	157	40
17	2.261	2.071	140	47	2.264	2.058	160	43
18	2.261	2.071	140	49	2.259	2.053	161	41
19	2.261	2.071	142	47	2.264	2.059	160	42
20	2.261	2.071	140	48	2.261	2.058	162	40
21	2.261	2.071	140	48	2.261	2.058	159	41
22	2.261	2.071	141	47	2.261	2.059	160	40

4.8. Conclusions

(1) 5,5'-Dmbpy analogs of compounds of Chapter 2 are available for early and middle lanthanide ions. The heavier ones give previously reported complex $[Cu(dmbpy)_2(NO_3)](NO_3)$.[1] All have 11-coordinate $Ln(NO_3)_5(OH_2)^{2-}$ anion and two $Cu(dmbpy)_2(NO_3)^+$ ions. All crystals contain one acetonitrile (solvent) molecule in the lattice. The bulkier ligand is therefore, less discriminatory with regards to *Ln* coordination number and number of aquo ligands. The EPR spectra show broad isotropic lines consistent with exchange averaging between the two Cu(II) complex ions.

(2) With regard to analogs of Chapter 3 crystals, the full series (except Pm) is available. The products from the first two early lanthanides contain $Ln(NO_3)_5(OH_2)^{2-}$, crystalling with two

solvent (acetonitrile) molecules, while all others contain $Ln(NO_3)_5^{2-}$. La and Ce compounds have higher tetragonality (T = 0.91-0.92) compared to the other compounds (T = 0.87-0.88). Consequently the former two compounds have greater temperature dependence in their EPR spectra compared to the others which give well resolved hyperfine patterns at RT as well as 77K.

4.9. References

1. G. A. van Albada, A. Mohamadou, I. Mutikainen, U. Turpeinen, J. Reedijk, *Eur. J. Inorg. Chem.* **2004**, 3733.
2. D. F. Perkins, L. F. Lindoy, A. McAuley, G. V. Meehan, P. Turner, *Proc. Nat. Acad. Sci. USA*, **2006**, *103*, 532.
3. *CrysAlisPro* version 1.171.33, Oxford Diffraction Ltd., Abingdon, Oxfordshire, UK, **2007**.
4. SAINTPLUS, Bruker AXS Inc., Madison, Wisconsin, USA **2003**.
5. G. M. Sheldrick, SADABS, Program for empirical absorption correction (University of Gottingen, Gottingen, Germany) **1996**.
6. G. M. Sheldrick, *Acta Crystallogr.*, **2008**, *A64*, 112.
7. C. F. Macrae, I. J. Bruno, J. A. Chisholm, P. R. Edgington, P. McCabe, E. Pidcock, L. Rodriguez-Monge, R. Taylor, J. van de Streek, P. A. Wood, *J. Appl. Cryst.*, **2008**, *41*, 466.
8. (a) M. B. Ferrari, G. G. Fava, C. Pelizzi, *J. Chem. Soc., Chem. Commun.*, **1977**, 8; (b) W. D. Harrison, B. J. Hathaway, *Acta Crystallogr., Sect.*, **1978**, *B34*, 2843; (c) P. Y. Zavalij, B. L. Burton, W. E. Jones Jr., *Acta Cryst.*, **2002**, *C58*, m330.
9. (a) S. Youngme, K. Poopasit, K. Chinnakali, S. Chantrapromma, H. –K. Fun, *Inorg. Chim. Acta*, **1999**, *292*, 57; (b) J. Foley, D. Kennefick, D. Phelan, S. Tyagi, B. J. Hathaway, *J. Chem. Soc., Dalton Trans.*, **1983**, 2333.

10. (a) W. Fitzgerald, B. J. Hathaway, C. J. Simmons, *J. Chem. Soc., Dalton Trans.*, **1985**, 141; (b) C. Escobar, O. Wittke, *Acta Crystallogr., Sect.*, **1983**, *C39*, 1643; (c) A. Wojciechowska, J. Jezierska, A. Bienko, M. Daszkiewicz, *Polyhedron*, **2011**, 30, 1547.

11. (a) K. Marjani, S. C. Davies, M. C. Durrant, D. L. Hughes, N. Khodamorada, A. Samodia, *Acta Cryst.*, **2005**, *E61*, m11; (b) S. Youngme, P. Phuengphai, S. Booncoon, N. Chaichit, *Polyhedron*, **2004**, *23*, 1685.

12. (a) C. -B. Ma, M. -Q. Hu, H. Chen, C. -N. Chen, Q. -T. Liu, *Eur. J. Inorg. Chem.*, **2011**, 5043; (b) G. Novitskii, A. Borta, D. Ganzhu, S. Shova, I. G. Filippova, Yu. A. Simonov, *Koord. Khim.(Russ.)*, **2009**, *35*, 386; (c) D. J. Evans, P. C. Junk, M. K. Smith, *New J. Chem.*, **2002**, *26*, 1043; (d) G. -L. Xue, Y. -X. Yang, H. -X. Li, S. -Y. He, J. Li, *Chin. J. Inorg. Chem.*, **2001**, *3*, 423; (e) G. Y. S. Chan, M. G. B. Drew, M. J. Hudson, N. S. Isaacs, P. Byers, *Polyhedron*, **1996**, *15*, 3385.

13. (a) B. Keshavan, Ramalingaiah, *Asian J. Chem.*, **1997**, *9*, 283; (b) K. Nakamoto, *Infrared Spectra of Inorganic and Coordination Compounds*, 4th Ed. (J. Wiley and Sons, New York), **1986**, 256.

14. (a) S. Youngme, K. Poopasit, K. Chinnakali, S. Chantrapromma, H.-K. Fun, *Inorg. Chim. Acta*, **1999**, *292*, 57; (b) B. Hathaway, *Struct. Bonding* , **1984**, *57*, 55.

15. A. Murphy, B. J. Hathaway, *J. Chem. Soc.,Dalton Trans.*, **1979**, 1646.

16. (a) B. Murphy, M. Aljabri, A. Mohamed Ahmed, G. Murphy, B. J. Hathaway, M. E. Light, T. Geilbrich, M. Hursthouse, *Dalton Trans.*, **2006**, 357; (b) A. Ch. Chamayou, Ch. Biswas, Ch. Janiaka, A. Ghosh, *Acta Crystallogr.*, **2007**, *E63*, m1936; (c) Md. Fayzauddin, N. C. Gangi Reddy, G. Siva Reddy, S. Lakshmi Reddy, P. Sambasiva Rao, R. L. Frost, *Spectrochim. Acta A*, **2007**, *68*, 807.

17. (a) B. Murphy, M. Aljabri, A. Mohamed Ahmed, G. Murphy, B. J. Hathaway, M. E. Light, T. Geilbrich, M. Hursthouse, *J. Chem. Soc., Dalton Trans*., **2006**, 357; (b) A. –C. Chamayou, C. Biswas, C. Janiaka, A. Ghosh, *Acta Cryst.,* **2007**, *E63*, m1936; (c) V. V. Pavlishchuk, A. V. Kalaida, E. A. Goreshnik, *Koord. Khim.*, **1999**, *25*, 542; (d) P. Majumdar, A. K. Ghosh, L. R. Falvello, S. -M. Peng, S. Goswami, *Inorg. Chem.*, **1998**, *37*, 1651; (e) Z. -M. Liu, Z. -H. Jiang, D. -Z. Liao, G. -L.Wang, *Polyhedron*, **1991**, *10*, 101; (f) J. M. Seco, M. J. Garmendia, M. Quitros, *J. Coord. Chem.*, **2002**, *55*, 345; (g) A. Wojciechowska, A. Pietraszko, W. Bronowska, Z. Staszak, J. Jezierska, M. C. Golonka, *Polyhedron*, **2010**, *29*, 2574; (h) A. Wojciechowska, J. Jezierska, A. Bienko, M. Daszkiewicz, *Polyhedron*, **2011**, *30*, 1547.

18. (a) D. M. Whittaker, T. L. Griffiths, M. Helliwell, A. N. Swinburne, L. S. Natrajan, F. W. Lewis, L. M. Harwood, S. A. Parry, C. A. Sharrad, *Inorg. Chem.*, **2013**, *52*, 3429; (b) M. W. Chorab, A. Gorczynski, M. Kubicki, Z. Hnatejko, V. Patroniak, *Polyhedron*, **2012**, *31,* 51; (c) E. B. Dhoot, J. Fawcett, R. A. Kresinski, A. W. G. Platt, *Polyhedron*, **2009**, *28,* 1497; (d) A. N. Georgopoulou, R. Adam, C. P. Raptopoulou, V. Psycharis, R. Ballesteros, B. Abarca, A. K. Boudalis, *Dalton Trans*., **2011**, *40*, 8199; (e) T. Otsuka, H. Cui, A. Kobayashi, Y. Misaki, H. Kobayashiz, *J. Solid State Chem.*, **2002**, *168*, 444; (f) C. G. Efthymiou, A. N. Georgopoulou, C. Papatriantafyllopoulou, A. Terzis, C. P. Raptopoulou, A. Escuer, S. P. Perlepes, *Dalton Trans*., **2010**, *39*, 8603; (g) H. Cui, T. Otsuka, A. Kobayashi, N. Takeda, M. Ishikawa, Y. Misaki, H. Kobayashi, *Inorg. Chem.*, **2003**, *42*, 6114; (h) W. Urland, E. Warkentin, *Z. Naturforsch*. **1983**, *88b*, 299.

CHAPTER V

Synthesis, structural and spectral characterization of Cu(II) isonicotinate adducts using 2,2'-bipyridine and 1,10-phenanthroline

5.1. Introduction

Pyridinecarboxylates can work as a good bridging ligands with oxygen and nitrogen donors, and also can be a good hydrogen bond donors and/or acceptors in assembly of supramolecular frameworks. Different coordination modes of the pyridinecarboxylates lead to formation of mononuclear,[1] polynuclear[2] and extended polymeric 1D, 2D and 3D structures.[3] While isonicotinic acid forms numerous complexes with Cu(II), the zwitter ion form was seen in only in five cases.[4]

As a part of a research on complexes bridged by water molecules with a view to the investigation of magnetic exchange interactions between adjacent magnetic nuclei, complexes with the core $[Cu(OH_2)_2Cu]^{+4}$ containing 2,2'-bipyridine (bpy) or 1,10-phenanthroline (phen) in presence of isonicotic acid (IN) have been synthesized. Although the aqua ligand usually exhibits the terminal coordination mode in Cu(II) complexes, but complexes with aqua bridges (single or double) are also reported in the literature.[5-7]

Only a few dinuclear Cu(II) complexes having the $[Cu_2(\mu\text{-}OH_2)_2]^{4+}$ core have been reported so far, which fall into two types based on core geometry: axial-equatorial[6] and equatorial-equatorial.[7] However, magnetic data are available only for two compounds.[6a,7a] One may also include among them two coordination chains[8] and one 2D-network[9] in which the dinuclear moieties are magnetically isolated. The magnetic coupling in both types of complexes

is generally weak with 2*J* value in the range –7 to 13.1 cm^{-1}. The coupling is enhanced when the diaquo bridges are complemented by other coordination bridges.[10]

Isonicotinic acids have been widely investigated to form coordination polymers, because these ligands have potential coordination sites involving both the nitrogen atom of pyridine and the carboxylate oxygen atoms to form extended networks, moreover the carboxylate groups also help to balance the metal charges. Many Cu(II) isonicotinate coordination polymers have been reported.[11] Several Cu(II)-isonicotinate coordination polymers with bipyridine type co-ligands such as 2,2'-bipyridine, 1,10-phenanthroline, 1,1'-(1,4-butanediyl)bis(imidazole), *trans*-1,2-bis(4-pyridyl)ethylene have been reported.[12-14] As a continuation of research, we prepare two copper coordination polymeric 1D chains containing isonicotinate and bpy. The 1D zig-zag chains are nearly same as that found in $\{[Cu(bpy)(IN)(OH_2)](NO_3)\cdot 2H_2O\}n$.[13]

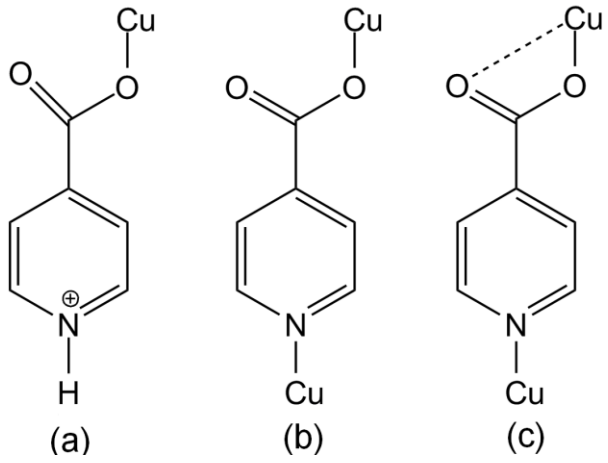

Scheme 5.1. Bonding modes of isonicotinate in the four Cu(II) complexes (a) in **1** and **2** (b) in **3** (c) in **4**

5.2. Experimental

5.2.1. Reagents

All chemicals were of reagent grade obtained from commercial sources and were used without further purification. Although no problem was aroused in our experiments, transition metal perchlorate salts are potentially explosive, only small quantity should be prepared.

5.2.2. Synthesis

Preparation of {[$Cu_2(\mu\text{-}OH_2)_2(bpy)_2(INH)_2(NO_3)_2](NO_3)_2$} (1)

To a warmed methanolic solution (30 mL) of 2,2′-bipyridine (0.156 g, 1.000 mmol) and isonicotic acid (0.123 g, 1.000 mmol), a warmed aqueous solution (10 mL) of $Cu(NO_3)_2{\cdot}3H_2O$ (0.241 g, 1.000 mmol) was added slowly with constant stirring at 75º C for 20 minutes. It was formed a dark blue color solution, kept at room temperature for crystallization. On standing for a week, blue crystals of **1** were obtained. They were filtered off, washed with methanol and air dried. From the filtrate, dark blue crystals of reported polymeric compound $\{[Cu(bpy)(IN)(OH_2)](NO_3){\cdot}2H_2O\}_n$[13] were obtained after 2 days along with small quantity of **1** confirmed by the unit cell determination. Yield of **1** is 0.480 g, (0.495 mmol, 50%). *Anal.* Calc. for $C_{32}H_{30}N_{10}O_{18}Cu_2$ (M.W. 969.76 g): C, 39.64; H, 3.12; N, 14.44%. Found: C, 39.65; H, 2.86; N, 14.35%. Important IR absorptions (KBr disc, cm^{-1}): 3396 ν(O−H), 3105 ν(C−H), 1601 ν_{as}(OCO), 1380 ν_s(OCO), 1439 $\nu_{as}(NO_3)$, 1315 $\nu_s(NO_3)$ and 1008 ν_s(N=O).

Preparation of {[$Cu_2(\mu\text{-}OH_2)_2(phen)_2(INH)_2(NO_3)_2](NO_3)_2$} (2)

Complex **2** was obtained as blue crystals by the same procedure adopted for complex **1** using 1,10-phenanthroline (0.198 g, 1.000 mmol) instead of 2,2′-bipyridine. From the filtrate, after separation of **2**, dark blue crystals of reported polymeric compound

{[Cu(phen)(IN)(OH_2)](NO_3)·H_2O}n[14] were obtained after 2 days along with small quantity of **2** confirmed by the unit cell determination. Yield of **2** is 0.488 g, (0.478 mmol, 48%). *Anal.* Calc. for $C_{36}H_{30}N_{10}O_{18}Cu_2$ (M.W. 1017.80 g): C, 42.48; H, 2.97; N, 13.76%. Found: C, 42.65; H, 2.71; N, 13.91%. Important IR absorptions (KBr disc, cm^{-1}): 3376 ν(O−H), 3099 ν(C−H), 1589 ν_{as}(OCO), 1385 ν_s(OCO), 1424 $\nu_{as}(NO_3)$, 1319 $\nu_s(NO_3)$ and 1005 ν_s(N=O).

Preparation of {[Cu(bpy)(IN)(OH_2)](ClO_4)}*n* (3)

Complex **3** was obtained as dark blue crystals by the same procedure adopted for complex **1** using $Cu(ClO_4)_2·7H_2O$ (0.370 g, 1.000 mmol) instead of $Cu(NO_3)_2·3H_2O$. From the filtrate, after separation of **3**, blue crystals of reported compound {[$Cu(bpy)_2$(μ-ClO_4)](ClO_4)}n[15] were obtained after 2 days along with small quantity of **3** confirmed by the unit cell determination. Yield of **3** is 0.216 g, (0.470 mmol, 47%). *Anal.* Calc. for $C_{16}H_{14}N_3O_7Cl_1Cu_2$ (M.W. 459.30 g): C, 41.84; H, 3.07; N, 9.15%. Found: C, 41.65; H, 3.48; N, 9.32%. Important IR absorptions (KBr disc, cm^{-1}): 3463 ν(O−H), 3005 ν(C−H), 1605 ν_{as}(OCO), 1380 ν_s(OCO), 1112 ν(Cl−O), 949 ν(Cl=O).

Preparation of {[Cu(bpy)($IN)_2$]$_2$·5H_2O}*n* (4)

Complex **4** was synthesized by the same procedure adopted for complex **1** using $CuCO_3$·$Cu(OH)_2·H_2O$ (0.060 g, 0.250 mmol) instead of $Cu(NO_3)_2·3H_2O$ in pure methanol. Blue color fine powder was obtained after 3 days. It was filtered off, and the mother solution kept at room temperature for crystallization. On standing for a week, blue crystals of **4** were obtained. The side product which could not be obtained in good crystalline form was not identified. Yield of **4** is 0.273 g, (0.268 mmol, 54%). *Anal.* Calc. for $C_{44}H_{42}N_8O_{13}Cu_2$ (M.W. 1017.95 g): C, 51.92; H, 4.16; N, 11.01%. Found: C, 51.85; H, 4.23; N, 11.14%. Important IR absorptions (KBr disc, cm^{-1}): 3484 ν(O−H), 3106 ν(C−H), 1600 ν_{as}(OCO), 1380 ν_s(OCO).

5.3. Physical measurements

IR spectra were obtained as KBr pellets on a Jasco FT-IR 5300 spectrometer in the range 4000-400 cm^{-1}. Elemental analysis for C, H and N was performed on a Perkin-Elmer 240C elemental analyzer. Diffuse reflectance spectra were measured by using a Shimadzu UV-3100 spectrometer. ESR spectra were recorded on Bruker Xenon EMX-ER-073 spectrometer. Powder X-ray diffraction patterns were recorded on a Bruker D8-Advance diffractometer using graphite monochromated $CuK_{\alpha 1}$ (1.5406 Å) and $K_{\alpha 2}$ (1.54439 Å) radiations. Simulation of the P-XRD patterns was carried out using the Mercury program. Magnetic susceptibilities were measured in the temperature range of 3−300 K on a Quantum Design PPMS-VSM. The samples were pressed into pellets to avoid orientation effects of the microcrystals during magnetic measurements. Diamagnetic corrections were made with Pascal's constants.[16] Fitting of the susceptibility data was done by using the program SUSCEP.[17]

5.4. X-ray crystallography

The unit cell parameters and intensity data at 100 K for **2** and 298 K for **1, 3** and **4** were obtained on a Bruker-Nonius SMART APEX CCD 1000 area detector, using graphite-monochromated Mo-Kα radiation (λ = 0.71073 Å). Data were reduced using SAINTPLUS[18] and a multiscan absorption correction using SADABS[19] was performed. The structure of complexes were solved by direct methods and refined on F^2 by full-matrix least-squares procedures. The non-hydrogen atoms were refined using anisotropic thermal parameters. The hydrogen atoms were included in the structure factor calculations at idealized positions using a riding model, and the hydrogen atoms attached to oxygen atoms were located from the difference maps. The structures were solved using SHELXS-97 and refined using SHELXL-97.[20] Drawings were made using Mercury.[21] Crystallographic data and structure refinement are given in Table 5.1. Selected

bond lengths and bond angles are listed in Table 5.2, Table 5.3, Table 5.6 and Table 5.7. Details of the hydrogen bonding and π–stacking interactions are given in Table 5.4, Table 5.5, Table 5.8 and Table 5.9.

Table 5.1: Crystallographic data and structure refinement parameters for complexes **1−4.**

	1	**2**	**3**	**4**
Formula	$C_{32}H_{30}N_{10}O_{18}Cu_2$	$C_{36}H_{30}N_{10}O_{18}Cu_2$	$C_{16}H_{14}N_3O_7ClCu$	$C_{44}H_{42}N_8O_{13}Cu_2$
Formula weight	969.76	1017.78	459.29	1017.94
Crystal system	Triclinic	Monoclinic	Monoclinic	Monoclinic
Space group	$P\bar{1}$	$P2_1/c$	Cc	$C2/c$
a (Å)	10.065(13)	10.280(6)	10.670(11	14.299(19)
b (Å)	10.465(14)	9.185(5)	14.461(14)	12.325(17)
c (Å)	10.470(14)	20.313(12)	12.405(12)	24.103(3)
α (˚)	98.673(2)	90	90	90
β (˚)	96.441(2)	96.695(10)	111.075(2)	93.496(2)
γ (˚)	118.281(2)	90	90	90
V (Å^3)	938.40(2)	1904.92(19)	1786.10(3)	4240.00(10)
Z	1	2	4	4
T (K)	298(2)	100(2)	298(2)	298(2)
λ (Å)	0.71073	0.71073	0.71073	0.71073
D_{cal} (g cm^{-3})	1.716	1.774	1.708	1.595
μ (mm^{-1})	1.228	1.215	1.419	1.082
F (000)	494	1036	932	2096
Crystal size (mm)	0.28 x 0.20 x 0.16	0.28 x 0.16 x 0.12	0.24 x 0.20 x 0.12	0.60 x 0.40 x 0.24
θ Range (˚)	2.01 to 25.00	1.99 to 24.99	2.48 to 24.98	1.69 to 25.00
h/k/l indices	-11,11/ -12,12/ -12,12	-12,12/ -10,10/ -24,24	-12,12/, -17,17/ -14,14	-16,16/, -14,14/ -28,28
Reflec. collected	9066	17674	8457	19760
Unique reflec. [R_{int}]	3299 [0.0264]	3349 [0.0402]	3150 [0.0349]	3732 [0.0490]
GooF	1.052	1.037	1.073	1.151
R_1 [I>2σ(I)]	0.0387	0.0304	0.0427	0.0444
wR_2	0.0996	0.0778	0.1014	0.1049

5.5. Crystal structures

5.5.1. Crystal structure of $[Cu_2(\mu\text{-}OH_2)_2(L)_2(INH)_2(NO_3)_2](NO_3)_2$ (L = bpy(1), phen(2))

The molecular structure of **1** and **2** consist of a dinuclear $[Cu_2(\mu\text{-}OH_2)_2(L)_2(INH)_2(NO_3)_2]^{2+}$ cation (Figure 5.1) and two uncoordinated nitrate anions in the lattice. The cations possess a crystallographic inversion centre. Selected bond lengths and angles are given in Table 5.2 and Table 5.3.

Each copper atom is six-coordinated with an elongated octahedral geometry. Two nitrogen atoms (N1, N2) of the chelated ligand (bpy/phen), one oxygen atom (O6) of a bridging water molecule and one oxygen atom (O4) of INH form the equatorial plane. The oxygen atom (O1) of the coordinated nitrate anion and the symmetry partner of O6 occupy the axial positions. The water molecules form two unsymmetrical bridges (2.03 Å, 2.72 Å, 103º for **1** and 2.00 Å, 2.68 Å, 99.7º for **2**) in the axial-equatorial mode. The bite angles of bpy is 81.42(12)º and 82.51(11)º for phen. The Cu···Cu distances of 3.768(1) Å in **1** and 3.605(1) Å in **2**. The copper atoms in both compounds are displaced by 0.20 Å from the mean plane formed by the four equatorial atoms.

The crystal packing analyses indicate that both intermolecular hydrogen-bonding and π-stacking interactions combine to stabilize the extended structure. The crystal packing of **1,** the lattice nitrate anions interconnect bridged water with O6–H6A···O7 (2.011(3) Å) interactions, zwitterion with N4–H4A···O8 (1.910(5) Å) interactions and bipyridine ligand with various C–H···O interactions (C1–H1···O9, 2.354(2); C4–H4···O8, 2.343(3); C8–H8···O5, 2.285(2) Å) give 2D hydrogen bonded chains. These 2D chains further extended into 3D by π-stacking interactions (3.312-3.370 Å) shown in Figure 5.2(a).

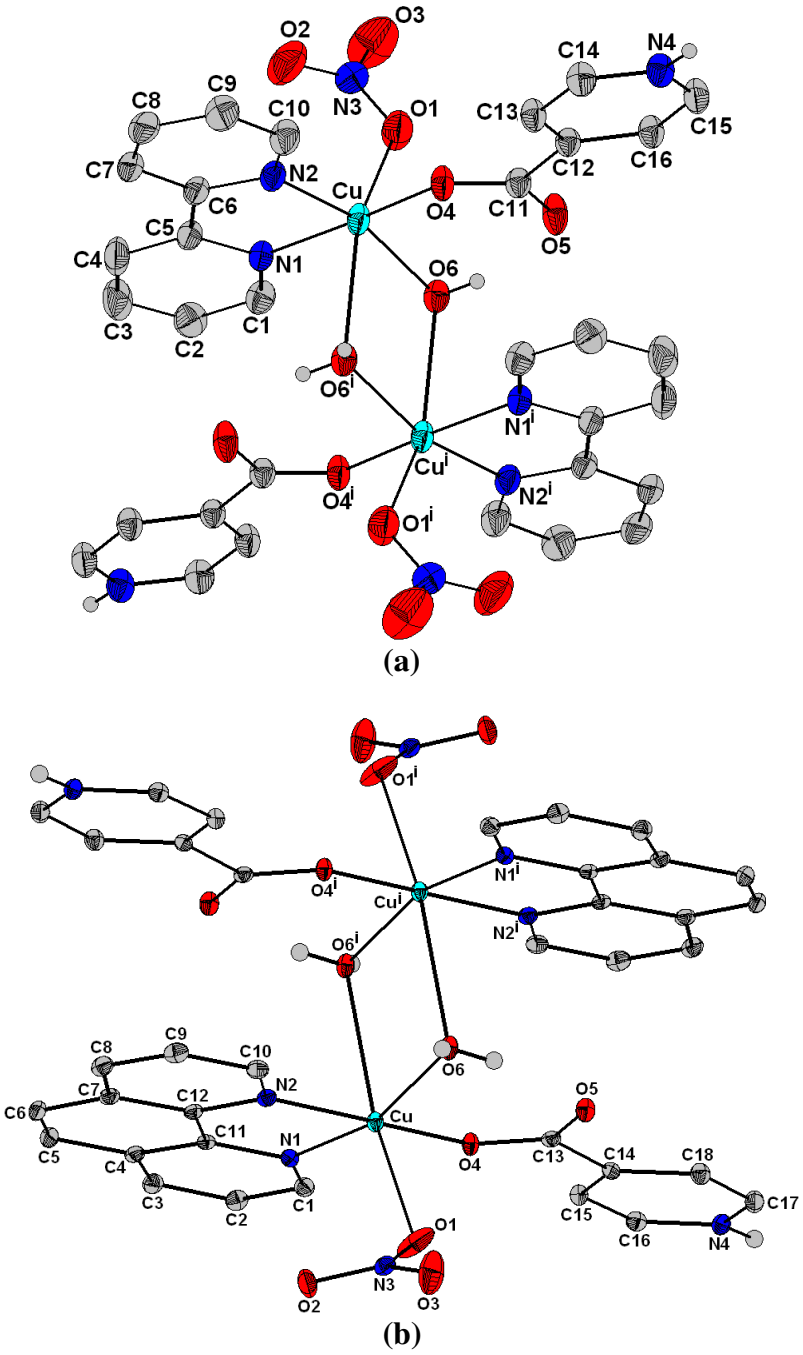

Figure 5.1. Thermal ellipsoid plots drawn at 30% probability level showing atom labeling (a) complex cation **1;** (b) complex cation **2**. Ring hydrogen atoms and uncoordinated nitrate anions have been omitted for clarity.

Table 5.2: Selected bond lengths (Å) and bond angles (˚) for **1**

Cu-N1	1.986(2)	Cu-N2	1.996(2)
Cu-O1	2.243(2)	Cu-O4	1.9630(18)
Cu-O6	2.033(2)	Cu-O6^{i}	2.723(2)
N1-Cu-N2	81.42(9)	N2-Cu-O1	113.82(9)
N1-Cu-O1	94.10(10)	N2-Cu-O4	90.08(9)
N1-Cu-O4	170.68(8)	N2-Cu-O6	161.68(9)
N1-Cu-O6	95.58(9)	N2-Cu-O6^{i}	85.63(9)
N1-Cu-O6^{i}	86.20(8)	O1-Cu-O4	92.82(9)
O4-Cu-O6	91.29(9)	O1-Cu-O6	84.36(9)
O4-Cu-O6^{i}	89.37(8)	O1-Cu-O6^{i}	160.40(8)
O6-Cu-O6^{i}	76.11(7)	Cu-O6-Cu^{i}	103.89(8)
Cu···Cu^{i}	3.768(6)	i = $-x+1, -y, -z+1$	

Table 5.3: Selected bond lengths (Å) and bond angles (˚) for **2**

Cu-N1	2.0022(18)	Cu-N2	2.0001(17)
Cu-O1	2.2263(18)	Cu-O4	1.9598(14)
Cu-O6	1.9998(17)	Cu-O6^{i}	2.680(2)
N1-Cu-N2	82.45(7)	N2-Cu-O1	98.17(7)
N1-Cu-O1	107.04(8)	N2-Cu-O4	172.10(7)
N1-Cu-O4	90.19(7)	N2-Cu-O6	93.94(7)
N1-Cu-O6	161.51(7)	N2-Cu-O6^{i}	84.57(6)
N1-Cu-O6^{i}	81.38(6)	O1-Cu-O4	86.70(6)
O4-Cu-O6	92.15(6)	O1-Cu-O6	91.41(8)
O4-Cu-O6^{i}	91.53(6)	O1-Cu-O6^{i}	171.37(6)
O6-Cu-O6^{i}	80.23(6)	Cu-O6-Cu^{i}	99.77(6)
Cu···Cu^{i}	3.606(4)	i = $-x+2, -y+1, -z$	

The crystal packing of **2,** the lattice nitrate anions interconnect bridged water with O6–H6B···O9 (1.952(2) Å) interactions, zwitterion with N4–H4A···O8 (1.930(2) Å) interactions form 2D hydrogen bonded chains and again interconnects isonicotinate and phenanthroline with

various C–H···O interactions (C18–H18···O9, 2.467(2); C16–H16···O2, 2.224(2); C2–H2···O1, 2.484(2); C6–H6···O3, 2.483(2); C9–H9···O2, 2.310(1) Å) give helical 3D network. Various π-stacking (3.387-3.498 Å) build more dense packing as shown in Figure 5.2(b). Details of the hydrogen bonding and π–stacking interactions are given in Table 5.4 and Table 5.5.

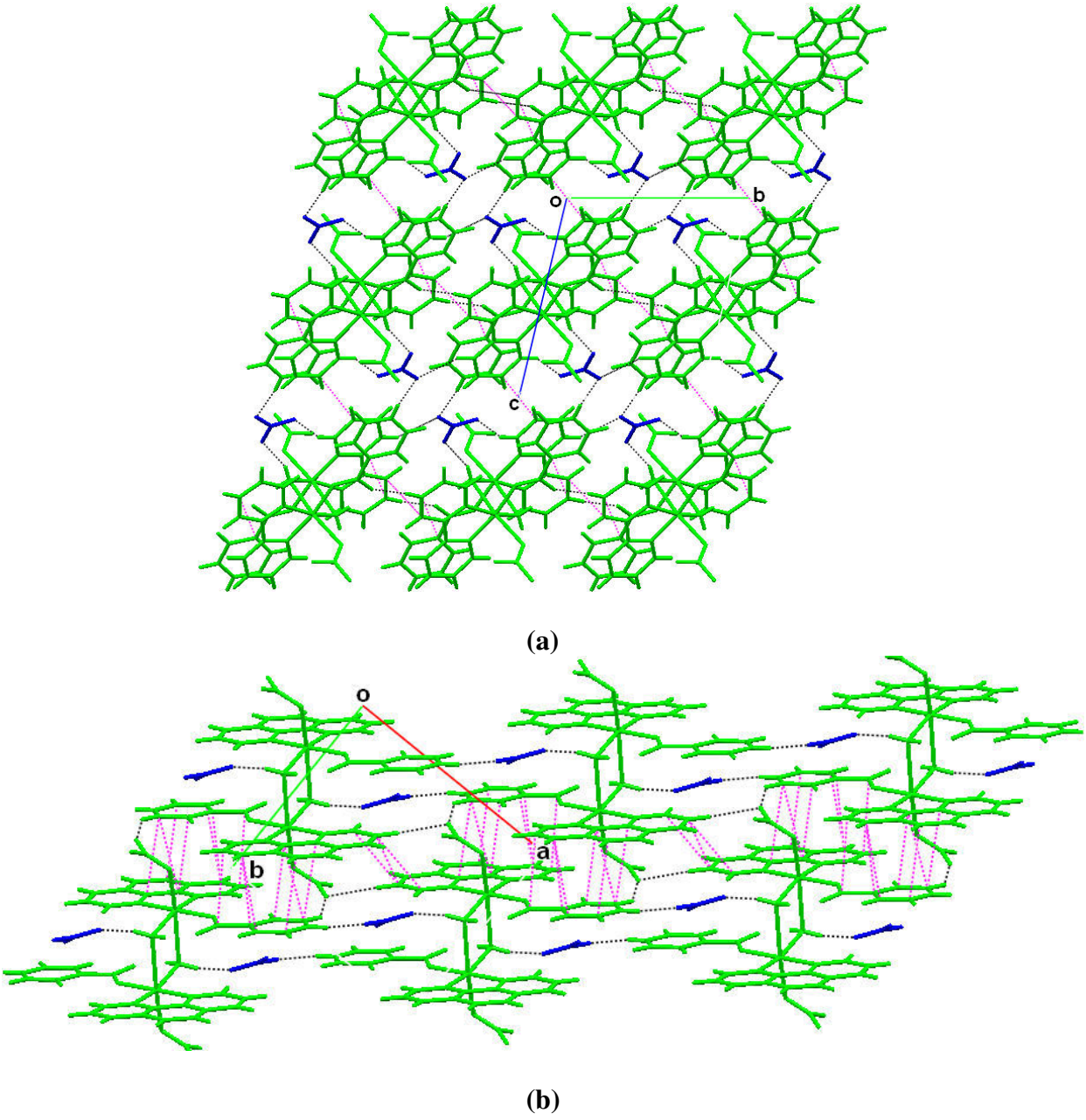

Figure 5.2. Molecular packing in the (a) *bc*-plane of **1**; (b) *ab*-plane of **2**

Table 5.4: Intermolecular interaction parameters

*H-bonding for **1***

D-H···A	**D-H(Å)**	**H···A(Å)**	**D···A(Å)**	**D-H···A(°)**
C4-H4···O8#1	0.93	2.34	3.14	144
C8-H8···O5#2	0.93	2.28	3.21	174
N4-H4A···O8#3	0.83	1.91	2.74	174
O6-H6A···O7#4	0.77	2.01	2.74	157
C1-H1···O9#4	0.93	2.35	3.17	146

(#1) $-x, -y, 1-z$; (#2) $1+x, 1+y, z$; (#3) $-x, 1-y, -z$; (#4) $1-x, 1-y, 1-z$

*H-bonding for **2***

C9-H9···O2#1	0.95	2.31	3.24	167
O6-H6B···O9#1	0.82	1.96	2.73	159
C2-H2···O1#2	0.95	2.48	3.07	120
C16-H16···O2#2	0.95	2.22	2.97	135
N4-H4A···O8#2	0.82	1.93	2.74	172
C6-H6···O3#3	0.95	2.48	3.20	132
C18-H18···O9#4	0.95	2.47	3.23	137

(#1) $1-x, 1-y, -z$; (#2) $-x, -y, -z$; (#3) $x, {}^{1}/_{2}-y, {}^{1}/_{2}+z$; (#4) $1+x, {}^{1}/_{2}-y, -{}^{1}/_{2}+z$

Table 5.5: π···π interaction (Å)

*π···π interaction for **1***

C2···C2#1	3.369(6)	C7···C7#2	3.311(5)
C8···C12#2	3.393(5)		

(#1) $1-x, -y, 2-z$; (#2) $-x,-y,1-z$

*π···π interaction for **2***

C2···C13#1	3.435(2)	C11···C15#1	3.435(3)
C3···C14#1	3.498(3)	C11···C16#1	3.457(3)
C3···C17#1	3.451(3)	C12···C16#1	3.493(3)
C5···C18#1	3.387(4)	C9···C9#2	3.451(3)
C9···C10#2	3.475(3)		

(#1) $2-x, -y, -z$; (#2) $1-x,1-y,-z$

5.5.2. Crystal structure of {[Cu(bpy)(IN)(OH_2)](ClO_4)}*n* (3)

The molecular structure of the compound **3** is shown in Figure 5.3(a). Selected bond distances and angles are given in Table 5.6. The coordination environment around each Cu(II) ion is five-coordinated distorted square pyramidal geometry. The equatorial plane is formed by the two nitrogen atoms (N1, N2) from the chelated bpy ligand and one nitrogen atom (N3), one oxygen atom (O3) from the two isonicotinates related by a screw axis [2.013(5), 2.003(5), 2.020(5) and 1.942(4) Å] respectively. The axial position is occupied by a coordinated water molecule [Cu-O3 = 2.294(4) Å]. The equatorial plane has a slight trigonal distortion from square pyramidal geometry with a τ value[22] (τ = [N3-Cu-N2]-[N1-Cu-O1]/60 of 0.22. The Cu atom lies out of the equatorial plane by 0.133 (2) Å. Isonicotinate is nearly perpendicular to the coordination equatorial plane with a dihedral angle of 71.6(4). Each isonicotinate anion bridges two neighboring Cu atoms through terminal oxygen atom of carboxylate and nitrogen atom of pyridine to form a zig-zag polymeric 1D chain (Figure 5.3(b)) along the crystallographic *b*-axis. The long bridging isonicotinate anion results in a long Cu···Cu distance of 8.845(9) Å. The 1D chain structure is nearly the same as that found in {[Cu(bpy)(IN)(OH_2)](NO_3)·2H_2O}*n*.[13] The main difference with compound **3** is in the intermolecular interactions. All the water molecules (coordinated and lattice) and both the nitrate and isonicotinate anions are involved hydrogen bonded 3D network, where as in our compound perchlorate anion is involved hydrogen bonding with the coordinated water molecule and with the bpy ligand to give a 2D network (Figure 5.3(c)). These are further interconnected with various π-stacking interactions [C(3)···C(8), 3.401(7) and C(15)···C(16), 3.439(8) Å] forming a 2D network. However, the voids are blocked by a two-fold parallel interpenetration of identical networks shown in Figure 5.3(d). Details of the hydrogen bonding and π–stacking interactions are given in Table 5.8 and Table 5.9.

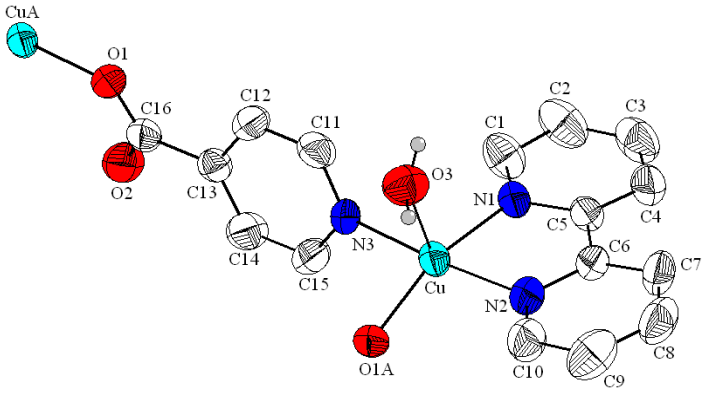

(a)

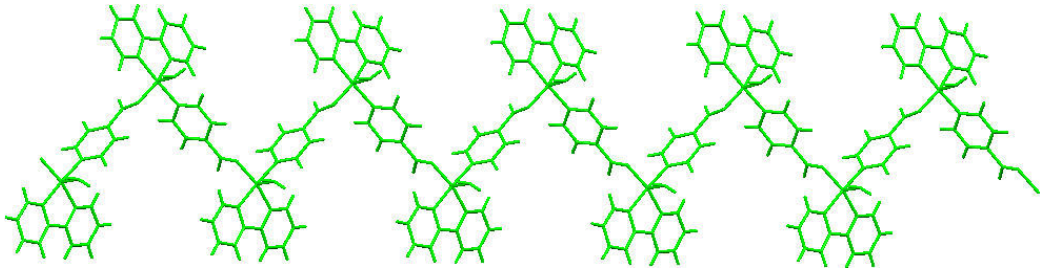

(b)

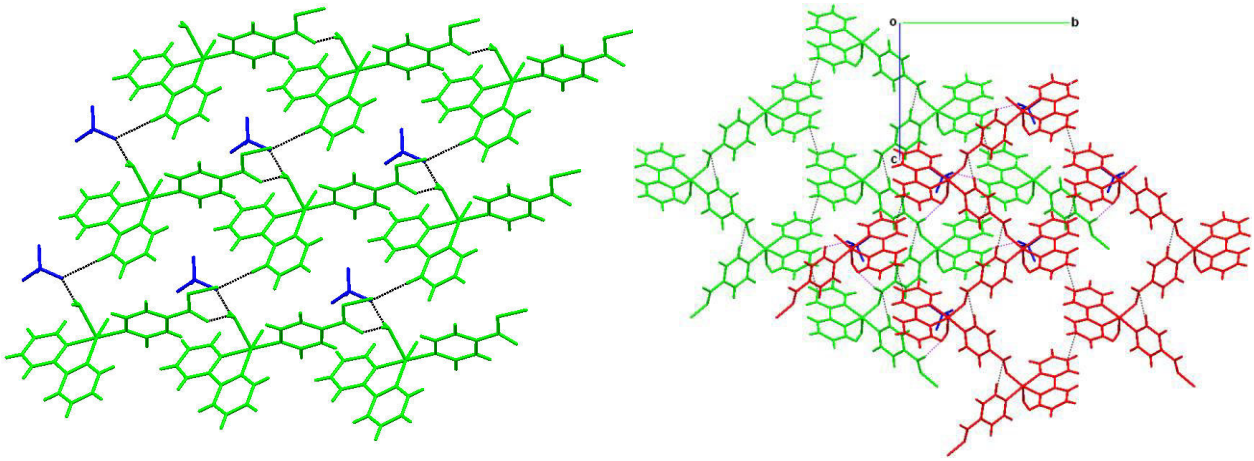

(c) **(d)**

Figure 5.3. (a) Thermal ellipsoid plot of the coordination environment of the complex **3**; (b) A view showing the zig-zag type of arrangement of 1D chains; (c) A view of the 2D structure formed by H-bonding; (d) Two-fold parallel interpenetrating H-bonded network.

Table 5.6: Selected bond lengths (Å) and bond angles (˚) for **3**

Cu-N1	2.013(4)	Cu-N2	2.003(4)
Cu-N3	2.019(4)	Cu-O3	2.294(4)
Cu-O1	1.942(4)		
N1-Cu-N2	81.22(15)	N2-Cu-N3	176.5(2)
N1-Cu-N3	95.56(18)	N2-Cu-O1	93.70(18)
N1-Cu-O1	162.82(15)	N2-Cu-O3	88.95(17)
N1-Cu-O3	104.18(17)	N3-Cu-O1	89.75(11)
O1-Cu-O3	92.06(17)	N3-Cu-O3	90.59(16)

5.5.3. Crystal structure of {[Cu(bpy)(IN)$_2$]$_2$·5H$_2$O}*n* (4)

The molecular structure of the compound **4** is shown in Figure 5.4(a). Selected bond distances and angles are given in Table 5.7. In this polymer, the bridging isonicotinate adopts a tridentate mode, that uses the nitrogen atom of the pyridine group and two oxygen atoms of the carboxylate group (Scheme 5.1(c)). This type of bonding mode has been observed previously.[23] The coordination environment around each Cu(II) ion is distorted square pyramidal, in which equatorial plane formed by the two nitrogen atoms (N1, N2) of the chelated bpy and one nitrogen atom (N4), one oxygen atom (O1) of the one isonicotinate [2.025(3), 1.997(2), 1.999(2) and 1.964(2) Å] respectively. The axial position is occupied by the nitrogen atom (N3) of another isonicotinate ligand [Cu-N3 = 2.274(3)]. A second oxygen atom (O2) of the bridged isonicotinate anion is at a semi-coordination distance [Cu-O2 = 2.749(2)]. The angles of the equatorial plane are 168.65(9)º and 168.38(10)º, the distortion parameter τ value is approximately zero. The Cu atom lies out of the equatorial plane by 0.180 (2) Å. The dihedral angle between the equatorial planes is 14º. The Cu···Cu distance for adjacent metals in the chains are 8.79(9) Å. Just like in the structure of **3**, here also the zig-zag type of arrangement of 1D chains (Figure 5(b)) is observed. The main difference with **3** is in the hydrogen bond network

which is formed by the lattice water molecules (Figure 5.4(c)). The zig-zag 1D chains are linked together through the lattice water molecules to give a 3D network (Figure 5.4(d)). Details of the hydrogen bonding and π–stacking interactions are given in Table 5.8 and Table 5.9.

Table 5.7: Selected bond lengths (Å) and bond angles (°) for **4**

Cu-N1	2.025(3)	Cu-N4	1.999(2)
Cu-N2	1.997(2)	Cu-O1	1.964(2)
Cu-N3	2.274(3)	Cu-O2	2.749(2)
N1-Cu-N2	80.47(10)	N2-Cu-N3	93.01(10)
N1-Cu-N3	94.59(10)	N2-Cu-N4	168.38(10)
N1-Cu-N4	94.12(10)	N2-Cu-O1	93.32(10)
N1-Cu-O1	168.65(9)	N2-Cu-O2	84.01(9)
N1-Cu-O2	117.00(9)	N3-Cu-N4	97.69(10)
O1-Cu-O2	52.48(8)	N3-Cu-O1	95.22(9)
N4-Cu-O1	90.21(9)	N3-Cu-O2	147.10(8)
N4-Cu-O2	89.40(8)		

Table 5.8: Intermolecular interaction parameters

*H-bonding for **3***

D-H···A	**D-H(Å)**	**H···A(Å)**	**D···A(Å)**	**D-H···A(°)**
O3-H3A···O2#1	0.93	2.01	2.76	166
O3-H3B···O4#2	0.93	2.25	3.00	163
C4-H4···O4#3	0.93	2.37	3.29	167

(#1) $^1/_2+x$, $^1/_2+y$, z; (#2) $^1/_2+x$, $^1/_2-y$, $½+z$; (#3) x, $1-y$, $½+z$

*H-bonding for **4***

O5-H5B···O2#1	0.93	2.02	2.81	165
O5-H5A···O4#2	0.93	2.03	2.83	165
O6-H6A···O4#3	0.93	2.31	2.98	156
O7-H7A···O3#4	0.93	1.95	2.75	174
O7-H7B···O6#5	0.93	2.07	2.85	163
C7-H7···O7#6	0.93	2.32	3.13	145

(#1) $^1/_2-x$, $^1/_2+y$, $^1/_2-z$ (#2) $1+x$, y, z (#3) $-x$, y, $^1/_2-z$ (#4) $1+x$, y, z (#5) $1-x$, y, $½-z$ (#6) $^1/_2-x$, $^1/_2-y$, $-z$

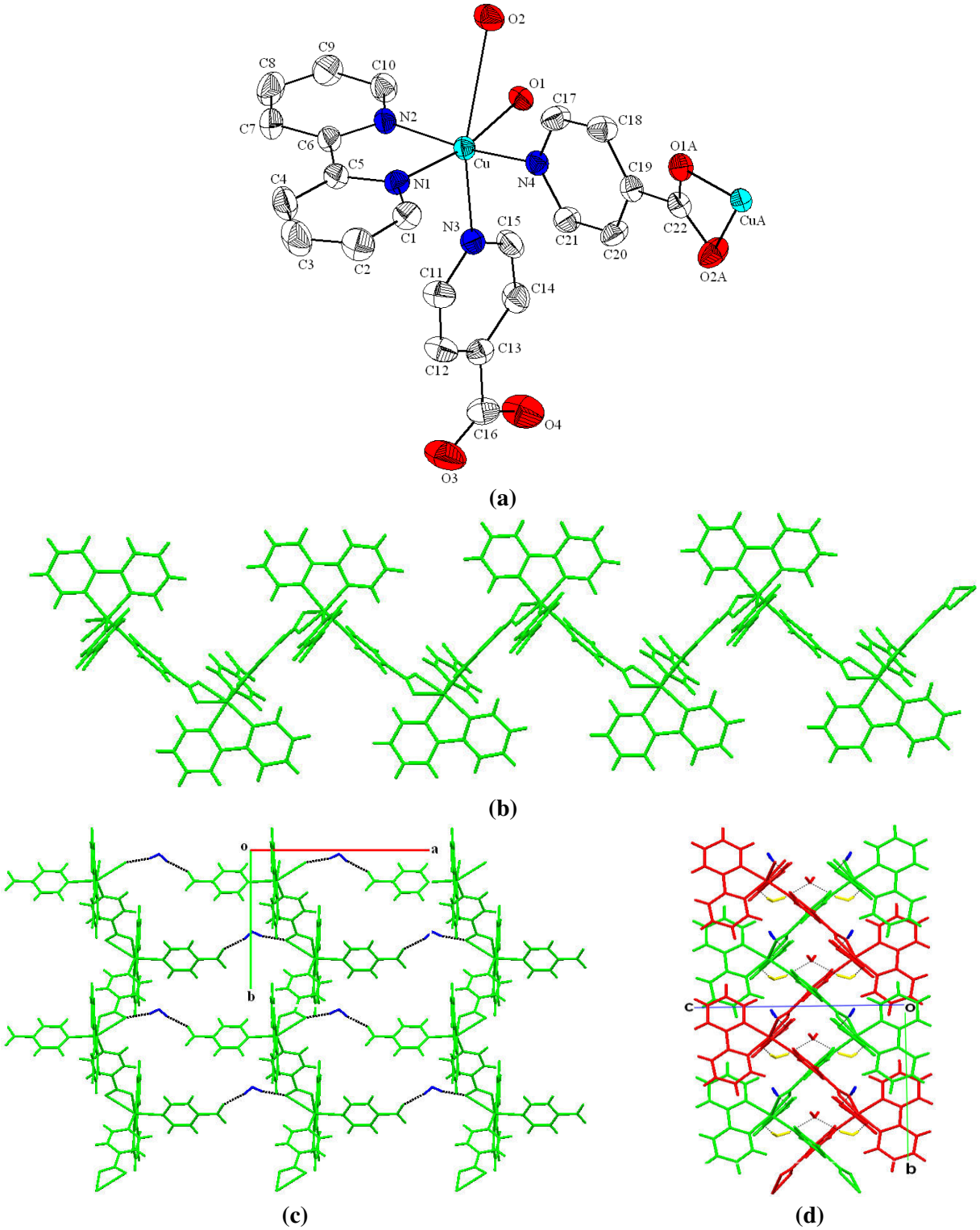

Figure 5.4. (a) Thermal ellipsoid plot of the coordination environment of the complex **4**; (b) A view showing the zig-zag type of arrangement of 1D chains; (c) A view of the 2D structure formed by H-bonding contacts in *ab*-plane; (d) A view of the 3D network in *bc*-plane.

Table 5.9: π···π interaction (Å)

*π···π interaction for **3***

C3···C8#1	3.401(7)	C15···C16#2	3.439(8)

(#1) *x*, 1–*y*, ½+*z*; (#2) *x*,–*y*,$^1/_2$+*z*

*π···π interaction for **4***

C2···C8#1	3.490(6)	C10···C22#2	3.302(4)
C16···C18#3	3.437(5)	C17···C22#4	3.448(4)

(#1) $^1/_2$–*x*, $^1/_2$–*y*, –*z*; (#2) $^1/_2$–*x*, $^1/_2$+*y*, $^1/_2$–*z*; (#3) –*x*, *y*,$^1/_2$–*z*; (#4) $^1/_2$–*x*,$^1/_2$+*y*,$^1/_2$–*z*

5.6. Spectroscopic properties

All of the compounds obtained gave satisfactory elemental analysis and were characterized by IR, diffuse reflectance spectroscopy and ESR spectroscopy.

5.6.1. Infrared spectra

IR spectra of the both compounds **1** and **2** are very similar. A broad band around 3396, 3376, 3463 and 3484 cm^{-1} is attributed to the absorptions of water molecules for **1–4** respectively. The intense bands at 1601, 1589, 1605 and 1600 cm^{-1} are associated with ν_{as}(COO), those at 1380, 1385, 1380 and 1380 cm^{-1} correspond to ν_s(COO) of **1–4**, respectively. This is consistent with the general observation that unidentate carboxylates show a difference of more than 200 cm^{-1} for the two frequencies.[24] The IR spectrum for **1** and **2** shows strong and medium bands at 1439, 1424 cm^{-1} and 1315, 1319 cm^{-1} corresponding to $\nu_{as}(NO_3)$ and $\nu_s(NO_3)$ absorption bands, respectively. The IR spectrum shows broad band corresponding to the ClO_4^- anion vibration near 1110 cm^{-1}.

5.6.2. Electronic spectra

The electronic reflectance spectrum of both compounds **1** and **2** show a broad peak at the approximately same frequency of 14,000 cm^{-1} ($d_{xy,}$ $d_{xz} \approx d_{yz} \rightarrow d_{x2-y2}$) with a poorly resolved shoulder to lower energy at approximately 10,380 cm^{-1} ($d_{z2} \rightarrow d_{x2-y2}$), consistent with the elongated octahedral coordination polyhedron. The spectrum of **3** involves a single broad peak at a lower energy of approximately 15,430 cm^{-1} (d_{xz}, $d_{yz} \rightarrow d_{x2-y2}$), consistent with the square-pyramidal geometry.[25] The compound **4** shows bands at around 15,527 and 10,976 cm^{-1}, which are considered normal transitions for square-pyramidal geometry.

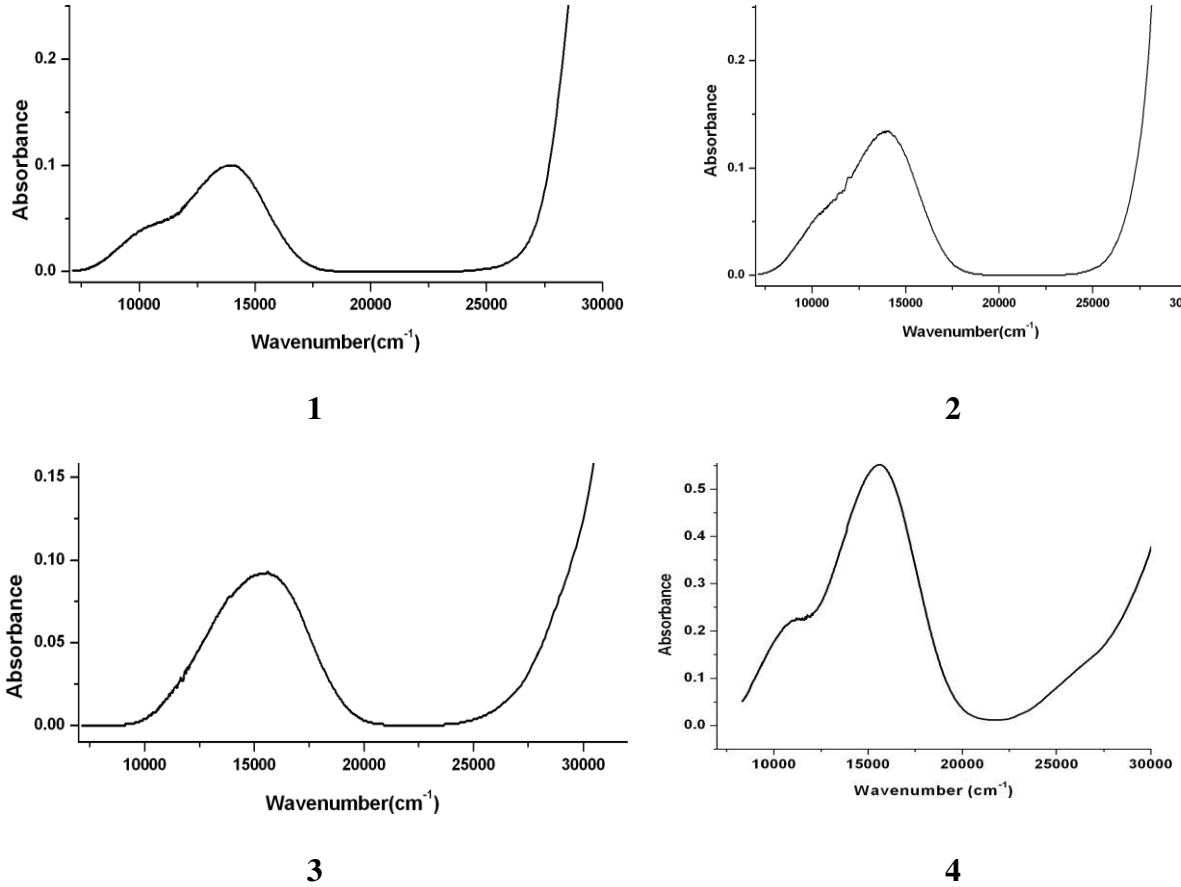

Figure 5.6. Diffuse reflectance spectra of **1-4**

5.6.3. EPR spectra:

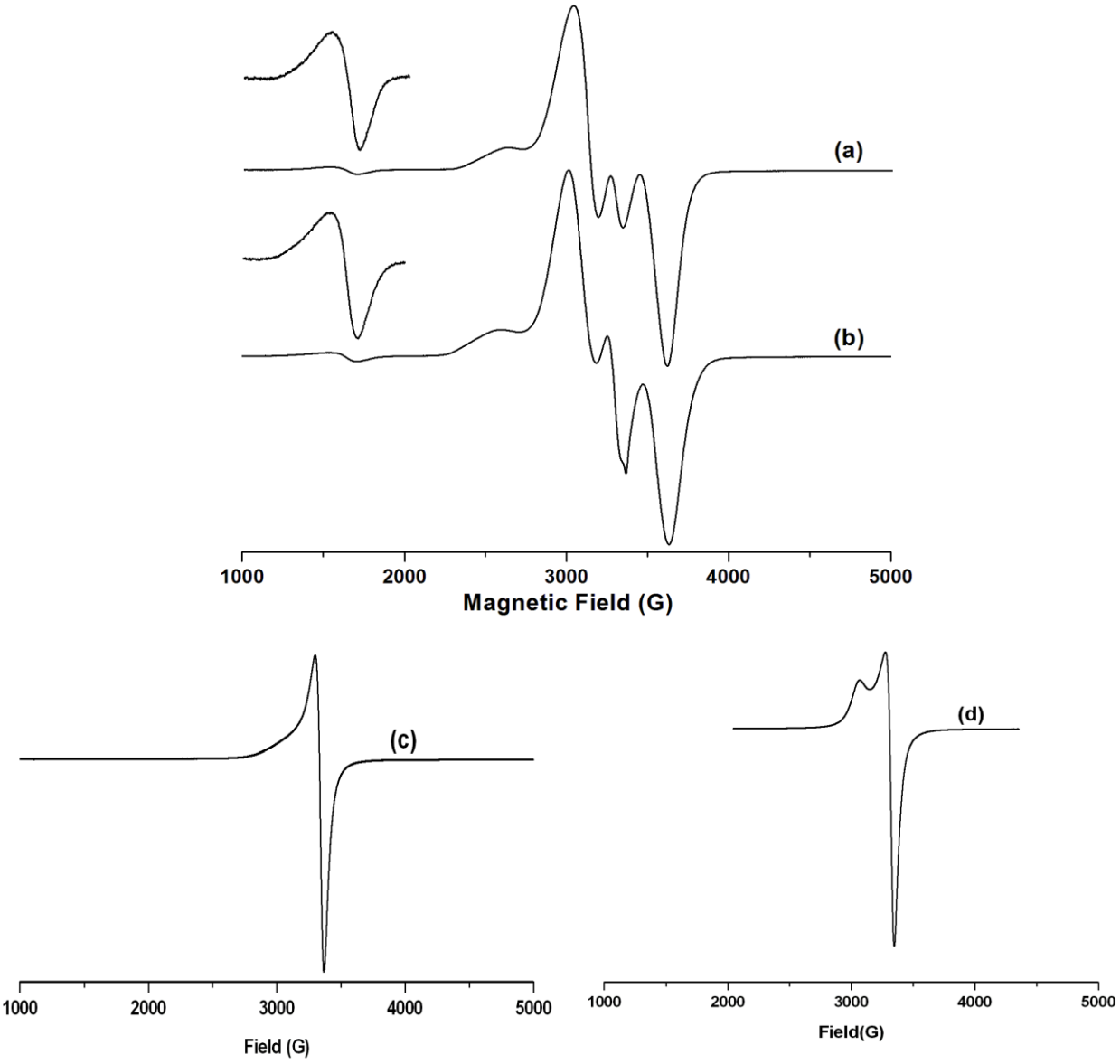

Figure 5.7. Room temperature X-band EPR spectra of polycrystalline-powder. (a) compound **1**, ν = 9.6818 GHz (b) compound **2**, ν = 9.6823 GHz. The low field portion is amplified to show the forbidden ("half-field") transition. (c) compound **3**, ν = 9.6826 GHz (d) compound **4**, ν = 9.6756 GHz. There is no significant change in spectra upon cooling the samples to 77 K.

The X-band EPR spectra of polycrystalline samples of **1** and **2** shown in Figure 5.7 are typical for triplet state dicopper(II) compounds with the zero-field splitting parameter $D < h\nu$ [26, 6a,10] Even though the hyperfine splitting is not resolved, the anisotropic components – three pairs of lines separated by the principal components (x, y, z) of the zero-field splitting – are partially resolved in both spectra. The axial (D) and rhombic components (E) of the zero-field interaction are related to the three field-separations by the following approximate equations:[27] $\Delta H_z = 2D$, $\Delta H_x = D - 3E$, $\Delta H_y = D + 3E$. Following assignments (field values in G) are consistent, within experimental error due to incomplete resolution, with the above formalism: compound **1**: z (2650, 3370); x (3320, 3570); y (3150, 3610); compound **2**: z (2600, 3380); x (3330, 3570); y (3140, 3640). Assuming the average g-values obtained by fitting the magnetic data the zero field parameters (cm^{-1}) are $D = 0.034$, $E = 0.003$ for **1** and $D = 0.038$, $E = 0.004$ for **2.** In both cases, a weak signal having an effective g-value of 4.3 is seen corresponding to ΔMs = ±2 transition of the triplet state. For **3**, the spectrum consists of a broad signal centered at about ~3330 G, as expected for a square-pyramidal Cu(II) system. The EPR spectra of **4** showed two broad signals (~3070 and ~3315 G) at room temperature.

5.7. Magnetic measurements:

The temperature-dependence of the magnetic susceptibility $\chi_m T$ of **1** and **2** were measured over the range 3-300 K. The room temperature $\chi_m T$ ($cm^3\ mol^{-1}\ K$) value for compound **1** (Figure 5.8(a)) per magnetic ion is 0.55 $cm^3\ mol^{-1}\ K$ at 300 K, which is higher than the expected spin-only value, 0.38 $cm^3\ mol^{-1}\ K$. While decreasing the temperature, the $\chi_m T$ value also slowly decreased and reached to 0.43 $cm^3\ mol^{-1}\ K$ at 15 K. Upon further cooling the $\chi_m T$ value increased and reached to 0.47 $cm^3\ mol^{-1}\ K$ per Cu^{II} at 3 K. The increase in $\chi_m T$ value is

characteristic of ferromagnetic exchange interaction between the two Cu^{II} ions. The best fit to the Bleaney–Bower equation[28] including temperature independent paramagnetism (TIP) yielded the parameters values $2J$ = 3.52(4) cm^{-1}, zJ' = –0.097(2) cm^{-1} g = 2.0498(9), TIP = 105 x10^{-5} cm^3mol^{-1} with a residual of 0.144 x 10^{-4}.

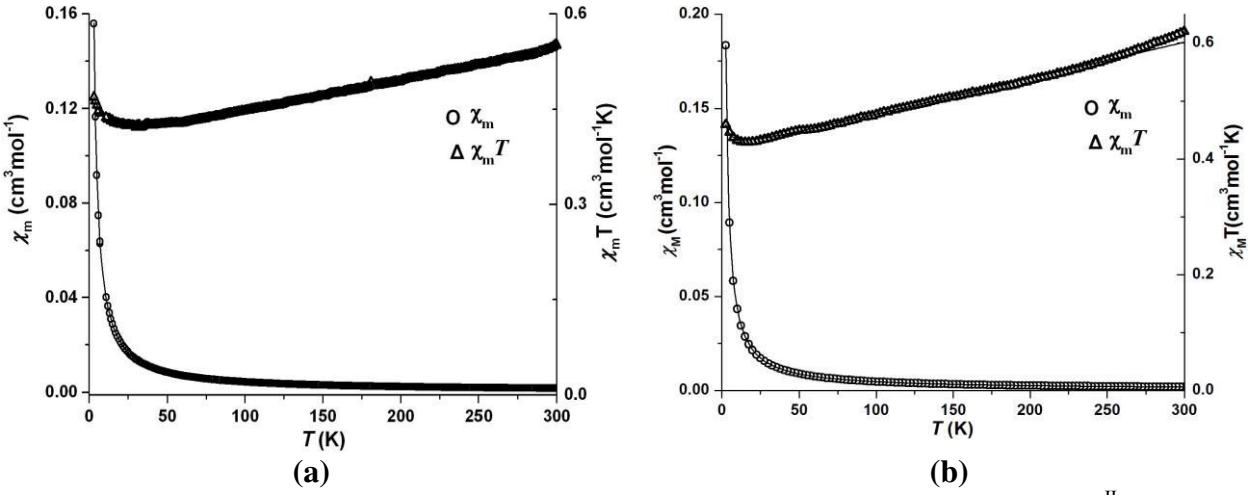

Figure 5.8. Temperature variation of the magnetic susceptibility χ_m and $\chi_m T$ product (per Cu^{II} ion) of (a) Compound **1**; (b) Compound **2**. The solid lines result from a least-square fit to the data of the theoretical values calculated with the Bleaney–Bower equation.

The room temperature $\chi_m T$ (cm^3 mol^{-1} K) value for compound **2** (Figure 5.8(b)) per magnetic ion is 0.62 cm^3 mol^{-1} K at 300 K which decreased to 0.43 cm^3 mol^{-1} K at 15 K. Further cooling increased the $\chi_m T$ value to 0.46 cm^3 mol^{-1} K at 2.5 K. The best fit parameters are $2J$ = 1.80(4) cm^{-1}, zJ' = –0.094(3) cm^{-1} g = 2.089(1), TIP = 125 x10^{-5} cm^3mol^{-1} with a residual of 0.700 x 10^{-5}. Table 5.10 collects together the magnetic data for the known diaquo-briged dinuclear Cu(II) complexes along with bridge geometries. It is seen that the super-exchange through water molecules is weak partly due to the unsymmetrical nature of the bridges and partly due to the unfavourable overlap between magnetic orbitals in the axial-equatorial mode. The lone example in the Table having equatorial-equatorial overlap corresponds to a significantly larger

coupling parameter. The data also show enhancement of the interaction when the diaquo-bridges are complemented by an additional bridge.

Table 5.10: Magnetostructural correlation of diaquo-bridged dicopper(II) complexes

Comp	Cu-O (Å)	Cu...O (Å)	Cu-O…Cu (˚)	Magnetic property ($2J/cm^{-1}$)	Ref.
1	2.033(2)	2.723(2)	103.89(8)	3.52	Present work
2	1.999(17)	2.680(2)	99.77(6)	1.80	
3	2.011(3)	2.680(3)	103.26(10)	1.50	5(a)
4	1.970(3)	2.667(3)	98.08(12)	–5.70	7
5	1.989(2)	2.663(2)	99.36(8)	–5.48	
6	1.971(3)	2.439(3)	97.33(10)	–14.00	8
7	1.957(3)	2.834(3)	78.35(10)	–51.0	9
8	1.936(15)	1.936(15)	97.13	–	6(a)

5.8. Conclusions

Herein we have described the synthesis and structural characterization of four mixed-ligand Cu(II) complexes containing 2,2'-bipyridine (bpy) or 1,10-phenanthroline (phen) in presence of isonicotinate (IN) $\{[Cu_2(\mu\text{-}OH_2)_2(INH)_2(L)_2(NO_3)_2](NO_3)_2\}$ [L = bpy (**1**), phen (**2**)] $\{[Cu(bpy)(IN)(OH_2)](ClO_4)\}n$ (**3**) and $\{[Cu(bpy)(IN)_2)]_2{\cdot}5H_2O)\}n$ (**4**) in which isonicotinate ligand exhibits three types of bonding modes, namely zwitterion in **1** and **2**; bidentate N, O bridging mode in **3** and tridentate N, O bridging mode in **4.** Compounds **1** and **2** are dinuclear with the core $[Cu(OH_2)_2Cu]^{+4}$ in equatorial–axial positions, while the compounds **3** and **4** contain 1D coordination polymer, created by the chains of Cu(II) ions bridged by isonicotinate ligands. The variable temperature (3–300 K) magnetic susceptibility measurements have suggested very weak ferromagnetic coupling interaction of the two Cu(II) ions, having J = 1.76 and 0.90 cm^{-1} respectively for **1** and **2**. Water molecules are weak transmitters of magnetic exchange compared

to for example hydroxo-bridges due to unsymmetrical nature of the bridges and unfavourable overlap of magnetic orbitals. A bridge angle of about 100º and above leads to a changeover from antiferro to ferromagnetic coupling.

5.9. References

1. (a) H. H. Monfared, M. Vahedpour, M. M. Yeganeh, M. Ghorbanloo, P. Mayer, C. Janiak, *Dalton Trans.,* **2011**, *40*, 1286; (b) K. Waizumi, M. Takuno, N. Fukushima, H. Masuda, *J. Coord. Chem.,* **1998**, *44*, 269.
2. (a) F. -P. Liang, M. -L. Huang, C. -F. Zhang, Y. Li, R. -X. Hu, *J. Coord. Chem.*, **2007**, *60*, 2343; (b) J. Lu, E. Shen, M. Yuan, Y. Li, E. Wang, C. Hu, L. Xu, J. Peng, *Inorg. Chem.*, **2003**, *42*, 6956; (c) X. -L. Wang, Q. Gao, G. -C. Liu, H. -Y. Lin, A. -X. Tian, J. Li, *Inorg. Chem. Commun.*, **2011**, *14*, 745; (d) M. -V. Sergio, V. -M. Jesús, I. M. Arturo, *J. Mol. Struct.*, **2011**, *1006*, 425; (e) M. -V. Sergio, I. M. Arturo, V. -M. Jesús, L. P. Dale, *J. Mol. Struct.*, **2013**, *1033*, 34.
3. (a) F. –M. Nie, F. Lu, S. –Y. Wang, M. –Y. Jia, Z. –Y. Dong, *Inorg. Chim. Acta*, **2011**, *365*, 309; (b) M. E. Chapman, B. M. P. Ayyappan, G. T. Foxman, W. L. Yee, *Cryst. Growth Des.*, **2001**, *1*, 159; (c) J. Y. Lu, A. M. Babb, *Inorg. Chem. Commun.*, **2001**, *4*, 716; (d) B. Rather, B. Moulton, R. D. Bailey Walsh, M. J. Zaworotko, *Chem. Commun.*, **2002**, 694; (e) J. Y. Lu, E. E. Kohler, *Inorg. Chem. Commun.*, **2002**, *5*, 600; (f) P. -O. Käll, J. Grins, M. Fahlman, F. Soderlind, *Polyhedron*, **2001**, *20*, 2747.
4. (a) C. -M. Wang, Y. -L. Chuang, S. -T. Chuang, K. -H. Lii, *J. Solid State Chem.*, **2004**, *177*, 2305; (b) G. -C. Liu, Y. -Q. Chen, W. -Y. Zheng, H. -Y. Lin, *Trans. Met. Chem.*, **2009**, *34*, 739; (c) Y. Ren, C. Du, S. Feng, C. Wang, Z. Kong, B. Yue, H. He, *Cryst. Eng.*

Comm., **2011**, *13*, 7143; (d) M. Almasi, Z. Vargova, R. Gyepes, R. Varga, V. Zelenak, *Inorg. Chem. Comm.*, **2014**, *46*, 118; (e) J. Li, Y. -G. Chen, C. -J. Zhang, Q. -J. Kong, *J. Mol. Struct.*, **2009**, *921*, 233.

5. (a) C. Biswas, M. G. B. Drew, S. Asthana, C. Desplanches, A. Ghosh, *J. Mol. Struct*., **2010**, *965*, 39; (b) P. Talukder, S. Sen, S. Mitra, L. Dahlenberg, C. Desplanches, J. -P. Sutter, *Eur. J. Inorg. Chem*., **2006**, 329; (c) M. Barquin, M. J. G. Garmendia, L. Larrinaga, E. Pinillab, M. R. Torres, *Z. Anorg. Allg. Chem*., **2005**, *631*, 2151.

6. (a) A. B. Caballero, A. R. Dieguez, L. Lezama, J. M. Salas, *Cryst. Growth Des.*, **2012**, *12*, 3583; (b) L. Klistincova, E. Rakovsky, P. Schwendt, G. Plesch, R. Gyepes, *Inorg. Chem. Commun.*, **2010**, *13*, 1275; (c) L. X. Xie, X. Li, P. H. Xie, Q. Jin, *Acta Cryst.*, **2009**, *E65*, m928; (d) O. Svajlenova, J. Vanco, J. Marek, *Acta Cryst.*, **2004**, *C60*, m275; (e) L. Hong, X. -M. Li, Q. -W. Wang, Z. -L. Xu, B. Liu, (Jiegou Huaxue) *CHIN. J. Struct. Chem.*, **2010**, *29*, 801.

7. (a) J. -W. Zhao, C. -M. Wang, J. Zhang, S. -T. Zheng, G. -Y. Yang, *Chem. Eur. J.*, **2008**, *14*, 9223; (b) B. Li, J. -W. Zhao, S. -T. Zheng, G. -Y. Yang, *Inorg. Chem.*, **2009**, *48*, 8294.

8. D. Ghoshal, T. K. Maji, G. Mostafa, S. Sain, T. -H. Lu, J. Ribas, E. Zangrandoe, N. R. Chaudhuri, *Dalton Trans.*, **2004**, 1687.

9. J. -Y. Zhang, X. -B. Li, K. Wang, Y. Ma, A. -L. Cheng, E. -Q. Gao, *Dalton Trans.*, **2012**, *41*, 12192.

10. M. Korabik, M. Materny, W. Surga, T. Gtowiak, J. Mroziflski, *J. Mol. Struct.*, **1998**, *443*, 255.

11. (a) J. Y. Lu, A. M. Babb, *Chem. Commu.*, **2002**, 1340; (b) T. -B. Lu, R. L. Luck, *Inorg. Chim. Acta*, **2003**, *351*, 345; (c) J. Zhang, Y. Kang, J. Zhang, Z. –J. Li, Y. –Y. Qin, Y. –G. Yao, *Eur. J. Inorg. Chem.,* **2006**, 2253; (d) H. S. Huh, S. W. Lee, *J. Mol. Struc.*, **2007**, *829*, 44; (e) T. –T. Lian, S. –M. Chen, *Inorg. Chem. Commun.*, **2012**, *18*, 8; (f) M. E. Chapman, P. Ayyappan, B. M. Foxman, G. T. Yee, W. Lin, *Cryst. Growth Des.,* **2001**, *1*, 161.

12. (a) J. -F. Ma, J. Yang, G. -L. Zheng, L. Li, Y. -M. Zhang, F. -F. Li, J. -F. Liu, *Polyhedron*, **2004**, *23*, 553; (b) J. Y. Lu, A. M. Babb, *Inorg. Chem.*, **2001**, *40*, 3261.

13. (a) A. -L. Xiea, D. -J. Xub, *J. Coord. Chem*., **2005**, *58*, 225; (b) L. Carlucci, G. Ciani, A. Gramaccioli, D. M. Proserpio, S. Rizzato, *Cryst. Eng. Comm*., **2000**, *29*, 1.

14. D. Xu, A. Xie, Y. Xu, K. Nishikawa, N. Yasuoka, *J. Coord. Chem*., **1998**, *43*, 237.

15. X. Zhou, C. Yang, X. Le, S. Chen, J. Liu, Z. Huang, *J. Coord. Chem*., **2004**, *57*, 401.

16. P. Pascal, *Ann. Chim. Phys.*, **1910**, *19*, 5.

17. G. V. R. Chandramouli, C. Balagopalakrishna, M. V. Rajasekharan, P. T. Manoharan, *Comput. Chem.*, **1996**, *20*, 353.

18. SAINTPLUS, Bruker AXS Inc., Madison, Wisconsin, USA, **2003**.

19. G. M. Sheldrick, SADABS*,* Program for empirical absorption correction (University of Gottingen, Gottingen, Germany), **1996**.

20. G. M. Sheldrick, *Acta Crystallogr.*, **2008**, *A64,* 112.

21. C. F. Macrae, I. J. Bruno, J. A. Chisholm, P. R. Edgington, P. Mc Cabe, E. Pidcock, L. Rodriguez-Monge, R. Taylor, J. van de Streek, P. A. Wood, *J. Appl. Cryst*., **2008**, *41*, 466.

22. A. W. Addison, T. N. Rao, J. Reedijk, J. van Rinj, C. G. Verscholar, *J. Chem. Soc., Dalton Trans*., **1984**, 1349.

23. (a) M. V. Sergio, V. M. Jesus, I. M. Arturo, *J. Mol. Struc.*, **2011**, *1006*, 425; (b) M. -M. Liu, J. -J. Hou, Z. -K. Qi, L.-N. Duan, W. -J. Ji, C. -Y. Han, X. -M. Zhang, *Inorg. Chem.*, **2014**, *53*, 4130; (c) J. Y. Lu, A. M. Babb, *Chem. Commun.*, **2001**, 821.

24. K. Nakamoto, *Infrared and Raman Spectra of Inorganic and Coordination Compounds*, third ed., John Wiley and Sons, New York, **1978**, 232.

25. B. J. Hathaway, D. E. Billing, *Coord. Chem. Rev*., **1970**, *5*, 143.

26. T. D. Smith, J. R. Pilbrow, *Coord. Chem. Rev.*, **1974**, *13*, 173.

27. E. Wasserman, L. C. Snyder, W. A.Yager, *J. Chem. Phys.*, **1964**, *41*, 1763.

28. B. Bleaney, K. D. Bowers, *Proc. R. Soc. London, Ser. A.*, **1952**, *214*, 451.

CHAPTER VI

Synthesis, structural and spectral characterization of mono-, di- and tri-chloroacetato bridged Cu(II) complexes with 2,2'-bipyridine

6.1. Introduction

Transition-metal complexes with carboxylate anions have been interesting for researchers, because these can be used for the chemical construction of molecular magnetic materials,[1] catalysts,[2] and, in some cases, photoluminescent systems.[3] The carboxylates can work as both bulk anions and multifunctional anions. The carboxylate groups are known to form a variety of bridging modes, such as *syn-syn*, *anti-anti* and *syn-anti* (Scheme 6.1).[4]

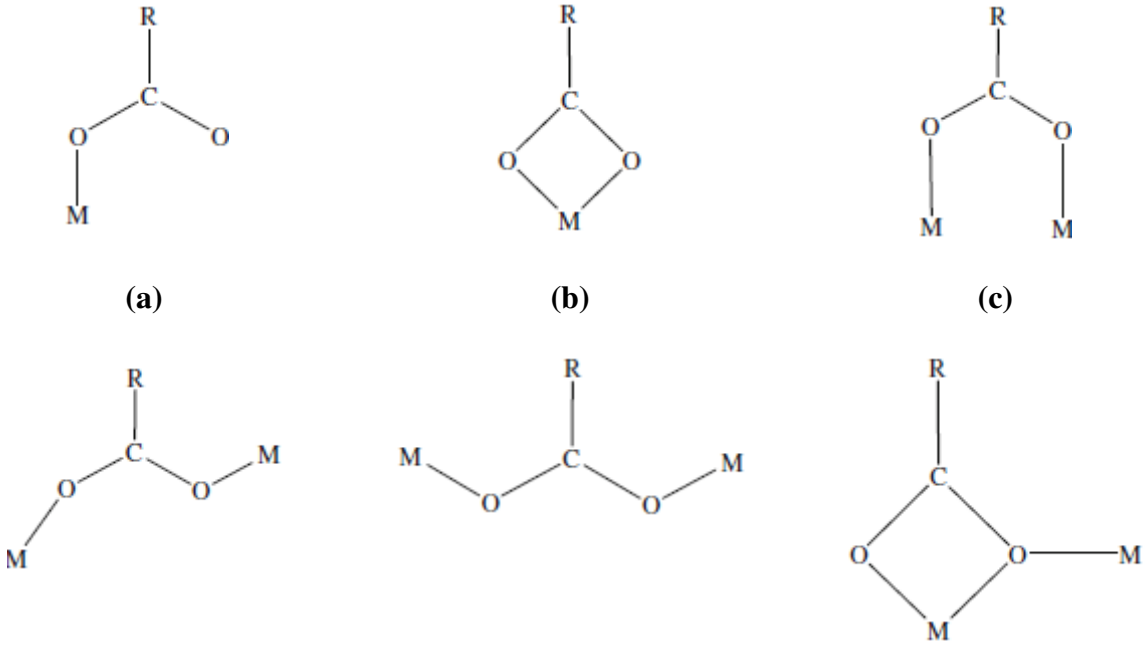

Scheme 6.1. Possible coordination modes for the carboxylate ions

Cu(II) carboxylates are commonly found as dinuclear compounds. A review published by Doedens[5a] reported that the average Cu – Cu distance in a range of dimeric carboxylate complexes was found to be 2.619Å. In complexes, metal ions are bridged with acetates or

substituted acetates in *syn-syn* fashion, the *J* value is high (antiferromagnetic or ferromagnetic), where acetate ligands directly interact with d_{x2-y2} orbitals of Cu(II) ions. In complexes having *syn-anti* bridging, the *J* value is smaller than that of *syn-syn* bridges because axial bonds are long and not directed towards d_{x2-y2} orbitals.[6] As a part of a research on complexes bridged by haloacetates with a view to the investigation of magnetic exchange interactions between adjacent magnetic nuclei, complexes with the core $[Cu(RCOO)_2Cu]^{+2}$ containing 2,2'-bipyridine (bpy) have been synthesized. Although several structures of polynuclear Cu(II) complexes with acetate bridges have been reported, not many were known with haloacetates in the literature.[5b] Accordingly it will be interesting to study polynuclear Cu(II) complexes of haloacetates which due to the electron withdrawing halo group will be more acidic. The pK_a value of haloacetic acids are less than that of the normal acetic acid (4.76). So in order to see the effect of acetate bridges on its magnetic properties we have synthesized some polynuclear Cu(II) complexes with haloacetic acids.

The Cu(II) haloacetates have been shown to have a diverse stereochemistry.[7-9] There are few structurally characterized metal haloacetates with aromatic nitrogen-donor ligands, in which organic ligands occupied the axial position in the square-pyramidal geometry.[7d-j] Only three compounds were reported with bpy, one dinuclear and two mononuclear: $[Cu_2(bpy)_2(\mu\text{-}OH)(\mu\text{-}OH_2)(\mu\text{-}ClCH_2COO)](NO_3)_2$,[7a] $[Cu(bpy)_2(Cl_2CHCOO)](Cl_2CHCOO)\cdot H_2O$[8] and $[Cu(bpy)(Cl_3CCOO)_2(CH_3OH)]$.[9] Presently we have synthesized four Cu(II) haloacetate complexes with bpy: a novel linear trinuclear Cu(II) complex $[Cu_3(bpy)_2(\mu\text{-}ClCH_2COO)_6]$ (**1**) with *syn-syn* chloroacetato bridge, two dinuclear complexes $[Cu_2(bpy)_2(\mu\text{-}Cl_2CHCOO)_2(Cl_2CHCOO)_2]$ (**2**) with monoatomic dichloroacetato bridge and $[Cu_2(bpy)_2(\mu\text{-}Cl_3CCOO)_2(Cl_3CCOO)_2]$ (**3**) with *syn-anti* trichloroacetato bridge. All of the complexes were

prepared by mixing Cu(II) carbonate with haloacetic acid and bpy ligands in methanol/water solvent. When 1 equivalent $NaClO_4 \cdot H_2O$ was added to the reaction solution, $[Cu_2(bpy)_2(\mu\text{-}OH)(\mu\text{-}OH_2)(\mu\text{-}ClCH_2COO)](ClO_4)_2$ (**4**) was obtained. Variable temperature magnetic susceptibility measurements in the range 3–300 K show antiferromagnetic behaviour for the complex **1** and ferromagnetic behaviour for the complex **4**. In addition, polycrystalline EPR spectra of all samples were measured at different temperature and the results are discussed.

6.2. Experimental

6.2.1. Reagents

All the chemicals were of reagent grade obtained from commercial sources and were used without further purification.

6.2.2. Synthesis

Preparation of $[Cu_3(bpy)_2(\mu\text{-}ClCH_2COO)_6]$ (1)

To a mixed warm methanol/water (3:1 v/v) solution (20 mL) of $CuCO_3 \cdot Cu(OH)_2 \cdot H_2O$ (0.120 g, 0.500 mmol), a methanolic solution (10 mL) of 2,2′-bipyridine (0.105 g, 0.670 mmol) and chloroacetic acid (0.189 g, 2.000 mmol) were added slowly with constant stirring at 75º C for 20 minutes. The resultant blue solution was filtered and allowed to cool to room temperature, kept for crystallization. On standing for a week, blue crystals of **1** were obtained along with a blue precipitate. They were washed with cold methanol and air dried. The side product could not be obtained in a pure crystalline form, it may probably mixed ligand complex. Yield of **1** is 0.173 g, (0.163 mmol, 49%). *Anal.* Calc. for $C_{32}H_{28}Cl_6Cu_3N_4O_{12}$ (M.W. 1063.9 g): C, 36.13; H, 2.65; N, 5.27%. Found: C, 36.22; H, 2.58; N, 5.43%. Important IR absorptions (KBr disc, cm^{-1}): 3109,

3034, 2961, 1620, 1496, 1477, 1446, 1415, 1363, 1315, 1253, 1230, 1157, 1057, 1032, 931, 779, 733, 686, 572, 495 and 422.

Preparation of $[Cu_2(bpy)_2(\mu\text{-}Cl_2CHCOO)_2(Cl_2CHCOO)_2]$ (2)

To a mixed warm methanol/water (3:1 v/v) solution (20 mL) of $CuCO_3{\cdot}Cu(OH)_2{\cdot}H_2O$ (0.120 g, 0.500 mmol), a methanolic solution (10 mL) of 2,2′-bipyridine (0.156 g, 0.100 mmol) and dichloroacetic acid (0.164 µL, 2.000 mmol) were added slowly with constant stirring at 75º C for 20 minutes. The resultant blue solution was filtered and allowed to cool to room temperature, kept for crystallization. On standing for a week, blue crystals of **1** were obtained along with a blue precipitate. They were washed with cold methanol and air dried. The side product could not be obtained in a pure crystalline form, it may probably mixed ligand complex. Yield of **2** is 0.441 g, (0.464 mmol, 46%). *Anal.* Calc. for $C_{28}H_{20}Cl_8Cu_2N_4O_8$ (M.W. 951.18 g): C, 35.36; H, 2.12; N, 5.89%. Found: C, 35.21; H, 2.21; N, 5.75%. Important IR absorptions (KBr disc, cm^{-1}): 3450, 3007, 1687, 1628, 1602, 1496, 1475, 1448, 1386, 1356, 1309, 1255, 1207, 1188, 1032, 823, 796, 769, 727 and 661.

Preparation of $[Cu_2(bpy)_2(\mu\text{-}Cl_3CCOO)_2(Cl_3CCOO)_2]$ (3)

Complex **3** was synthesized by the same procedure adopted for complex **2** using trichloroacetic acid (0.202 µL, 2.000 mmol) instead of dichloroacetic acid. Yield of **3,** 0.260 g, (0.238 mmol, 24%). *Anal.* Calc. for $C_{28}H_{16}Cl_{12}Cu_2N_4O_8$ (M.W. 1088.95 g): C, 30.88; H, 1.48; N, 5.14%. Found: C, 30.75; H, 1.41; N, 5.43%. Important IR absorptions (KBr disc, cm^{-1}): 3377, 3111, 3076, 3034, 1601, 1568, 1494, 1475, 1446, 1352, 1161, 1105, 1028, 912, 852, 771, 731, 684, 657, 634, 493 and 412.

Preparation of $[Cu_2(bpy)_2(\mu\text{-}OH)(\mu\text{-}OH_2)(\mu\text{-}ClCH_2COO)](ClO_4)_2$ (4)

To a mixed warm methanol/water (3:1 v/v) solution (20 mL) of $CuCO_3{\cdot}Cu(OH)_2{\cdot}H_2O$ (0.120 g, 0.500 mmol), a methanolic solution (20 mL) of 2,2′-bipyridine (0.156 g, 1.000 mmol) and

chloroacetic acid (0.094 g, 1.000 mmol) were added slowly with constant stirring at 75º C for 20 minutes. To the resultant solution, $NaClO_4 \cdot H_2O$ (0.140 g, 1.000 mmol) dissolved in methanol (5 mL) was added. The clear blue solution was allowed to cool to room temperature, kept for crystallization. On standing for a week, blue crystals of **4** were obtained. They were washed with cold methanol and air dried. Yield is 0.394 g, (0.514 mmol, 51%). *Anal.* Calc. for $C_{22}H_{21}Cl_3Cu_2N_4O_{12}$ (M.W. 766.88 g): C, 34.46; H, 2.76; N, 7.31%. Found: C, 34.35; H, 2.65; N, 7.25%. Important IR absorptions (KBr disc, cm^{-1}): 3528, 3389, 3117, 3082, 3065, 1602, 1593, 1564, 1496, 1473, 1446, 1429, 1315, 1267, 1122, 1051, 1032, 925, 775, 731, 700, 623, 542, 491, 459 and 416.

6.3. Physical measurements

IR spectra were obtained as KBr pellets on a Jasco FT-IR 5300 spectrometer in the range 4000-400 cm^{-1}. Elemental analysis for C, H and N was performed on a Perkin-Elmer 240C elemental analyzer. Diffuse reflectance spectra were measured by using a Shimadzu UV-3100 spectrometer. ESR spectra were recorded on Bruker Xenon EMX-ER-073 spectrometer. Powder X-ray diffraction patterns were recorded on a Bruker D8-Advance diffractometer using graphite monochromated $CuK_{\alpha 1}$ (1.5406 Å) and $K_{\alpha 2}$ (1.54439 Å) radiations. Simulation of the P-XRD patterns was carried out using the Mercury. Magnetic susceptibilities were measured for compound **1**and **4** in the temperature range of 3−300 K on a Quantum Design PPMS-VSM. The samples were pressed into pellets to avoid orientation effects of the microcrystals during magnetic measurements. Diamagnetic corrections were applied using Pascal's constants.[10] Fitting of the susceptibility data was done by using the program SUSCEP[11] based on the trimer

equation[12] for compound **1** and Bleaney–Bower equation[13] for compound **4** including temperature independent paramagnetism (TIP).

6.4. X-ray crystallography

The unit cell parameters and intensity data at 298 K for **1-4** were obtained on a Bruker-Nonius SMART APEX CCD 1000 area detector, using graphite-monochromated Mo-Kα radiation (λ = 0.71073 Å). Data were reduced using SAINTPLUS[14] and a multiscan absorption correction using SADABS[15] was performed. The structure of complexes were solved by direct methods and refined on F^2 by full-matrix least-squares procedures. The non-hydrogen atoms were refined using anisotropic thermal parameters. The hydrogen atoms were included in the structure factor calculations at idealized positions using a riding model, and the hydrogen atoms attached to oxygen atoms were located from the difference maps. The structures were solved using SHELXS-97 and refined using SHELXL-97.[16] Drawings were made using Mercury.[17] Crystallographic data and structure refinements are given in Table 6.1. Selected bond lengths and bond angles are listed in Table 6.2, Table 6.3, Table 6.5 and Table 6.6.

6.5. Results and discussion

6.5.1. Synthesis

We realize that new types of bridged species may occur when the ratio of Cu(II), bpy and haloacetates is not high enough to lead to mononuclear products. Keeping the 1:1:2 molar ratio, we notice some interesting phenomena during this systematic observation. Firstly, treatment of $CuCO_3 \cdot Cu(OH)_2 \cdot H_2O$ with 1 equivalent of bpy and 2 equivalent of haloacetates in methanol/water at room temperature led to the formation of different structures, for example, a linear trinuclear complex $[Cu_3(bpy)_2(\mu\text{-}ClCH_2COO)_6]$ (**1**) and dinuclear complexes

$[Cu_2(bpy)_2(\mu\text{-}Cl_2CHCOO)_2(Cl_2CHCOO)_2]$ (**2**) and $[Cu_2(bpy)_2(\mu\text{-}Cl_3CCOO)_2(Cl_3CCOO)_2)]$ (**3**) under analogous reaction conditions. The reactions are summarized in Eq. (1).

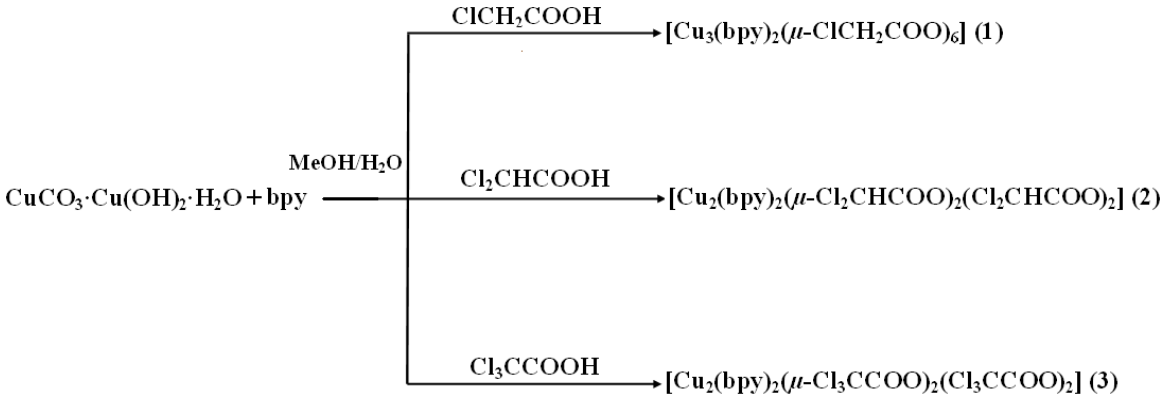

(1)

Secondly, in the presence of a high ionic strength anion such as ClO_4^-, the reaction system was driven to produce only dinuclear complexes. For example, treatment of the reaction solution with 1 equiv. $NaClO_4$ leads to the formation of a triply-bridged dinuclear complex $[Cu_2(bpy)_2(\mu\text{-}OH)(\mu\text{-}OH_2)(\mu\text{-}ClCH_2COO)](ClO_4)_2$ (**4**), compound **2** or compound **3**, respectively. The reactions are summarized in Eq. (2).

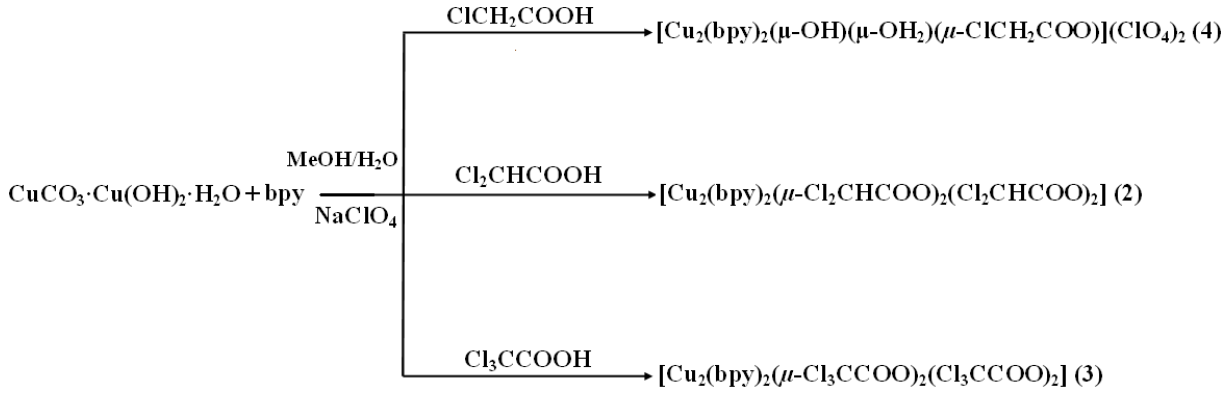

(2)

In each preparation, a small amount of crystalline precipitate was obtained along with the main compounds. The powder patterns of the compounds **1-4** were matched with those simulated powder patterns based on the results from crystal structure. The nature of the acid strongly affects the composition of the products. The presence of a larger number of electron-withdrawing

substituents on the α-C atom, makes the copper center more acidic and the bridging haloacetates less prone to form additional bond with other units.

In order to study the influence of the aromatic heterocycle ligand on the product identity, we used 1,10-phenanthroline (phen) instead of bpy. The reaction of $CuCO_3{\cdot}Cu(OH)_2{\cdot}H_2O$ with 1 equivalent of phen and 2 equivalent of haloacetates in methanol/water afforded only mononuclear complexes, $[Cu(phen)(ClCH_2COO)_2(H_2O)]$,[18] $[Cu(phen)(Cl_2CHCOO)_2(H_2O)]$[19] and $[Cu(phen)(Cl_3CCOO)_2(H_2O)]$[20] respectively.

6.5.2. Crystal structure of $[Cu_3(bpy)_2(\mu\text{-}ClCH_2COO)_6]$ (1)

The molecular structure of **1** is shown in Figure 6.1. Selected bond lengths and angles are listed in Table 6.2. The crystal structure of **1** consists of a trinuclear unit $[Cu_3(bpy)_2(\mu\text{-}ClCH_2COO)_6]$, in which each terminal Cu(2) atom is linked by three chloroacetate ligands to the central Cu(1) atom, which is located at an inversion center. Two of them act as *syn-syn* bridging mode and the third one function in the monoatomic bridging plus chelate mode. The coordination environment of Cu(2) is completed by two nitrogen atoms of a bpy ligand to form a distorted CuN_2O_4 octahedral and the Cu(1) has a CuO_6 octahedral geometry. The $[Cu_3(bpy)_2(ClCH_2COO)_6]$ core is similar to those found in $[Mn_3(bpy)_2(ClCH_2COO)_6]$,[21] $[M_3(bpy)_2(CH_3COO)_6]$ (M = Co(II) and Mn(II)),[22] $[Mn_3(bpy)_2(OOCPh)_6]$,[23] $[M_3(bpy)_2(L)_6]$ (M = Co(II), Mn(II); L = 2,4-dichlorobenzoate)[24] and $[Mn_3(bpy)_2(L)_6]$ (L = 3,5-dimethylbenzoate).[25] The Cu···Cu distance (3.536 Å) is comparable to those observed in $[Mn_3(bpy)_2(ClCH_2COO)_6]$ (3.624 Å),[21] $[M_3(bpy)_2(CH_3COO)_6]$ (M = Co(II) (3.495 Å) and Mn(II) (3.614 Å)),[22] $[Mn_3(bpy)_2(OOCPh)_6]$, (3.588 Å)[23] $[M_3(bpy)_2(L)_6]$ (M = Co(II) (3.586 Å), Mn(II) (3.627); L = 2,4-dichlorobenzoate)[24] and $[Mn_3(bpy)_2(L)_6]$ (L = 3,5-dimethylbenzoate) (3.549 Å).[25]

Table 6.1: Crystallographic data and structure refinement parameters for complexes **1−4**

	1	**2**	**3**	**4**
Formula	$C_{32}H_{28}N_4O_{12}Cl_6Cu_3$	$C_{28}H_{20}N_4O_8Cl_8Cu_2$	$C_{28}H_{16}N_4O_8Cl_{12}Cu_2$	$C_{22}H_{21}N_4O_{12}Cl_3Cu_2$
Formula weight	1063.90	951.16	1088.93	766.86
Crystal system	Triclinic	Triclinic	Monoclinic	Triclinic
Space group	$P\,\bar{1}$	$P\,\bar{1}$	$P2_1/c$	$P\,\bar{1}$
a (Å)	7.957(10)	9.398(2)	16.058(13)	8.0719(5)
b (Å)	10.444(14)	10.052(2)	16.997(14)	11.126(6)
c (Å)	13.283(17)	10.898(2)	14.026(12)	17.169(10)
α (˚)	69.46(2)	63.077(3)	90	71.597(10)
β (˚)	77.66(2)	72.101(3)	99.84(10)	89.61(10)
γ (˚)	68.33(2)	82.249(4)	90	76.04(10)
V (Å^3)	956.2(2)	873.5(3)	3771.8(5)	1415.8(14)
Z	1	1	4	2
λ (Å)	0.71073	0.71073	0.71073	0.71073
T(K)	298(2)	298(2)	298(2)	298(2)
D_{calc} (g cm^{-3})	1.848	1.808	1.918	1.799
μ (mm^{-1})	2.140	1.884	2.033	1.855
F(000)	533	474	2152	772
Crystal size (mm)	0.68 x 0.60 x 0.24	0.28 x 0.20 x 0.16	0.60 x 0.32 x 0.24	0.32 x 0.28 x 0.16
θ Range(˚)	1.64 to 25.00	2.18 to 25.00	1.29 to 26.01	1.25 to 25.00
h/k/l indices	-9,9/ -12,12/ -15,15	-11,11/ -11,11/ -12,12	-19,19/ -20,20/ -17,17/	-9,9/ -13,13/ -20,20
Reflection collected	9216	8396	38669	13732
Unique reflect.,[R_{int}]	3369 [0.0406]	3071 [0.0287]	7398 [0.0503]	4993 [0.0225]
GooF	1.046	1.030	1.048	1.055
R_1 [I>2σ(I)]	0.0552	0.0422	0.0595	0.0458
wR_2 (all data)	0.1312	0.1042	0.1627	0.1262

$w = 1/[\sigma^2(F_0^2) + (AP)^2 + BP]$; where $P = [2F_C^2 + Max(F_0^2, 0)]/3$

The acute N(1)–Cu(2)–N(2) (80.4(2)°) and O(1)–Cu(2)–O(2) (51.8(1)°) bond angles produce marked differences in the coordination sphere with respect to regular octahedral coordination. The smaller difference (23.3°) between the angles Cu(2)–O(1)–C(11) (109.5(4)°) and Cu(1)–O(1)–C(11) (132.8(2)°) indicates significant tilt of the carboxylate toward Cu(2). The bridging angle of Cu(1)–O(1)–Cu(2) is 109.1(2).

Hydrogen bonding interactions between the oxygen atom of chloroacetato and bpy generate a 1D chain (C4–H4···O2, 2.509(4); C7–H7···O2, 2.440(4)Å). Further H-bonding involving C-H…Cl interactions ((C3–H3···Cl2, 2.879(3); C14–H14···Cl3, 2.881(2) Å) as well as π-stacking interactions between bpy rings (3.435-3.466 Å) generates a 3D network (Figure 6.2). Details of the H-bonding and π-stacking interactions are given in Table 6.7.

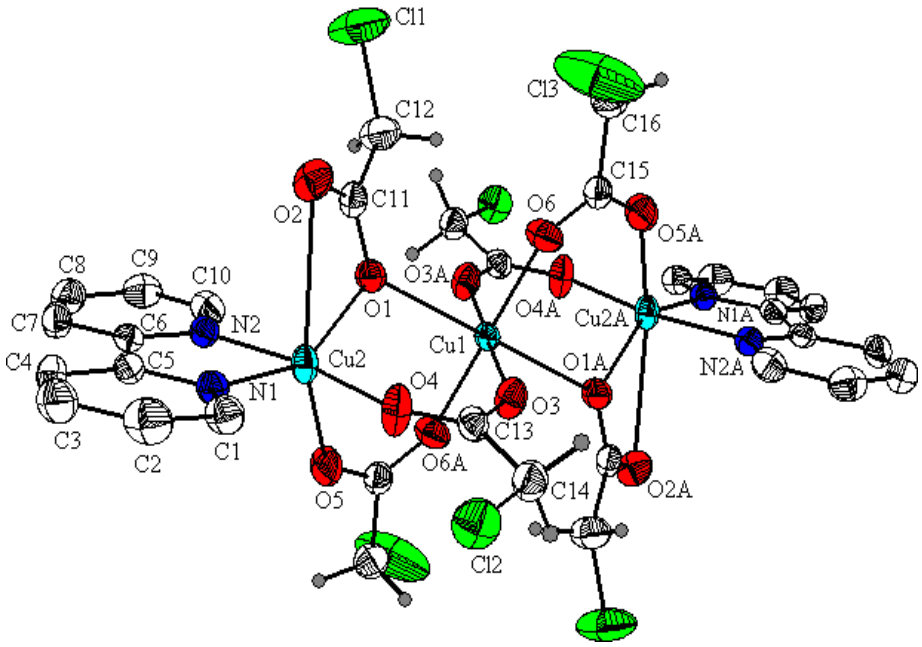

Figure 6.1. Thermal ellipsoid plot of the coordination environment of the complex molecules **1**: Atoms are represented as 30% probability ellipsoids. Ring hydrogen atoms have been omitted for clarity. Symmetry code: A, –*x*+1, –*y*+1, –*z*

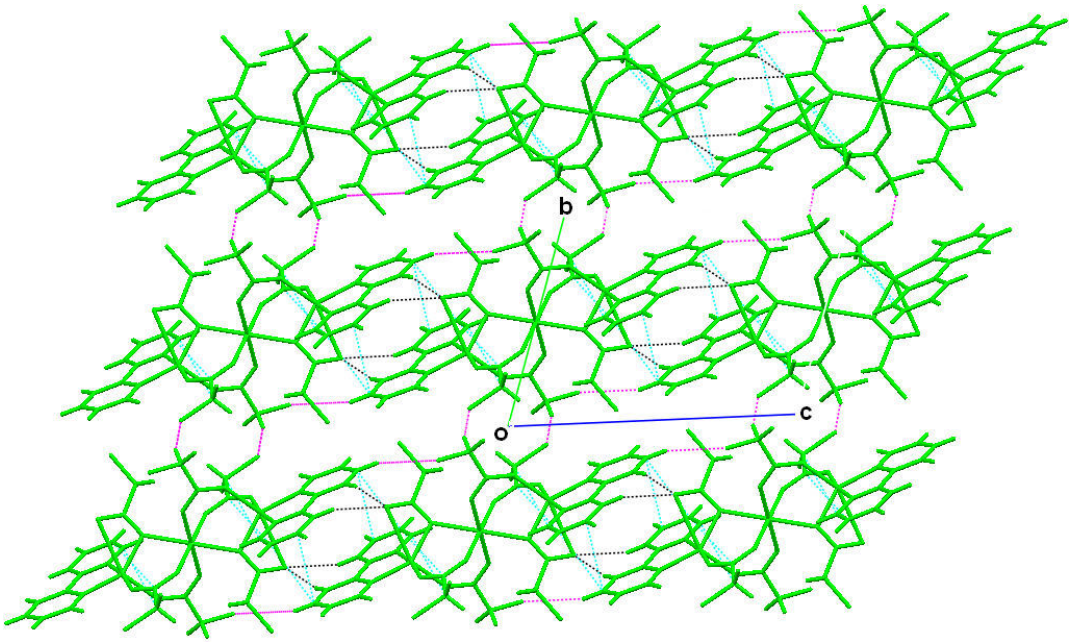

Figure 6.2. Molecular packing in the *bc*-plane of **1**

Table 6.2: Selected bond lengths (Å) and bond angles (˚) of **1**

Cu(1)-O(6)	1.952(3)	O(1)-Cu(2)-O(2)	51.81(15)
Cu(1)-O(3)	1.993(4)	O(1)-Cu(2)-O(4)	98.74(15)
Cu(1)-O(1)	2.350(3)	O(1)-Cu(2)-O(5)	97.00(16)
Cu(2)-O(1)	1.983(3)	O(1)-Cu(2)-N(1)	144.30(16)
Cu(2)-O(5)	1.928(3)	O(1)-Cu(2)-N(2)	91.97(16)
Cu(2)-N(2)	1.984(4)	O(2)-Cu(2)-O(4)	149.57(16)
Cu(2)-N(1)	2.006(4)	O(2)-Cu(2)-O(5)	100.34(16)
Cu(2)-O(4)	2.119(4)	O(2)-Cu(2)-N(1)	92.57(16)
Cu(2)-O(2)	2.793(3)	O(2)-Cu(2)-N(2)	83.52(16)
O(1)-Cu(1)-O(3)	93.80(14)	O(4)-Cu(2)-O(5)	89.64(17)
O(1)-Cu(1)-O(3)#1	86.20(14)	O(4)-Cu(2)-N(1)	116.11(16)
O(1)-Cu(1)-O(6)	88.46(13)	O(4)-Cu(2)-N(2)	91.12(16)
O(1)-Cu(1)-O(6)#1	91.54(13)	O(5)-Cu(2)-N(1)	91.00(16)
O(3)-Cu(1)-O(6)	89.44(16)	O(5)-Cu(2)-N(2)	170.77(16)
O(3)-Cu(1)-O(6)#1	90.56(16)	N(1)-Cu(2)-N(2)	80.41(17)
Cu(1)-O(1)–Cu(2)	109.13(16)	#1, *–x*+1, *–y*+1, *–z*	

6.5.3. Crystal structure of $[Cu_2(bpy)_2(\mu\text{-}Cl_2CHCOO)_2(Cl_2CHCOO)_2]$ (2)

The molecular structure of **2** is shown in Figure 6.3. Selected bond lengths and angles are listed in Table 6.3. The molecule has a crystallographic inversion center. The crystal structure of **2** consists of a dinuclear unit, $[Cu_2(bpy)_2(\mu\text{-}Cl_2CHCOO)_2(Cl_2CHCOO)_2]$, in which each pair of Cu(II) ions are linked by two monoatomic dichloroacetate bridges (μ_2-κ^2O). The second oxygen atom of the dichloroacetate group remains uncoordinated and is involved only in H-bonding interactions. The bond lengths C11–O1 1.280(5) and C11–O2 1.203(6) Å also indicate coordination through single oxygen only.

Each of the Cu(II) ions are further coordinated by one oxygen atom of additional bidentate dichloroacetate group and two nitrogen atoms of a chelating bpy ligand, forming two equivalent but distorted octahedral geometry. The bond distances of Cu–N(1) 1.997(3), Cu–N(2) 1.989(3), Cu–O(1) 1.964(2), Cu–O(3) 1.964(2), Cu–O(1A) 2.416(2) and Cu–O(4) 2.770(3) Å). The bond length of Cu–O(1A) 2.416(2) Å) is notably longer than that of Cu–O(3) 1.964(2) Å), which may be due to the monoatomic bridging mode of the O(1) atom. The bond distances Cu–O1 and Cu–O1A are 1.964(2) and 2.416(2) Å, respectively, which show that the bridging is highly unsymmetrical through a single oxygen O1 of the dichloroacetate group (A = $-x$, $-y$, $-z+1$). The two square pyramids in the dimer are sharing one equi-to-axial edge with parallel equatorial planes. The oxygen atom of a bridging dichloroacetate group occupies an equatorial position of one Cu(II) ion and the axial position of the neighboring Cu(II) ion. The most distorted angle in the octahedron around the Cu(II) atom N(1)–Cu–N(2) is 81.12(11)° produces significant differences in the coordination sphere with respect to regular octahedral coordination. The Cu···Cu distance is 3.319(9)Å. The bridging angle of Cu–O(1)–Cu(A) is 98.0(1)º. This complex is quite similar to the previously reported analogous complexes [Cu_2(μ-

$ClCH_2CO_2)_2(ClCH_2CO_2)_2(NITpPy)_2(H_2O)_2]\cdot CH_3OH$, (NITpPy = 4,4,5,5-tetramethyl-2-(4-pyridyl)-2-imidazoline-N^1-oxy N^3-oxide)[26a] $[Cu_2(bpy)_2(L)_4]\cdot 2H_2O$ (L= 2-phenylacetato),[26b] $[Cu_2(bpy)_2(L)_4]\cdot 0.5H_2O$ (L= iodoacetato),[26c] $[Cu_2(bpy)_2(L)_4]$ (L= benzoate),[26d] $[Cu_2(bpy)_2(OAc)_4]\cdot 2H_2O$,[22] $[Cu_2(phen)_2(L)_4]\cdot 2H_2O$ (L= 2-chlorobenzoato).[26e]

The crystal packing analyses indicate that both intermolecular H-bonding and π…π interactions combine to stabilize the extended structure (Figure 6.4). The crystal structure forms 2D network with various C–H···O interactions (C14–H14···O4, 2.262(3); C4–H4···O4, 2.352(3) Å). These chains are further extends into 3D network with C–H···Cl interactions (C1–H1···Cl(1), 2.882(1); C10–H10···Cl(1), 2.958(2) Å) as well as π-stacking (3.410-3.493 Å) between the bpy rings. Details of the H-bonding and π-stacking interactions are given in Table 6.7.

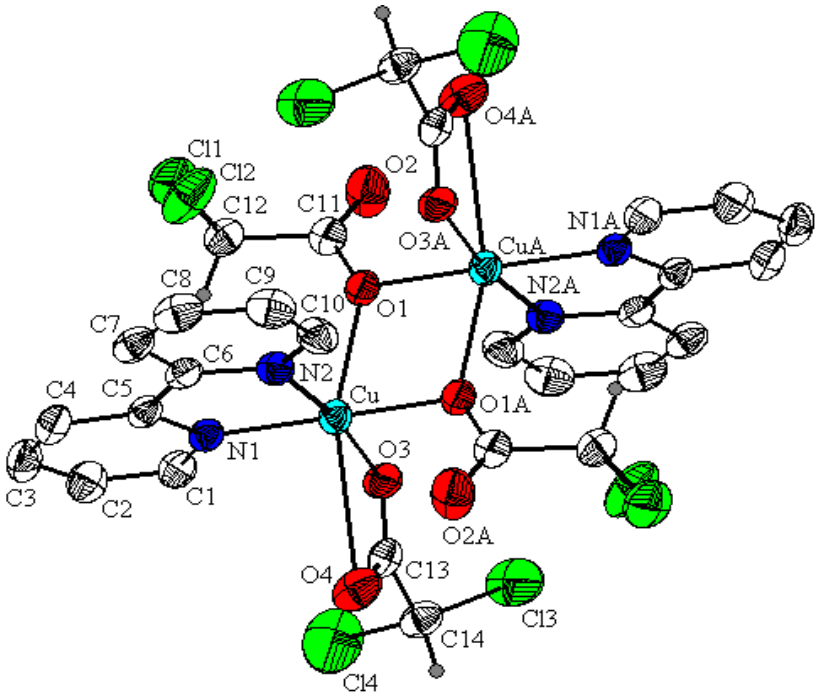

Figure 6.3. Thermal ellipsoid plot of the coordination environment of the complex molecules **2**: Atoms are represented as 30% probability ellipsoids. Ring hydrogen atoms have been omitted for clarity. Symmetry code: A, –*x*, –*y*, –*z*+1.

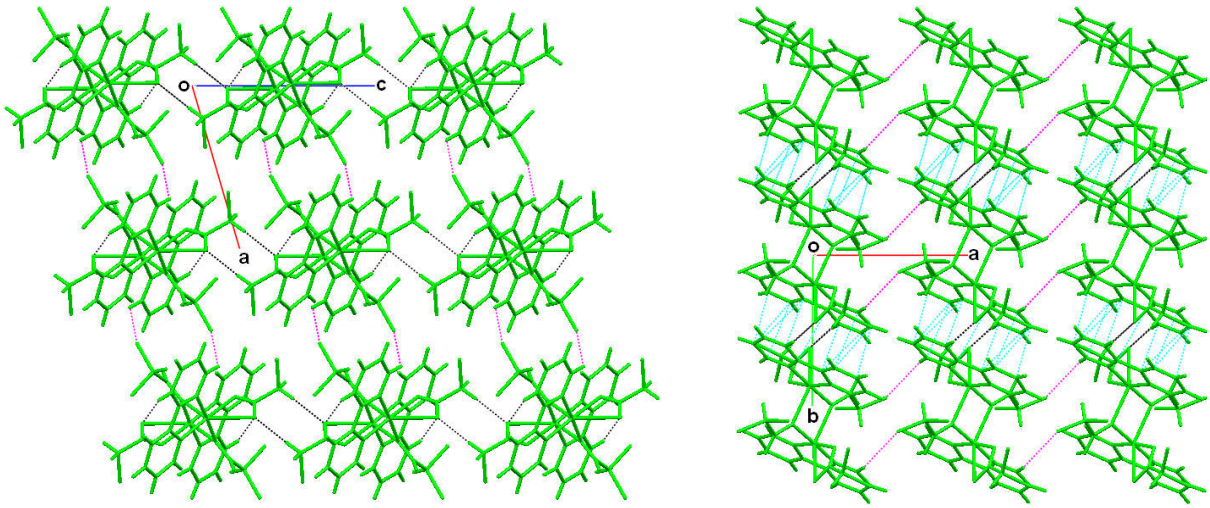

(a) **(b)**

Figure 6.4. The molecular packing of **2** viewed down the (a) *b*-axis and (b) *c*-axis.

Table 6.3: Selected bond lengths (Å) and bond angles (˚) of **2**

Cu–O(1)	1.964(2)	Cu–O(1)#1	2.416(2)
Cu–O(3)	1.964(2)	Cu–O(4)	2.770(3)
Cu–N(1)	1.997(3)	Cu–N(2)	1.989(3)
O(1)–Cu-O(1)#1	82.00(9)	O(3)–Cu-O(1)#1	90.44(9)
O(1)–Cu-O(3)	89.54(10)	O(3)–Cu-O(4)	52.34(11)
O(1)–Cu-O(4)	94.21(10)	O(3)–Cu-N(1)	93.43(11)
O(1)–Cu-N(1)	176.90(10)	O(3)–Cu-N(2)	170.77(11)
O(1)–Cu-N(2)	95.82(11)	O(4)–Cu-O(1)#1	142.74(11)
N(1)–Cu-O(1)#1	98.85(10)	O(4)–Cu-N(1)	86.92(11)
N(2)–Cu-O(1)#1	97.73(10)	O(4)–Cu-N(2)	119.52(11)
N(1)–Cu-N(2)	81.12(11)	Cu-O(1)-Cu#1	98.00(9)
#1, –*x*, –*y*, –*z*+1			

6.5.4. Crystal structure of $[Cu_2(bpy)_2(\mu\text{-}Cl_3CCOO)_2(Cl_3CCOO)_2]$ (3)

The molecular structure of **3** is shown in Figure 6.5. Selected bond lengths and angles are listed in Table 6.5. The crystal structure of **3** consists of a dinuclear unit, $[Cu_2(bpy)_2(\mu\text{-}Cl_3CCOO)_2(Cl_3CCOO)_2]$, in which each pair of Cu(II) ions are linked by two *syn-anti*

trichloroacetate bridges. Each of the Cu(II) ions are further coordinated with one additional monodentate terminal trichloroacetate group and two nitrogen atoms from a chelating bpy ligand, forming two non-equivalent distorted square-pyramidal geometry. The second oxygen atom of the trichloroacetate group remains uncoordinated and is involved only in H-bonding interactions. The equatorial plane is formed by the two nitrogen atoms from the chelated bpy ligand, one oxygen atom from the monodentate trichloroacetate group and another oxygen atom from the bridging trichloroacetate group [Cu(1)–N(1) 2.001(4), Cu(1)–N(2) 1.997(4), Cu(1)–O(1) 1.941(3), Cu(1)–O(3) 1.928(3) Å and Cu(2)-N(3) 1.997(4), Cu(2)-N(4) 1.998(4), Cu(2)-O(7) 1.942(3), Cu(2)-O(6) (1.926(3) Å)]. The axial site of each copper square pyramid is occupied by the second oxygen atom from the bridging trichloroacetate groups [Cu(1)–O(5) 2.249(3) and Cu(2)-O(4) 2.255(3) Å]. The oxygen atom of a bridging trichloroacetate group occupies an equatorial position of one Cu(II) ion and the axial position of the neighboring Cu(II) ion. Cu(1) lies only 0.1565, above the N(1), N(2), O(1), O(3) least-squares plane toward O(5) and Cu(2) lies 0.1586 towards O(4). This complex is very similar to the previously reported complexes $[Cu_2(O_2CMe)_4(bpy)_2]\cdot 2H_2O$,[27c] $[Cu_2(L)_4(phen)_2]\cdot 2H_2O$ (L = 2,3,4,5-tetrafluoro benzoate).[27d] The unusual *syn-anti* bridging mode results in a significant lengthening of the Cu···Cu distance [4.481(7) Å], which is very long for a doubly-bridged complex (Table 6.4). In dinuclear complexes, the Cu···Cu distance generally increases as the number of bridging ligands decreases, with that of four bridging ligands falling in the range 2.58-2.76 Å, that of three bridging ligands falling in the range 2.85-3.39 Å and that of two bridging ligands falling in the range 3.01-4.50 Å but only few examples, with a Cu···Cu separation above 4.0 Å. For one bridging ligand, only few examples reported, with a distance of 5.25 Å (Table 6.4). In the crystal packing, uncoordinated oxygen atom of trichloroacetate groups are interconnect bpy ligands with

various C–H···O interactions (C9–H9···O8, 2.425(3); C17–H17···O8, 2.463(3) Å) forming intermolecular hydrogen bonds. These are further linked through intermolecular C–H···Cl interactions (C2–H2···Cl10, 2.809(1); C8–H8···Cl8, 2.851(1); C18–H18···Cl5, 2.861(1); C3–H3···Cl4, 2.863(1) Å) as well as π-stacking between bpy rings (3.346-3.434 Å) forming zig-zag chains along the *a*-axis (Figure 6.6). Details of the H-bonding and π-stacking interactions are given in Table 6.7.

Table 6.4 : Magnetic behavior of dinuclear Cu(II) complexes with μ-O_2CR previously studied

	No. of bridges	Cu···Cu (Å)	Mag. behavior	Reference
1	1 μ-O_2CR	5.25	AF	[28]
2	2 μ-O_2CR (di atomic)	4.50	AF	[27], pw
3	2 μ-O_2CR (mono)	3.24-3.53	F or AF	[26, 29], pw
4	3 μ-O_2CR	2.85-3.39	F	[30]
5	4 μ-O_2CR	2.58-2.76	AF	[31]

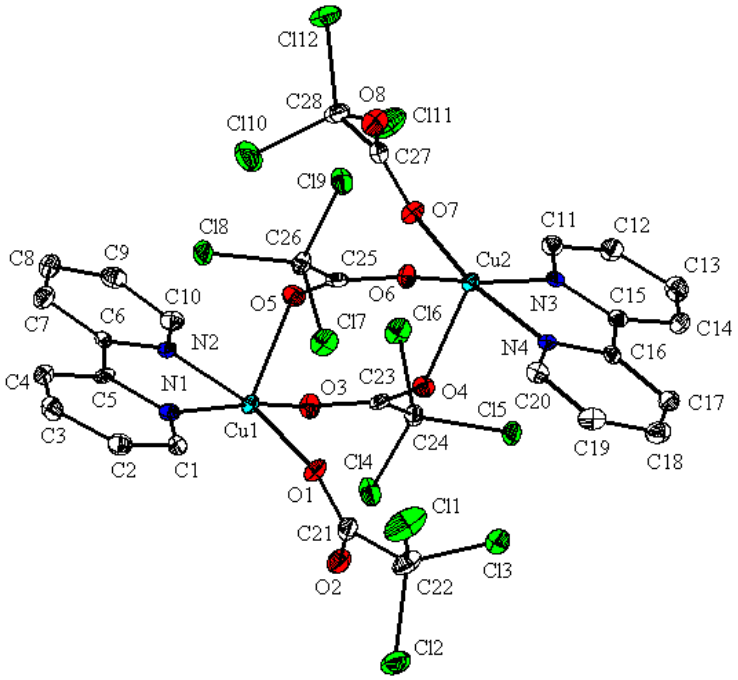

Figure 6.5. Thermal ellipsoid plot of the coordination environment of the complex molecules **3**: Atoms are represented as 30% probability ellipsoids. Ring hydrogen atoms have been omitted for clarity.

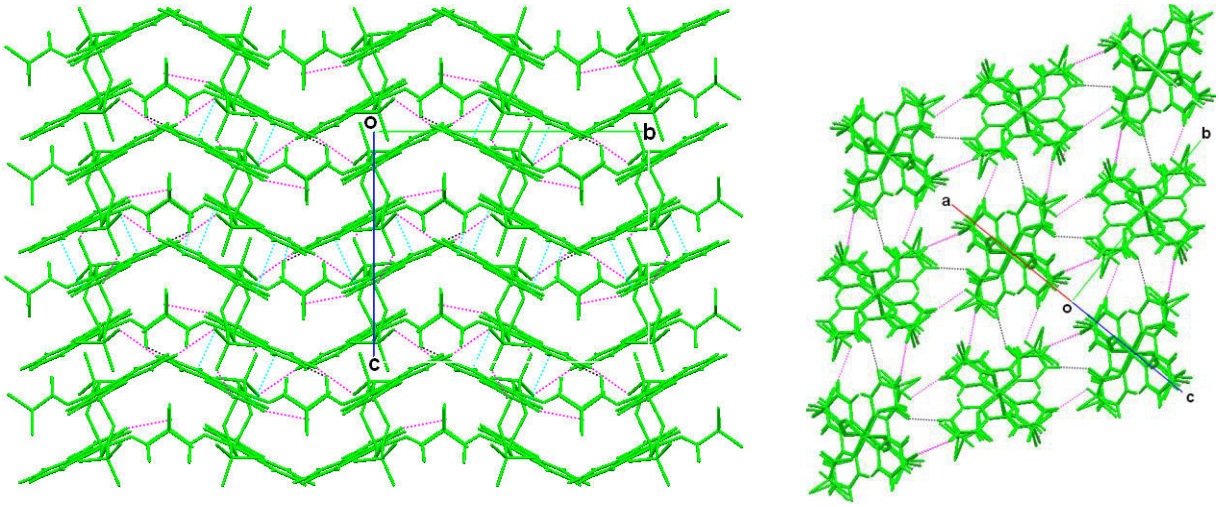

(a) **(b)**

Figure 6.6. crystal packing showing C-H…O (black), C-H…Cl (pink) and π…π (blue) interactions in **3**

Table 6.5: Selected bond lengths (Å) and bond angles (˚) for **3**

Cu(1)-N(1)	2.001(4)	Cu(2)-N(3)	1.997(4)
Cu(1)-N(2)	1.997(4)	Cu(2)-N(4)	1.998(4)
Cu(1)-O(1)	1.941(3)	Cu(2)-O(4)	2.255(3)
Cu(1)-O(3)	1.928(3)	Cu(2)-O(6)	1.926(3)
Cu(1)-O(5)	2.249(3)	Cu(2)-O(7)	1.942(3)
N(1)-Cu(1)-N(2)	80.86(14)	N(3)-Cu(2)-N(4)	81.30(15)
N(1)-Cu(1)-O(1)	90.00(14)	N(3)-Cu(2)-O(4)	92.16(13)
N(1)-Cu(1)-O(3)	166.38(14)	N(3)-Cu(2)-O(6)	166.78(14)
N(1)-Cu(1)-O(5)	91.38(12)	N(3)-Cu(2)-O(7)	90.18(14)
N(2)-Cu(1)-O(1)	169.01(14)	N(4)-Cu(2)-O(4)	90.84(13)
N(2)-Cu(1)-O(3)	90.92(14)	N(4)-Cu(2)-O(6)	90.51(14)
N(2)-Cu(1)-O(5)	90.64(13)	N(4)-Cu(2)-O(7)	169.06(14)
O(1)-Cu(1)-O(3)	96.84(13)	O(4)-Cu(2)-O(6)	98.36(12)
O(1)-Cu(1)-O(5)	95.70(12)	O(4)-Cu(2)-O(7)	96.37(12)
O(3)-Cu(1)-O(5)	99.60(12)	O(6)-Cu(2)-O(7)	96.55(13)

6.5.5. Crystal structure of $[Cu_2(bpy)_2(\mu\text{–}OH)(\mu\text{–}OH_2)(\mu\text{–}ClCH_2COO)](ClO_4)_2$ (4)

The molecular structure of **4** is shown in Figure 6.7. Selected bond lengths and angles are listed in Table 6.6. The dinuclear Cu(II) unit of **4** is triply bridged by three different ligands and consists of a dinuclear $[Cu_2(bpy)_2(\mu\text{-}OH)(\mu\text{-}OH_2)(\mu\text{-}ClCH_2COO)]^{2+}$ cation with two uncoordinated ClO_4^- anions. Each Cu(II) ion has a distorted square pyramidal environment (τ = 0.19 and 0.21 for Cu(1) and Cu(2), respectively). The equatorial plane is formed by the two nitrogen atoms from a chelated bpy ligand (Cu–N distances range between 1.992(3) and 1.996(4) Å), one oxygen atom from the diatomic bridging chloroacetato (μ_2-κO:κO'), [Cu(1)–O(3) 1.933(3) and Cu(2)–O(4) 1.947(2) Å, respectively] and one oxygen atom from the hydroxo ligand, which is same for both Cu(1) and Cu(2) [Cu(1)–O(1) and Cu(2)–O(1) distance of 1.920(3) Å]. The discrimination between OH^- and H_2O was made from the Cu–O distances. The chloroacetate ligand adopts a bidentately bridging *syn-syn* coordination mode with oxygen atoms linking two Cu(II) centers. The axial position is occupied by a bridging water molecule at a longer distance of 2.421(4) and 2.402(3) Å for Cu(1) and Cu(2) respectively. The copper atoms are displaced from the equatorial plane towards the axial O(2) atom of aqua by 0.1067(4) and 0.1314(4)Å. The CuN2O2 chromophores are non-planar with dihedral angles of 11.54(1) and 13.87(1)º between the CuN2 and CuO2 planes for Cu(1) and Cu(2) respectively. The dihedral angle between the equatorial planes is 58.25°. The bridging Cu(1)–O(1)–Cu(2) angle is 105.94(1)º. The Cu···Cu separation is 3.065(8) Å, noticeably shorter than in **1-3** due to the greater number of monoatomic bridges. Comparisons of structural and magnetic properties of the complex moiety, $[Cu_2(bpy)_2(\mu\text{-}OH)(\mu\text{-}OH_2)(\mu\text{-}ClCH_2COO)]^{2+}$ are made with isostructural compounds having similar cationic units but different counter ions (Table 6.9). The lattice is stabilized by hydrogen bonding between the bridging hydroxo group and the oxygen atom of the

perchlorate anion with a O1–H1A···O8 distance of 2.25(5)Å; between the oxygen atom of bridging aqua group and the oxygen atom of perchlorate anion with O2–H2A···O8 contacts of 2.21(5)Å.

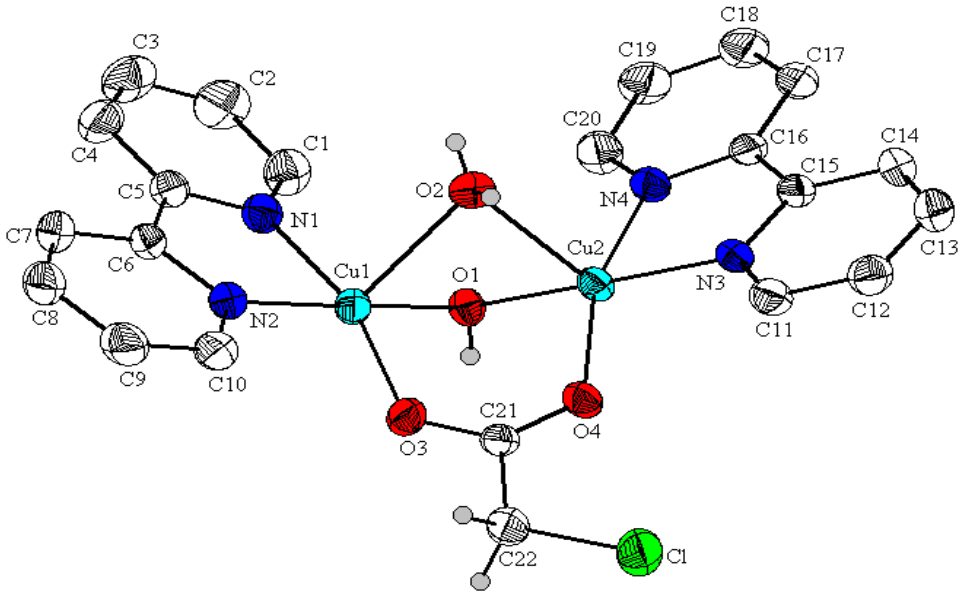

Figure 6.7. Thermal ellipsoid plot of the coordination environment of the complex molecules **4**: Atoms are represented as 30% probability ellipsoids. Lattice perchlorate and ring hydrogen atoms have been omitted for clarity.

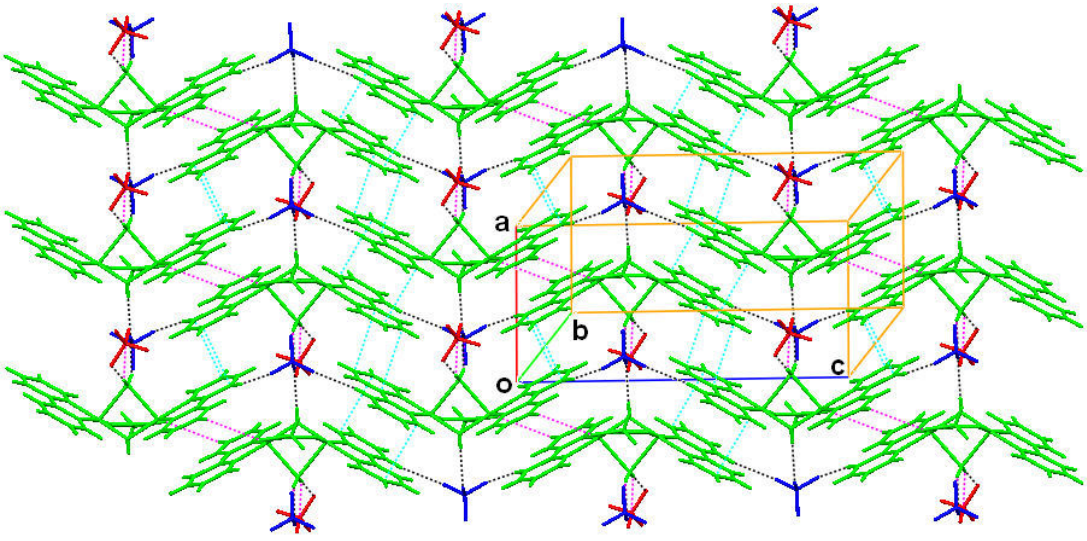

Figure 6.8. crystal packing showing C-H…O (black), C-H…Cl (pink) and π…π (blue) interactions in **4**

These are further linked through intermolecular O–H···Cl interactions (O2–H2A···Cl(2), 2.93(4); O2–H2B···Cl(3), 2.96(4) Å) as well as π- stacking between bpy rings (3.346-3.434 Å) forming zig-zag chains (Figure 6.8). Details of the H-bond geometry and π-stacking interactions are given in Table 6.7.

Table 6.6: Selected bond lengths (Å) and bond angles (˚) of **4**

Cu(1)-N(1)	1.992(3)	Cu(2)-N(3)	1.996(3)
Cu(1)-N(2)	1.996(3)	Cu(2)-N(4)	1.988(3)
Cu(1)-O(1)	1.920(3)	Cu(2)-O(1)	1.920(3)
Cu(1)-O(2)	2.421(3)	Cu(2)-O(2)	2.401(3)
Cu(1)-O(3)	1.933(3)	Cu(2)-O(4)	1.947(3)
Cu(1)-Cu(2)	3.065(3)		
N(1)-Cu(1)-N(2)	81.13(14)	N(3)-Cu(2)-N(4)	81.06(13)
N(1)-Cu(1)-O(1)	95.23(13)	N(3)-Cu(2)-O(1)	175.77(12)
N(1)-Cu(1)-O(2)	96.08(13)	N(3)-Cu(2)-O(2)	101.63(12)
N(1)-Cu(1)-O(3)	165.06(13)	N(3)-Cu(2)-O(4)	89.12(12)
N(2)-Cu(1)-O(1)	176.30(13)	N(4)-Cu(2)-O(1)	94.88(12)
N(2)-Cu(1)-O(2)	101.42(12)	N(4)-Cu(2)-O(2)	99.15(13)
N(2)-Cu(1)-O(3)	89.19(13)	N(4)-Cu(2)-O(4)	163.20(13)
O(1)-Cu(1)-O(2)	79.59(11)	O(1)-Cu(2)-O(2)	80.10(12)
O(1)-Cu(1)-O(3)	94.23(12)	O(1)-Cu(2)-O(4)	94.55(12)
O(2)-Cu(1)-O(3)	96.99(12)	O(2)-Cu(2)-O(4)	96.16(12)
Cu(1)-O(1)-Cu(2)	105.94(12)	Cu(1)-O(2)-Cu(2)	78.93(12)

Table 6.7: Intermolecular interaction parameters

*H-bonding for **1***

D-H···A	**D-H(Å)**	**H···A(Å)**	**D-H···A(˚)**
C(4)-H(4)···O(2)#1	0.95	2.51	163
C(7)-H(7)···O(2)#1	0.95	2.44	159
C(3)-H(3)···Cl(2)#2	0.95	2.88	155
C(14)-H(14A)···Cl(3)#3	0.95	2.88	157
(#1) *–x, 1–y, 1–z*	(#2) *x, y, 1+ z*	(#3) *x, 1+y, z*	

H-bonding for ***2***

C(4)-H(4)···O(4)#1	0.95	2.35	160
C(7)-H(7)···O(4)#1	0.95	2.51	155
C(14)-H(14)···O(4)#2	0.95	2.62	172
C(1)-H(1)···Cl(1)#3	0.95	2.88	128
C(10)-H(10)···Cl(1)#4	0.95	2.96	147
(#1) *–x, 1–y, 1–z*	(#2) *–x,*1*–y, –z*	(#3) 1+*x, y, z*	(#4) –1-*x, –y, 1–z*

H-bonding for ***3***

C(4)-H(4)···O(2)#1	0.95	2.55	146
C(9)-H(9)···O(8)#2	0.95	2.43	172
C(14)-H(14)···O(8)#3	0.95	2.56	147
C(17)-H(17)···O(8)#3	0.95	2.46	139
C(19)-H(19)···O(8)#4	0.95	2.43	172
C(2)-H(2)···Cl(10)#5	0.95	2.81	154
C(3)-H(3)···Cl(4)#1	0.95	2.86	138
C(8)-H(8)···Cl(8)#2	0.95	2.85	159
C(18)-H(18)···Cl(5)#4	0.95	2.86	152

(#1) 2*–x, –y,* 1*–z* (#2) *x, –*$^1/_2$*–y,* $^1/_2$*+z* (#3) 1*–x, –y, –z* (#4) *x,*$^1/_2$*–y,*$^1/_2$*+z* (#5) 2*–x,*$^1/_2$*+y,*$^1/_2$*–z*

H-bonding for ***4***

O(1)-H(1A)···O(8)	0.95	2.25	179
O(2)-H(2B)···O(9)	0.95	2.26	175
O(2)-H(2A)···O(8)#1	0.95	2.21	153
C(4)-H(4)···O(5)#2	0.95	2.42	172
C(14)-H(14)···O(7)#3	0.95	2.48	172
C(18)-H(18)···O(7)#4	0.95	2.49	157
O(2)-H(2B)···Cl(3)	0.95	2.96	152
O(2)-H(2A)···Cl(2)#5	0.95	2.93	162
C(18)-H(18)···Cl(1)#6	0.95	3.06	122

(#1) 1+*x, y, z;* (#2) 1-*x,* 1*–y,* 1*–z*; (#3) 1-*x,1-y,-z*; (#4) *x, 1+y, z*; (#5) –1+*x, y, z*; (#6) 1*–x,* 1*–y, –z*

π···π interaction for ***1***

C(3)···C(8)#1	3.466(7)	C(3)···C(9)#1	3.435(7)
C(9)···C(15)#2	3.219(7)	C(10)···C(16)#2	3.477(7)
(#1) *–x,* 1*–y,* 1*–z*	(#2) *–x,*1*–y, –z*		

π···π interaction for ***2***			
C(1)···C(7)#1	3.475(5)	C(3)···C(6)#1	3.493(5)
C(2)···C(7)#1	3.490(5)	C(4)···C(6)#1	3.442(5)
C(2)···C(8)#1	3.463(5)	C(5)···C(5)#1	3.410(5)
(#1) *–x*, 1*–y*, 1*–z*			
π···π interaction for ***3***			
C(2)···C(10)#1	3.352(6)	C(7)···C(21)#1	3.418(6)
C(12)···C(20)#2	3.346(6)	C(17)···C(27)#2	3.434(6)
(#1) 2*–x, –y,* 1*–z*	(#2) 1*–x, –y, –z*		
π···π interaction for ***4***			
C(1)···C(9)#1	3.427(8)	C(6)···C(8)#2	3.454(8)
C(12)···C(14)#3	3.471(8)		
(#1) 1*–x,* 1*–y,*1*–z*; (#2) *–x,*1*–y,*1*–z*; (#3) *–x,*1*–y, –z*			

6.6. Spectroscopic properties

All of the compounds obtained gave satisfactory elemental analysis and were characterized by IR, PXRD, diffuse reflectance spectroscopy and ESR spectroscopy.

6.6.1. PXRD measurements

Powder X-ray diffraction experiments have been done to check the homogeneity of the bulk crystalline powders of **1–4** by comparison of the simulated and experimental X-ray powder diffraction patterns. As shown in Figure 6.9, the peak positions of the experimental patterns agree with the corresponding simulated patterns from the single-crystal X-ray diffraction data for **1–4**.

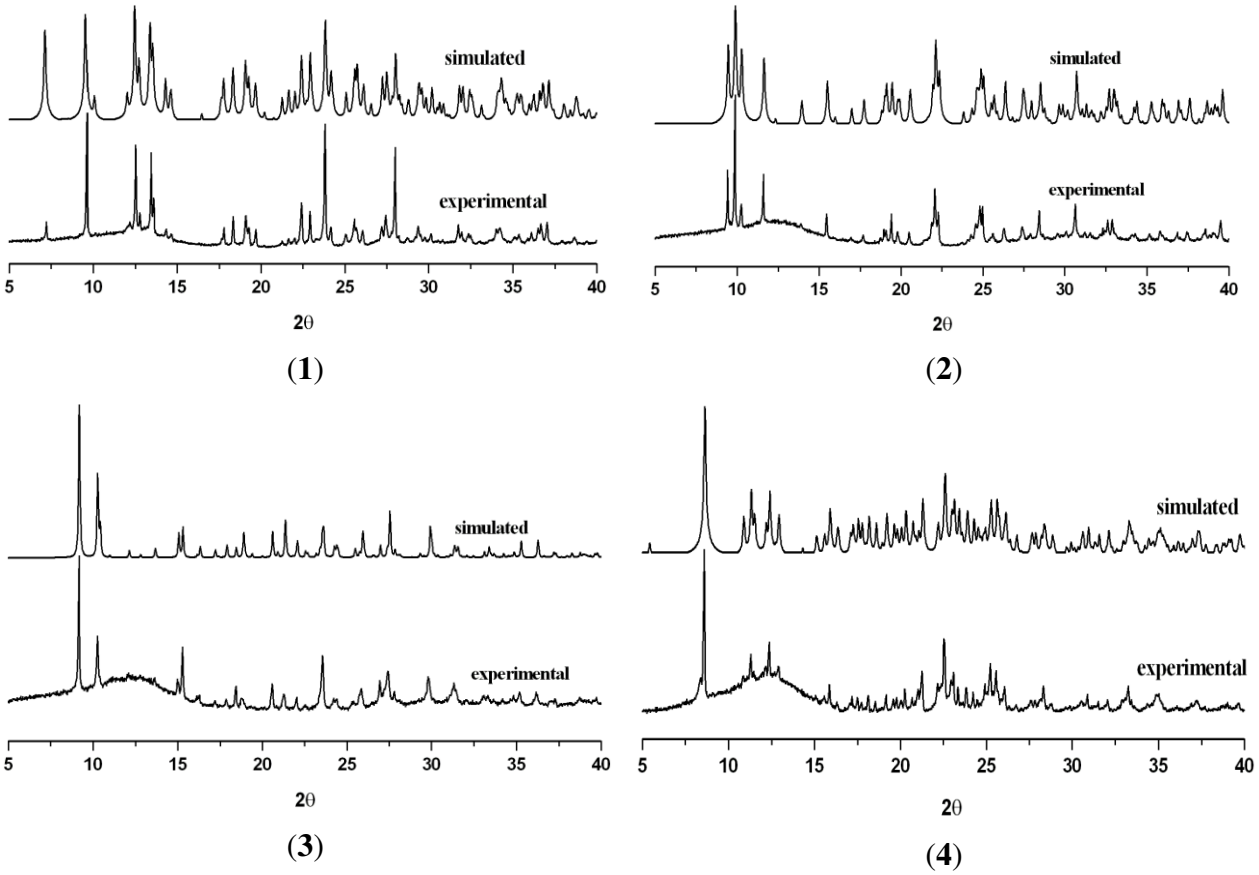

Figure 6.9. Powder X-ray diffraction computer simulated and experimental patterns of complexes **1-4**

6.6.2. Infrared spectra

The IR spectra of **1-3** exhibit two ν_{as}(COO) and two ν_s(COO) stretching bands, indicating the presence of two carboxylate ligands involved in different coordination modes. The intense bands at 1605 and 1380 cm^{-1} ($\Delta\nu$ = 225 cm^{-1}) are attributed to the monoatomic carboxyl group, the bands at 1555 and 1397 cm^{-1} ($\Delta\nu$ = 158 cm^{-1}) are attributed to the asymmetric monoatomic carboxylate bridging ligand and the bands at 1555 and 1448 cm^{-1} ($\Delta\nu$ = 107 cm^{-1}) are attributed to the triatomic carboxylate bridging ligand. The IR spectra of **4** exhibits a intense band at 3528 cm^{-1} due to the bridging O−H and a broad medium band at 3389 cm^{-1} is attributed to the absorptions of water molecule. A broad band corresponding to the ClO_4^- anion vibration near

1120 cm^{-1} indicating the involvement of anion in H-bonding. The stretching vibrations corresponding to those typical of coordinated bpy occur at 730, 830, 1030, 1210 and 1600 cm^{-1}.

6.6.3. Electronic spectra

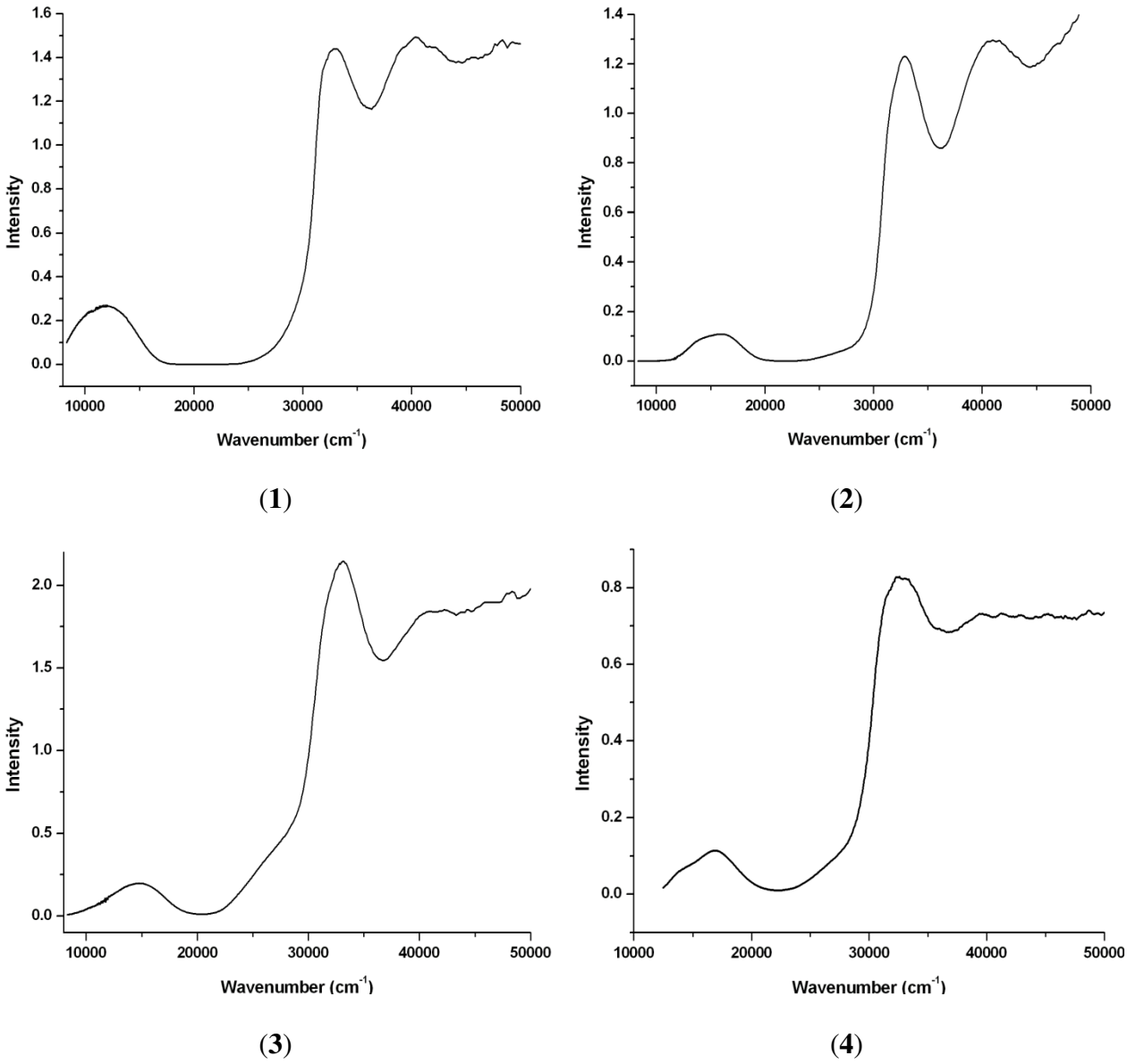

Figure 6.10. Diffuse reflectance spectra of complexes **1-4**

Diffuse reflectance spectra of **1-4** were shown in Figure 6.10. The spectrum of **1** shows a broad band centered at 12,200 cm^{-1} ($d_{xy,}$ $d_{xz} \approx d_{yz} \rightarrow d_{x2-y2}$) and a poorly resolved shoulder peak at approximately 10,380 cm^{-1} ($d_{z2} \rightarrow d_{x2-y2}$), is consistent with the distorted octahedral coordination polyhedron. The spectrum of **2** consists an asymmetric broad band approximately at 16,200 cm^{-1} (d_z^2, d_{yz}, $d_{xz} \rightarrow d_{x2-y2}$) and a lower energy shoulder peak at 14,000 cm^{-1} ($d_{xy} \rightarrow d_{x2-y2}$). These features are consistent with the distorted square pyramidal geometry with a much larger elongation in the axial position.[32] The spectrum of **3** consists of a single broad band centered at 14,700 cm^{-1} (d_{z2}, d_{xy}, d_{xz}, $d_{yz} \rightarrow d_{x2-y2}$) is consistent with the distorted square-pyramidal stereochemistry.[33] The spectrum of **4** consists an asymmetric broad band approximately at 17,000 cm^{-1} and a lower energy shoulder peak at 14,000 cm^{-1}. These features are typical and can be assigned to the d_{xy}, d_{yz}, $d_{xz} \rightarrow d_{x2-y2}$ and $d_{z2} \rightarrow d_{x2-y2}$ transitions for the square pyramidal geometry of the triply-bridged dinuclear Cu(II) compounds.[27] Notice that according to strict symmetry considerations for the distorted square pyramidal geometry, the d_{xy}, d_{yz}, d_{xz} orbitals are not triply degenerated which is the origin of the broad band mentioned above. Band near 33,000 cm^{-1} is due to ligand-to-metal charge transfer transition, while the band near 41,000 cm^{-1} is associated with intra-ligand $\pi \rightarrow \pi^*$ excitation.

6.6.4. ESR spectra

The X-band polycrystalline-powder electron spin resonance (ESR) spectra of **1-3** were measured at both room temperature and 77 K. Compound **4** was measured only at room temperature. All spectra have been normalized to the same microwave frequency (ν = 9.6763 GHz). As discussed in the next section, compound **1** is an antiferromagnetically linear trimer while compound **4** is a ferromagnetically coupled dimer. Based on the reports of similar

compounds, **2** and **3** are also likely to have antiferromagnetic ground states. The EPR of compound **4** shows half field signal (Figure 6.14), characteristic of $S = \mathbf{1}$ ground state, along with the "axial" signals for the allowed transitions with no resolution of the hyperfine splittings.

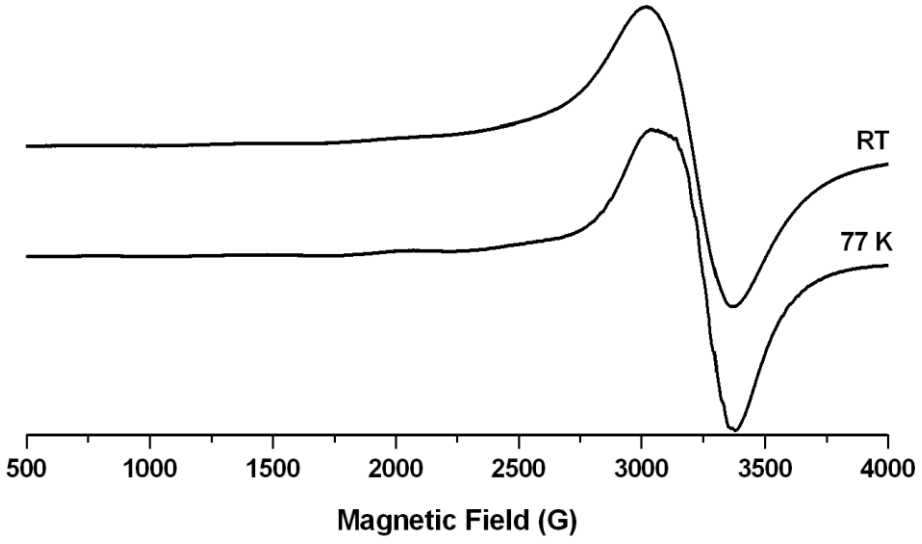

Figure 6.11. EPR spectra at two different temperatures for compound **1**

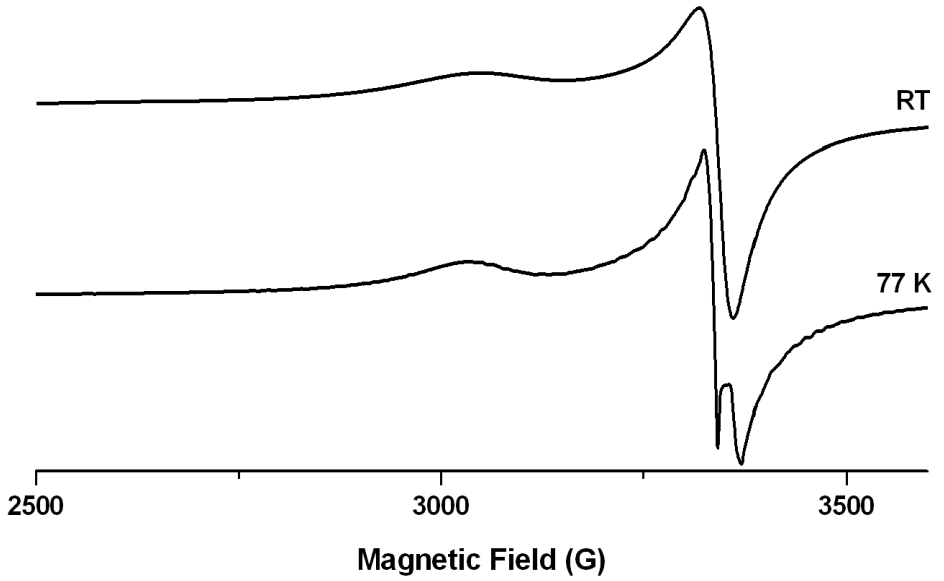

Figure 6.12. EPR spectra at two different temperatures for compound **2**

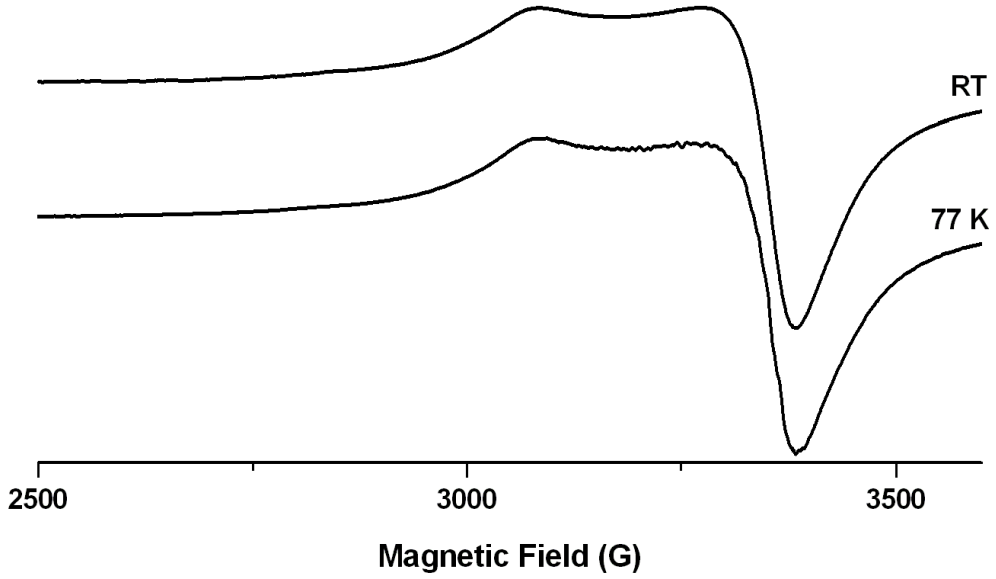

Figure 6.13. EPR spectra at two different temperatures for compound **3**

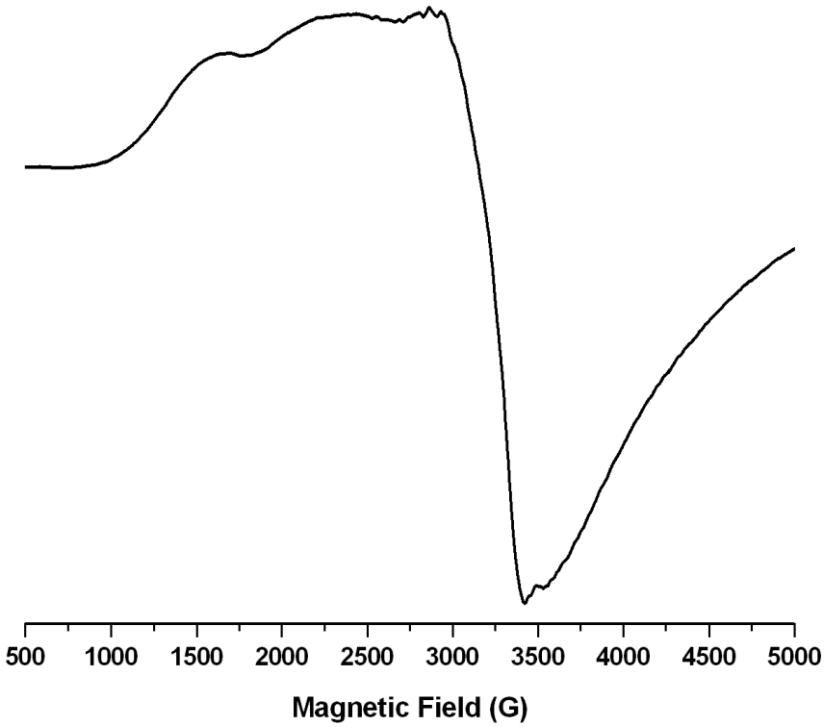

Figure 6.14. EPR spectra of compound **4** at room temperature.

Compounds **2** and **3** show spectra corresponding to axial symmetry with hyperfine couplings averaged out; compound **2** shows rhombic splitting at 77 K. The EPR *g*-values ($g_{||}$ =

2.27, $g_{\perp}$ = 2.069 for **2** and $g_{\parallel}$ = 2.24 and $g_{\perp}$ = 2.07 for **3** respectively) are consistent with a d_{xy} ground state of Cu(II) in low symmetry five coordinate environment (Figure 6.12 and Figure 6.13).[34] The three Cu(II) centres in compound **1** are six-coordinate. Its EPR shows a broad signal at g ~ 2.0 with some unresolved very broad features at lower field (Figure 6.11).

6.7. Magnetic properties

The temperature-dependence of the magnetic susceptibility $\chi_m T$ of **1** and **4** were measured over the range 3-300 K and diamagnetic corrections were calculated from the Pascal constants.[6] The room temperature $\chi_m T$ (cm^3 mol^{-1} K) value for compound **1** (Figure 6.15) per magnetic ion is 0.52 cm^3 mol^{-1} K at 300 K, which is higher than the expected spin-only value, 0.38 cm^3 mol^{-1} K. The moment decreases upon cooling and reaches a plateau around 15−3 K range with a value of 0.15 cm^3 mol^{-1} K per mole. This feature is typical of an isolated trinuclear Cu(II) species with intramolecular antiferromagnetic coupling between adjacent metal ions. Upon further cooling the $\chi_m T$ value decreases to 0.12 cm^3 mol^{-1} K per Cu^{II} at 3 K. The best fit to a linear trimer equation[12] with including temperature independent paramagnetism (TIP) yielded the parameters values J = −51.4(9) cm^{-1}, zJ' = –0.72(1) cm^{-1} g = 2.129(4), TIP = 84 x10^{-5} cm^3mol^{-1} with a residual of 0.4242 x 10^{-3}.

To the best of our knowledge no compound has been reported with a linear trinuclear chloroacetate bridge. The antiferromagnetic interaction observed in compound **1** through the chloroacetate bridges can be explained from the magneto-structural correlations established for the triply-bridged dinuclear $[Cu_2(RCOO)_3]^+$ core (Table 6.8). As the superexchange interaction is operative only through the acetate bridges, the magnitude of the antiferromagnetic interaction ($2J$) might be expected to be dependent on the number of bridging acetate ligands. An

examination of the structure of compound **1** shows that only one chloroacetate bridge links the copper magnetic orbitals directly. Cu(1) and Cu(2) have d_{x2-y2} ground states, but connections to O(1) (Cu(2)–O(1) 1.980 Å, Cu(1)–O(1) 2.350 Å) are axially oriented relative to the magnetic planes, thus creating orthogonal bridging connections, which would lead to insignificant antiferromagnetic exchange. The two *syn-syn* chloroacetate bridge is therefore associated with moderate net intramolecular exchange situation ($J = -51.4(9)$ cm^{-1}).[30,35]

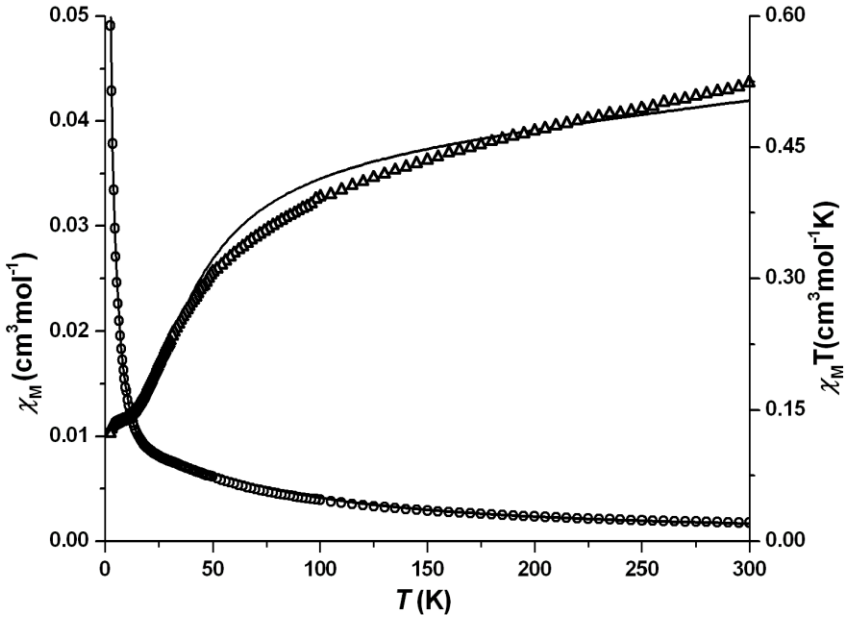

Figure 6.15. Temperature variation of magnetic susceptibility (circle) and $\chi_M T$ product (triangle) per magnetic ion for $[Cu_3(bpy)_2(\mu\text{-}ClCH_2COO)_6]$ (**1**). The solid lines result from a least-square fit to the data of the theoretical values calculated with the trimer equation including TIP.

Table 6.8: Structural and magnetic parameters of triply-bridged Cu(II) complexes with a $[Cu_2(\mu\text{-}OCOR)(\mu\text{-}O_2CR)_2]^+$ core

Complex	Cu···Cu (Å)	Cu−O−Cu	J	Ref.
$[Cu_2(bpy)_2(\mu\text{-}OCOPh)(\mu\text{-}O_2CPh)_2](ClO_4)$	3.386	109.7	−39.4	36
$[Cu_2(bpy)_2(\mu\text{-}OCOPh)(\mu\text{-}O_2CPh)_2](BF_4)$	3.386	109.5	−39.7	36
$[Cu_2(bpy)_2(\mu\text{-}OCOPh)(\mu\text{-}O_2CPh)_2](PF_6)$	3.384	108.3	−31.4	36
$[Cu_3(bpy)_2(\mu\text{-}OCOCH_2Cl)_2(\mu\text{-}O_2CH_2Cl)_4]$	3.536	109.1	−51.4	pw

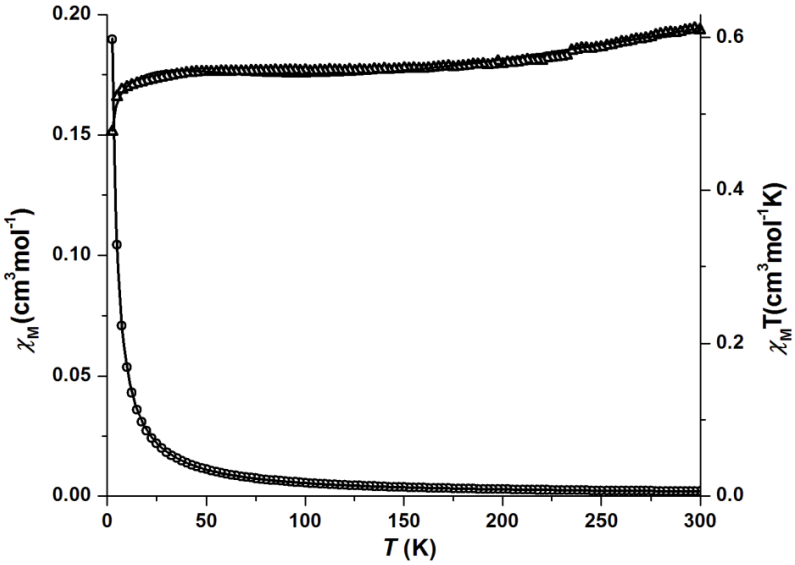

Figure 6.16. Temperature variation of magnetic susceptibility (circle) and $\chi_M T$ product (triangle) per magnetic ion for **4**. The solid lines result from a least-square fit to the data of the theoretical values calculated with Bleaney-Bowers equation including TIP.

Table 6.9: Structural and magnetic data for triply-bridged $[Cu_2(bpy)_2(\mu\text{-OH})(\mu\text{-OH}_2)(\mu\text{-RCOO})]^{2+}$ core

Comp.	τ	Cu···Cu	Cu-O		Cu-OH-Cu	*J* (cm^{-1})	Ref.
			Axial	Equatorial			
1	0.24, 0.25	3.024	2.394, 2.323	1.921–2.009	103.39	102.1	[37]
2	0.14, 0.25	3.035	2.379, 2.405	2.006–2.010	103.8	19.3	[38]
3	0.21, 0.19	3.049	2.347, 2.460	1.938–2.017	104.0	n.d.	[39]
4	0.20, 0.16	3.037	2.382, 2.415	1.920–2.005	104.50	148.9	[40]
5	0.02, 0.14	2.989	2.360, 2.375	1.933–2.020	101.30	120.0	[40]
6	0.21, 0.16	3.002	2.374, 2.390	1.925–2.008	102.10	120.8	[39]
7	0.19, 0.21	3.026	2.344, 2.368	1.925–2.029	103.60	98.4	[36]
8	0.10, 0.22 0.08, 0.26	3.010 3.034	2.419, 2.379 2.425, 2.369	1.911–2.015 1.893–2.012	103.8 0 105.30	151.2	[36]
9	0.10, 0.38	3.077	2.324, 2.409	1.908–1.999	107.26	72.6	[37]
10	0.11, 0.30	3.055	2.323, 2.442	1.918–1.999	105.55	90.2	[37]
11	0.21, 0.22	2.984	2.329, 2.346	1.929–2.003	101.07	104.3	[37]
12	0.34, 0.31	3.007	2.310, 2.323	1.923–2.003	102.57	92.1	[37]
13	0.23, 0.27	2.979	2.321, 2.339	1.931–1.996	100.80	103.1	[37]
14	0.17, 0.19	3.008	2.320, 2.333	1.921–2.012	102.40	98.7	[37]
15	0.19, 0.21	3.065	2.421, 2.401	1.920–1.996	105.94	38.2	pw

1. $[Cu_2(bpy)_2(\mu\text{-}OH)(\mu\text{-}OH_2)(\mu\text{-}O_2CCH_3)](CF_3SO_3)_2$
2. $[Cu_2(bpy)_2(\mu\text{-}OH)(\mu\text{-}OH_2)(\mu\text{-}O_2CCH_3)](ClO_4)_2$
3. $[Cu_2(bpy)_2(\mu\text{-}OH)(\mu\text{-}OH_2)(\mu\text{-}O_2CCH_3)](NO_3)_2$
4. $[Cu_2(bpy)_2(\mu\text{-}OH)(\mu\text{-}OH_2)(\mu\text{-}O_2CCH_2CH_3](ClO_4)_2$
5. $[Cu_2(phen)_2(\mu\text{-}OH)(\mu\text{-}OH_2)(\mu\text{-}O_2CCH_3)](ClO_4)_2$
6. $[Cu_2(phen)_2(\mu\text{-}OH)(\mu\text{-}OH_2)(\mu\text{-}O_2CCH_3)](BF_4)_2\cdot(H_2O)_{0.5}$
7. $[Cu_2(phen)_2(\mu\text{-}OH)(\mu\text{-}OH_2)(\mu\text{-}O_2CCH_2CH_3)](NO_3)_2$
8. $[Cu_2(phen)_2(\mu\text{-}OH)(\mu\text{-}OH_2)(\mu\text{-}O_2CC(CH_3)_3)](ClO_4)_2(CH_3CH_2OH)$
9. $[Cu_2(4,4'\text{-}dmbpy)_2(\mu\text{-}OH)(\mu\text{-}OH_2)(\mu\text{-}OCH)](ClO_4)_2$
10. $[Cu_2(4,4'\text{-}dmbpy)_2(\mu\text{-}OH)(\mu\text{-}OH_2)(\mu\text{-}OCCH_3)](ClO_4)_2$
11. $[Cu_2(5,5'\text{-}dmbpy)_2(\mu\text{-}OH)(\mu\text{-}OH_2)(\mu\text{-}OCCH_3)](ClO_4)_2$
12. $[Cu_2(5,5'\text{-}dmbpy)_2(\mu\text{-}OH)(\mu\text{-}OH2)(\mu\text{-}OCCH_3)](CF_3SO_3)_2$
13. $[Cu_2(5,5'\text{-}dmbpy)_2(\mu\text{-}OH)(\mu\text{-}OH_2)(\mu\text{-}OCCH_2CH_3)](CF_3SO_3)_2$
14. $[Cu_2(5,5'\text{-}dmbpy)_2(\mu\text{-}OH)(\mu\text{-}OH_2)(\mu\text{-}OCC(CH_3)_3)](ClO_4)_2$

The room temperature $\chi_m T$ ($cm^3\ mol^{-1}\ K$) value for compound **4** (Figure 6.16) per magnetic ion is 0.61 $cm^3\ mol^{-1}\ K$ at 300 K, which is higher than the expected spin-only value, 0.38 $cm^3\ mol^{-1}\ K$. While decreasing the temperature, the $\chi_m T$ value also slowly decreased and reached to 0.55 $cm^3\ mol^{-1}\ K$ at 50 K. On further cooling, the $\chi_m T$ value to 0.47 $cm^3\ mol^{-1}\ K$ at 2.5 K. The best fit to the Bleaney-Bower equation including temperature independent paramagnetism (TIP) yielded the parameters values J = 38.2(1) cm^{-1}, zJ' = –0.206(1) cm^{-1} g = 2.10, TIP = 110 x10^{-5} $cm^3 mol^{-1}$ with a residual of 0.700 x 10^{-4}. Table 6.9 collects together the magnetic data for the known triply-briged dinuclear Cu(II) complexes.

6.8. Conclusions

The present work describes the synthetic investigation of the $CuCO_3\cdot Cu(OH)_2\cdot H_2O$ /haloacetates/bpy general reaction system. The influence of various synthetic parameters, such as the molar ratio of the reactants, the absence or presence of externally added perchlorates, the

nature of the nature of the aromatic N-N chelates has been examined. Our studies revealed that the use of haloacetate/bpy 'ligand blend' in reactions with $CuCO_3 \cdot Cu(OH)_2 \cdot H_2O$ in MeOH/H_2O solutions in the presence of $NaClO_4$ yielded triply-bridged dinuclear complex $[Cu_2(bpy)_2(\mu\text{–}OH)(\mu\text{–}OH_2)(\mu\text{–}ClCH_2COO)](ClO_4)_2$ (**4**), whereas in the absence of $NaClO_4$ yielded a linear trinuclear Cu(II) complex $[Cu_3(bpy)_2(\mu\text{–}ClCH_2COO)_6]$ (**1**), the dinuclear Cu(II) complexes $[Cu_2(bpy)_2(\mu\text{–}Cl_2CHCOO)_2(Cl_2CHCOO)_2]$ (**2**) with *syn-syn* dichloroacetato bridges and $[Cu_2(bpy)_2(\mu\text{–}Cl_3CCOO)_4]$ (**3**) with *syn-anti* coordination mode were isolated. The variable temperature (3–300 K) magnetic susceptibility measurements have suggested antiferromagnetic coupling interaction for the complex **1**, having $J = -51.4(9)$ cm^{-1} and ferromagnetic behaviour for the complex **4**, having $J = 38.2(1)$ cm^{-1}.

6.9. References

1. (a) J. A. Sheikh, A. Adhikary, H. S. Jena, S. Biswas, S. Konar, *Inorg. Chem.*, **2014**, *53*, 1606; (b) R. Kulmaczewski, J. Olguin, J. A. Kitchen, H. L. C. Feltham, G. N. L. Jameson, J. L. Tallon, S. Brooker, *J. Am. Chem. Soc.*, **2014**, *136*, 878; (c) N. V. Gogoleva, E. N. Z. Tikhonova, N. N. Efimov, E. A. Ugolkova, A. S. Bogomyakov, S. V. Kolotilov, M. A. Kiskin, G. G. Aleksandrov, V. V. Minin, A. A. Sidorov, V. M. Novotortsev, I. L. Eremenko, *Russ.Chem.Bull., Int.Ed.*, **2014**, *63*, 1301.
2. (a) D. M. Reinoso, M. L. Ferreira, G. M. Tonetto, *J. Mol. Catal. A: Chem.*, **2013**, *377*, 29; (b) J. W. Boer, W. R. Browne, B. L. Feringa, R. Hage, *C. R. Chimie*, **2007**, *10*, 341.
3. (a) H. Y. Yuan, M. M. Han, X. R. Jiang, Z. G. Jiang, Y. L. Feng, *J. Solid State Chem.*, **2013**, *202*, 191; (b) G. Peng, L. Ma, B. Liu, J. B. Cai, H. Deng, *Inorg. Chem. Commun.*, **2010**, *13*, 599; (c) E. K. D. Dermitzaki, K. F. Konidaris, E. E. Moushi, C. P.

Raptopoulou, V. Psycharis, A. J. Tasiopoulos, V. Bekiari, E. M. Zoupa, S. P. Perlepes, T. C. Stamatatos, *Polyhedron*, **2013**, *52*, 467.

4. (a) E. Colacio, J. M. Dominguez-Vera, R. Kivekas, J. M. Moreno, A. Romerosa, J. Ruiz, *Inorg. Chim. Acta*, **1993,** *212*, 115; (b) S. Sen, M. K. Saha, T. Gupta, A. K. Karmakar, P. Kundu, S. Mitra, M. B. Hursthouse, K. M. Abdul Malik, *J. Chem. Cryst.*, **1998**, *28*, 771.
5. (a) R. J. Doedens, *Prog. Inorg. Chem*., **1976**, *21*, 209; (b) M. Melnik, *Coord. Chem. Rev.,* **1981**, *36***,** 1.
6. (a) O. K. Towle, S. K. Hoffmann, W. E. Hatfield, P. Singh, P. Choudhuri, *Inorg. Chem.*, **1988,** *27*, 394; (b) P. K. Coughlin, S. J. Lippard, *J. Am. Chem. Soc.*, **1984**, *106,* 2328; (c) P. J. Corvan, W. E. Estes, R. R. Weller, W. E. Hatfield, *Inorg.Chem.*, **1980,** *19,* 1297.
7. (a) S. Sarkar, S. Majumder, S. Sasmal, L. Carrella, E. Rentschler, S. Mohanta, *Polyhedron*, **2013**, *50*, 270; (b) G. Mukerjee, K. Biradha, Cryst. Growth Des., 2011, 11, 5649; (c) L. Chena, X. –W. Wanga, J. –Z. Chena, J. –H. Liu, *Z. Naturforsch.* **2007**, *62b,* 1271; (d) J. Moncol, M. Mudra, P. Lonnecke, M. Hewitt, M. Valko, H. Morris, J. Svorec, M. Melnik, M. Mazur, M. Koman, *Inorg. Chim. Acta*, **2007**, *360*, 3213; (e) F. Calderazzo, N. Donati, U. Englert, F. Marchetti, G. Pampaloni, V. Passarelli, *Inorg. Chim. Acta*, **2003**, *346*,100; (f) Q. Shi, R. Cao, M. -C. Hong, Y. -Y. Wang, Q. -Z. Shi, *Trans. Met. Chem.*, **2001**, *26*, 657; (g) H. -H. Lin, H. -H. Wei, G. -H. Lee, W. Wang, *Polyhedron*, **2001**, *20*, 3057; (h) J. F. J. Laugier, D. Luneau, P. Rey, *Inorg. Chem.*, **2000**, *39*, 5510; (i) F. A. Cotton, E. V. Dikarev, M. A. Petrukhina, *Inorg. Chem.*, **2000**, *39*, 6072; (j) A. Grodzicki, E. Szlyk, A. Wojtczak, G. Vrzeszcz, L. Pazderski, T. Muziol, *Polyhedron*, **1999**, *18*, 519.
8. Y. –F. Li, L. –T. Wang, F. –F. Jian, *Acta Cryst.*, **2010**, *E66*, m141.

9. X. –Y. Ma, X. –D. Dong, Y. –P. Li, Z. –G. Zhang, *Acta Cryst.*, **2006**, *E62*, m3467.

10. P. Pascal, *Ann. Chim. Phys.*, **1910**, *19*, 5.

11. G. V. R. Chandramouli, C. Balagopalakrishna, M. V. Rajasekharan, P. T. Manoharan, *Comput. Chem.*, **1996**, *20*, 353.

12. D. B. Brown, J. R. Wasson, J. W. Hall, W. E. Hatfield, *Inorg.Chem.*, **1977,** *16,* 2526.

13. B. Bleaney, K. D. Bowers, *Proc. R. Soc. London, Ser. A.*, **1952**, *214*, 451.

14. SAINTPLUS, Bruker AXS Inc., Madison, Wisconsin, USA, **2003**.

15. G. M. Sheldrick, SADABS, Program for empirical absorption correction (University of Gottingen, Gottingen, Germany), **1996**.

16. G. M. Sheldrick, *Acta Crystallogr.*, **2008**, *A64,* 112.

17. C. F. Macrae, I. J. Bruno, J. A. Chisholm, P. R. Edgington, P. Mc Cabe, E. Pidcock, L. R. Monge, R. Taylor, J. van de Streek, P. A. Wood, *J. Appl. Cryst*., **2008**, *41*, 466.

18. R. Yang, Y. Li, J. Sun, J. Li, C. Chu, *Acta Cryst.*, **2008**, *E64*, m348.

19. Y. Liu, J. Ning, J. Sun, C. Zhang, *Acta Cryst.*, **2009**, *E65*, m113.

20. P. Yin, M. –L. Hu, Q. Miao, *Acta Cryst.*, **2005**, *E61*, m1854.

21. G. Fernandez, M. Corbella, J. Mahia, M. A. Maestro, *Eur. J. Inorg.Chem.*, **2002**, 2502.

22. B. –H. Ye, X. –M. Chen, F. Xue, L. –N. Ji, T. C. W. Mak, *Inorg. Chim. Acta*, **2000**, *299*, 1.

23. H. –C. Yao, N. Wang, L. Zhang, Z. –J. Li, *Acta Crystallogr.*, **2008**, *E64*, m774.

24. Y. Xu, Y. –X. Che, J. –M. Zheng, *Z. Anorg. Allg. Chem.*, **2013**, *639*, 784.

25. W. Li, C. –H. Li, Y. –L. Li, C. –H. Zhang, *Jiegou Huaxue(Chin. J. Struct. Chem.)*, **2012**, *31*, 1507.

26. (a) H. -H. Lin, H. -H. Wei, G. -H. Lee, Y. Wang, *Polyhedron*, **2001**, *20*, 3057; (b) W. Xu, L. Jin, B. B. Liu, *Acta Cryst.*, **2011**, *E67*, m1334; (c) Z. –G. Zhang, X. –D. Dong, Y. –P. Li, X. –H. Pu, F. –J. Huo, M. –L. Zhu, *Acta Cryst.*, **2006**, *E62*, m2326; (d) J. Kaizer, R. Csonka, G. Speier, M. Giorgi, M. Reglier, *J. Mol. Cat. A: Chem.*, **2005***, 236,* 12; (e) Z. F. Zhang, *Acta Cryst.*, **2011**, *E67*, m1158.

27. (a) P. Segla, M. Palicova, D. Miklos, M. Koman, M. Melnik, M. Korabik, J. Mrozinski, T. Glowiak, M. R. Sundberg, P. Lonnecke, *Z. Anorg. Allg. Chem.*, **2004**, *630*, 470; (b) G. Psomas, C. P. Raptopoulou, L. Iordanidis, C. Dendrinou-Samara, V. Tangoulis, D. P. Kessissoglou, *Inorg. Chem.*, **2000,** *39,* 3042; (c) S. P. Perlepes, E. Libby, W. E. Streib, K. Folting, G. Christou, *Polyhedron*, **1992,** *11*, 923; (d) J. Sun, *Acta Cryst.*, **2014**, *E70*, m365; (e) G. Psomas, C. P. Raptopoulou, L. Iordanidis, C. Dendrinou-Samara, V. Tangoulis, D. P. Kessissoglou, *Inorg. Chem.*, **2000,** *39,* 3042.

28. (a) K. S. Burger, P. Chaudhuri, K. Wieghardt, *Inorg. Chem.*, **1996**, *35*, 2704; (b) J. A. Guevara-Garcia, N. Barba-Behrens, A. R. Tapia-Benavides, M. J. Rosales-Hoz, M. Contreras, *Inorg. Chim. Acta*, **1995**, *239*, 93.

29. (a) A. Rodriguez-Fortea, P. Alemany, S. Alvarez, E. Ruiz, *Chem.–Eur. J.*, **2001**, *7*, 627; (b) Watanabe, M. Nakashima, Y. Muto, M. Morooka, S. Ohba, Y. Saito, *Bull. Chem. Soc. Jpn.*, **1990**, *63*, 364.

30. G. Christou, S. P. Perlepes, E. Libby, K. Folting, J. C. Huffman, R. J. Webb, D. N. Hendrickson, *Inorg. Chem.*, **1990**, *29*, 3657.

31. (a) F. P. W. Agterberg, H. A. J. Provo-Kluit, W. L. Driessen, H. Oevering, W. Buijs, M. T. Lakin, A. L. Spek, J. Reedijk, *Inorg. Chem.*, **1997**, *36*, 4321; (b) O. W. Steward, B. S. Johnston, S. C. Chang, A. Harada, S. Ohba, T. Tokii and M. Kato, *Bull. Chem. Soc. Jpn.*,

1996, *69*, 3123; (c) T. C. W. Mak, J. C. Fulwood, C. H. L. Kennard, E. J. O'Reilly, D. S. Sagatys, G. Smith, *Polyhedron*, **1987**, *6*, 855; (d) G. Smith, E. J. O'Reilly, C. H. L. Kennard, A. H. White, *J. Chem. Soc., Dalton Trans.*, **1985**, 243.

32. (a) S. Youngme, T. Chotkhun, S. Leelasubcharoen, N. Chaichit, C. Pakawatchai, G. A. van Albada, J. Reedijk, *Polyhedron*, **2007**, *26*, 725; (b) R. N. Patel, *Inorg. Chim. Acta*, **2010**, *363*, 3838.

33. (a) B. J. Hathaway, in: G. Wilkinson, R. D. Gill, J. A. McCleverty (Eds.), *Comprehensive Coordination Chemistry*, vol. 5, Pergamon Press, Oxford, **1987**; (b) J. Kaizer, R. Csonka, G. Speier, M. Giorgi, M. Reglier, *J.Mol. Catalysis A: Chemical,* **2005***, 236,* 12.

34. B. J. Hathaway, D. E. Billing, *Coord. Chem. Rev.,* **1970**, *5***,** 143.

35. K. Geetha, A. R. Chakravarty, *J. Chem. Soc., Dalton Trans.*, **1999**, 1623.

36. N. Wannarit, K. Siriwong, N. Chaichit, S. Youngme, R. Costa, I. de P. R. Moreira, F. Illas, *Inorg. Chem.*, **2011**, *50*, 10648.

37. N. Wannarit, C. Pakawatchai, I. Mutikainen, R. Costa, I. de P. R. Moreira, S. Youngme, F. Illas, *Phys. Chem. Chem. Phys.*, **2013**, ***15***, 1966.

38. G. Christou, S. P. Perlepes, E. Libby, K. Folting, J. C. Huffman, R. J. Webb, D. **N.** Hendrickson, *Inorg. Chem.*, **1990**, *29,*3657.

39. S. Youngme, J. Phatchimkun, N. Wannarit, N. Chaichit, S. Meejoo, G. A. van Albada, J. Reedijk, *Polyhedron*, **2008**, *27*, 304.

40. C. Chailuecha, S. Youngme, C. Pakawatchai, N. Chaichit, G. A. van Albada, J. Reedijk, *Inorg. Chim. Acta*, **2006**, *359*, 4168.

List of publications:

1. Synthesis and structural studies of copper(II) and nickel(II) complexes containing 4,5-diazafluoren-9-one and pseudohalides: Metal ion directed isomer preference.

   B. Kishore Babu, S. M. Elahi, **T. Krishna Chary**, M. V. Rajasekharan*, *Indian J. Chem., Sec. A*, **2011**, *50*, 1318-1323.

2. Supramolecular architecture and photophysical and biological properties of ruthenium(II) polypyridyl complexes.

   Satish S. Bhat, Vidyanand K. Revankar, Ayesha Khan, Raymond J. Butcher, **Krishnachary Thatipamula**, *New J. Chem.*, **2015**, *39*, 3646-3657.

3. Di-aqua-bridged dinuclear Cu(II) isonicotinate adducts using 2,2'-bipyridine and 1,10-phenanthroline.

   Krishna Chary Thatipamula, G. Bhargavi, M.V. Rajasekharan, *Polyhedron*, **2015**, *97*, 182-187.

4. Synthesis, structural and spectral characterization of the lanthanide nitrato complex anions crystallised using Cu(II) nitrate and 2,2'-bipyridine.

   Krishna Chary Thatipamula, M.V. Rajasekharan *To be communicated*.

5. Synthesis, structural and spectral characterization of the lanthanide nitrato complex anions crystallised with Cu(2,2'-bipyridine)$_3^{2+}$

   Krishna Chary Thatipamula, M.V. Rajasekharan *To be communicated*.

6. Synthesis, structural and spectral properties of the lanthanide nitrato complex anions crystallized using Cu(II) nitrate and 5,5'-dimethyl-2,2'-bipyridine.

   Krishna Chary Thatipamula, M.V. Rajasekharan *To be communicated*.

7. Synthesis, structural and magnetic properties of Cu(II) isonicotinate polymers using 2,2'-bipyridine.

Krishna Chary Thatipamula, M.V. Rajasekharan *To be communicated*.

8. Synthesis, structural and magnetic properties of mono-, di- and tri-chloroacetato bridged Cu(II) complexes with 2,2'-bipyridine.

   Krishna Chary Thatipamula, M.V. Rajasekharan *To be communicated*.

9. Synthesis, structural and spectral characterization of the lanthanide nitrato complex anions crystallised using Ag(I) nitrate and 4,5-diazafluoren-9-one.

   Krishna Chary Thatipamula, M.V. Rajasekharan *To be communicated*.

10. Synthesis, structural and spectral characterization of the lanthanide nitrato complex anions crystallised using Zn(II) nitrate and 2,2'-bipyridine.

    Krishna Chary Thatipamula, M.V. Rajasekharan *To be communicated*.

Posters and workshops:

1. Workshop on crystallography school, School of Chemistry, University of Hyderabad (India) 22 Nov – 4 Dec, **2010**.
2. Workshop at Agilent Single Crystal X-ray Diffractometer User Meet, IIT-Indore, March 19-20, **2012**.
3. A Flash Presentation entitled, The plasticity of Cu(II) in $[Cu(bpy)_2X]^{n+}Y$. Crystal and molecular structures of mixed copper—lanthanide complexes; at Agilent Single Crystal X-ray Diffractometer User Meet, IIT-Indore, March 19-20, **2012**.
4. R. Babu, **T. Krishna chary**, S. M. Elahi, P. M. Vimal, N. Srinivasan, G. Bhargavi and M. V. Rajasekharan, Abstract presented at School of Chemistry, University of Hyderabad (India) NSFOC-2013 Symposium, **2013**.